Measuring Progression in Glaucoma

Thesis submitted for the degree of

Doctor of Medicine at the University of London

Nicholas G Strouthidis MBBS MRCOphth

Supervisors

Mr DF Garway-Heath MD FRCOphth

Professor FW Fitzke PhD

Institutions

Glaucoma Research Unit, Moorfields Eye Hospital, London, UK

Institute of Ophthalmology, London, UK

I declare that this thesis, submitted for the degree of Doctor of Medicine, conducted at University College London, is my own composition and the data presented herein are my own original work, unless otherwise stated. NG Strouthidis, September 2006

ProQuest LLC
789 East Eisenhower Parkway
P.O. Box 1346
Ann Arbor, MI 48106-1346

1 SECTION I: Overview

1.1 Abstract

Background: Primary open angle glaucoma is characterised by progressive optic neuropathy associated with characteristic visual field loss. The ability to measure disease progression is of vital importance in the management of patients with glaucoma. Conventionally, disease progression has been monitored using static automated perimetry. Recently, devices which image the optic nerve head quantifiably have been introduced. This thesis sets out to compare structural and functional progression in ocular hypertensive subjects followed longitudinally using novel progression algorithms.

Plan of research: The investigations may be considered in three parts. Firstly, the factors affecting the test-retest variability of the Heidelberg Retina Tomograph (HRT) are identified and methods to improve repeatability are investigated. Secondly, novel HRT trend and event analyses, based on the findings of the test-retest studies, are compared with established field progression techniques in ocular hypertensive and control subjects. Thirdly, a previously described novel spatial filter is assessed in terms of its impact on the monitoring of visual field progression and in terms of its agreement with a previously described 'structural' map.

Results: Rim area was identified as the most repeatable HRT parameter; its variability can be improved by using the 320μm reference plane and by using only good quality images. Agreement as regards structural and functional progression was poor, regardless of the estimated specificities of the algorithms used or technique adopted. The novel spatial filter appeared to confer some advantage in terms of specificity, comparable to the effect of confirmatory testing. The functional relationship between test-points, characterised by the filter, correlated well with the expected structural pattern.

Clinical significance: The poor agreement suggests that the monitoring of both structure and function is essential to provide the best chance of detecting progression at all stages of the disease. Spatial filtering techniques may provide some additional benefit in the monitoring of progression, particularly once structural data are incorporated.

1.2 Table of contents

1.3 List of figures

1.4 List of tables

1.5 List of abbreviations

AGIS	Advanced glaucoma intervention study
AUROC	Area under receiver operating characteristic
C	Cortical
CCT	Central corneal thickness
CIGTS	Collaborative initial glaucoma treatment study
CND	Central nuclear dip
CNTG	Collaborative normal tension glaucoma (study)
CPSD	Corrected pattern standard deviation
CSLO	Confocal scanning laser ophthalmoscopy
CV_w	Within subject coefficient of variation
dB	Decibel
DLS	Differential light sensitivity
EA	Event analysis
EGPS	European glaucoma prevention study
EMGT	Early manifest glaucoma trial
ETW	Edward Thomas White
FC	Functional correlation
GAT	Goldmann applanation tonometry
GCP	Glaucoma change probability
GDx-VCC	'Glaucoma diagnosis' - variable corneal compensator
GON	Glaucomatous optic neuropathy
GPA	Glaucoma probability analysis
GPS	Glaucoma probability score
HFA	Humphrey field analyser
HRP	Horseradish peroxidase
HRT	Heidelberg retina tomograph
HTG	High tension glaucoma
ICC	Intraclass correlation coefficient
IN	Inferonasal

IOP	Intraocular pressure
IT	Inferotemporal
LOCS	Lens opacity classification system
MD	Mean deviation
MPHSD	Mean pixel height standard deviation
MRA	Moorfields regression analysis
N	Nasal
NC	Nuclear colour
NFI	Nerve fibre indicator
NGS	Nicholas Gabriel Strouthidis
NO	Nuclear opalescence
NTG	Normal tension glaucoma
OAG	Open angle glaucoma
OBF	Ocular blood flow
OCT	Optical coherence tomography
OHT	Ocular hypertension
OHTS	Ocular hypertension treatment study
ONH	Optic nerve head
ONHd	Angular distance at the optic nerve head
P	Posterior subcapsular
PLR	Point-wise linear regression
POAG	Primary open angle glaucoma
PAC	Primary angle closure
PACG	Primary angle closure glaucoma
RA	Rim area
RC	Repeatability coefficient
RETd	Retinal distance
RGC	Retinal ganglion cell
RNFL	Retinal nerve fibre layer
ROC	Receiver operating characteristic

RP	Reference plane
RSD	Residual standard deviation
SAP	Static/standard automated/achromatic perimetry
SIM	Statistic image mapping
SITA	Swedish interactive thresholding algorithm
SN	Superonasal
ST	Superotemporal
SWAP	Short wavelength automated perimetry
T	Temporal
TCA	Topographical change analysis
VF	Visual field
WFA	Wavelet-Fourier analysis

1.6 Acknowledgements

I would like to acknowledge the guidance and support of my supervisors, Mr Ted Garway-Heath (Moorfields Eye Hospital) and Professor Fred Fitzke (Institute of Ophthalmology). In particular I would like to thank Mr Garway-Heath for all of his invaluable advice, time and patience. His influence has been central to my development as an ophthalmologist and as a scientist. I would also like to thank Dr David Crabb (City University) and Mr Ananth Viswanathan (Moorfields Eye Hospital) for their advice regarding perimetry.

Specifically, I would like to thank my co-investigators:

Victoria Owen (Nottingham Trent University) for providing statistical advice relating to the test-retest variability of the HRT and HRT-II. (sections 3.2, 3.3)

Stuart Gardiner (Devers Eye Institute) for providing the novel spatial filter. (sections 3.6, 3.7)

Allan Tucker and Veronica Vinciotti (Brunel University) for the computational analysis performed in comparing structure-function using the novel spatial filter. (sections 3.6)

I would like to thank all of the technical staff at the Glaucoma Research Unit, led by Mr Ed White, without whom I would not have had access to any longitudinal data. Ed White was also an observer in the HRT test-retest studies (sections 3.2, 3.3). I am most grateful to Tuan Ho for his great skill and experience in technical writing; he has been central to my development as a scientific writer. Special mention must also be made of Mr David Spalton (St Thomas's Hospital) and of Professor Roger Hitchings (Moorfields Eye Hospital) without whom I would never have had the opportunity to undertake this project.

I gratefully acknowledge the generous support of *The Friends of Moorfields* and of Heidelberg Engineering in funding my research fellowship at the Glaucoma Research Unit (2002-2004).

2 SECTION II: Introduction

2.1 Glaucoma

2.1.1 Definition and classification

Glaucoma is defined as a progressive optic neuropathy with associated characteristic visual field (VF) deficits (Gupta and Weinreb, 1997). The disease results in a loss of retinal ganglion cells and their neurons. The characteristic, pathognomic, sign of optic nerve head (ONH) 'cupping' – glaucomatous optic neuropathy (GON) – is a result of remodelling of the ONH and retina. The eventual outcome of nerve fibre loss and ONH remodelling is VF loss which, if allowed to progress, may impact upon the patient's ability to function.

A causal relationship between raised intraocular pressure (IOP) and GON was first espoused by von Graefe (1857). Historically, a diagnosis of glaucoma required an IOP greater than 21 mmHg. Epidemiological surveys have established that the mean IOP is approximately 15-16 mmHg in various populations (Armaly, 1965; Bankes et al., 1968; Kahn et al., 1977a; Klein et al., 1992b). The figure of 21 mmHg is taken as the upper limit of normal and has been derived from the mean IOP + 2 standard deviations. This 'cut-off' between normal and abnormal is not entirely valid as IOP is not normally distributed, with an increasing right skewness with age (Colton and Ederer, 1980). There is considerable evidence to suggest that greater than 30% of subjects with GON and VF loss have an IOP less than 21 mmHg (Sponsel, 1989). Elevated IOP is therefore considered a major risk factor for the development of glaucoma and, to this date, remains the only treatable cause. Where a consistently elevated IOP exists in the absence of GON or VF loss, the term ocular hypertension (OHT) is used.

IOP may be elevated by reduced outflow of aqueous humour, with the obstruction usually located at the irido-corneal angle and at the trabecular meshwork. Where the raised IOP can be attributed to significant obstruction of the functional trabecular meshwork by the peripheral iris this is classified as primary angle closure (PAC) with secondary OHT; if this is associated with GON, it is classified as ' primary angle closure glaucoma' (PACG).

Open angle glaucoma (OAG) is defined as GON occurring in the absence of any features suggestive of irido-trabecular contact. Primary open angle glaucoma (POAG) occurs where no underlying cause of raised IOP is identified. Where there is an identifiable cause for raised

IOP, such as pseudoexfoliation, pigment dispersion, uveitis or steroid response, the term secondary open angle glaucoma is used. POAG may therefore be considered a diagnosis of exclusion. POAG patients include subjects with high IOP, high tension glaucoma (HTG), and with normal IOP, normal tension glaucoma (NTG).

2.1.2 Prevalence of POAG and of blindness due to glaucoma

Prevalence estimates of POAG vary around the world; the wide variation in estimates results from differences in study population characteristics (especially age and ethnicity) and differences in glaucoma defining criteria.

Estimates from Europe:

2.1% in white subjects aged 40-49 years in Segovia (Anton et al., 2004)

1.4% (2.1% OHT) in white subjects aged ≥ 40 years in Egna-Neumarkt (Bonomi et al., 1998)

2.5% (6.0% OHT) in white subjects aged ≥ 40 years in Ponza (Cedrone et al., 1997)

1.2% (4.3% OHT) in white subjects aged ≥ 40 years in Sicily (Giuffre et al., 1995)

1.9% in white subjects aged ≥ 50 years in County Roscommon (Coffey et al., 1993)

1.1% in white subjects ≥ 55 years in Rotterdam (Dielemans et al., 1994)

Estimates from the Americas:

2.1% in white subjects aged 43-84 years in Beaver Dam (Klein et al., 1992b)

1.3% in black and white subjects aged ≥ 40 years in Baltimore (Tielsch et al., 1991b)

0.9% in white subjects, 1.2% in black subjects aged 40-49 years "

2.2% in whites subjects, 11.3% in black subjects ≥ 80 years "

1.9% in Hispanic subjects aged ≥ 40 years in Arizona (Quigley et al., 2001)

4.7% (3.6% OHT) in Hispanic subjects aged ≥ 40 years in Los Angeles (Varma et al., 2004)

7.0% in black subjects aged 40-84 years in Barbados (Leske et al., 1994)

Estimates from Africa:

3.1% in black subjects aged ≥ 40 years in Kongwa, Tanzania (Buhrmann et al., 2000)

2.9% in black subjects aged ≥ 40 years in Temba, South Africa (Rotchford et al., 2003)

2.7% in black subjects aged ≥ 40 years in Kwazulu-Natal, South Africa (Rotchford and Johnson, 2002)

Estimates from Australia:

3.0% (3.7% OHT) in white subjects aged ≥ 49 years in Blue Mountains (Mitchell et al., 1996)

1.7% in white aged ≥ 40 years in Melbourne subjects (Wensor et al., 1998)

Estimates from Asia:

2.6% (0.4% OHT) in Indian subjects aged ≥ 40 years in Hyderabad (Dandona et al., 2000)

1.7% in Indian subjects aged ≥ 40 years in Tamil Nadu (Ramakrishnan et al., 2003)

4.1% in Indian subjects aged 30-60 years in Vellore (Jacob et al., 1998)

3.1% in Bangladeshi subjects aged ≥ 40 years in Dhaka (Rahman et al., 2004)

2.3% in Thai subjects aged ≥ 50 years in Rom Klao (Bourne et al., 2003)

0.5% in Mongolian subjects aged ≥ 40 years in Hovsgol Province (Foster et al., 1996)

2.4% in Chinese subjects aged 40-79 years in Singapore (Foster et al., 2000)

3.9% in Japanese subjects aged ≥ 40 years in Tajimi (Iwase et al., 2004)

Quigley (1996) has estimated the worldwide prevalence of glaucoma (both POAG and PACG) at approximately 66.8 million, rising to 79.6 million by 2020 (Quigley and Broman, 2006), of which 74% will have OAG. A median age-adjusted prevalence, taken from population surveys conducted before 1997, is 1.5% for a white population > 40 years and 4.6% for a black population > 40 years (Quigley and Vitale, 1997).

The World Health Organisation estimated the number of people with visual impairment worldwide in 2002 was more than 161 million, of whom approximately 37 million were blind. GON accounts for 12.3% of cases of blindness, second only to cataract which accounts for 47.8% (Resnikoff et al., 2004). In the United States, the Eye Diseases Prevalence Research Group has reported that glaucoma accounts for 6.4% of blindness (taken as best corrected visual acuity of the better-seeing eye at < 20/200) in white subjects, 26.0% of black subjects and 28.6% of Hispanic subjects (Congdon et al., 2004). In the same study, rates of vision impairment (taken as best corrected visual acuity of the better-seeing eye at < 20/40) caused by glaucoma were estimated at 3.3% for white subjects, 14.3% for black subjects and 7.6% for Hispanic subjects. In a survey of a rural and of an urban area of Beijing, POAG accounted for 7.7% of blindness and 8.1% of visual impairment (Xu et al., 2006). This compares with 7.4% bilateral blindness and 7.1% bilateral low vision due to POAG in a Chinese population in Singapore (Saw et al., 2004). An estimated 4.3% of bilateral blindness in a South Indian

population is caused by glaucoma (Vijaya et al., 2006). In the UK, glaucoma accounts for 10.9% of all blind registrations and 10.2% of partial sight registrations (Bunce and Wormald, 2006). Caution is required in extrapolating these figures to the general population, as over half of eligible subjects are not registered despite consultation with an ophthalmologist (Robinson et al., 1994).

2.1.3 Incidence of POAG

Unlike prevalence of POAG, very little data have been published regarding incidence of POAG from population studies. The Barbados Eye Study Group reported a 2.2% 4-year risk of OAG in black subjects; the incidence increased from 1.7% in subjects aged 40-49 years to 4.2% in subjects aged 70 years and older (Leske et al., 2001). The 5 year incidence of OAG in Melbourne was estimated at 0.5% for 'definite' OAG and 1.1% for combined 'probable' and 'definite' OAG (classification of OAG was based on the consensus of 6 ophthalmologists, 2 of whom were glaucoma specialists), with the incidence of 'definite' OAG increasing from 0% in subjects aged 40-49 years to 4.1% in subjects aged 80 years and older (Mukesh et al., 2002). A 1 year incidence of 0.24% was observed in 1093 white subjects in Dalby, Sweden (Bengtsson, 1989) and of 0.25% in 3842 white subjects in Rotterdam, Holland (de Voogd et al., 2005). It should be noted that local factors such as ethnic origin (Racette et al., 2003) or a high prevalence of pseudo-exfoliation (Vesti and Kivela, 2000) make it difficult to apply incidence estimates across differing populations. Further measurement of population-based POAG incidence is desirable; this will enable the cost of screening to be calculated and to help estimate the optimal screening interval. Techniques for monitoring disease progression will have an important role to play in future estimates of glaucoma incidence.

2.1.4 Risk factors for POAG

POAG may be considered a primary degenerative mono-neuropathy influenced by a complex interaction of ocular and systemic factors. Genetic and environmental factors also play a role in the development of POAG.

2.1.4.1 Raised intraocular pressure

Raised IOP undoubtedly plays a significant role in the development of POAG. The Baltimore survey identified 1.2% of the population with an IOP less than or equal to 21 mmHg to have glaucoma; 10.3% with an IOP greater than 22 mmHg were found to have glaucoma. This equates to a relative risk of OHT of 8.6 times that of lower IOP (Sommer et al., 1991b). Other prospective epidemiological studies have supported the concept of increasing risk of glaucoma with raised IOP (Armaly et al., 1980; Dielemans et al., 1994; Leske et al., 1997; Leske et al., 2001).

The magnitude of IOP is positively correlated with risk of glaucoma (Sommer et al., 1991b) and greater magnitude of IOP is associated with more severe visual field deficit at presentation (Jay and Murdoch, 1993; Quigley et al., 1996). It should be noted that over half the number of subjects with glaucoma in some population studies have IOPs less than 21 mmHg (Sommer et al., 1991b; Dielemans et al., 1994; Leske et al., 2001). IOP still plays a role in subjects with NTG, with the eye with the higher IOP having the more severe field loss (Cartwright and Anderson, 1988) and the magnitude of IOP being a risk factor for progression (Crichton et al., 1989; Orgul and Flammer, 1994).

Until recently, the lowering of IOP, either surgically or pharmacologically, to retard the progression of glaucoma has been based on indirect evidence. An indication of an effect of IOP control of visual function in glaucoma has been gleaned from comparative studies (Jay and Murray, 1988; Migdal et al., 1994; 2000). Two recently reported randomised control trials, the Ocular Hypertension Treatment Study (OHTS) and the Early Manifest Glaucoma Trial (EMGT) have provided substantial weight to support the notion that lowering IOP reduces the risk of glaucomatous progression (Heijl et al., 2002; Kass et al., 2002). In the OHTS (Kass et al., 2002), a 20% reduction in IOP achieved a 5.1% absolute reduction in risk of progression to glaucoma, defined as either VF loss or optic disc change (hazard ratio 0.4, 95% confidence interval 0.27 to 0.59). The effect was less but still significant if a stricter definition of onset of disease (VF only) was used, with an absolute risk reduction of 2.4%. The EMGT established the benefit of lowering IOP in subjects with pre-existing glaucoma (Heijl et al., 2002). 255 people with glaucoma were recruited from a Swedish population based survey of 40,000 people. Each subject was randomised to receive either treatment with laser and topical

ß blockers or no treatment. Treatment reduced the risk of progression by 24% (P=0.004, number needed to treat 6).

A third randomised controlled trial, the European Glaucoma Prevention Study (EGPS) failed to detect a statistically significant difference between medical therapy and placebo in reducing the incidence of POAG in OHT subjects at risk of developing POAG (Miglior et al., 2005). The discrepancy in the results of the EGPS and the OHTS may be explained by methodological differences in study design. The failure of the EGPS to demonstrate a benefit of lowering IOP comparable to the OHTS may be due to failure to achieve adequate IOP lowering and selective drop out of those with higher IOP; the reported IOP lowering effect of placebo during the course of the study is most likely a combination of regression to the mean (Parrish, 2006).

Recent evidence suggests that variation in IOP over time in subjects with treated glaucoma may influence disease progression. A retrospective analysis of data from the Advanced Glaucoma Intervention Study (AGIS) indicated that IOP variation over time was more important than absolute level of IOP in increasing the odds of VF progression (Nouri-Mahdavi et al., 2004). A retrospective sub-analysis of the Moorfields 'More Flow' Surgery Study found a similar relationship with optic disc progression following trabeculectomy (Kotecha A, et al. *IOVS* 2006; 47: ARVO E-abstract 4345). Recently, the EMGT group have reported a contradictory relationship, with absolute IOP being strongly associated with glaucomatous progression and no significant relationship between IOP fluctuation and progression was found (Bengtsson et al., 2006).

Both the EMGT and OHTS confirm the importance of lowering IOP in the retardation of disease progression in OHT subjects and patients with an established diagnosis of early glaucoma. A vital factor in the success of both studies was the importance placed on meticulous and repeatable detection of the study end-points, both structural (optic disc changes) and functional (perimetric changes). As the role of IOP in glaucoma is established, and the methods for lowering IOP are readily available, the ability to detect disease progression must now play a central role in the management of patients with OHT and POAG.

2.1.4.2 Central corneal thickness

Central corneal thickness (CCT) has been identified as both a potential determinant of measured IOP, and as a potential independent risk factor for glaucoma. The 'gold standard'

method of measuring IOP in clinical practice in the UK is Goldmann applanation tonometry (GAT). GAT applies the Imbert-Fick principle to measure IOP, whereby an external force (exerted by the tonometer) against a sphere (the eye) is equivalent to the pressure within the sphere multiplied by the area flattened by the force (3.06 mm^2); the mean CCT is approximately 520 µm. GAT IOP measurements have been shown to vary with CCT (Shimmyo et al., 2003; Li et al., 2004), with thicker corneas resulting in an over-reading error and vice versa for thinner corneas. The influence of CCT upon IOP being acknowledged over thirty years ago (Ehlers, 1970) – indeed Goldmann, when first describing the tonometer (Goldmann and Schmidt, 1957) was aware of the association but did not think CCT varied to a degree that it would significantly affect IOP measurement. However, the clinical relevance of CCT in glaucoma has only recently become appreciated with the report of OHTS (Gordon et al., 2002). The results of that study suggest that thinner CCT in OHT subjects may be an independent risk factor for development of glaucoma, over and beyond the influence of any underestimation of IOP, although the effect of CCT on measured IOP is non-linear (Liu and Roberts, 2005). This may be explained by the possibility that less aggressive IOP-lowering therapy is given to subjects with thinner corneas (and therefore lower measured IOP). Alternatively, a thinner cornea may be an indicator of the response of the corneoscleral shell and the ocular vasculature to raised IOP. A recent report suggests that more elastic or distensible ocular tissues may be associated with glaucomatous progression (Congdon et al., 2006).

Although the relationship of CCT to risk of glaucoma has been supported by some studies (Medeiros et al., 2003a; Medeiros et al., 2003b; Herndon et al., 2004), it has not been observed in two population based studies, the EMGT (Leske et al., 2003) and the Barbados Eye Study (Nemesure et al., 2003). The precise role of CCT and corneal biomechanics has yet to be fully elucidated in the context of glaucoma. A recent classic twin study has identified CCT to be highly heritable (Toh et al., 2005), suggesting that CCT may influence the family history component of risk of progression. The measurement of CCT should now, along with IOP measurement, gonioscopy, optic disc and VF assessment, be considered as an essential part of the baseline examination of any subject with, or at risk of, glaucoma.

2.1.4.3 Ageing

The prevalence of POAG increases with age (Klein et al., 1992b; Coffey et al., 1993). In the Blue Mountains Eye Study an exponential increase in the prevalence of glaucoma with increasing age was found; there was, however, no significant age related increase in prevalence of OHT (Mitchell et al., 1996). Other reports identify a positive relationship between age and mean level of IOP, itself a risk factor for the development of POAG (Carel et al., 1984; Mason et al., 1989; Klein et al., 1992a; Wu and Leske, 1997; Bonomi et al., 1998). Glaucomatous VF loss has also been shown to increase with age (Armaly et al., 1980; Nouri-Mahdavi et al., 2004). There is also strong evidence from both the OHTS and EMGT that age is a significant baseline risk factor for glaucomatous progression (Gordon et al., 2002; Heijl et al., 2003).

Age specific prevalence of POAG varies with ethnic origin, with approximately 1% of white subjects having POAG at the age of 50 years, rising to approximately 4% at the age of 80 years compared to 3% at 50 years and 13% at 80 years in black subjects (Quigley and Vitale, 1997).

2.1.4.4 Ethnicity

The Baltimore eye survey demonstrated that African Americans (as a 'self-reported' ethnic origin) have a 6 times greater prevalence (age-adjusted) of POAG and develop POAG 10 years earlier than whites (Tielsch et al., 1991b). Using data from the same survey, POAG was found to be 4 times more likely to cause blindness in African Americans than in whites (Javitt et al., 1991). African Americans are 16 times more likely to have visual dysfunction as a consequence of POAG than whites (Munoz et al., 2000). The latter two observations may be explained partly by lower socio-economic status and by difficulty with access to healthcare services resulting in late presentation (Tielsch et al., 1991a). Higher prevalences of POAG have also been reported in black races in Caribbean island populations. In Barbados a prevalence of 7.0% is reported for blacks compared with 3.3% in mixed-race subjects and 0.8% in whites (Leske et al., 1994); similar prevalences are reported in a population study performed in St Lucia (Mason et al., 1989). A 3% prevalence of POAG has been reported in subjects over 40 years in several population studies conducted in rural Africa (Buhrmann et al., 2000; Rotchford and Johnson, 2002; Rotchford et al., 2003).

There is scant evidence to suggest that ethnic origin relates to an increased risk of glaucomatous progression, or conversion to POAG from OHT (Wilson et al., 1985). OHTS showed an increased risk of developing POAG in the African American group (Gordon et al., 2002), although it should be noted that the increased risk lost significance when adjusted for racial differences in cup-to-disc ratio and corneal thickness. This may imply that the higher rate of conversion may be mediated in part by structural factors which are more prevalent in the African American population. Although a relationship between ethnic origin and risk of glaucoma progression may be suggested by incidence studies (Leske et al., 2001; Mukesh et al., 2002) and by the re-examination of previous retrospective series (Wilson, 2002), studies comparing progression in racial groups prospectively are required for confirmation.

2.1.4.5 Heredity

Family history is often regarded as a risk factor for glaucoma. Recall bias precludes accurate estimates of risk of positive family history in population studies. Likewise, patients are more likely than controls to be aware of family history in case control studies. A positive association has been reported in some studies (Tielsch et al., 1994; Leske et al., 1995). It is important to note that OHTS did not identify positive family history as a significant risk factor for the development of POAG in OHT subjects (Lee and Wilson, 2003), perhaps suggesting that OHT itself is inherited, rather than susceptibility to OHT.

The prevalence of POAG in first-degree relatives of affected patients has been documented to be as high as 7 to 10 times that of the general population (Hart et al., 1979; Drance et al., 1981). A high concordance of POAG has been observed in monozygotic twins (Goldschmidt, 1973; Teikari, 1987). These observations suggest that the heritability of POAG is high, however a single gene theory is unlikely given the variability in the age at disease onset and the prevalence of the disease. It is likely that more than one gene contributes to POAG.

POAG often occurs in multiple family members, but does not follow a clear inheritance pattern, suggesting that inherited risk factors (such as ethnicity, CCT, size of optic disc) can result in a susceptibility to the disease.

Mutations of the MYOC gene, which codes for myocilin, have been identified in patients with adult and juvenile open-angle glaucoma; the gene has been mapped to the open-angle glaucoma locus (GLC1A) region of chromosome 1q25 (Stone et al., 1997). Mutations of this

gene are found in 3% to 5% of adult-onset POAG (Wiggs et al., 1998; Fingert et al., 1999). Myocilin was first identified in cultures of trabecular meshwork cells, where increased expression of the protein was observed following treatment with dexamethasone (Polansky et al., 1997). A role for myocilin in aqueous outflow has been purported, although the function of the normal protein is incompletely understood.

Genes predisposing to glaucoma, described in a further two loci, have been identified from single large pedigrees affected by POAG; GLC1E, optineurin (Rezaie et al., 2002); and GLC1G, WDR36 (Monemi et al., 2005). Polymorphisms in OPA1, which is responsible for an autosomal dominant form of primary optic neuropathy, may be associated with NTG (Aung et al., 2002).

2.1.4.6 Myopia

Clinic-based studies have reported an association between high myopia and risk of POAG (Perkins and Phelps, 1982; Wilson et al., 1987; Mastropasqua et al., 1992), of NTG (Leighton and Tomlinson, 1973; Perkins and Phelps, 1982) and of OHT (Seddon et al., 1983; David et al., 1985). Three population-based studies have identified a relationship between POAG and refractive error. POAG was found to be two to three times more frequent in myopic eyes than emmetropic or hypermetropic eyes in the Blue Mountains Eye Study (Mitchell et al., 1999). Myopia was identified as a risk factor in adult black people with POAG in the Barbados Eye Study (Wu et al., 1999; Wu et al., 2000). In the Beaver Dam Eye Study, which examined a predominantly white population aged 43-86 years, subjects at baseline with myopia were 60% more likely to have glaucoma than those with emmetropia, after controlling for age and gender (Wong et al., 2003). Interestingly this study reports an increased risk of incident (over 5 years) OHT in subjects with hypermetropia but not myopia. Precise estimates of incident glaucoma were not available to determine whether refractive error was related to the risk of glaucoma.

2.1.4.7 Systemic factors

Lagrange (1922) noted that a glaucomatous eye is "a sick eye in a sick body". This statement is pertinent, as a large variety of systemic findings have been observed more commonly in glaucomatous subjects than in normal controls. However evidence is frequently contradictory and it is not clear whether the associations occur by chance. Where independent studies are

in agreement over a particular factor, then there is a higher probability that the association is real. It is also often unclear whether systemic factors are primary or secondary to POAG, and whether the factor has some causal link to POAG; precise mechanisms of causality remain hypothetical.

A number of case control studies have identified a significant association between POAG (including NTG) and arterial hypertension (Leighton and Phillips, 1972; Goldberg et al., 1981; Wilson et al., 1987; Kashiwagi et al., 2001). Population-based data from the Wisconsin epidemiologic study of diabetic retinopathy (Klein et al., 1984) and the Egna-Neumarkt Glaucoma Study (Bonomi et al., 2000) suggest that subjects with POAG have an increased chance of arterial hypertension. There is considerable evidence to suggest that in POAG, and in particular NTG, progression is linked to arterial hypotension (Drance et al., 1973; Kaiser et al., 1993; Bechetoille and Bresson-Dumont, 1994; Leske et al., 1995; Leske et al., 2002). Demailly (Demailly et al., 1984) demonstrated that postural hypotension was of significantly greater magnitude in NTG subjects compared to HTG and control subjects. 24-hour ambulatory blood pressure monitoring studies have demonstrated a significantly lower nocturnal mean diastolic blood pressure in NTG than in acute ischaemic optic neuropathy (Hayreh et al., 1994). Subjects with systemic hypertension taking oral hypotensive medications have shown a significant relationship between VF progression and nocturnal blood pressure 'dip' (Hayreh et al., 1999b). In a case control study of 8 NTG and HTG subjects, all nocturnal blood pressure parameters were lower in subjects with progressive VF loss compared with those in whom the parameters were stable (Graham et al., 1995). The VF series of these subjects were re-examined after 5 years; patients who had experienced greater nocturnal blood pressure dips were more likely to have VF deterioration, despite good IOP control (Graham and Drance, 1999). It is therefore plausible that nocturnal drops in blood pressure may play a role in the progression of glaucoma, perhaps by compromising ONH blood flow.

Vasospasm – vascular dysregulation – has been proposed as a further risk factor for glaucoma, particularly NTG (Flammer et al., 1999). Vasospasm may render the eye more susceptible to IOP-mediated insult. It is possible that endothelium-derived vasoactive substances may play a role in glaucomatous progression. Increased plasma levels of

endothelin-1 have been detected in patients with progressive glaucoma (Sugiyama et al., 1995; Emre et al., 2005) although it is not clear whether this represents a secondary phenomenon or is directly a cause of glaucomatous progression. A link between glaucoma and functional vasospasm of the cerebral vasculature, migraine, has been suspected (Phelps and Corbett, 1985; Wang et al., 1997; Cursiefen et al., 2000). The Collaborative Normal Tension Glaucoma (CNTG) Study Group found migraine to be an independent risk factor for a faster course of VF deterioration (Drance et al., 2001). Although some contradictory reports have been published (Usui et al., 1991; Klein et al., 1993), it seems likely that both migraine and vasospasm are associated with glaucoma, particularly NTG. There is very little evidence to suggest that dyslipidaemia, hypercholesterolaemia and smoking – all of which are risk factors for arteriosclerosis – are independently associated with POAG (Winder, 1977; Wilson et al., 1987; Tanaka et al., 2001). Diabetes is also a significant risk factor in the development of arteriosclerosis. A number of large epidemiological studies have found a positive relationship between diabetes and POAG; the Rotterdam Study (Dielemans et al., 1996), the Wisconsin Study of Diabetic Retinopathy (Klein et al., 1984), the Beaver Dam Eye Study (Klein et al., 1997) and the Blue Mountains Eye Study (Mitchell et al., 1997). These findings were not, however, supported by the Framingham Eye Study (Kahn et al., 1977b; Leibowitz et al., 1980) or the Barbados Eye Study(Leske et al., 1995). The Baltimore Eye Survey similarly found no association between POAG and diabetes, although an association between raised IOP and diabetes was identified (Tielsch et al., 1995). Indeed, the OHTS was contradictory to the extent that diabetes was found to have a significant protective effect against converting to POAG (Gordon et al., 2002). A meta-analysis, conducted before the results of OHTS were available, concluded that there was too much conflicting evidence to warrant screening of diabetic patients for glaucoma (Ellis et al., 1999).

A number of other conditions have been identified as having a potential relationship with POAG, including thyroid eye disease (Cockerham et al., 1997; Ohtsuka and Nakamura, 2000), Cushing syndrome (Haas and Nootens, 1974; Rozsival et al., 1981), altered platelet aggregation (Drance et al., 1973; Hoyng et al., 1992) and higher blood viscosity (Klaver et al., 1985; Trope et al., 1987). Sleep disorders such as obstructive sleep apnoea have been reported to have a greater prevalence in glaucoma subjects (Mojon et al., 1999; Marcus et al.,

2001), however a recent case-control study (Girkin et al., 2006) did not identify pre-existent sleep apnoea to have a great impact on the eventual development of glaucoma.

2.1.5 Pathophysiology of glaucomatous optic neuropathy

The exact mechanism by which the characteristic clinical hallmarks of GON, with progressive displacement of the surface of the ONH and excavation of the prelaminar tissues beneath Elschnig's ring (Ernest and Potts, 1968), is not yet fully understood. Two distinct mechanisms are mooted; a mechanical mechanism whereby IOP-related physical stress is the inciting 'insult' to the ONH and a vascular mechanism whereby compromise to ONH blood flow is the 'insult'. Differing credence is given to both mechanisms by various research groups.

The mechanical theory is based on the understanding that IOP generates mechanical stress (force/cross sectional area) which in turn causes strain (a measure of local deformation) within the load bearing connective tissues of the ONH (Burgoyne et al., 2005). The load bearing tissues of the ONH are the connective tissues of the peripapillary sclera, the lamina cribrosa and the wall of the scleral canal. It is the physical deformation of local tissue (strain) which can induce physiological changes (physical and metabolic changes at a cellular level) to adjacent axons and supporting tissues. The notion that ONH tissues respond to the presence of IOP related strain is based on a number of observations:

a) Axonal transport is compromised at the level of the lamina cribrosa at normal levels of IOP (Ernest and Potts, 1968; Minckler, 1986), and is further compromised with acute (Quigley and Anderson, 1976; Minckler et al., 1977; Quigley and Anderson, 1977; Minckler, 1986) and chronic (Quigley and Anderson, 1976; Minckler et al., 1977; Quigley and Anderson, 1977) elevation of IOP. Retrograde (towards the cell body) flow is important for cellular maintenance as it allows passage of neurotrophic factors. Prolonged interruption of flow may therefore trigger ganglion cell apoptosis.

b) A predictable pattern of connective tissue deformation occurs in glaucomatous cupping (Quigley et al., 1983). The ONH surface (Quigley, 1977; Burgoyne et al., 1994; Burgoyne et al., 1995b) and lamina cribrosa (Levy and Crapps, 1984; Yan et al., 1994) are compliant structures, bowing posteriorly with acute elevations of IOP and then returning to baseline with the return of IOP to normal levels.

c) A predictable pattern of axonal loss underpins glaucomatous visual field loss (Quigley and Green, 1979; Quigley et al., 1982).

d) The ONH surface in experimental early glaucoma demonstrates exaggerated ease of deformation (hypercompliance) to an applied load, suggesting that connective tissue damage occurs early (in this model) in the IOP mediated mechanical hypothesis (Burgoyne et al., 1995a).

e) Extracellular matrix changes occur in the load baring connective tissues, both as part of ageing (Hernandez et al., 1989; Repka and Quigley, 1989) and of glaucoma (Minckler and Spaeth, 1981; Hernandez et al., 1990; Morrison et al., 1990). Cellular synthetic activity in these tissues may be altered by an IOP-induced mechanism (Hernandez et al., 1994).

The vascular paradigm has favour with some researchers as the mechanism is independent of IOP, unlike the mechanical hypothesis outlined previously. The vascular theory considers GON to be a consequence of insufficient blood supply due to either increased IOP or to other risk factors which may reduce ocular blood flow (OBF). The clinically observed relationship between nocturnal 'dips' in arterial blood pressure and disease progression in NTG (Hayreh et al., 1994; Graham et al., 1995; Graham and Drance, 1999; Hayreh et al., 1999b) has already been mentioned in section 2.1.4.7. Further evidence to support a vascular mechanism is provided by in vivo measurements of OBF (measured either directly or indirectly) which generally demonstrate a reduction in OBF in glaucoma subjects, principally:

a) Reduced pulsatile OBF has been observed in patients with POAG, in particular NTG (Silver et al., 1989; Trew and Smith, 1991; Kerr et al., 1998; Schmidt et al., 1998; Fontana et al., 1998b; Kerr et al., 2003), with the OBF changes being apparent before visual field deficit (Fontana et al., 1998b).

b) Reduced blood flow in the retina, choroid and ONH has been observed using fluorescein angiography (Hitchings and Spaeth, 1977; Schwartz et al., 1977; Yamazaki et al., 1996); reduction in choroidal blood flow appears to be most pronounced in NTG patients (Duijm et al., 1997). Peripapillary filling defects have also been observed, particularly using indocyanine green angiography (O'Brart et al., 1997).

c) Reduction in ONH and retinal blood flow has been demonstrated in glaucoma subjects using the Heidelberg retina flowmeter (Michelson et al., 1996; Michelson et al., 1998a; Michelson et al., 1998b; Findl et al., 2000), although Hollo could not detect a reduction (Hollo, 1997).

d) Colour Doppler Imaging studies have found reduced systolic and diastolic velocities in retrobulbar vessels of glaucomatous eyes when compared to normal controls ((Rankin et al., 1995; Nicolela et al., 1996c; Nicolela et al., 1996d; Cheng et al., 2001), with retrobulbar blood flow reduction being greater in the eye with the greater glaucomatous damage (Nicolela et al., 1996b).

e) Baseline peripheral blood flow is slightly decreased in glaucoma patients compared with normal controls. The difference increases following cold provocation, particularly in NTG subjects (Drance et al., 1988; Gasser and Flammer, 1991).

The findings that peripheral blood flow is reduced in glaucoma and that OBF reduction may precede GON (Nicolela et al., 1996c) counter the possibility that reduced OBF is a secondary effect of GON. Flammer and co-workers have suggested that GON may be a consequence of vascular dysregulation/vasospasm, causing OBF fluctuation which damages the ONH through reperfusion injury (Flammer et al., 2001).

The separation of the effects of IOP and of blood flow into two separate pathophysiological mechanisms is likely to be an artificial distinction. Recently, the concept of the ONH as a 'biomechanical' structure has been put forward by Burgoyne and co-workers (Burgoyne et al., 2005). In this new paradigm, glaucomatous structural progression is a result of the interplay between connective tissue damage, axonal compromise and the physiological age of the tissues, with the primary insult being the physiological strain on the ONH supporting tissues, regardless of the level of IOP.

2.2 Structure – anatomy, histology and morphometry

2.2.1 The normal retinal nerve fibre layer

The retinal nerve fibre layer (RNFL) refers to the innermost layer of the retina. Clinically it may be observed ophthalmoscopically as a pattern of subtle striations near the most superficial layer of the retina. Ophthalmoscopic examination may be improved with the use of red-free (ie green) light (Hoyt et al., 1973; Hoyt, 1976). Histologically the retinal nerve fibre layer is comprised of ganglion cell axons organised into bundles, separated by tunnels comprised of glial (Müller cell) processes (Radius and Anderson, 1979a; Radius and Anderson, 1979b). The RNFL also contains the elongated processes of astrocytes (Ogden, 1978). When the RNFL is observed clinically – either using ophthalmoscopy or red-free photography – the 'silvery' striations correspond to axon bundles (Radius and de Bruin, 1981). The 'dark' striations correspond to intervening neuroglial tissue, namely thickened Müller cell end-plates near the retinal surface (Radius and Anderson, 1979a). At higher magnifications, each nerve fibre bundle is seen to be divided into sub-bundles by septa of Müller cell processes (Ogden, 1983c).

The 'retinotopic' organisation of the RNFL can be described in two planes – horizontal and in depth. Horizontal retinotopy, based on the collection of fibres from neighbouring retinal areas into neighbouring bundles which are directed towards the optic nerve head, is clearly apparent as the topography of the RNFL may be observed in vivo by ophthalmoscopy. Nerve fibres arising from the nasal retina follow a direct course to enter the nasal portion of the optic disc, whereas fibres from the temporal retina curve around the fovea to enter the disc at the superior and inferior poles of the optic nerve (Radius, 1987). Neurons arising from ganglion cells located between the fovea and optic nerve enter the temporal portion of the disc within the papillomacular bundle. The temporal raphe extends from the temporal portion of the disc and passes horizontally through the fovea. Ganglion cells superior to the temporal raphe project to the superior and superotemporal portions of the optic nerve and ganglion cells inferior to temporal raphe project to the inferior and inferotemporal portions of the disc (Vrabec, 1966). Fibres arising from locations more temporal to the optic disc arch over those more proximal to the disc.

The vertical ('in depth') retinotopic organisation of the RNFL remains controversial; a number of studies using the techniques of focal xenon arc photocoagulation, horseradish peroxidase (HRP) injection and radioactive amino acid injection in various primate species have provided conflicting and contradictory evidence (Ogden, 1974; Radius and Anderson, 1979b; Minckler, 1980; Ogden, 1983a; Ogden, 1983b). Photocoagulation studies performed in owl monkeys *(Aotes trivirgatus)* and rhesus monkeys *(Macaca mulatta)* demonstrated that nerve fibres within bundles travel together towards the disc with little tendency for lateral displacement and that axons arising peripherally were located deeply (close to the scleral surface) compared to more central axons which lie superficially (close to the vitreal surface), although this was more apparent in the owl monkeys (Radius and Anderson, 1979b). Direct retinal and nerve head injections of HRP in the eyes of Philippine cynomolgus monkeys *(Macaca fasicularis)* agree with this vertical retinotopic organisation (Minckler, 1980). Furthermore the 'Bjerrum' axons, thought to correspond to the axons most susceptible to glaucoma in man, were reported to be primarily confined to a central wedge-shaped 30° area of the supero- and infero-temporal quadrants and maintained the same predictable superficial to deep topography. In contrast, HRP injections into the RNFL of crab-eating macacques *(Macaca irus)* and bonnet monkeys *(Macaca radiata)* identified long (peripheral) fibres as being vitreal to the shorter (more central) fibres, with a relatively 'meandering' course of individual fibres across the retina (Ogden, 1983a). Using the same technique on the eyes of owl monkeys *(Aotes trivirgatus)* identified a lateral dispersion of temporal but not nasal fibres, an absence of vertical retinotopic organisation nasally and a well-defined vertical organisation temporally with long fibres scleral to the shorter fibres (Ogden, 1983b). The variation in vertical axonal distribution seems in part due to species differences – the owl monkey has a rod-dominated system lacking a fovea, and so may not be equivalent to the human RNFL (Ogden, 1983a) – and due to differences in analysis technique. In contrast to the extensive studies on primate eyes, very little has been published regarding the vertical retinotopy of human eyes. Injections of the carbocyanine dyes DiI and DiA demonstrated that peripheral nerve fibres were scattered through the depth of the nerve fibre layer, although axons of the arcuate bundles tended to demonstrate a more scleral bias (Fitzgibbon and Taylor, 1996). The lack of a conclusive description of the organisation of the RNFL in humans is a major stumbling block in the

understanding of the structural and functional relationship in glaucoma. Until such evidence is available, extrapolations of the results of perimetric and imaging studies in glaucoma subjects will remain, in part, speculative.

2.2.2 Glaucomatous changes at the retinal nerve fibre layer

Changes in the appearance of the RNFL in glaucoma subjects, including slit- and wedge-shaped defects (focal atrophy) as well as diffuse atrophy, are detectable ophthalmoscopically (Hoyt and Newman, 1972; Hoyt et al., 1973; Hoyt, 1976). RNFL atrophy has been demonstrated before perimetric loss in glaucoma subjects by as much as five years and to be at least as accurate in predicting later damage as examination of the optic disc (Sommer et al., 1977; Sommer et al., 1979a; Sommer et al., 1979b; Quigley et al., 1982). Atrophy of the RNFL in glaucoma is usually first seen at the superior or inferior arcuate regions (or both), with loss of the striate pattern, and increased visibility of the retinal vessels (Quigley, 1986; Quigley and Sommer, 1987). Localised wedge-shaped defects may develop in the superior/inferior arcuate regions, beginning near the disc margin and fanning out towards the retinal periphery; these may be associated with notches of neural rim tissue at the disc. With progression, the wedge defects increase in size and become diffuse (although some may start diffuse), resulting in the further loss of striations.

As discussed in section 2.2.1, RNFL defects may be induced by xenon arc retinal photocoagulation; histological examination of such defects in rhesus monkeys identified thinning of the RNFL and scattered cystic degeneration (Radius and Anderson, 1979a). This experimental model causes RNFL defects by ascending axonal degeneration. In a model which used descending axonal degeneration, by applying direct trauma to the orbital optic nerve, RNFL thinning was induced in the retinas of cynomolgus monkeys (Quigley and Addicks, 1982). Upon histological examination, RNFL thickness was diminished by at least 50% in the mid-portion of each localised defect; after 3 months following insult the injured axons had disappeared with the space formerly occupied by axons replaced by compacted tissue. An increase in the number of visible astrocyte processes was also observed. An experimental model of glaucoma in cynomolgus monkeys, which raises IOP by argon photocoagulation of the trabecular meshwork has been shown to induce wedge-shaped

RNFL defects, identical to those observed in human glaucoma subjects (Iwata et al., 1985). The wedge-shaped RNFL defects correspond histologically to localised areas of cystic degeneration and loss of axon bundles.

There is very little evidence to suggest that there are differences in the topographical organisation of the RNFL between subjects with HTG and NTG. In a study comparing RNFL defects in 50 NTG eyes and 36 HTG eyes, NTG RNFL defects were significantly closer to the fovea and wider than RNFL defects in the HTG eyes (Woo et al., 2003). These observations are, however, of relatively small magnitude and cannot account for the observation that high tension eyes tend to be associated with 'diffuse' visual field loss whereas NTG eyes tend to be associated with focal perimetric loss. It would seem more likely that the pattern of response to glaucomatous 'insult' is different between NTG and HTG as opposed to any genuine difference in topographical arrangement.

As changes to the RNFL may precede glaucomatous visual field loss as measured by convensional perimetry, technologies which are capable of imaging the RNFL reliably should prove useful in the detection, as well as in the follow-up, of glaucoma.

2.2.3 The normal optic nerve head

2.2.3.1 Anatomy and histology

The optic nerve may divided, along its length, into four distinct components (Ritch et al., 1989; Bron et al., 1997): the intraocular (approximately 3 mm in length), intraorbital (approximately 25 mm in length), intracanalicular (approximately 10 mm in length) and the optic tract (approximately 30 mm in length). The intraocular portion may further be subdivided into:

1) The pre-laminar portion
2) The laminar portion
3) The post-laminar portion

The pre-laminar and laminar zones are of particular clinical interest, as it is believed that these constitute the primary site of injury in glaucoma. The pre-laminar zone, or optic disc, is that which is clinically observable by ophthalmoscopy. The optic disc is a vertically oval structure comprising of a neuroretinal 'rim', containing unmyelinated optic nerve fibres, astrocytes and glial processes. Central to the rim is a 'cup' which is devoid of neural tissue.

The proportion of glial tissue in the pre-laminar optic nerve increases from 5% at the disc surface to 23% at the posterior pre-laminar zone, with a corresponding relative decrease in the axonal area (Minckler et al., 1976). The retinotopic organisation of the optic disc is such that fibres from the papillomacular bundle occupy a large temporal quadrant of the disc, with ganglion cells arising closer to the fovea occupying a more central location and those arising away from the fovea a peripheral location (Minckler, 1980). The fibres from the superior and inferior half of the retina occupy the superior and inferior halves of the disc, with a similar distribution seen for the nasal and temporal fibres. The edge of the optic disc is defined by Elschnig's ring, which is the termination of Bruch's membrane at the scleral foramen; it contains dense collagenous tissue and elastic fibres (Bron et al., 1997). The central part of the optic disc is occupied by the central retinal vessels; their connective tissue collagen is covered by glial processes which split to form a sheath around the vessels (Hogan et al., 1971).

The laminar zone, or lamina cribrosa, corresponds to the segment of the optic nerve which receives collagenous extensions from the surrounding sclera. The lamina cribrosa is a series of approximately 10 cribriform 'plates' of collagenous tissue which stretch across the scleral canal (Anderson, 1969; Emery et al., 1974; Radius and Gonzales, 1981). The laminar beams which make up the cribriform plates are comprised of a core of elastic fibres, collagens type I, III, IV, V, VI, as well as laminin and fibronectin (Hernandez et al., 1987; Hernandez et al., 1990). The cribriform plates are perforated by laminar pores which number 500 to 600 in the humans (Ogden et al., 1988). The number of pores increases from the superficial to deeper plates such that pores are not aligned in descending plates (Emery et al., 1974; Ogden et al., 1988). The pore areas are significantly larger in the superior and inferior quadrants compared to the nasal and temporal quadrants (Quigley and Addicks, 1981; Radius and Gonzales, 1981). The laminar beams are thicker in the nasal-temporal axis of the nerve head, and thinner in the superior-inferior axis, giving the lamina cribrosa a saddle-like shape, with the nasal-temporal axis being closer to the vitreous face (Quigley and Addicks, 1981). Within the lamina, axon bundles follow a relatively direct course, passing through successive pores (Quigley et al., 1981), running with their neighbours to be grouped in a retinotopic arrangement in the post-laminar region and beyond (Hoyt and Luis, 1962). In a detailed

examination of two normal cadaveric eyes following direct injection of HRP into the optic nerve head, the majority of axons were seen to pass directly through the lamina cribrosa, whereas approximately 10% deviate, passing through adjacent cribriform plates (Morgan et al., 1998). This tangential, perhaps precarious, course was identified both in central and peripheral parts of the lamina cribrosa. It is possible that such topographical imprecision is a reflection of the lack of retinotopic organisation seen in non-primate mammals (Horton et al., 1979). The concept that these meandering fibres are more susceptible to glaucomatous damage – perhaps representing the larger axons purportedly selectively lost in glaucoma (Quigley et al., 1987; Quigley et al., 1988) – would appear to be insufficient to account for visual field loss in glaucoma, given the small number of axons involved.

2.2.3.2 Blood supply

The most anterior part of the optic nerve head, the surface nerve fibre layer, receives its blood supply from retinal arterioles although the temporal region may be supplied by the posterior ciliary artery from the deeper pre-laminar region (Hayreh, 1978). In vivo fluorescein angiographic studies suggest that the pre-laminar region is supplied by centripetal branches from the peripapillary choroid (Hayreh, 1975), and this is supported by histological studies in humans and primates (Anderson and Braverman, 1976). However some post-mortem morphometric studies have suggested that the anterior blood supply to the optic nerve head is derived primarily from the scleral short posterior ciliary artery distribution, with minimal contribution from the choriocapillaris (Lieberman et al., 1976; Onda et al., 1995). The laminar zone is supplied either directly by short posterior ciliary arteries or indirectly via the circle of Haller and Zinn (Hayreh, 2001). The circle of Haller and Zinn is located in the peripapillary sclera and is formed by anastamoses between posterior ciliary arteries. It is present in 75% of eyes (Olver et al., 1990) and gives three sets of branches – to the lamina cribrosa, to the peripapillary choroid and to the retrolaminar region (Olver et al., 1994). As the posterior ciliary arteries are end arteries, the boundary between the territories of distribution between two such arteries represent a 'watershed zone'. These zones are of significance as if there is a fall in the perfusion pressure in the vascular bed of one or more end arteries, the area of watershed will be susceptible to ischaemic damage (Hayreh, 1990). The importance of watershed zones in ischaemic optic neuropathies is, therefore, self evident. However, their

role in glaucoma, where the exact pathophysiological mechanism, whether related to blood flow, mechanical stress, or both, is not yet fully understood. A recent report, based on indocyanine green angiography, has suggested that the size and location of watershed zones at the ONH influences the depth of visual field loss in NTG subjects (Sato et al., 2000). It should, however, be noted that these findings were only apparent in seven eyes.

2.2.3.3 Morphometry and ophthalmoscopy

The optic disc area shows considerable inter-individual variability in Caucasian populations from approximately 0.80 mm^2 to approximately 6.00 mm^2 (Franceschetti and Bock, 1950; Bengtsson, 1976; Britton et al., 1987; Jonas et al., 1988a). The optic disc area is approximately 12% larger in black populations (Varma et al., 1994). In general, men have larger optic discs than women (Quigley et al., 1990; Varma et al., 1994). Optic discs are significantly smaller beyond +5 diopters refractive error and significantly larger beyond -8 diopters of refractive error compared to emmetropic eyes (Britton et al., 1987; Jonas et al., 1988a; Jonas et al., 1988b). Optic disc size is positively correlated to the size of the cup and neuroretinal rim, such that the larger the optic disc, the larger the cup and rim (Caprioli and Miller, 1987; Jonas et al., 1988a). The optic disc has a slightly vertically oval form, with the vertical diameter being up to 10% larger than the horizontal diameter (Jonas et al., 1988a). The optic disc shape in highly myopic eyes is more oval and elongated, with an oblique orientation of the disc (Jonas et al., 1988b). There is no significant difference in optic disc shape in myopic eyes less than -8 diopters compared to emmetropic eyes (Jonas et al., 1999). The neuroretinal rim has a characteristic configuration, based on the vertically oval shape of the disc and the horizontally oval shape of the cup. The neuroretinal rim is broadest in the inferior disc region, followed by the superior disc region, the nasal region then finally the temporal region. This pattern, which is usually abbreviated as the ISNT rule (Jonas et al., 1988a) is important in the clinical evaluation of glaucomatous optic discs, whereby changes in this sequence are highly suggestive of glaucomatous damage. The depth of the cup varies according to optic disc size, with deeper cups being associated with larger cups (Jonas and Budde, 2000). Given the relationship between optic disc size and cup size, the expression of the size of the cup as a 'cup to disc' ratio (CDR) is of limited informative value unless the size of the disc is known, particularly in the detection of glaucoma in small optic discs (Garway-

Heath et al., 1998a). CDR varies from 0.0 to 0.9 in a normal white population (Jonas et al., 1988a), although a CDR of greater than 0.65 is found in less than 5% of non-glaucomatous subjects (Sommer et al., 1979b). Cupping tends to be symmetrical between the two eyes, with the vertical CDR being within 0.2 in over 96% of normal subjects (Carpel and Engstrom, 1981; Jonas et al., 1988a).

2.2.4 Ageing changes at the optic nerve head

2.2.4.1 Anatomy and histology

Ageing changes are evident at a histological level at the lamina cribrosa, with an increase in collagen type I within the cribriform plates with advancing age (Hernandez et al., 1989; Morrison et al., 1989). The total collagenous content of the lamina cribrosa increases with age from 20% in the young eye to 50% in the adult eye (Albon et al., 2000a), explaining why flexibility of the lamina cribrosa diminishes with age (Albon et al., 2000b). The density of elastin also increases with age (Hernandez et al., 1989), with elastin fibres increasing in thickness to form long tubular structures (Hernandez, 1992). A 5% reduction in the number of laminar pores above the age of 50 years has been reported (Minckler, 1989). A reduction in the number of axons in the optic nerve head ranging between 4000 and 6723 (0.4-0.6%) per annum has been reported (Johnson et al., 1987; Jonas et al., 1992b). Within the length of the optic nerve, progressive diminution of axons, an increase in fibrous septa, age-related deposits such as corpora amylacea and lipofuscin, as well as vascular sequelae such as swollen axons and cavernous degeneration have been observed with increasing age (Dolman et al., 1980).

2.2.4.2 Morphometry and ophthalmoscopy

Much controversy exists within the literature as to whether an age-related increase in cupping occurs. Two longitudinal studies, which used optic disc stereophotographs, failed to identify a loss of rim area (RA) over time which exceeded the RA variability of repeated photographs (Airaksinen et al., 1992; Caprioli, 1994). A further investigation, which used disc photographs from the Framingham study found that measurement imprecision prevented the identification of an appreciable rate of rim/disc area change (Moya et al., 1999). In a study using the Rodenstock optic disc analyser, neuroretinal RA was found to be significantly smaller in

elderly compared to younger subjects, although it should be noted that there was a tendency to smaller optic discs in that particular group of elderly subjects (Tsai et al., 1992). An earlier study, using the same device, failed to identify any relationship between RA and age (Funk et al., 1989). Population studies also provide conflicting evidence, with an increase in cup diameter of 0.002 mm per year reported in a series of non-stereoscopic optic photographs from 2274 eyes (Bengtsson, 1980), whereas digital photogrammetric analysis of simultaneous stereoscopic pairs taken from 6378 eyes failed to identify a relationship between any optic disc variable and age (Varma et al., 1994). An age-related neuroretinal RA decline of 0.28-0.39% in normal subjects has been reported using computer-assisted planimetry and confocal scanning laser ophthalmoscopy (Garway-Heath et al., 1997).

2.2.5 Glaucomatous changes at the optic nerve head

2.2.5.1 Anatomy and histology

Post-mortem examination of glaucomatous eyes have identified changes at the lamina cribrosa which include a mechanical outward movement (posterior bowing) and vertical compression of the laminar sheets (Emery et al., 1974; Quigley et al., 1983). As glaucoma advances, the lamina pores lose their round shape, becoming elongated (Emery et al., 1974) (Fontana et al., 1998a). Pores which may be visible clinically by ophthalmoscopy also demonstrate elongation with increasing severity of glaucoma (Miller and Quigley, 1988). Histopathological studies of the glaucomatous optic nerve head demonstrate persistent glial activation, which is accompanied by an increased synthesis of extracellular matrix (Hernandez et al., 1990; Morrison et al., 1990; Quigley et al., 1991; Varela and Hernandez, 1997; Ricard et al., 1999). Astrocytes located within the cribriform plate have been identified as migrating to the laminar pores in glaucoma (Hernandez, 2000); this migration is activated by elevated IOP in vitro (Tezel et al., 2001). Astrocyte remodelling of the optic nerve head may therefore play a central role in the characteristic appearance of glaucomatous optic neuropathy.

Histological sections of optic nerves indicate that axons of larger diameter are more susceptible to glaucomatous damage, both in humans (Quigley et al., 1988) and in animal models of glaucoma (Quigley et al., 1987). However, a more recent histological study

performed on a glaucoma model in *Macaca fascicularis* indicated that axonal shrinkage preceding cell death may account for the observed pattern of axon loss, rather than a selective process (Morgan et al., 2000). Axons are lost throughout the optic disc, but are preferentially lost (in eyes with glaucomatous visual field loss) in the superior and inferior sectors of the nerve (Quigley et al., 1982; Quigley et al., 1983). In a primate model of glaucoma, an increase in CDR of 0.1 corresponded to a loss of 10% of nerve fibres, equivalent to 120,000 nerve fibres in humans (Varma et al., 1992a).

2.2.5.2 Morphometry and ophthalmoscopy

A central challenge in the detection of glaucomatous changes at the optic disc – namely enlargement of the optic disc cup, focal (notching) and diffuse narrowing of the neuroretinal rim, as well as loss of the nerve fibre layer (Tuulonen and Airaksinen, 1991) – is that the pattern of loss is superimposed onto the wide interindividual variability of 'normal' optic disc morphology. The pattern of RA loss over time is uncertain, due to measurement variability; stereophotographic examination of 123 OHT and 43 glaucomatous eyes identified a linear decay of RA over time in nearly half of subjects, with the remainder having either episodic or curvilinear loss (Airaksinen et al., 1992). It has been suggested that, although the pattern of loss is most likely to be episodic on an individual axonal basis, the cumulative structural loss will be linear over time (Anderson, D.R. - *personal communication*, 2006).

A variety of glaucomatous optic disc appearances have been categorised (Spaeth et al., 1976; Spaeth, 1994; Nicolela and Drance, 1996a; Nicolela et al., 2003):

1) Type 1 - focal glaucomatous optic disc

In these discs, localised neuroretinal rim loss occurs from within the cup, preferentially at the superior and inferior poles of the disc (Kirsch and Anderson, 1973; Hitchings and Spaeth, 1976; Caprioli and Spaeth, 1985). It is possible, however, that notching is more easily detectable at the poles as this is where the rim is broadest, and where no major vessels are present. It has been suggested that rim loss in the nasal sector is underestimated, based on an experimental glaucoma model (Burgoyne, C.F. – *personal communication*, 2006). Focal rim 'sharpening' occurs if the notch extends to the edge of the disc. A deep notch, extending to the edge of the disc, may take on a greyish, shadowy hue in its depth which is often described as an 'acquired optic disc pit', although subretinal fluid does not accumulate in the

affected region, unlike congenital optic disc pits (Javitt et al., 1990). Notching progresses by notch area enlargement, deepening and sharpening of the polar edge, eventually leading to narrowing and loss of neuroretinal rim in the region of the original loss, which may be associated with 'bayonetting' of vessels (Read and Spaeth, 1974).

2) Type 2 - Myopic glaucomatous optic disc

These discs are characteristically tilted, shallow, have a myopic temporal crescent of peripapillary atrophy and typically demonstrate glaucomatous damage in the form of superior and inferior rim narrowing (Nicolela et al., 1996d).

3) Type 3 - senile sclerotic (atrophic glaucomatous) optic disc

These discs are characterised by diffuse rim loss, resulting in rim narrowing (Geijssen and Greve, 1987); the appearance of the rim may be described as 'moth eaten'. A complete ring of peripapillary atrophy and choroidal sclerosis (where exposure of larger choroidal vessels is visible) is typically present in such discs. As rim loss progresses, gently sloping, shallow cupping occurs, leading down to a centralised, pale area of the cup – saucerisation of the disc (Chandler and Grant, 1965). Rim pallor may precede tissue loss, although this may be a feature of other types of glaucomatous disc (Schwartz, 1973).

4) Type 4 - generalised enlargement of the optic disc cup

Discs of this type possess enlarged round cups in the absence of focal neuroretinal rim loss and with healthy-looking residual neuroretinal tissue; it has been suggested that this is the most frequently observed glaucomatous optic disc (Pederson and Anderson, 1980).

Progressive disc damage may occur by 'concentric atrophy' whereby the neuroretinal rim decays in a concentric, circular fashion with associated cup enlargement in an inferior-temporal, superior-temporal or horizontal direction (Portney, 1976; Spaeth et al., 1976).

'Temporal unfolding' refers to the expansion of the cup more on the temporal side, which may progress nasally to cause 'nasal cupping' nasal to the retinal vessels as they emerge from the disc (Read and Spaeth, 1974; Spaeth et al., 1976).

Cup deepening occurs in most forms of progressive glaucomatous disc damage and is due to a combination of neuroretinal tissue loss and posterior movement of the lamina. Deepening of the cup results in the exposure of the lamina cribrosa such that the lamina pores may become visible (Read and Spaeth, 1974). 'Overpass cupping' is an early sign which is most apparent

in small discs with little or shallow cupping, whereby a central, deep, pallor gives the appearance of a hollow beneath the disc surface (Hitchings and Spaeth, 1976). The characteristic 'bean pot cupping' of end stage glaucoma occurs when the cup enlarges to form a bowl behind the scleral opening of the optic nerve head (Hitchings and Spaeth, 1976; Spaeth et al., 1976).

2.2.6 Other features of glaucomatous optic neuropathy

2.2.6.1 Changes to the optic disc vasculature

As the optic disc cup progressively enlarges, the main trunk of disc vessels may migrate towards the nasal edge of the disc; however nasal exit of vessels is a common feature in physiologically cupped discs (Kirsch and Anderson, 1973). As such, nasal displacement of vessels should not be considered as a sign of progressive glaucoma, unless the movement has been observed over time. An early sign of cup enlargement is 'baring' of circumlinear vessels. These vessels lie within the inner edge of the rim and as neural tissue is lost, the vessel loses its supporting tissue so as to appear exposed or 'bared' (Herschler and Osher, 1980; Osher and Herschler, 1981); the vessel may 'hang' superficially or may progress to lie on the floor of the cup or the edge of the inner rim slope. Unfortunately a bared circumlinear vessel may be seen in normal subjects and in some non-glaucomatous pathologies (Osher and Herschler, 1981; Sutton et al., 1983), and so may not be considered a pathognomonic sign of GON. 'Bayonetting' refers to the appearance of a vessel as it courses up a steep cup slope or undermined rim, and is a feature of progressive notch enlargement.

2.2.6.2 Optic disc haemorrhages

The connection between optic disc haemorrhages and glaucoma was first made over a century ago (Bjerrum, 1889), although their importance in terms of glaucomatous progression was not appreciated in the modern era until as late as 1977 (Drance et al., 1977).

Disc haemorrhages associated with POAG are located on or close to the disc, usually reaching the disc border and are most frequently seen at the disc poles (Sonnsjo et al., 2002). Disc haemorrhages are usually located in the pre-laminar region of the disc and the superficial nerve fibre layer, less often deeper. Disc haemorrhages may appear thin and stretched radially when located at the disc border ('splinter haemorrhage') or round when

occurring centrally on the disc. When extravasation of the haemorrhage is extensive, the haemorrhage may appear flame- or fan-shaped. In one study, 92% of disc haemorrhages in glaucoma subjects were detectable up to two months after first presentation, with recurrences occurring in 64% of eyes, the majority within 1 month (Kitazawa et al., 1986). Disc haemorrhage represents a significant prognostic factor in glaucoma, (Ishida et al., 2000), being associated with, and predictive of, notching and progressive loss of rim tissue (Airaksinen and Tuulonen, 1984; Jonas and Xu, 1994; Ahn and Park, 2002), focal nerve fibre layer loss (Airaksinen et al., 1981; Sugiyama et al., 1997; Sugiyama et al., 1999) and progression of visual field loss (Siegner and Netland, 1996; Rasker et al., 1997). It should be noted that up to 70% optic disc haemorrhages may occur in subjects with no definite evidence of glaucoma (Healey et al., 1998); within glaucoma subjects, haemorrhages may be more common in the normal tension subtype (Kitazawa et al., 1986; Jonas and Xu, 1994; Healey et al., 1998).

2.2.6.3 Peripapillary atrophy

Peripapillary atrophy can be divided into a peripheral 'alpha zone', characterised by chorioretinal thinning associated with irregular hypo- and hyper-pigmentation, and a central 'beta' zone, characterised by marked atrophy of the chorioretinal tissue and the retinal pigment epithelium, with visibility of choroidal vessels (Jonas et al., 1989). The two zones are larger, and the beta zone occurs more frequently, in glaucomatous compared to normal eyes (Jonas et al., 1989; Jonas et al., 1992a). Some studies have suggested that increasing peripapillary atrophy may be indicative, or predictive, of progressive glaucomatous damage (Rockwood and Anderson, 1988; Tezel et al., 1997a; Tezel et al., 1997b; Uchida et al., 1998). However, a recent study identified progressing atrophy of zone beta in only 2.7% of glaucomatous eyes, with a minimum follow-up of 1.5 years, although this proportion was slightly increased with the exclusion of myopic eyes (Budde and Jonas, 2004). A large beta zone and small neuroretinal rim have been identified as significant risk factors for the development and progression of visual loss in OHT and POAG subjects (Jonas et al., 2004). The same morphological features have been identified as being predictive of glaucomatous disc damage in subjects with raised IOP, but not normal tension (Martus et al., 2005).

2.3 Imaging of the ONH and the RNFL

2.3.1 The importance of quantitative measurement

The glaucomatous optic disc morphometric changes, as well as the wide inter-individual morphometric variations seen in normal subjects, described in section 2.2, have been based on the subjective appreciation of clinical appearance, either by ophthalmoscopy or the use of photographs. Agreement as regards subjective appearance of optic disc photographs (viewed either monoscopically or stereoscopically) is poor, even amongst experienced observers (Varma et al., 1992b; Azuara-Blanco et al., 2003). Such a shortcoming would suggest that the non-quantitative examination of serial optic disc photographs may be of limited value in the follow-up of glaucoma subjects. Unfortunately, in much of UK clinical practice, the only record of optic disc appearance remains a drawing in the patient's notes, perhaps annotated with the cup to disc ratio. Given the notoriously high inter-observer variability in measuring cup to disc ratio (Lichter, 1976), this method is unlikely to be of any real value in the monitoring of glaucomatous progression.

One approach which attempts to improve inter-observer variability of clinical examination of the disc has been the introduction of 'standardised' methods of interpretation. A novel optic disc scaling method, the 'disc damage likelihood scale', gauges neuroretinal rim appearance corrected for disc diameter (Spaeth et al., 2002). Although this technique takes into account important physiological and morphometric principles, it is no more repeatable than the interpretation of cup to disc ratio in vivo; it is, however, more repeatable when stereophotographs are used (Henderer et al., 2003). In OHTS, independent optic disc reading centres were used to grade glaucomatous change in stereophotographs over time. The inter-observer agreement for detecting glaucomatous disc change by masked graders in that study has been reported as 'good to excellent' with kappa values in the range of 0.65 to 0.83 (Parrish et al., 2005), comparing favourably with other masked grading studies (Caprioli et al., 1996; Coleman et al., 1996; Azuara-Blanco et al., 2003; Zeyen et al., 2003). However the sensitivity of the masked graders, estimated from the number of stereophotographs correctly 're-graded' as not demonstrating deterioration in OHTS was poor, being as low as 64% after the first year of the study (Parrish et al., 2005). This highlights the marked difficulties encountered in trying to consistently detect the small optic disc changes which occur at the

earliest stages of glaucoma and ocular hypertension, despite the presence of experienced graders and a robust protocol.

A number of technological advances, including computer-assisted planimetry, video-ophthalmography and simultaneous stereo disc photography with digital photogrammetry have offered a quantitative, repeatable analysis of optic disc characteristics (Betz et al., 1982; Mikelberg et al., 1984a; Jonas et al., 1988a; Varma et al., 1989). However, these methods have largely been superseded in modern clinical practice by three devices, each of which employs a different technology. These devices are the Heidelberg Retina Tomograph (HRT, Heidelberg Engineering, Heidelberg GmbH, Germany) which uses confocal scanning laser ophthalmoscopy, the GDx-VCC (Carl Zeiss Meditec, Dublin, California) which uses scanning laser polarimetry and the Optical Coherence Tomography scanner (OCT, Carl Zeiss Meditec, Dublin, California). As these devices are pre-eminent at the time of writing, they will be described in this section, whereas other technologies such as the Discam and the Retinal Thickness Analyzer will be omitted. As the HRT has been available in the clinical setting for well over a decade, a greater amount of longitudinal patient data are available compared to the other two devices. As such, the HRT is described in particular detail in this section.

2.3.2 Confocal scanning laser ophthalmoscopy (HRT)

2.3.2.1 Historical perspective and principles

The first landmark in the genesis of confocal scanning laser ophthalmoscopy (CSLO) was the development of 'TV ophthalmoscopy', over fifty years ago (Ridley, 1951). The device, developed at St Thomas's Hospital, London, with the assistance of the Marconi Wireless Telegraph Company, used the principle of indirect ophthalmoscopy to transfer an image of the fundus, free of the corneal reflex, onto a television monitor. Although the system was successful, it was too bulky and impractical to use in routine clinical practice. The principle was subsequently adapted to use low-powered laser light, instead of direct illumination, in a device called 'the flying spot TV ophthalmoscope' (Webb et al., 1980). The same group, based in Boston, Massachusetts, described the operating principle of scanning laser ophthalmoscopy, whereby a single point on the fundus is illuminated at any one time by a beam of laser light sweeping across the fundus in a raster-like fashion (Webb and Hughes,

1981; Mainster et al., 1982). The scanning of sections of the fundus enables a piece-by-piece retinal image to be cumulatively constructed and to be viewed on a television monitor. The use of a focussed laser beam enabled the acquisition of a high quality image of the fundus using less than 1/1000 of the light necessary to illuminate the fundus with conventional light ophthalmoscopy; scanning laser ophthalmoscopy requires irradiance of less than 70 $\mu W/cm^2$ compared with 100,000 $\mu W/cm^2$ for conventional indirect ophthalmoscopy (Webb and Hughes, 1981). The confocal principle refers to the fact that the light reflected from the fundus is received at a photodetector via an aperture which is confocal (having the same focal length) with the light source. Signal to noise ratio is increased as the aperture or pinhole excludes reflected light which is not from the point of interest on the fundus, such as diffuse fundal, corneal and lenticular reflections.

2.3.2.2 Image acquisition

The HRT and its successor, the Heidelberg Retina Tomograph-II (HRT-II), both use a 675 nm diode laser as a light source. The emitted beam is directed in a flat plane, in a horizontal direction (x-axis) and vertical direction (y-axis) onto a plane of focus perpendicular to the optic disc (z-axis) (Girkin, 2005; Zinser, 2005). In order to produce the two dimensional planes, the laser beam is periodically deflected perpendicular to the optical axis using scanning mirrors. The field of view for the acquisition of these two dimensional sections can be varied from 10° x 10°, 15° x 15°, or 20° x 20° when using the HRT; the field of view is set at 15° x 15° when using the HRT-II (Heidelberg Engineering, 2003). The optical section of the point of interest (in this case, the optic disc) is reflected back to the imaging device through the subject's pupil and directed to a photodirector, using a beam splitter. Prior to reaching the photodetector, the reflected light passes through a pinhole which is confocal with the illuminating system (Figure 2-1). The confocal pinhole allows light reflected from the point of interest which is at the focal plane to be focussed, passing through the pinhole to the detector. Light reflected from structures above and below the focal plane are not focussed to the pinhole; a minimal amount of light from these structures will reach the detector. The location of the focal plane in depth can be adjusted by moving the confocal aperture – this allows multiple sections of the optic disc at different depths (from the vitreous face to the lamina cribrosa) to be collected. This

generates a three-dimensional image of the disc, a process called scanning laser tomography (Figure 2-2).

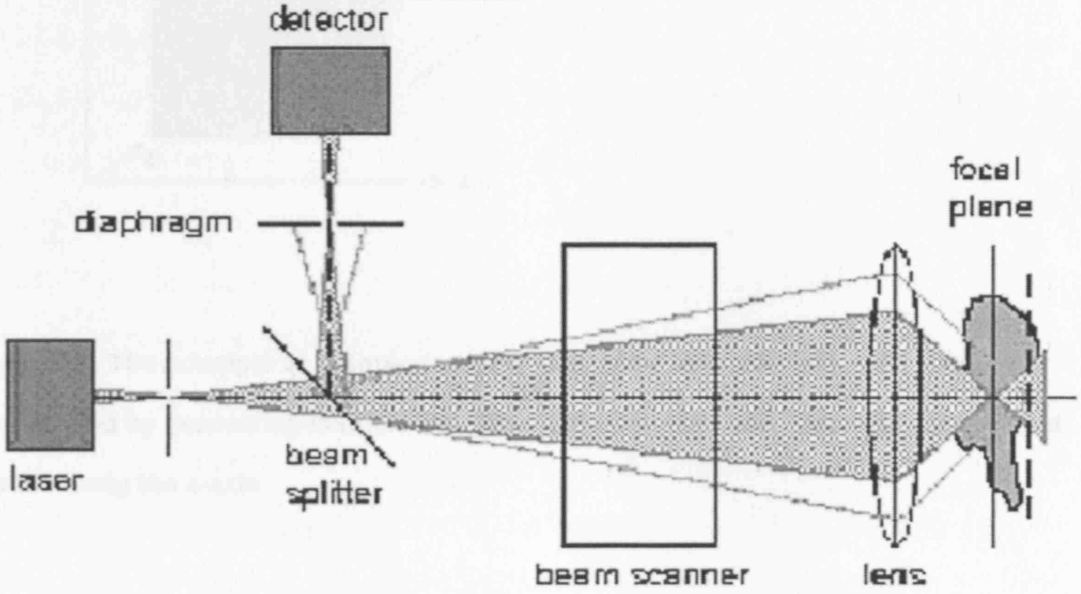

Figure 2-1. The principle of confocal scanning laser ophthalmoscopy as applied using the Heidelberg Retina Tomograph and the Heidelberg Retina Tomograph-II

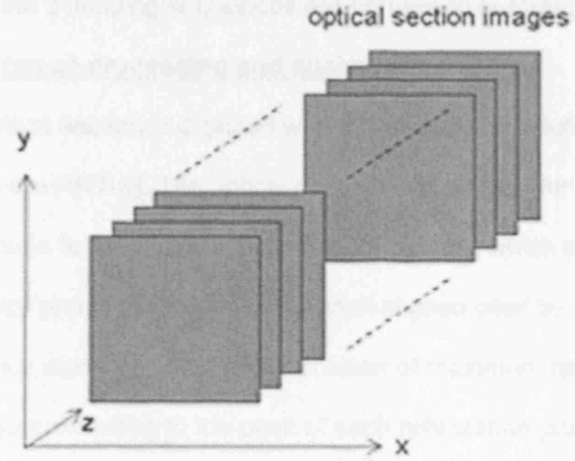

Figure 2-2. The principle of scanning laser tomography. A three dimensional image is constructed by generating multiple two dimensional optical section images at different depths along the z-axis

The HRT acquires 32 optical sections (or 'reflectance images') in 1.6 seconds – the HRT-II on the other hand acquires sections at 16 to 64 planes up to a scan depth of 4mm. In terms of the practical aspects of image acquisition, the manufacturers suggest that pupil dilation is not required as a 1 mm pupil diameter is sufficient to acquire high quality images (Heidelberg Engineering, 2003). However, it is accepted that pupil dilation may allow a small improvement in image quality, particularly in patients with cataracts and small pupils (Zangwill et al., 1997b). Image acquisition takes place with the subject's head placed on a head-rest and chin-rest, as in the standard slit lamp, with a distance between the imaging head and the subject's eye of approximately 1.5 cm. The HRT requires external fixation, and the use of trial lenses to be placed in front of the fellow eye to correct for refractive error. The HRT-II, on the other hand, has an internal fixation light and the focus may be adjusted for spherical refractive error; latterly additional lenses to correct for cylindrical error have been made available. The manufacturers do not recommend using the HRT II beyond + or -6 diopters of spherical refractive error (Heidelberg Engineering, 2003). Using the HRT, discrete individual scan

acquisitions (a minimum of 3) are required to generate a mean topography image; using the HRT-II, the 3 imaging sequences are performed automatically at the same acquisition.

2.3.2.3 Image processing and analysis

Each optical section is digitised with a transverse resolution of 256 x 256 pixels (384 x 384 pixels in the HRT-II). The optical sections are aligned for horizontal and vertical shift, to compensate for any head movements or blinking which occur during image acquisition. A 'reflectivity profile' is generated for each aligned pixel by plotting light reflectivity as a function of distance along the z-axis. The position of maximum reflectivity ('centre of gravity') for each pixel – approximating to the peak of each reflectance profile – determines the topographical height value for the pixel. When summated, over 60,000 height measures per image acquisition are generated. The result is a 'topographic image' (single topography) representing the topographical height of each pixel from the focal plane of the eye (Chauhan et al., 2000). As mentioned in section 2.3.2.2, a minimum of 3 single topographies is obtained in each session (Weinreb et al., 1993); a mean topography and reflectance image is generated from these topographies. In order to achieve this, horizontal, vertical and rotational alignment is achieved using a correlation function performed on the reflectance images; depth and tilt alignment are made using the topography images (Chauhan et al., 2000). The variability of pixel heights across the single topographies used to generate the mean topography is calculated as the mean pixel height standard deviation (MPHSD), this value may be used as a proxy measure of image quality (Dreher et al., 1991). As the light source used by the HRT and HRT-II is monochromatic, the mean topography and reflectance image are monochromatic – a colour coding according to signal intensity is applied by post-hoc image processing. In order to generate the 'stereometric parameters' of an individual optic disc image, the operator needs to draw a contour line onto the mean topography image. This is placed at the edge of the optic disc, at the internal limit of Elschnig's ring – visual cues observed in the mean reflectance image and the mean topography image are useful in defining the limits of the disc. Contour lines may be drawn freehand, or by using disc photographs or clinical examination to assist definition. In a study comparing contour lines drawn freehand, with the assistance stereoscopic photographs and with monoscopic photographs, very little difference in inter-observer variability was detected with intraclass

correlation coefficients of 0.89-0.99, 0.86-0.99 and 0.81-0.99 generated, respectively (Watkins and Broadway, 2005). It may therefore be sufficient, in most circumstances, to base contour line placement on the HRT-generated images. However, use of photographic assistance may be of benefit in large or tilted discs where the true size of the optic disc may be underestimated using the HRT (Bhermi et al. *IOVS* 2004; 45: ARVO E-Abstract 955).

The original operating software of the HRT was MS-DOS based. With the introduction of the HRT-II, which was intended as a tool primarily designed for routine clinical practice, as opposed to the largely research-orientated HRT, a new Windows based platform was introduced. The new platform, Eye Explorer, in keeping with the requirements of the newer device, was much faster and more intuitive, being largely operator independent, other than for the placement of the contour line. In creating the new software, a number of useful operator-dependent facilities were lost; the ability to access individual single topographies, the ability to tailor disc sector size and the ability to define reference plane being chief amongst them (although these facilities have very recently become available in research versions of the software). It is possible to analyse images acquired using the HRT on the new software, by importing the images as HRTport files. The MS-DOS operating system was phased out; indeed the system cannot be supported by any operating system later than Windows 98 (Reutter, M. *Personal communication*, 2003). In its place, a facility on the Explorer software called 'HRT Classic' was introduced which replicated the operating characteristics of the older software. It should be noted, however, that it is not possible to analyse images acquired using the HRT-II with the HRT Classic option.

At the time of writing, a new version of the HRT, the HRT-III has been introduced. This is not, as the name suggests, a wholesale redevelopment of the system comparable to the difference between HRT and HRT-II. The HRT-III uses the same laser unit as the HRT-II, but the practicality of use has been improved by replacing the desk-top interface with a laptop unit. In terms of image processing, the HRT-III has improved image quality assessment and uses a new alignment algorithm. In terms of software modifications, the HRT-III has expanded, ethnicity-based, normative databases and a new diagnostic algorithm named glaucoma probability score (GPS), discussed in section 2.3.2.6 (Heidelberg Engineering, 2006).

2.3.2.4 Reference plane

The reference plane (RP) is an imaginary plane set below, and parallel to the retinal surface within an HRT topographic image (Strouthidis, 2005). Space that is above the RP, within the scleral ring, is defined as 'neuroretinal rim' and below is defined as 'cup' (Figure 2-3).

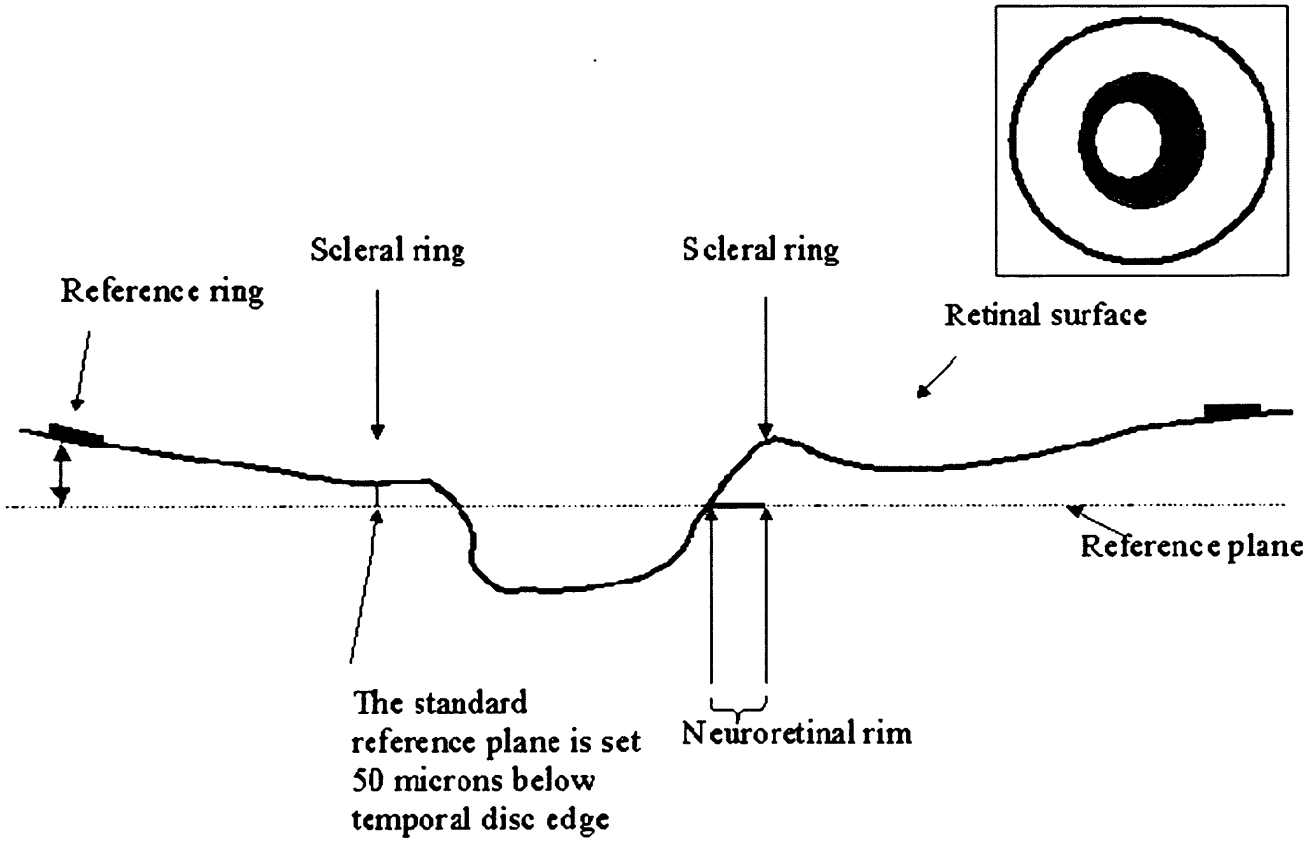

Figure 2-3. Schematic diagram of a cross-section through the optic nerve head and retinal nerve fibre layer demonstrating the position of the reference plane. The reference plane (dashed line) is parallel to the retinal surface at the peripheral reference ring. The 'Standard' reference plane is set at 50µm below the contour line at the temporal disc margin. An alternative reference plane may be set 320µm below the mean height of the peripheral reference ring

Most stereometric parameter values are dependent on the position of the RP; a deeply placed plane generates a smaller cup and a greater rim, whereas a superficially placed plane generates a greater cup and a smaller rim. Disc area, height variation contour and cup shape measure are parameters which are independent of RP.

The Standard RP is the default plane in Explorer. It is located 50μm below the contour line at the temporal disc margin, between -10° and -4°. The choice of location was based on the mean surface inclination angle of the optic nerve head and because it coincides with the papillomacular bundle (Burk et al., 2000). It was assumed that the papillomacular bundle maintains a stable thickness, as central visual acuity is not affected until the latter stages of glaucoma. This has not been supported by OCT studies which demonstrate reduced bundle thickness despite maintenance of good visual acuity (Chen et al., 2001): it is therefore possible that the RP height changes as glaucoma progresses. RP height variability may also occur as a consequence of tomographic 'artefacts' dipping over Elschnig's ring.

There is evidence to suggest that alternative RP locations may result in less measurement variability (Tan et al., 2003a). The 320μm RP, previously available on the old HRT MS-DOS system, was introduced as an option on later versions of Explorer (1.6.0 onwards). This plane has a fixed off-set situated 320μm posterior to the reference ring located in the image periphery. This RP has the advantage of greater stability, which is reflected in reduced between-image RA variability compared with the standard RP (Tan and Hitchings, 2003c). This plane may not be appropriate for use in discs with oblique insertions where the difference between the retinal height and the cup level may exceed 320μm. Likewise, disease processes occurring outside the disc margin such as peripapillary atrophy may influence measurements.

More recently an experimental RP has been described with the intention that it should have an unchanging height relationship with the optic nerve head in a longitudinal image series (Tan and Hitchings, 2003c). The position of the RP is calculated from the mean height of the contour line, and a fixed off-set from the contour line's lowest region (previously identified as giving rise to the least RA variability). Reduced inter-image RA variability has been reported using this experimental plane however as the plane height is determined by the height of the

disc margin contour it might be expected to shift posteriorly as glaucoma progresses, as with the standard RP.

2.3.2.5 Reproducibility

A prerequisite of any imaging device used in the detection of structural changes secondary to glaucomatous disease progression is that it generates highly reproducible measurements. Changes outside of those expected from measurement error may be ascribed to the disease process, thereby enabling the discrimination of disease stability from progressing disease. Much has been reported regarding the reproducibility of the HRT. The earliest reproducibility study of the HRT's immediate predecessor, the Laser Tomographic Scanner (LTS, Heidelberg Instruments GmbH, Heidelberg, West Germany) examined ten repeated measurements in eight normal subjects (Kruse et al., 1989). The mean coefficient of variation for the eight subjects was 9.5% (3.9-18.2%). In a later study, using the same instrument, Dreher and co-workers acquired five images in eight normal and eight glaucomatous eyes (Dreher et al., 1991). There was no significant difference between measurement variability between the two groups, with the standard deviation for pixel height at the disc being 41.2µm in the normal eyes and 49.4µm the glaucomatous eyes. A study which analysed five 10° x 10° images from five normal and five glaucomatous eyes generated reproducibility coefficients ranging from 60.5 to 99.4% (Mikelberg et al., 1993). With the introduction of the HRT, coefficients of variation of 5.5% ± 4.5% for cup area and 8.6% ± 6.1% for RA were reported using 3 repeated measurements acquired from thirty nine glaucoma, glaucoma suspect and control subjects (Rohrschneider et al., 1994). An alternative study identified a statistically significant difference between mean pixel height standard deviation in thirty glaucomatous (31.2 µm) and thirty control subjects (25.9 µm) imaged on three occasions (Chauhan et al., 1994). In the same study, a significant increase in variability with increasing age was identified. The highest variability was found along the cup border and along blood vessels, which was confirmed in a later study examining regional variability of the HRT (Brigatti et al., 1995). The Halifax group later showed that scanning with pulse synchronicity, thereby removing some of the noise occurring around major blood vessels, reduced mean image variability by 13.6% (Chauhan and McCormick, 1995). Variability is also associated with misalignment of the patient and the laser scanner (Orgul et al., 1996) and choice of RP (Tan

et al., 2003a). Inter-observer variability has been shown to improve in one study with the use of stereoscopic photographs to assist in contour-line drawing (Iester et al., 2001), although later studies have been less convincing as regards this matter (Miglior et al., 2002; Watkins and Broadway, 2005). Perhaps the most striking demonstration of the reproducibility of the HRT was a comparison made with computer-assisted planimetry, a previous 'gold-standard' disc assessment methodology, which demonstrated 50% less inter-observer RA variability using the HRT (Garway-Heath et al., 1999). A potential role for the HRT in the monitoring of glaucomatous progression is therefore supported by the large amount of evidence indicating that it generates highly reproducible measurements.

By way of contrast, very little has been published regarding the reproducibility of the HRT-II, or of variability studies using Explorer software. One study which assessed the test-retest variability of the HRT-II reported similar levels of variability as the HRT (Sihota et al., 2002). This did not, however, hold true for image acquisitions in eyes with greater than one dioptre of uncorrected cylindrical error; in this circumstance the newer device fared less well than the HRT. This is unlikely to be a significant problem now as cylindrical correcting lenses have become available for use with the HRT-II.

2.3.2.6 Diagnostic potential

A number of early studies have confirmed that the HRT was capable of discriminating normal subjects from glaucoma subjects, with cup shape measure, cup volume and RA being the most useful discriminatory parameters (Hatch et al., 1997; Iester et al., 1997a). Zangwill and co-workers (Zangwill et al., 1996) found significant differences in all topographic measurements between age-matched glaucomatous and normal eyes, and significant differences for disc area, contour height , RA and rim volume between age-matched OHT and glaucomatous eyes. In a comparison between 50 normal subjects and 102 OHT subjects, a sensitivity for RA of 24.8% and for rim volume of 25.5% in the superior disc sector were estimated at a predetermined specificity of 95% (Mardin et al., 1999). A major weakness of all the aforementioned studies is that they sought to estimate sensitivity using subjects in whom optic disc appearance, the very parameter under investigation, was used as an inclusion criterion. The studies were therefore subject to considerable selection bias (Garway-Heath and Hitchings, 1998).

A sensitivity of 84.3% has been reported for RA as the discriminating parameter (taking disc area into account) with a specificity of 96.3% (Wollstein et al., 1998). In other studies, cup shape measure (or 'third moment') has been identified as the parameter with the best discriminatory power (Mikelberg et al., 1995; Uchida et al., 1996).

Improved discriminatory power, over individual parameters, has been achieved by combining a number of parameters and by segmentation of the disc (Mikelberg et al., 1995; Iester et al., 1997c; Bathija et al., 1998; Wollstein et al., 1998; Miglior et al., 2003). One method of combining variables is to perform a discriminant function analysis, whereby the variables included are weighted according to their discriminatory power. The linear discriminant function described by Mikelberg et al., (1995; 2003) is included in the Explorer software. In this formula, weighted values for rim volume, height variation contour and age-corrected cup shape measure are used to define whether the optic disc is normal or glaucomatous. Burk et al., (1998; 2003) described a linear discriminant function which omitted RP dependant parameters by combining weighted values of the difference in contour line height between the temporal and superotemporal sector, the difference in contour line height between temporal and inferotemporal sector, and the superotemporal cup shape measure. A third linear discriminant function formula was described by Bajitha et al., (1998) which combines weighted values of cup shape measure, height variation and mean retinal nerve fibre retinal thickness. Although all of these linear discriminant functions achieved respectable sensitivity and specificities when originally described, this was not replicated by a later study which achieved sensitivities of 39%, 55% and 44%, respectively, at a cut-off specificity of 95% (Ford et al., 2003). None of these tests would be sufficient to enable the HRT to be used as a stand-alone test in a mass screening program for glaucoma (Ford et al., 2003).

Other than the Mikelberg discriminatory function, the other classification system available on the Explorer software is the Moorfields Regression Analysis (MRA) (Wollstein et al., 1998; 2003). This algorithm is based on the understanding that RA is dependent on optic disc size (Jonas et al., 1988a), may decline with advancing age (Garway-Heath et al., 1997) and that it may narrow in any sector of the disc in glaucoma (Read and Spaeth, 1974; Tuulonen and Airaksinen, 1991). The MRA algorithm is derived from measurement data derived from a group of 112 normal Caucasian eyes. A logarithmic transformation of RA, performed to

normalise the variability distribution, is plotted against optic disc area to define the normal ranges. By plotting linear regression lines at the lower 95%, 99% and 99.9% prediction limits, one may define the number of normal eyes which would be expected to have a particular RA size at each cut-off value. The process is performed for the global RA, as well as for each of the six predefined RA sectors. An ONH is defined as 'within normal limits' if the global and segmental RA values are all greater than the 95% prediction interval (represented as green ticks in the HRT-II printout). A disc is defined as 'borderline' if the RA value of any segment lies between the 95% and 99.9% prediction interval (represented as yellow exclamation marks in the HRT-II printout). Finally, a disc is defined as 'outside normal limits' if the RA value of any segment lies below the 99.9% prediction interval (represented as red crosses in the HRT-II printout). It should be noted that the values used are RP dependent; the MRA is only valid if the standard RP is used. When this technique was first described, a sensitivity of 84.3% and specificity of 96.3% was reported in discriminating normal subjects from early glaucoma cases (Wollstein et al., 1998). A subsequent study reported MRA sensitivity and specificity at 78% and 81%, respectively, when 'borderline' outcomes were regarded as test-positives (Ford et al., 2003). When 'borderline' outcomes were classified as test negatives, MRA sensitivity was 58% with a specificity of 96%. Sensitivity of 74% and specificity of 94% have been reported by another group (Miglior et al., 2003), suggesting a somewhat more favourable diagnostic accuracy. Despite this, it is vital that operators of the HRT, or for that matter any other optic nerve head imaging device, do not base diagnoses or management decisions solely on the outcome of a scan, but rather in concert with clinical examination and VF results. One particularly encouraging result pertaining to MRA, is that global, inferotemporal, inferonasal and superotemporal MRA were found to be predictive of glaucoma in OHTS (Zangwill et al., 2005b).

A potential criticism of the MRA is that the normative database was derived from white subjects. It may therefore not be applicable to other ethnic groups, in whom different optic disc morphometric characteristics may be present, such as larger discs in black subjects (Varma et al., 1994), although a recent study comparing black and white American subjects did not support this (Girkin et al., 2005). The normative database has been expanded in the HRT-III to include African and Indian ethnic groups. An additional classification system,

Glaucoma Probability Score (GPS), has been added to the HRT-III operating software. The GPS is based on a system described by Swindale (Swindale et al., 2000) which discriminates between normal and glaucomatous eyes using a mathematical model of the ONH shape. The model includes ten parameters which describe the morphology of the ONH; a least squares fitting-technique is used to approximate the model's morphological parameters to those of the nerve under examination. Discrimination between normal and glaucomatous discs is achieved by applying a linear discriminant function on seven of the aforementioned parameters. The method has an advantage in that it is operator independent, not requiring contour line placement and being independent of RP position. The GPS does not, however, confer any advantage over MRA or the Mikelberg linear discriminant function in terms of sensitivity and specificity (Swindale et al., 2000; Coops et al., 2006). A strong disc size-dependence has been found for both MRA and GPS, with high false-positives identified in large discs and poor sensitivity in small discs (Coops et al., 2006). Rather confusingly, the same graphical system of classification as MRA is used with red crosses denoting 'outside normal limits', yellow exclamation marks denoting 'borderline' and green ticks denoting 'within normal limits'.

A promising method of discriminating between glaucomatous and normal subjects is the use of machine-learning classifier systems. These systems 'learn' from the data available to them either in a supervised fashion, whereby the machine compares the HRT parameter input with predefined glaucoma characteristics such as VF, or in an unsupervised fashion whereby predefined characteristics are not used but classification is based on patterns identified in the inputted data. An advantage of these systems over linear discriminant functions is that they adapt to the distribution of the data. However they are also prone to 'over-fitting' of the data and need to be validated against independent data sets. Examples of machine learning classifiers applied to HRT parameters include the multi-layer perceptron with back-propagated learning (Uchida et al., 1996), 'boot-strap aggregating' classification trees (Mardin et al., 2003), and support vector machines (Bowd et al., 2002). The latter system allows for identification of which parameters are most useful in classification, thereby enabling an optimisation of technique; a significant improvement in discriminating ability has been demonstrated for this technique over non-optimised neural networks and linear discriminant functions (Bowd et al., 2002).

2.3.2.7 Monitoring progression

The first indication that the HRT could be used to identify glaucomatous changes was provided by Kamal et al., (1999). This study was the first to demonstrate that the HRT could identify structural changes prior to the identification of repeatable glaucomatous VF loss, thereby highlighting the great clinical potential of ONH imaging devices in the monitoring of glaucomatous progression. The investigators compared sequential HRT images acquired one year apart from two cohorts; a cohort of thirteen eyes of eleven normal control subjects and a cohort of thirteen eyes from thirteen OHT subjects who developed repeatable glaucomatous VF loss at a date subsequent to their second HRT image. The Wilcoxon signed rank statistical test was used to identify whether a significant change in the magnitude of stereometric parameters had occurred between the first and second image acquisitions. No significant global or segmental parameter changes were identified in the control cohort. In the OHT cohort, significant ($p < 0.05$) changes were identified in global RA, SN RA, ST RA, T rim volume and IT rim volume.

The same group later refined their progression technique by estimating 95% confidence limits for change in sequential HRT images acquired from normal control eyes, which was used as an estimate of normal measurement variability (Kamal et al., 2000). Subjects examined were 21 OHT subjects who had converted to early glaucoma on the basis of visual field criteria (24-2 program on the Humphrey perimeter), 164 OHT subjects with normal VFs, and 21 normal controls. The parameters demonstrating significant change between baseline and follow-up HRT imaging in the 'conversion group' were identified, as in the preceding paper, using the Wilcoxon signed rank test ($p < 0.05$). The 95% limits of normal variability were calculated from mean magnitude of difference in parameter values between baseline and follow-up images in the normal cohort; this was only performed for those parameters which demonstrated significant change in the converter group, namely cup area (global, SN, ST), cup volume (global, IT, IN, ST), RA (global, SN, ST) and rim volume (global, IT, IN, SN, ST). The 95% normal variability limits were used to define thresholds for glaucomatous change in each of these parameters, whereby any change exceeding the limits was ascribed to glaucomatous damage and within the limits as measurement noise. 'Glaucomatous change' was identified in 13 out of 21 converter eyes and in 47 of 164 OHT eyes with normal VFs, with global cup

volume, inferonasal cup volume, inferotemporal cup volume, and superotemporal cup area being the parameters which changed most frequently.

A potential shortcoming of the limits of change used in this latter study is that variability limits are derived from a population. Some individuals vary more than others, and these limits may be too wide for individuals with reproducible imgae series, and too narrow for those with greater inter-session variability. This problem was avoided by Tan and Hitchings (2003d) who derived limits for change for each ONH based on RA variability in each of the single topography images used to construct the mean topography image. Limits of variability were calculated for 30° disc sectors from the standard deviation of all possible permutations of paired intra-visit (between single topographies) RA differences. In the initial description of this technique, limits of variability were defined at $p < 0.05$, equivalent to a 95% confidence limit (Tan and Hitchings, 2003d). In a longitudinal HRT image series, when the RA value for a particular 30° sector exceeds the sector's variability limits for that series, this was defined as 'tentative progression'. 'Definite progression' required confirmation in at least two out of three consecutive tests, thereby accounting for spurious change or potential reversal on subsequent testing. This approach yielded a sensitivity of 85% and specificity (1 - false positive rate) of 95% when performed using HRT series acquired from 20 OHT subjects demonstrating glaucomatous VF conversion and 20 normal control subjects. The 95% statistical limit and two-of-three confirmatory criterion were subsequently shown to be optimal in terms of sensitivity and false positive rate, compared to alternative statistical limits (80%, 90%, 99%) and different confirmatory permutations (single test, two of two consecutive tests, three of three consecutive tests, two adjacent sectors in a single test, two adjacent sectors in two of three consecutive tests) yielding sensitivity of 83.3% and a false positive rate of 3.1% (Tan and Hitchings, 2004a). The technique was subsequently applied to 32 normal control eyes, 97 OHT, 30 OHT VF 'converters', 26 NTG suspect eyes, 5 NTG suspect VF 'converter' eyes and 26 established NTG eyes followed longitudinally (Tan et al., 2004b). Repeatable rim loss was identified in 6.2% of normal controls (effectively false positive rate), 11% of the OHT subjects, 90% of the OHT converters, 58% of suspected NTG subjects, 60% of NTG 'converters' and 54% of established NTG cases. It should be noted that the control image series was far shorter, giving less opportunity for spurious 'events' to occur, likewise the

confidence limits are wide: as such the rim loss in controls is likely to be an underestimate using this technique. Rim loss was most frequently observed at the inferior pole in all subsets. Rim loss was more frequently observed in the nasal compared to temporal sector in high tension subsets; this relationship was reversed in the normal tension subsets. It is important to note that the limits of variability-based technique, although elegant and robust, was designed using the old HRT MS-DOS software. At present it is not possible to access the individual single topography images in the HRT-II, which precludes the use of this technique with the newer equipment. The HRT-II and HRT-III acquire three single topographies in rapid succession (automated) unlike the HRT 'Classic' such that the intra-session variability may underestimate the inter-session variability, suggesting that the technique may be too sensitive and less specific if applied using the newer iterations of the device. Similarly, the technique uses an experimental RP (Tan and Hitchings, 2003c), which cannot yet be applied to images acquired using the HRT-II, although it may be applied to HRT acquisitions using the 'HRT Classic' option on Explorer. This technique has yet to be validated using alternative RPs.

The aforementioned techniques use changes in stereometric parameters to define glaucomatous progression. The RP dependent parameters, particularly RA, equate to clinically understandable optic disc morphometric characteristics. However critics argue that progression techniques using individual parameters do so at the cost of ignoring a significant proportion of the potentially useful topographical information generated by the HRT.

Topographical change analysis (TCA), which is the progression algorithm native to the Explorer software, examines changes in topographical height at the super-pixel level (Chauhan et al., 2000; 2003). Superpixels are discrete areas of the ONH image, measuring 4 x 4 pixels; there are 64 x 64 superpixels within a topography image. TCA identifies change within the disc margin contour and is dependent on the location of the reference ring (Chauhan, 2005). The key determinant in TCA is the variability in topographical height values within the superpixel over the two sets of three images (single topography images) taken at baseline and at follow-up. The statistical method estimates the probability of the difference in height value between images occurring by chance alone. Where $p < 0.05$, the probability is low and the change is therefore unlikely to be due to chance and is ascribed to glaucoma. Where the variability is high between images, which typically occurs at the edge of the cup

and along blood vessels, a much greater difference in height values needs to be identified to reach significance. TCA generates a 'change probability map' – the reflectivity map is overlaid with colour coded pixels, red pixels representing significant height depression and green pixels representing significant elevation. By default, superpixels will only be flagged as changing in this manner if the significant change occurs in three consecutive images, although it is possible to select two consecutive images only (Heidelberg Engineering, 2003). A major shortcoming of TCA in both clinical practice and research is that there is no clear-cut method of defining glaucomatous progression and until recently, quantifying glaucomatous change, as the recently introduced HRT-III software can now plot the areas and volumes of significant clusters over time. In two longitudinal studies, TCA progression was based on empirical data from normal subjects, whereby less than 5% of normal controls have greater than 20 significantly depressed superpixels within the optic disc margin (Chauhan et al., 2001; Nicolela et al., 2003). Progression was therefore identified where clusters of 20 or more significantly depressed superpixels within the disc margin were observed in three consecutive images. In a later study, the same group defined criteria for change by expressing the size of the largest cluster of depressed superpixels within the disc as a percentage of the total number of superpixels within the contour line, thereby accounting for variability in optic disc size (Artes and Chauhan, 2005). The Dalhousie group, responsible for the development of TCA, has recently described novel TCA progression criteria based on both cluster size and height change (Artes et al. *IOVS* 2006; ARVO-E Abstract 4349). In this study, which utilised the new alignment algorithm available on HRT-III, the greatest separation between glaucomatous and normal subjects was observed with red clusters of small size (between 1% and 2% of disc area) and moderate height changes (20 to 50 μm). The results of this study suggest that criteria incorporating both cluster size and height changes will enable improved detection of structural progression.

A newer pixel-based progression strategy, statistic image mapping (SIM), has recently been described by our group (Patterson et al., 2005). SIM is an established technique in the radiology milieu, being used for the analysis 3 dimensional images of the brain acquired using positron emission tomography and magnetic resonance imaging (Arndt et al., 1996; Holmes et al., 1996; Bullmore et al., 1999; Nichols and Holmes, 2002). SIM estimates topographic

change by linear regression of topographic height of each pixel within the disc over time. This generates a test statistic summarising the amount of change at each pixel. The sequence of images is then shuffled in time in a permuation analysis and the test statistic is recalculated for each pixel; this step is repeated a number of times, using a unique re-ordering sequence on each occasion. A distribution of test statistics is therefore generated for each pixel. Change is identified by comparing the observed test statistic to the test statistic distribution for that pixel. A pixel is flagged as progressing if it exceeds the 95^{th} percentile ($p < 0.05$). A global probability value for the entire image series is derived by comparing the largest cluster of active pixels in the observed image series to the distribution of largest clusters. When applied to simulated and real longitudinal HRT data, SIM performed favourably compared to TCA in detecting change (Patterson et al., 2005). A full comparison of detection of change using SIM and using stereometric parameters has yet to be published (Patterson, 2006; PhD Thesis, Nottingham Trent University).

All of the aforementioned progression strategies constitute 'event analyses', although strictly speaking, SIM is trend-based at the pixel-level and is converted to an 'event' when change has occurred. An event analysis defines change as occurring when a predetermined threshold or cut-off value is exceeded. Effectively, such techniques generate a binary outcome – either change ('progression') or no change ('stable'). This approach is particularly useful in clinical trials where disease classification is used as an end-point. A shortcoming, previously explained in the context of TCA, is that event analyses do not allow the quantification of rate of change. This may be achieved using a trend analysis technique whereby the relationship of the measurement over time is examined. Very little has been published in the literature regarding trend analyses applicable to longitudinal HRT data. The Explorer software is capable of performing a simple trend analysis of global and stereometric summary indices by comparing the values at any follow-up to those at the baseline. This is illustrated graphically as the normalised change from baseline over time. Normalisation is performed to enable the same scaling of change for each parameter from +1 (maximum improvement) to -1 (maximum deterioration). Normalisation is achieved by using the ratio of the difference between a given value and baseline to the difference between the average value in a normal eye and in an eye with advanced glaucoma (Chauhan, 2005). The trend

analysis is therefore interpreted in terms of empirical values; a formal regression analysis is not performed.

Artes and Chauhan (2005) have described a trend analysis in which a Spearman rank correlation is performed on longitudinal series of sectoral RA values. The statistical rationale for this approach is that the Spearman rank correlation identifies the likelihood that the slope generated from the sequence of observed sectoral RA values over time occurred by chance in a random sequence. The significance values for the four sectors were graded according to level of significance and were summated to give an overall 'evidence of change' score. In that particular study, the evidence of change score was used to allow an objective comparison between different tests – HRT, static automated perimetry (SAP) and high pass resolution perimetry. It is of interest that there is very little difference in the detection rate when sectoral RA progression identified using a Spearman rank correlation is compared with linear regression over time, with disagreement identified in only 1 subject from 198 ocular hypertensive and 21 control subjects (Strouthidis, 2004; Unpublished work). No particular technique, whether event- or trend-analysis based, has yet to been identified as optimal for detecting progression using the HRT; the thresholds and significance levels by which progression is defined are selected on a largely arbitrary basis.

2.3.3 Scanning laser polarimetry (GDx-VCC)

2.3.3.1 Principles, image acquisition and image processing

The GDx was initially developed by Laser Diagnostic Technologies (LDT, San Diego, California); subsequent iterations of the device have been released by Carl Zeiss Meditec (Dublin, California) following a commercial takeover of LDT. The name 'GDx' originally stood for 'glaucoma diagnosis' although the association with this name has been abandoned. This is perhaps a reflection of the potential overconfidence an 'unenlightened' operator may have in the device's abilities as a result of such a name. It is clear from experience with the HRT that imaging devices should not be used in isolation to make diagnostic decisions; naming such a device on an unproved ability to diagnose glaucoma was somewhat inappropriate.

The GDx differs from the HRT in that it is optimised for quantitative measurement of the RNFL. The device works on the principle of scanning laser polarimetry, exploiting the

birefringent properties of the RNFL to measure its thickness. Birefringence is the property of a material that 'decomposes' a light ray as it passes through the structure into two rays (an 'ordinary' and an 'extraordinary' ray), depending on the plane of polarisation of the light. One of the rays travels more quickly throught the material than the other (one is 'retarded'). The closely spaced microtubules in the RNFL give it birefringent properties (Huang and Knighton, 2002; Huang and Knighton, 2005). The parallel arrangement of the microtubules within the retinal ganglion cell axons causes a quantifiable change in the polarisation of light that passes through them. The change is the 'retardation' of the extraordinary ray with respect to the ordinary ray when light is reflected from the retina and is proportional to the birefringence of the RNFL and to the thickness of the RNFL (Weinreb et al., 1990; Weinreb et al., 1995b). The principle of scanning laser polarimetry is summarised in Figure 2-4.

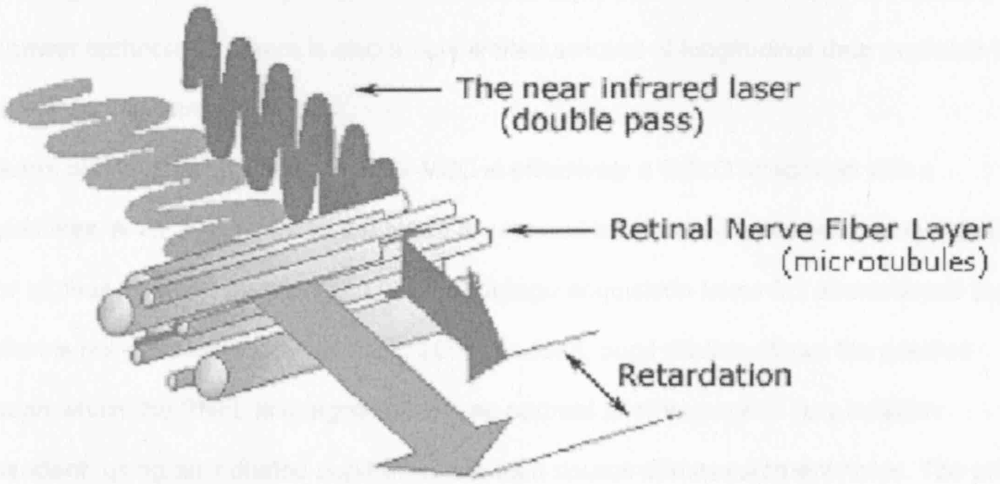

Figure 2-4. Scanning laser polarimetry. As polarised light (near infrared laser) passes through the parallel organisation of microtubules in the nerve fibre layer, retardation of light occurs. Retardation is proportional to the birefringence and to the nerve fibre layer thickness

The RNFL is not the only birefringent structure in the eye; the cornea and, to a much lesser degree the vitreous and lens all have birefringent properties. This additional birefringence, particularly from the cornea, is a confounding factor in the assessment of nerve fibre layer thickness. Initially the GDx used a fixed corneal compensator to account for this, which was based on the assumption that most eyes have a slow axis of corneal birefringence of 15 degrees in the nasal and downward direction with a magnitude of 60 nm. Studies have, however, shown that there is a wide variation in the polarisation properties of the cornea in different subjects (Greenfield et al., 2000; Knighton and Huang, 2002). A variable corneal compensator (VCC) has therefore been developed to allow customisable compensation based on individual corneal properties. The VCC uses the radial birefringence of Henlé's fibre layer in the macula to act as a control for the measurement of corneal birefringence (Choplin et al., 2003). Although the GDx has been available for a number of years with a fixed corneal compensator, the introduction of the VCC is a relatively recent development. As such, many of the original reproducibility studies and discriminatory studies have had to be repeated using the newer technology. There is also a very limited amount of longitudinal data available for analysis, for the same reasons.

In terms of image acquisition, the GDx-VCC is effectively a CSLO integrated with a polarimeter. A 15° x 15° area of the retina is scanned in a raster-like fashion using a diode laser at near infra red wavelength (780 nm). Image acquisition takes 0.7 seconds and pupil dilation is not necessary (Horani et al., 2006). Indeed, pupil dilation allows the position through which the RNFL is imaged to vary; as corneal birefringence is very location dependent, using an indilated pupil limits this as a source of measurement noise. The printout of the GDx-VCC includes three different images requiring interpretation, the 'reflectance map', the 'retardation map' and the 'deviation map' (Choplin et al., 2005). The reflectance map is a fundus image constructed by the scanning laser; it is used primarily for orientation and assessment of image quality. The retardation map colour codes the thickness of the nerve fibre layer such that bright, 'warm' colours represent thicker readings and dark, 'cool' colours represent thinner readings. The deviation map divides the image into superpixels (as for HRT TCA) and compares the retardation values of each superpixel with an age- and ethnicity-

matched database. A 5th percentile cut-off is used to identify the superpixels which are thinner compared to normal values.

2.3.3.2 Reproducibility

High inter-operator reproducibility has been reported for the GDx, prior to the introduction of the VCC (Hollo et al., 1997; Zangwill et al., 1997a; Hoh et al., 1998). Reproducibility data for the GDx-VCC are, on the other hand, sparse; it is however assumed that the newer version will have improved reproducibility. One study reports mean intra-observer coefficient of variation values for retardation index ranging from 2.2% to 13.1% for the GDx-VCC in 60 normal and OHT subjects (Lleo-Perez et al., 2004). A group from Israel has demonstrated that the GDx-VCC has, unsurprisingly, a high inter-device reproducibility by testing 13 separate device units (Blumenthal and Frenkel, 2005). The same group examined inter-observer reproducibility and learning effect by using three operators, naïve to the use of the GDx-VCC, to image one eye each of 15 normal subjects and 15 glaucoma subjects over the period of an hour (Frenkel et al., 2005). A high inter-observer reproducibility and no learning effect were reported.

Intraclass correlation coefficients of 0.79 to 0.91 in healthy subjects and of 0.92 to 0.97 in glaucoma subjects (TSNIT average and standard deviation, superior and inferior average, Nerve Fiber Indicator values) have been reported recently for intra-observer testing using the GDx-VCC at a testing interval of one week (Iacono et al., 2006).

Corneal refractive surgery can affect corneal retardation. LASIK-induced corneal healing can cause a significant change in corneal polarising properties leading to apparent thinning of the nerve fibre layer when measured using scanning laser polarimetry with a fixed corneal compensator, although most measurements return to pre-operative values after three months post-operatively (Hollo et al., 2002; Hollo et al., 2003; Katsanos et al., 2004). It seems likely that the GDx measurements are largely unaffected by LASIK when using the VCC (Hollo et al., 2003; Halkiadakis et al., 2005; Zangwill et al., 2005a), although one group has suggested that customised corneal compensation after LASIK does not normalise TSNIT (temporal-superior-nasal-inferior-temporal plot) and NFI (nerve fibre index) measurements (Centofanti et al., 2005); in this study the corneal compensation was re-set following LASIK.

The use of the patient's own macula as an 'intraocular polarimeter' to neutralise the effect of corneal birefringence is not without problems. Eyes with macular degeneration, central serous retinopathy and cystoid macula oedema have indeterminate macula bow-tie patterns when using scanning laser polarimetry (Bagga et al., 2003). A similar effect may be expected in eyes with subfoveal choroidal neovascular membranes (Katsanos et al., 2005). The 'screen' method for corneal compensation, which measures an average birefringence over a wide area of the fundus, has been recommended for use in subjects with co-existent macular pathologies (Bagga et al., 2003).

2.3.3.3 Diagnostic potential

The GDx-VCC generates a variety of numerical parameters which are intended to facilitate the discrimination of glaucomatous eyes from normal eyes, by providing probability measures of abnormality based on comparison with a normative database derived from data collected from 540 normal eyes (Medeiros et al., 2004). These values are TSNIT (temporal-superior-nasal-inferior-temporal) average, superior average, inferior average, and TSNIT standard deviation. An additional numerical indicator, the NFI is provided. This value is calculated using a support vector machine algorithm based on several retardation measures throughout the whole image. A number from 0 to 100 is allocated to each eye, with the higher the value equating to greater likelihood that the patient has glaucoma; the manufacturers recommend 0 to 30 for within normal limits, 31 to 50 for borderline, and 51 to 100 for outside normal limits (Medeiros et al., 2004). Of the numerical parameters, the nerve fibre index has been shown to consistently generate the largest area under receiver operating characteristic curve (AUROC) values, varying between 0.87 (Da Pozzo et al., 2006) and 0.98 (Reus and Lemij, 2004a). This suggests that the NFI is the best discriminatory parameter currently provided by the GDx-VCC.

An alternative approach to discriminating glaucomatous from normal eyes is to try to quantify the shape of the 'double hump' of the TSNIT pattern of nerve fibre layer thickness. This has been addressed by Essock and colleagues (Essock et al., 2005), who have developed a discriminant function which combines a Wavelet analysis followed by a Fourier analysis. The Wavelet-Fourier analysis (WFA) outperformed the NFI in one study, with an AUROC of 0.98

for WFA compared to 0.90 for the NFI. The discriminatory power of the 'shape-based' analysis was most impressive at the earliest stages of glaucomatous damage.

As with the HRT, the use of machine learning classifiers has been advocated to assist the diagnostic potential of the GDx-VCC. Both relevance vector machine and support vector machine learning classifiers have been shown to have greater discriminatory power than individual GDx-VCC parameters, when trained on nerve fibre layer measurements acquired by the GDx-VCC (Bowd et al., 2005).

2.3.3.4 Monitoring progression

The GDx-VCC has been shown to be repeatable, and performs well in terms of discriminating between glaucomatous and normal eyes. Unfortunately its performance as a tool for monitoring glaucomatous progression has yet to be ascertained. This is purely a reflection of the dearth of longitudinal data currently available for the device. Some centres have collected longitudinal data using the older, fixed corneal compensator device. However, any progression algorithms developed using this data would be redundant using the GDx-VCC, so complete has the overhaul been in terms of image analysis software, as well as the normative database. RNFL progression analysis software is evolving for the GDx-VCC, but as yet the GDx (albeit without variable corneal compensation) has not been found to be useful for the detection of progression (Boehm et al., 2003).

2.3.4 Optical Coherence Tomography (OCT)

2.3.4.1 Principles, image acquisition and processing

The technique of optical coherence tomography (OCT) was first described by a group at the Massachusetts Institute of Technology, when it was used to image the peripapillary retina and the coronary artery *in vitro* (Huang et al., 1991). OCT is frequently described as the optical equivalent of B-scan ultrasonography, with reflected light replacing sound waves. The light source in the OCT is a near-infra red (wavelength 850 nm) low-coherence super-luminescent diode. The incident beam of light is split into two arms, one which reaches the target tissue, and the other a reference mirror that translates back and forth (Shuman et al., 2004). The two beams of light recombine using the principle of interferometry, whereby their pulses need to arrive at nearly the same time. A constructive interference signal is generated when the path

lengths of the reference and measurement beams are closely matched to within the coherence length of the light. By panning the light source across the target tissue, a series of scans is obtained which is used to generate a two dimensional colour-coded map based on the detection of the previously described interference signals. The device may be used to scan the macula, the peripapillary retina and the ONH. Both the macula and ONH scans are comprised of six linear scans arranged in a spoke-like fashion with a 30° separation. The device identifies the ONH margin as the end of the retinal pigment epithelium layer, thereby eliminating the necessity for an operator to manually input a contour line, although there is a facility to 'correct' the automated placement. The peripapillary scan is a circular scan with an optimal diameter of 3.4 mm centred at the ONH (Schuman et al., 1996). Although the manufacturers recommend pupil dilation for optimal image acquisition, it is possible to generate reproducible nerve fibre layer measurements without pupil dilation (Zafar et al., 2004).

In the current commercially available OCT model, the OCT 3 or Stratus ($STRATUS_{OCT}$, Carl Zeiss Meditec Inc, Dublin, California) there is an axial resolution of 8 to 10μm. The operator may vary sampling density as 512, 256, or 128 vertical A-scans. Irrespective of scan length, A-scans are acquired at a rate of 400 per second.

2.3.4.2 Reproducibility

Limited data are available for the $STRATUS_{OCT}$, due to its relatively recent introduction. Budenz et al., (2005) have investigated short-term intra-observer nerve fibre layer thickness variability in 88 normal and 59 glaucomatous eyes, stratified according to severity of perimetric damage. Excellent intraclass correlation coefficients were reported for mean RNFL thickness, using the 'standard' acquisition protocol – 0.97 for normal eyes and 0.98 for glaucomatous eyes. Reproducibility data for disc segments are considerably poorer because of the difficulty in scanning in exactly the same location; migration of the scan circle position will not have a great effect on mean values but may considerably affect segmental values. A very minimal reduction in intraclass correlation acquisition was observed when acquisitions were performed using the 'fast' protocol. The nasal quadrant was identified as the most variable sector of the peripapillary nerve fibre layer. The use of high density scans is associated with improved reproducibility of RNFL measurements (Paunescu et al., 2004).

Although good reproducibility has been reported for previous generations of the OCT (Blumenthal et al., 2000), comparisons between RNFL measurements made with older OCT devices and the current model should be interpreted with caution, if at all, even with the use of correction factors (Bourne et al., 2005).

2.3.4.3 Diagnostic potential

A number of recently published studies have investigated the ability of the $STRATUS_{OCT}$ to discriminate between glaucomatous and normal eyes. In a comparison between the abilities of the $STRATUS_{OCT}$, the HRT-II and the GDx-VCC, to discriminate between healthy eyes and eyes with glaucomatous visual field loss, the best AUROC curve value (0.92) was found for $STRATUS_{OCT}$ inferior nerve fibre layer thickness (Medeiros et al., 2004), although the difference between devices was not statistically significant. The same result, albeit with a marginally higher AUROC (0.94) was reported in a similar study performed at the Moorfields Glaucoma Research Unit (Schlottmann et al *IOVS* 2006; ARVO E-abstract 3627). In general, peripapillary nerve fibre thickness measurements have been found to be more useful than ONH parameters or macular thickness in the discrimination between healthy and glaucomatous eyes (Leung et al., 2005; Wollstein et al., 2005a; Medeiros et al., 2005b).

2.3.4.4 Monitoring progression

To date there has been only one published report of the OCT being used to monitor glaucomatous progression (Wollstein et al., 2005b). In this study, OCT progression was defined as a reproducible thinning of the mean RNFL thickness of at least 20μm, a value chosen on the basis of known reproducibility error of the OCT. It should be noted that this study utilised older OCT technology, which is known to have poorer test-retest variability than the newer $STRATUS_{OCT}$.

As with the GDx-VCC, the lack of available longitudinal data for the OCT prevents any meaningful discussion relating to its ability to monitor progression. In many respects, great potential in terms of the monitoring of progression may be expected given the excellent reproducibility and discriminatory power of the $STRATUS_{OCT}$. However, it is the HRT, with its older and more slowly evolving technology, as well as backward-compatible software, which has the longevity necessary for researchers to be able to examine long series of ONH images over time. Progression algorithms will be developed and tested, as the newer technologies

become more established. OCT is poised to become the pre-eminent ocular imaging technology; not least because of its versatility in imaging multiple anatomical sites – the macula, the optic nerve, the peripapillary nerve fibre layer and anterior segment structures (albeit using a different device). The commercial success of the $STRATUS_{OCT}$ has occurred concurrently with the development of newer treatments for macular pathologies, such as photodynamic therapy and anti-VEGF agents for exudative macular degeneration as well as intravitreal steroids for uveitic macular oedema. Further improvements in the technology of the OCT may be expected in the next few years, including ultra-high resolution OCT (Drexler et al., 2001) which can offer axial resolution of 2-3 μm, compared with the current 10 μm, giving an unprecedented level of intraretinal visualisation. En-face OCT is a developing technique which has similarities with scanning laser tomography, as it constructs an image of the ONH by using the OCT to create stacks of transverse ONH images which are aligned to form a three-dimensional image (Guo et al., 2005). The en-face OCT is capable of providing ten times the depth resolution of the CSLO; however, at present, acquisition time is too long to make the technology clinically applicable. Perhaps the most exciting development in OCT technology is spectral domain OCT (Nassif et al., 2004). This technique allows much faster image acquisition time – the Heidelberg Spectral OCT, which includes image stabilisation during acquisition, performs 40,000 A-scans per second. Such high speed imaging can allow the measurement of true optic nerve topography and optic disc cupping as well as visualise changes in small retinal blood vessels, although movement artefact from axial motion is still a feature. Its future impact on the management of glaucoma subjects and patients with macular pathologies may be inestimable.

2.4 Measuring functional change in glaucoma

2.4.1 Basic Principles

From the perspective of a patient with glaucoma, the most important aspect of their diagnosis is the impact it will have on their visual function. Progressive VF loss may deteriorate to the extent that it may impinge upon the patient's ability to carry out day to day activities, and in particular driving. It is therefore imperative that an effective measure of visual function is available in the clinic to allow an assessment of visual deficit at the time of presentation and to enable longitudinal assessment of VF change over time.

The best-established technique for assessing visual function in glaucoma subjects is by perimetry; a method of examining the VF. The VF was defined by Tate and Lynn (1977) as 'all the space one eye can see at any given instant'. The normal extent of the VF for a bright stimulus is 60° superiorly, 75° inferiorly, 100° temporally and 60° nasally (Henson, 1998). The oldest perimeters assessed the VF using a 'kinetic technique'; this exploits the principal that the centre of the VF is more sensitive than the periphery. Stimuli of insufficient intensity to be visible at the periphery are brought towards the centre of the field until they are seen. The process is repeated using stimuli of differing size and intensity; isopters may be drawn around the points where the same stimulus becomes first visible around the field. The process may be conducted within a bowl (such as the Goldmann bowl perimeter) or using a screen (such as the Bjerrum tangent screen). Using a bowl allows stimuli to be presented at further eccentricities (up to 90°) whereas tangent screens allow a greater magnification of the central field, allowing a more accurate plotting of central defects. The advantage of kinetic perimetry is that the perimetrist has full control of the examination technique, modifying it according to the specific problems presented by the patient. It is time consuming, precluding its use as a screening test and it is less sensitive when it comes to the detection of scotomata (Coffey et al., 1993).

An alternative approach, and one which has become pre-eminent in the routine examination of glaucomatous and ocular hypertensive subjects, is SAP. This technique differs from kinetic perimetry in that the stimuli do not move, appearing in fixed locations within the perimeter, with the intensity of the stimulus varying. SAP has become the technique of choice at it is largely operator independent and relatively quick. As the technique is computer controlled, the

numerical output generated by SAP may be stored and analysed, thereby facilitating longitudinal assessment.

A number of newer perimetric testing strategies have recently become available for the assessment of glaucomatous subjects, namely short wavelength automated perimetry (SWAP), frequency doubling technology and high pass resolution perimetry. Although these techniques may have advantages, particularly in terms of earlier detection of functional loss, SAP's smaller test-retest variability and larger dynamic range (Gardiner et al., 2006) make it the current technique of choice for monitoring of glaucomatous VF progression. Of the available automated perimeters available, the Humphrey Field Analyser (HFA-II, Carl Zeiss Meditec, Dublin, Ca) is the prevalent device in current UK practice. The previous incarnation of the device, the HFA, was used in 56.3% of patients involved in the Royal College of Ophthalmologists Trabeculectomy audit (Edmunds et al., 1999); this percentage is likely to be much higher now as the subjects in that audit were recruited prior to 1996.

2.4.2 HFA – Principles of threshold examination

The HFA and HFA-II are projection bowl static automated perimeters. The patient faces a white hemispherical bowl of 330 mm radius. The background luminance of the bowl is 31.5 asb, generated by two separate diffuse light sources. Stimulus size can be varied according to the five sizes available using the Goldmann perimeter (I to V), with stimuli being presented for 0.2 seconds. The stimulus intensity may be varied from 0.08 to 10,000 asb (51 dB) using neutral density filters. In examining glaucomatous subjects, three central threshold strategies of stimulus presentation may be selected, covering the central 10°, 24° and 30°. The test-points are arranged in a grid pattern with a horizontal and vertical spacing of 6° between adjacent test-points. The 24 and 30 test patterns may be off-set by 3° horizontally and vertically (24-2 and 30-2 strategies, as opposed to 24-1 and 30-1 without the off-set). Although screening strategies ('suprathreshold') are available using the HFA, full threshold strategies are more useful in the longitudinal assessment of visual function in glaucoma subjects and are therefore described in detail here.

Using the HFA (and HFA II) the maximal intensity (which is inversely proportional to retinal sensitivity) is ascribed the value of 0 dB. The relationship between log units and decibel units

is 1 to 10. Table 2-1 illustrates the relationship between decibels, logarithmic scale and stimulus intensity. In general most humans cannot respond to stimuli below 40 dB (0.1/1000 = 1/10000 of the maximal stimulus intensity), which means that the dynamic range of the HFA is equivalent to 0-40 dB.

Decibel Scale (dB)	Log Unit scale	Intensity Luminance Units (asb)
0	0	1000.0
10	1	100.0
20	2	10.0
30	3	1.0
40	4	0.1

Table 2-1. Relationship between decibel and logarithmic attenuation scales and intensity scale

Thresholding ascertains the retinal sensitivity by calculating the stimulus intensity seen 50 % of the time at each test-point location. The technique adopted by the HFA is the repetitive bracketing strategy which optimises both time and accuracy (Spahr, 1975; Bebie et al., 1976a). In this technique, a 'double reversal' strategy is used. A stimulus is presented which is expected to be close to threshold; successive stimuli are presented at decreasing sensitivity until they are not seen. Stimuli are then re-presented at increasing intensity until seen again. If the initial stimulus is not seen, the process is reversed – ie stimuli increase in intensity until seen and then decrease in intensity until not seen. In the Humphrey, initial changes in stimulus intensity are in 4 dB increments until the threshold is crossed, after which reversal stimuli change in 2 dB increments. At the beginning of the test, the Humphrey thresholds one test-point in each quadrant and uses these values as the basis for the surrounding secondary points. Other than a plot of raw threshold sensitivity data, the

Humphrey outputs two further numerical plots. The total deviation map is derived from the difference between the observed threshold value for each test-point and the age-corrected normal value. Pattern deviation is defined as the deviation from the age-corrected sensitivity values adjusted for the 'general height' of the visual field, taken (arbitrarily) as the relative depression of the 15th percentile of the total deviation values (Artes et al., 2005). The latter plot is considered to be useful in discriminating focal glaucomatous field loss from the diffuse loss which may be caused by media opacity such as cataract (Heijl et al., 1989b), although recent work has suggested that pattern deviation may underestimate diffuse field loss in glaucoma (Artes and Chauhan, 2005).

Recently, a new thresholding algorithm has been developed – Swedish Interactive Thresholding Algorithm (SITA) – which is the default option on the HFA-II. The technique has enabled large reductions in examination time compared to full thresholding, by up to 50% when examining the central 30° in normal subjects (Bengtsson et al., 1998). The reductions in test time are achieved by adapting the time between stimuli presentations according to the patient's response speed, by estimating false-positive response rates without using catch trials and by reducing the number of stimulus presentations using Bayesian principles to estimate threshold values (Bengtsson et al., 1997b). SITA is associated with lower test-retest variability than the full threshold technique and as such may be a more appropriate method for the long term assessment of glaucoma patients (Artes et al., 2002). It should be noted that the use of SITA is associated with a 1.9 dB higher sensitivity in normal individuals and up to 2.4 dB in glaucoma subjects. This presents a particular problem when analysing longitudinal series of Humphrey visual field tests in which both full threshold and SITA tests are included. The developers of SITA have suggested that total deviation and pattern deviation maps may be more appropriate measures than 'raw' sensitivity values when comparing between full threshold and SITA tests (Heijl et al., 2000). However, the same authors have suggested that it is probably best to establish a new baseline when switching between algorithms and therefore not to mix full threshold and SITA tests in the same series (Heijl et al., 2000).

2.4.3 Measurement variability

In order to be best able to quantify VF change in glaucoma subjects, an appreciation of measurement variability and an understanding of sources of variability are essential (Hutchings et al., 2000). Measurement variability may be considered a confounding effect when monitoring VF progression, as changes in threshold sensitivity must be of sufficient magnitude to exceed variability. A well-established observation is that measurement variability increases in areas of established reduced sensitivity, where glaucomatous visual field loss already exists (Heijl et al., 1989a; Chauhan and Johnson, 1999; Henson et al., 2000). Some authors have suggested that this increase in test-retest variability over time may, in itself, be considered as evidence of progressive glaucoma (Flammer et al., 1985). Test-retest variability has been shown to increase, and differential light sensitivity (DLS) to decrease, with increasing retinal eccentricity (Heijl et al., 1989a), and with variability being higher nasally than temporally and higher superiorly than inferiorly (Flammer et al., 1984a; Heijl et al., 1987). Measured DLS decreases with age; the slope of sensitivity reduction with age increases with eccentricity such that the 'hill of vision' is steeper with greater age (Katz and Sommer, 1986; Heijl et al., 1987).

Two different methods of quantifying variability are available on the Humphrey perimeter full threshold program – short-term fluctuation and long-term fluctuation. These are not measures of test-retest variability, but rather of intra-test and inter-test variability within a given individual. Short-term fluctuation is effectively a gauge of intra-test variability and is derived from the average standard deviation of the differences between two threshold estimates in ten predetermined test-point locations (Flammer et al., 1984c; Flammer et al., 1985). It is important to note that ten double determinations is a small number and may not sample areas of established glaucomatous deficit, resulting in a less reproducible estimate than would be obtained if more locations were utilised (Casson et al., 1990). Long-term fluctuation is the clinical equivalent of inter-test variability and equates to physiological fluctuation in retinal sensitivity; it is the long-term variability not explained by short-term fluctuation (Bebie et al., 1976b; Flammer et al., 1984b). As with short-term fluctuation, long-term fluctuation is influenced by severity of disease. These two measures are distinct from test-retest variability, which is a quantification of the scatter of measures made on two or more examinations at

different test sessions. It may be considered as a compound measure of within- and between-test variability (Spry and Johnson, 2002).

2.4.4 Visual field changes in glaucoma

Hart and Becker (1982) have retrospectively characterised the focal visual field defects occurring in 98 eyes of 72 subjects, examined four monthly by Goldmann kinetic perimetry, with visual field defects being confirmed by static perimetry. The first types of field defect presenting, in descending order of frequency were:

1) Nasal steps in 54% of subjects (33% superior, 21% inferior)
2) Paracentral scotomata (within 10° of fixation) and Bjerrum scotomata (between 10° and 20° of fixation) in 41% of subjects
3) Arcuate enlargement of the blind spot (polar extension of 5° or more) in 30% of subjects
4) Other defects corresponding to nerve fibre bundle distribution, including Bjerrum scotomata isolated from the blind spot (20%) and temporal defects (3%).

Within a single hemifield, the pattern of progression is likely to correspond to increasing nerve fibre damage. Small paracentrally-located areas of sensitivity loss may extend, deepen and become arcuate in appearance, with nasal defects extending temporally in the same fashion. The defects may progress to join the blind spot, widening to affect both central and peripheral vision. End-stage loss equates to islands of only temporal and central vision, which may also eventually disappear. Mikelberg and Drance (1984b) have demonstrated that, in 42 glaucomatous eyes followed-up for a mean period of 8.2 years, visual defects become deeper in 79% of eyes, larger in 52% of eyes, with new defects occurring in 50% of eyes. The finding that glaucoma progresses by deepening and expansion of established scotomata has recently been confirmed by glaucoma change probability using total deviation and pattern deviation plots (Boden et al., 2004). Based on this observation, newer perimetric strategies such as fundus orientated perimetry and scotoma orientated perimetry have been developed to increase spatial resolution in areas of established glaucomatous damage (Schiefer et al., 2003)(Paetzold et al. *IOVS* 2005; 46: ARVO E-Abstract 636). It should be noted that VF loss

in glaucoma is unlikely to be exclusively focal. Several authors have suggested that focal VF loss in glaucoma is usually accompanied by a diffuse component (Drance, 1991; Henson et al., 1999). Others have observed a minority of patients in whom glaucoma may present with exclusively diffuse VF loss (Chauhan et al., 1997). There are, however, considerable difficulties involved in the detection of diffuse loss, given that it is non-specific change also occurring with lens opacity and miosis.

Mikelberg et al., (1986) studied the pattern of VF loss over time and identified four distinct patterns: linear (49%), curvilinear (20%), episodic (7%) and non-progressing (24%). The observation that much of the VF loss is characterised by linear decay has been confirmed by other authors (McNaught et al., 1995; Rasker et al., 2000). McNaught et al., (1995) modelled series of VFs of 12 initially normal fellow eyes of subjects with untreated NTG in the other eye. From a potential 221 different models, complex polynomial models were the best fit (median $r^2 = 0.95$) for visual field sensitivity over time in 47 test point locations of 5 eyes demonstrating VF deterioration. It is possible that such a model reflected the measurement variability (model over-fitting) as opposed to the underlying trend of sensitivity over time. Best fit models were then applied to the first five fields and projected to the last field in the series (all eyes had a minimum of fifteen available field tests). In this circumstance, a simpler linear model was found to be best able to predict the sensitivity at the end of the study period. The assumption that VF progression is best characterised by linear decay (which may also be the best fit for episodic loss with infrequent testing) is the rationale for the adoption of linear regression techniques for monitoring glaucomatous VF progression.

2.4.5 Monitoring visual field progression

2.4.5.1 Observer judgement

Field series may be examined by the observer using experience and intuition to make a clinical judgement as to whether a series is progressing. This technique remains perhaps the approach adopted most frequently in UK clinical practice. It has a number of advantages in that it does not require additional computation, is flexible and simple to perform. However, it is not objective, poorly reproducible and time consuming, requiring all VF printouts to be arranged manually in the correct sequence. In one study which compared clinical assessment

of VF change by six expert observers, some observers identified twice as many series as progressing as others and there were extreme disagreements, such as a progressing series being declared as an improving series by a different observer (Werner et al., 1988). Such gross inter-observer differences may be explained by different observers using different criteria for change and observers changing criteria over time according to recent experience. It is unrealistic to expect an observer to be able to collate and interpret the vast array of numerical outputs generated by SAP. Computer-assisted progression algorithms may represent a solution to the problems encountered with the manual approach.

2.4.5.2 Event analyses

As with HRT progression techniques, VF progression strategies may be broadly categorised as either 'event analyses' or 'trend analyses'.

AGIS (1994) developed a defect scoring system to grade the severity of visual field loss, which may be used to define whether or not a field is glaucomatous, and in a series, whether glaucomatous progression has occurred. The field defect score is calculated using total deviation values for each test point in the HFA 24-2 program. The VF is divided into three regions; nasal (which crosses the midline), upper hemifield and lower hemifield (both of which respect the midline). The minimum amount of depression (dB) required to label a point as defective is loosely based on the distribution of total deviation values found within a normal population – the deficit required to fall within the lowest 5% of normal subjects. The deficit required varies according to location, being larger with increasing eccentricity and larger superiorly than inferiorly. Defects in a single hemifield are only considered if three or more adjacent points are depressed. A nasal step equates to a single depressed point in the nasal region, whereas a cluster of three or more points in the nasal region is considered a nasal defect. Scoring is allocated as follows:

1) Nasal step = +1
2) 4 or more depressed nasal points = +1
3) 3 to 5 test points in a hemifield cluster = +1
4) 6 to 12 test points in a hemifield cluster = +2
5) 13 to 20 test points in a hemifield cluster = +3
6) 20 or more test points in a hemifield cluster = +4

7) Half of adjacent points in a hemifield cluster depressed by 12 or more dB = +1

8) Half of adjacent points in a hemifield cluster depressed by 16 or more dB = +2

9) Half of adjacent points in a hemifield cluster depressed by 20 or more dB = +3

10) Half of adjacent points in a hemifield cluster depressed by 24 or more dB = +4

11) Half of adjacent points in a hemifield cluster depressed by 28 or more dB = +5

12) 2 adjacent points depressed by 12 dB or more, in absence of 3 point cluster = +1

13) Points above summed to give AGIS visual field score

A score change of four or more on two or more consecutive tests from a single baseline test is generally considered as signifying progression (Katz, 1999a; Katz et al., 1999b).

A defect classification system, based on total deviation values from the HFA 24-2 program, was also adopted by the Collaborative Initial Glaucoma Intervention Treatment Study (CIGTS) (Musch et al., 1999). The system differs from AGIS in that it is based on probability as opposed to defect depth. Locations are deemed to be depressed if the probability value of the measured threshold is less than 5% (falling within the lowest 5% of the normal distribution on total deviation probability). Scores are given for clusters of three or more contiguous depressed points, based on their probability values such that the score increases with decreasing probability (probability values of 5 %, 2 %, 1 % and 0.5 % are equivalent to scores of 1, 2, 3 and 4, respectively). Given the reliance on probability values, it is more appropriate to use the CIGTS scoring system with early defects, as opposed to the AGIS system which was designed for use with advanced defects. In general, an increase in CIGTS score of 3 or more from baseline (taken as the mean of two baseline tests) and confirmed in two further consecutive tests may be used to define glaucomatous progression.

The CNTG study initially defined progression as a decline of 10 dB or greater, or three times the average baseline short-term fluctuation, in two adjacent points within or next to an established defect. The sensitivity of the depressed points needed to be outside the range of values for those points in the three baseline examinations. Confirmation was sought on two further tests performed within a month of the first suspect test. A high false positive progression rate was identified using this strategy, so the investigators modified the technique to minimise false positives by also requiring progression in the same points to be demonstrated in at least two of three tests three months later (Schulzer, 1994).

In OHTS, VF examinations were performed at six monthly intervals. The Glaucoma Hemifield Test (which classifies fields as 'within normal limits', 'borderline', 'outside normal limits', 'abnormally high sensitivity', 'generalised reduction in sensitivity' and 'borderline/generalised reduction in sensitivity') and the Corrected Pattern Standard Deviation (CPSD – interpreted as the PSD corrected for the general height measure) were the indexes monitored to detect the development of possible glaucomatous visual field loss (Keltner et al., 2000). Prior to 1997, if a technically acceptable follow-up VF was abnormal on the Glaucoma Hemifield Test ('outside normal limits' or 'general reduction of sensitivity'), the CPSD ($p < 0.05$), or both, a re-test was performed on the eye in question within the same six month follow-up visit interval. The defect was confirmed if the same index was involved in both test and re-test and if the abnormality was in the same general location in both tests. As a high proportion of re-tests were found to return to normal during follow-up, a more stringent criterion, requiring confirmation in two consecutive tests was adopted from 1998 onwards.

In the EMGT, progression was suspected if three or more not necessarily contiguous locations are depressed from baseline ($p < 0.05$) using pattern deviation probability maps (Bengtsson et al., 1997a). Definite VF progression occurred when the significant depression in three or more locations is detected in three consecutive tests using pattern deviation probability maps (Heijl et al., 2003). This technique, renamed Glaucoma Probability Analysis (GPA) is the progression algorithm most recently available in Statpac, the software package native to the HFA-II. The previous technique, Glaucoma Change Probability (GCP) was similar, except that it used total deviation probability maps.

2.4.5.3 Trend analyses

In a trend analysis, the test parameter of interest is evaluated sequentially in order to determine temporal behaviour. The technique has a number of potential advantages compared to event analyses. Trend analyses employ all available VF tests (unlike event analyses, which usually compare baseline to follow-up) and are therefore theoretically more adept at discriminating subtle visual changes from wide degrees of variability (Fitzke et al., 1996). By plotting the perimetric parameter over time, and fitting the line of best fit, it is possible to estimate the rate of change over time. Knowledge of rate of change is of particular value in the management of glaucomatous patients, in terms of monitoring effect of treatment,

and in OHT subjects, any significant negative change may represent development of glaucoma. As previously discussed, linear regression may be best able to predict the behaviour of visual field parameters over time and therefore constitutes the most appropriate trend model (McNaught et al., 1995).

Linear regression analysis is available commercially in the Statpac 2 program (Heijl et al., 1990). The so-called 'change analysis' technique plots a linear regression of summary parameters, such as mean deviation (MD) and PSD, over time. MD is a weighted average deviation of points in the observed field from the normal reference field. MD declines with progressing glaucomatous loss; however, it is non-specific, also declining with progressive lens opacity. As MD is an estimate of the uniform component of deviation for the entire field (ie a global index) it may be unable to detect subtle, localised VF change. Reports have indicated that MD has poor sensitivity in the detection of progressive VF change (Chauhan et al., 1990), as indeed has the equivalent global index on the Octopus perimeter (Interzeag, Schlieren-Zurich, Switzerland) (O'Brien and Schwartz, 1992).

An alternative approach is to perform linear regression analysis of sensitivity (dB) over time for each point in the visual field, a technique known as point-wise linear regression (PLR). The improved ability of PLR to detect VF change compared to linear regression techniques which monitor summary measures over time has been demonstrated by a number of groups (Birch et al., 1995; Smith et al., 1996; Katz et al., 1997). Some commentators, in particular Heijl (Heijl et al., 1998), have been critical of the PLR approach, suggesting that the use of a single point to identify progression is likely to yield high sensitivity, but at the cost of a high false positive rate unless strict significance criteria are applied. It should be noted that, as yet, no independent gold standard exists by which to define glaucomatous progression. Distinction needs to be made between 'clinical significance' and 'statistical significance' in the context of PLR; management decisions should not be taken in isolation from other clinical data such as optic disc appearance, level of IOP and patient history. No consensus yet exists as to the optimal approach of PLR in terms of slope, significance level, or indeed whether a 'cluster-based' approach should be used. A number of different progression criteria have been reported in the literature; worse than -2.4 dB/year and $p < 0.05$ (Noureddin et al., 1991), worse than -1.0 dB/year and $p < 0.05$ (Viswanathan et al., 1997), worse than -1.0 dB/year and

$p < 0.001$ (Bhandari et al., 1997) and worse than 0 dB/year and $p < 0.0009$ in 2 contiguous points (Nouri-Mahdavi et al., 1995). In general, it is probably advisable to select a minimum slope requirement which exceeds that which may be expected with age-related decay. Cross-sectional studies have estimated the age-related slope of dB/decade to vary from -0.6 dB/decade centrally to -1.2 dB/decade peripherally (Heijl et al., 1987). The selection of a minimal slope of -1.0 dB/year therefore comfortably exceeds the predicted age related loss ten-fold, allowing for inaccuracies in the age-related estimate.

There is a statistical source of false positives when using point-wise linear regression, namely the multiple testing in space (at 52 points) and in time (at each follow-up). This potential risk of high false positive progression may be addressed in a number of approaches. Firstly the significance criteria may be made stricter, such that a steeper slope and a tighter significance level are required. Secondly, intermediate-sized VF areas or clusters may be used (Nouri-Mahdavi et al., 1997). A third option is to include additional confirmatory visual field tests. In an elegant study by Gardiner and Crabb (2002a), the sensitivity and specificity of different PLR criteria were compared using VF series incorporating simulated measurement noise. The study defined progression according to the 'standard criteria' (worse than -1.0 dB/year and $p < 0.01$) and compared various confirmatory permutations each requiring the same minimum slope standard criteria – two of two consecutive tests, three of three consecutive tests, two of three consecutive tests, three of four consecutive tests. Two further methods were proposed in the study. In the two-omitting strategy a point n is identified as progressing if it satisfies standard criteria and if the slope obtained by adding one confirmatory point (n+1) but excluding point n also satisfies standard criteria. Three-omitting is similar except that it requires standard criteria to be satisfied by an additional slope constructed from a second confirmatory point (n+2) with omission of point n+1. Using the simulation model, after six years the standard criteria (without confirmatory steps) yielded the highest sensitivity at 97.1% (at three years) but at the cost of falsely labelling virtually all stable eyes as progressing. In contrast the three-omitting approach falsely labelled 11.6% of stable eyes as progressing after six years, with a sensitivity of 65.7%. Although the three-omitting approach was found to have the best estimated specificity, other groups have elected to use the two-omitting option by way of compromise as it affords better sensitivity than three-omitting and

requires only one confirmatory step, resulting in less time to identified progression (Nouri-Mahdavi et al., 2005).

The detection of progression by linear regression is influenced by a number of factors such as examination frequency, underlying rate of progression, degree of variability and position of the VF tests within the time series (Wild et al., 1997). The performance of linear regression improves with the amount of available data points included in the analysis. Some authors have suggested that a minimum of seven or eight tests is required for PLR to achieve satisfactory sensitivity and specificity (Katz et al., 1997; Spry et al., 2000). Gardiner and Crabb (2002b) have more recently shown that the optimal frequency of VF testing to detect progression was three tests per year with more frequent testing resulting in increased false positive rate.

A Windows-based software package called PROGRESSOR (Institute of Ophthalmology, London) is available for the computation of PLR analyses (Fitzke et al., 1996). The software is independent from the HFA and therefore requires the collection of VF tests (either using floppy discs, but now possible by direct transfer using serial port) and transfer to a database held on an external terminal. PROGRESSOR enables linear regression analysis of VF sensitivity over time for each test-point, with adjustable slope and significance criteria. PROGRESSOR outputs a graphical display, with each test-point being represented by a bar chart. Each bar of the bar chart represents a single VF examination in the series. The length of each bar equates to the sensitivity loss of the test location at that examination, with increasing length indicating decreasing sensitivity. Each bar is colour-coded according to the level of significance of the slope generated by the inclusion of the examination in the series, with 'hotter' colours (red, white) indicating higher levels of significance. An example of a PROGRESSOR output is shown in Figure 2-5. The level of agreement between expert observers in assessing progressive VF deterioration has been shown to improve with the use of PROGRESSOR relative to the unaided inspection of VF printouts (Viswanathan et al., 2003). PROGRESSOR has also been shown to detect progression earlier than GCP (total deviation based) when the same significance criteria ($p < 0.05$) are used by both techniques (Viswanathan et al., 1997), although this is with the caveat that the techniques were not necessarily matched for specificity.

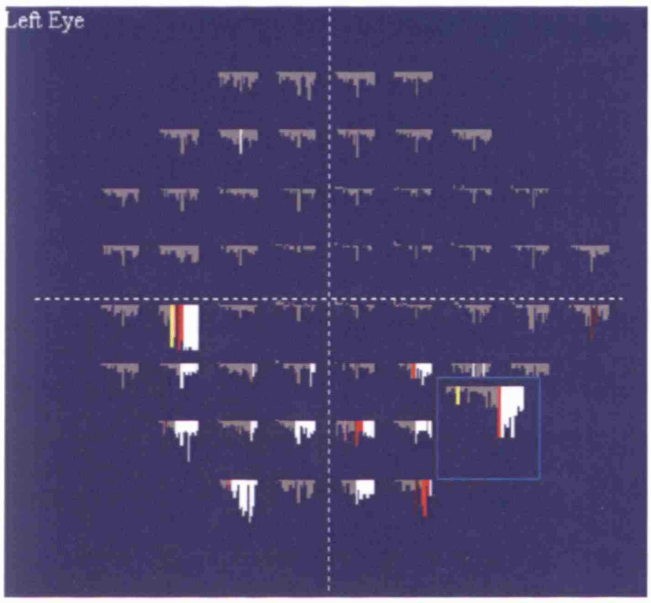

Figure 2-5. An example of a PROGRESSOR output for a subject's left eye. Progression criteria have been set at slope < -1 dB/year and p < 0.01. A progressing point's bar graph has been enlarged (bottom right)

2.4.5.4 Comparison of Methods

The absence of an independent reference by which to classify glaucomatous progression limits our ability to draw meaningful conclusions from methodological comparisons. One must also appreciate that, in the case of event analyses designed for use in large scale clinical trials, the criteria by which progression are judged may be optimised for the stage of disease. Katz et al., (1999b) have compared detection of progression in 67 glaucomatous eyes using AGIS, CIGTS and EMGT criteria. 'Positive detection rates' of 11% for AGIS, 22% for CIGTS and 23% for EMGT were estimated. Although the incidence rates were similar for the CIGTS and EMGT techniques, only half of the subjects identified as progressing by one test were identified by the other. In another study using the same glaucomatous eyes, a higher temporal variability of CIGTS scores was identified compared to AGIS scores over a one year period (Katz, 1999a). Katz subsequently applied both the total deviation-based GCP technique and the pattern deviation-based GCP used in the EMGT (which subsequently was

introduced to the Statpac software as GPA) to the same 67 glaucomatous eyes (Katz, 2000). The total deviation technique detected glaucomatous progression in 35.7% of subjects at six years, compared to 23.2% using the pattern deviation technique, with only moderate agreement between methods (kappa = 0.51). The suggestion that pattern deviation techniques may be 'superior' to total deviation based techniques (as they can attenuate apparent glaucomatous change resulting from diffuse change due to cataract) has recently been challenged. Artes et al., (2005) performed total and pattern deviation analyses (both trend and event analyses) on VFs from 168 eyes with early to moderately advanced glaucomatous field loss. Although the pattern deviation techniques identified fewer progressing cases, consistent with previous reports, a diffuse VF loss based on MD and general height change was found in all progressing eyes. This suggests that pattern deviation-based techniques may underestimate the true amount of glaucomatous progression. Indeed there is very little in the literature assessing the performance of the pattern deviation-based GPA software, which is of concern as this is now the algorithm native to the Humphrey and likely to be considered by some operators, if somewhat erroneously, as the 'gold standard' technique. The developers of the EMGT visual field criteria have reported a pilot study comparing the AGIS, CIGTS and EMGT progression criteria in 40 eyes (Heijl et al. *IOVS* 2003; 44: ARVO E-Abstract 44). The EMGT technique was found to identify progression earlier and more often than CIGTS or AGIS and without loss of specificity. It should be noted that the study was not without shortcomings, chiefly that the independent standard by which specificity was estimated was based on expert observer opinion. Interestingly, a recently reported study, with the same methodological limitation of using expert observation as the reference, reported an improved sensitivity for total deviation-based PLR compared with pattern deviation-based PLR (Manassakorn et al., 2006).

It is therefore clear that it is impossible to select an 'optimal' technique by which to monitor glaucomatous progression. An indication of sensitivity and specificity may be derived by applying the change criteria to computer-modelled VF data. In this circumstance the VF status at the end of the assessment period may be predetermined by the operator, thereby removing the need for an independent reference. A study of particular interest is that reported by Vesti et al., (2003) which compared AGIS criteria, CIGTS criteria, three GCP-based criteria (total

deviation-based) and two PLR techniques. Real patient VF tests, separated by seven years, were used as the initial and final tests with a further 14 interim computer simulated tests included with moderate, high or no variability levels. The AGIS method was the most conservative, identifying the fewest eyes as progressing, with CIGTS identifying twice as many and at 1.4 to 2.3 years earlier, despite a similar level of specificity. The PLR and GCP techniques had higher progression rates than AGIS and CIGTS, suggesting that they are more adept at detecting smaller field changes. The GCP techniques were, however, less resistant to increasing levels of threshold variability compared to the PLR techniques, unless additional confirmatory tests were applied. The PLR techniques varied in specificity from 80 % to approaching 100 %, with an increased time to detection compared to the other techniques. This latter feature may be explained in part by the fact that PLR identifies more progressing eyes, and these additional eyes may have more subtle changes which take longer to detect. It may be concluded that PLR may be an appropriate choice when the number of tests and length of follow-up increases. PLR also has the additional advantage of allowing a rate of change to be calculated.

2.4.6 Spatial filtering

A potential strategy for the reduction of threshold variability, without recourse to additional testing or exclusion of 'noisy' tests, is the post-hoc application of a spatial filter to the VF data (Fitzke et al., 1995; Crabb et al., 1997b). Spatial filtering (or 'processing') is adapted from digital image processing techniques. Medical images, such as those obtained by magnetic resonance imaging, may be digitally represented as a matrix of numerical values; measurement noise is reduced and image quality is improved by applying a mathematical process which exploits the spatial relationship between neighbouring values. A graphical illustration of spatial processing applied to an image is depicted in Figure 2-6.

As the field may be considered as a similar numerical matrix, the same rationale may be applied to VF data. In this context, the measured threshold sensitivity of each test-point within the VF is replaced by a 'weighted' sensitivity value, which is estimated according to the magnitude of neighbourhood sensitivity values. The first spatial filter applied to VF data, the Gaussian filter (based on a three-by-three test-point grid, Figure 2.7), has been shown to

reduce test-retest variability and to attenuate measurement noise (Fitzke et al., 1995; Crabb et al., 1997b). However, it has also been shown to attenuate useful signal, particularly small VF defects (Spry et al., 2002). This suggests that Gaussian filtering may be of limited benefit in the earliest stages of the disease process.

More recently, a novel spatial filter has been designed with the intention to incorporate the physiological relationship between measured sensitivity at all test-points within the VF (Gardiner et al., 2004). The filter was derived by examining the correlations and covariances between sensitivities among all pairs of VF test-point locations, within 98,821 predominantly glaucomatous VFs.

Figure 2-6. An example of spatial image processing. A noisy, pixelated image (left) is rendered clearer and with higher resolution following the application of a Gaussian filtering process

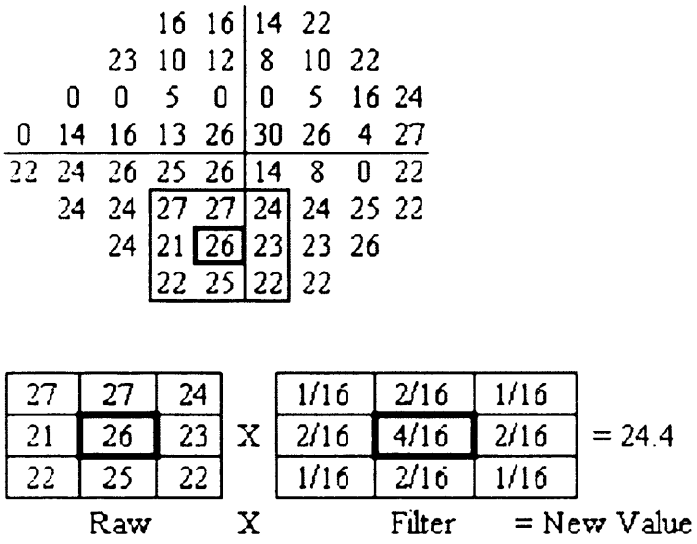

Figure 2-7. The Gaussian filter. The sensitivity of the point of interest, 26 dB (in the centre of the grid) is adjusted according to weightings applied to the sensitivities of the neighbouring locations in the grid

2.5 Comparing structure and function

In this section an account of studies which have compared structure and function is given. Various methods have been used to assess structure – by clinical assessment, by imaging and by histological examination. A number of different approaches has been used to assess visual function in these comparative studies, including conventional perimetry (both static and kinetic), specialised perimetry methods (SWAP, flicker perimetry) and electrodiagnostic testing. However, for the purposes of this thesis, emphasis has been placed on those comparisons which have been performed using conventional perimetry, as this is the predominant technique of measuring visual function in current clinical practice.

2.5.1 Clinical assessment of ONH and RNFL

2.5.1.1 Cross sectional data

Balazsi et al., (1984) estimated the neuroretinal RA of 39 normal, glaucoma suspect and early glaucoma subjects (with the diagnosis based on VF and not optic disc status) using magnification-corrected stereoscopic photographs. RA was correlated to the overall retinal sensitivity and root mean square retinal sensitivity acquired using the JO program of the Octopus static perimeter (Interzeag, Schlieren-Zurich, Switzerland), as well as contrast sensitivity and colour vision. Using linear regression, a strong correlation was reported for RA with retinal sensitivity ($r = 0.37$, $p < 0.05$ for RA corrected for magnification and $r = 0.68$, $p < 0.01$ for uncorrected RA).

Airaksinen et al., (1985a) also correlated magnification-corrected RA from stereoscopic optic disc photographs with VF indices derived from the Octopus JO program in 23 normal subjects, 49 glaucoma suspects and 51 subjects with POAG. Using linear regression, RA was found to be significantly correlated with both 'mean damage' and 'corrected loss variation' ($R^2 = 0.32$ and 0.29, respectively, p value not given). The scatter plots of log corrected loss variation with RA and mean deviation with RA in this study were curvilinear, although some subjects did appear to have advanced field loss (up to 24 dB mean damage). A quadratic function was found to improve the fit, increasing the R^2 for mean damage and corrected loss variation to 0.41 and 0.34, respectively.

A curvilinear relationship was also observed by Jonas and Grundler (1997), who compared magnification-corrected optic disc stereophotographs from 360 glaucoma subjects (POAG, pseudo-exfoliative and NTG) with VF indices from the G1 program of the Octopus perimeter. It should be pointed out that the study was potentially biased in that subjects were included on the basis of optic disc appearance and on the presence of specific VF defects. As the relationship between RA and mean defect was found to be curvilinear, a transformation was performed plotting RA against the square root of the mean defect. A linear relationship was found following the transformation, and the correlation coefficient marginally improved from -0.66 ($p < 0.0001$) to -0.70 ($p < 0.0001$) for POAG subjects. The description of neuroretinal rim shape was found, overall, to have the best correlation with mean defect in POAG subjects ($r = 0.71$, $p < 0.001$).

A number of other authors have reported strong correlations between neuroretinal rim and VF defects, both for global measures and localised lesions (Guthauser et al., 1987; Funk et al., 1988; Weber et al., 1990; Nyman et al., 1994). Throughout the literature, RA appears to be the most consistent amongst optic disc parameters to correlate with VF measures.

Airaksinen et al., (1985b) have also reported high correlations between RNFL scores and VF indices. Monochromatic RNFL photos and stereo disc photographs from 29 normal, 52 POAG suspect and 51 POAG subjects were assessed by dividing the optic disc circumference into ten sectors and by scoring each sector from 0-4 for diffuse and localised nerve fibre loss. The RNFL scores were correlated to VF indices from the Octopus JO program. A linear relationship was found between localised corrected loss variation index and localised RNFL score. VF indices were found to be related to diffuse nerve fibre loss score. The relationship appeared curvilinear and the fit was significantly improved when a quadratic component was included in the model. Using a multiple linear regression model, 50-60% of the total variation in visual function indices could be accounted for by diffuse RNFL loss. These findings have been supported by the work of Autzen et al., (1990). Airiksanen's group have subsequently shown that conventional perimetry tests are sometimes unable to detect function losses associated with RNFL loss and that high resolution microperimetry may be necessary to reveal the earliest functional losses (Tuulonen et al., 1993). This work supports the view that RNFL defects may be detectable prior to VF loss using current conventional techniques.

2.5.1.2 Structure-function maps

A number of studies have proposed 'maps' relating VF test-points to positions at the ONH using cross-sectional data. Wirtschafter et al., (1982) projected illustrations of primate RNFL patterns onto an appropriately scaled VF template, with the border of the ONH defined as the physiological blind spot covering 13° x 9°. The authors intended the map to justify an anatomical basis for the subdivision of the VF into sectors, as opposed to a method of relating disc sectors exactly to field sectors. Despite this caveat, a number of other authors have used Wirtschafter's map for this latter purpose (Kono et al., 1997; Reyes et al., 1998).

Weber et al., (1990) constructed a map using data from 15 subjects with focal glaucomatous disc damage. The anatomical site of damage at the ONH was defined according to the sector with the thinnest rim by planimetric examination. A functional map based on 21 regions of the 'perimetric nerve fibre bundle map' was used to evaluate the VF data (Weber and Ulrich, 1991). The site of the affected rim and the number of the corresponding RNFL bundles showed a linear correlation over a limited range of the superior and inferior pole of the disc. These comparisons were used as the basis of a 'functional disc map' divided into six sectors.

Garway-Heath et al., (2000a) proposed a structure-function map constructed by projecting the Humphrey 24-2 visual field template onto 69 red-free RNFL photographs from NTG patients in which there were either prominent RNFL bundles or defects. By noting the proximity of each test-point to the nearest RNFL defect/bundle and then tracing the course of the RNFL to the ONH, the relationship between the test-point location and circumferential location at the ONH was estimated. These data were used to construct a map relating structure and function (Figure 2-8). Garway-Heath's map differed from that described by Wirtschafter in that paracentral and arcuate areas of the field are represented by sectors at the superior and inferior poles of the disc, whereas they are nearer the temporal horizontal meridian in Wirtschafter's map. Garway-Heath's map is also somewhat asymmetrical, in keeping with the partial map of Weber, reflecting the position of the disc superior to the horizontal meridian. Garway-Heath's map has received wide acceptance, and has been used in a variety of subsequent studies, particularly those mapping structural parameters derived from imaging devices to VF data (Lan et al., 2003; Schlottmann et al., 2004; Reus and Lemij, 2004b; Danesh-Meyer et al., 2006; Strouthidis et al., 2006a).

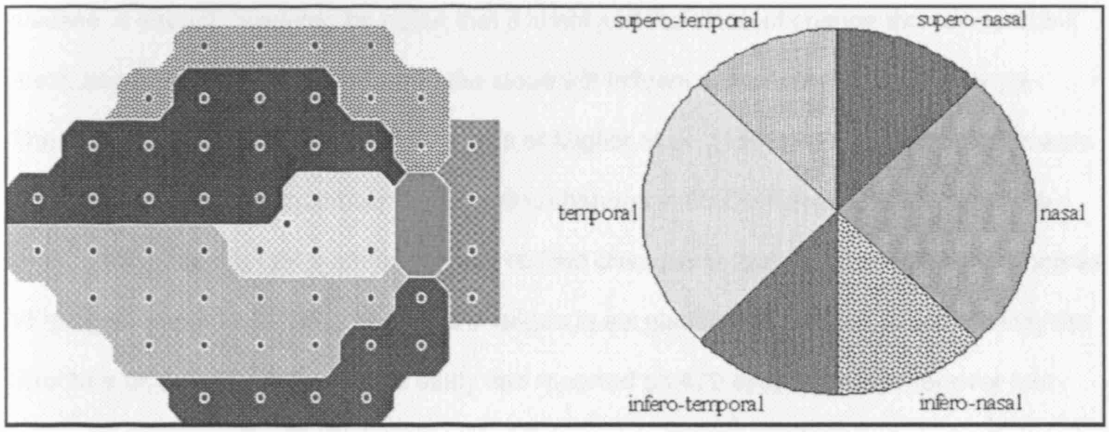

Figure 2-8. Diagram showing the anatomical relationship between Humphrey 24-2 visual field test-points (left) and optic nerve head disc sectors (right). Adapted from (Garway-Heath et al., 2000a)

2.5.1.3 Longitudinal data

There are few longitudinal investigations of structural and functional losses in glaucoma using clinical examination published in the literature. Studies performed using stereophotographs or RNFL photographs suggest that structural changes occur prior to VF loss as determined by white-on-white perimetry. Planimetric optic disc measurements and automated static threshold measurements were compared in a study of fifteen patients with asymmetrical early POAG (early reproducible field loss in one eye, normal field in the fellow eye) over a mean follow-up of 6.1 years (Zeyen and Caprioli, 1993). Eight of the fifteen eyes with an initially normal field went on to demonstrate disc progression, 75% of which did not develop field abnormalities. The mean rate of RA loss was 1.7 %/year in eyes with initially normal fields and 2.1 %/year in eyes with initial field loss. The mean rate of change of corrected loss variation was 0.3 dB^2/year in eyes with a normal field at baseline and 3.6 dB^2/year in eyes with a baseline field defect. These findings are in keeping with the concept of a curvilinear relationship between structure and function, suggesting that structural assessment is more

useful for detecting progression at the earliest stages of the disease (before field loss has occurred) and that perimetry is more useful for detecting progression at the later stages of the disease. It should, however, be noted that it is not just the slope of change that is important; measurement variability in relation to the slope will influence the detectability of change.

These results are supported by the findings of Miglior et al., (1996) who compared perimetric changes and optic disc manual morphometric changes in 86 OHT eyes and 16 glaucoma eyes. Optic disc changes were found prior to field changes in four hypertensive eyes whereas VF progression was found prior to disc changes in six glaucomatous eyes. More recently the Structure and Function Evaluation study has reported on 479 eyes assessed for over four years using stereo disc photographs (assessed at an optic disc reading centre), SAP and SWAP (Johnson et al., 2003). A strong relationship existed between glaucomatous optic disc damage at the time of study entry and the subsequent development of glaucomatous field defects detected using SAP, with 75-80% of field 'converters' having abnormal discs at baseline. Amongst eyes with unchanging VFs (82.5-90% of eyes), there was an equal division of normal and glaucomatous discs at baseline. A higher percentage of glaucomatous optic discs was present in subjects with SWAP defects at baseline, and in those subjects who later went on to develop SWAP defects.

In terms of longitudinal studies using RNFL photographs, Sommer et al., (1991a) examined RNFL photographs in 1344 eyes over a six year period. Depending on the observer, 50-85% of eyes with VF loss at baseline had nerve fibre defects. In 60% of cases, RNFL defects were present six years before the development of visual field loss. The same group subsequently compared optic disc photographs and RNFL photographs in 37 OHT eyes that developed VF loss after a five year period and 37 OHT eyes which retained normal VFs over the same period (Quigley et al., 1992). 49% of converter eyes and 8% of stable eyes demonstrated progressive RNFL loss, with the hemiretinal position of loss being highly correlated with the location of subsequent VF loss.

2.5.2 Quantitative imaging of ONH and RNFL

With the development of each objective imaging system, an ever increasing number of investigations evaluating the relationship between structural parameters and VF

measurements is being published. Studies involving the HRT/HRT-II, GDx-VCC and OCT are discussed in this section.

2.5.2.1 Cross sectional data - HRT

Brigatti and Caprioli (1995) compared HRT parameters, calculated using the 320 μm RP, with MD and CPSD (both Octopus and Humphrey programs) in 46 subjects with early to moderate glaucomatous field loss. The only parameter to achieve statistical significance was the 'third moment', the third central moment of the frequency distribution of the depth values for optic disc structures (a measure now referred to as 'cup shape measure' on more recent software iterations). The third moment achieved a Pearson correlation coefficient of 0.65 with MD and 0.55 with CPSD ($p < 0.0001$). Cup volume and mean cup depth also showed a degree of correlation with VF indices, but not reaching statistical significance. This study did not, however, include assessment of RA. Iester et al., (1997b) found RA to be the best optic nerve predictor of MD, with Pearson's $r = 0.44$, $p < 0.001$. Unlike the previous study, the standard RP was used to define the HRT cup. The same group went on to demonstrate that superior and inferior optic nerve measures were significantly correlated with the corresponding VF hemifields (Iester et al., 1997d).

Emdadi et al., (1998) performed a quantitative comparison of the HRT disc topography with focal VF deficits in 39 subjects with focal glaucomatous field loss. The topographic measurements were divided into 10° sectors and the comparisons made using sector RA to sector disc area ratio. Approximately half of the subjects had diffuse optic disc damage despite having focal field loss. Focal optic disc deficits were observed in 25-35% of subjects and 15% of subjects had no detectable optic disc deficit. A stronger relationship between topographical sectors and VF loss was subsequently reported by the same group in a study which included subjects with focal disc damage as well as focal field loss (Anton et al., 1998). Applying a similar methodology, strong global topographic correlations were observed using SWAP (Yamagishi et al., 1997).

In a study by Gardiner et al., (2005) the relationship between HRT RA in 10° sectors and Humphrey threshold sensitivity was examined in a cross section of healthy subjects and glaucoma subjects. The 'healthy' eye RA sectors were used to construct a 'normal' model. The 'glaucoma' sectors were divided by the matching healthy sector average RA values. The

sectors (glaucoma/healthy) were then normalised to account for absolute differences in RA between eyes. The normalised RA sector values were correlated against the sensitivities of all 52 VF test-points. A map, correlating structure and function, was constructed, allowing easy visualisation of the ONH sectors with the highest correlation with each VF test-point. In particular, locations within the superior hemifield were highly correlated with the inferior and temporal ONH and locations in the inferior hemifield were highly correlated with the superior and temporal ONH. This map differed from that proposed by Garway-Heath et al., (2000a) in that test-points in the central field tended to be more vertically located in the HRT map compared to the RNFL map. There were also some incongruous relationships, such as locations in the superotemporal VF locations tending to relate to sectors in the superior (when inferior would be expected) part of the disc and locations in the field temporal to the blind spot were more often associated with temporal disc sectors (when nasal would be expected). The map did not include many discs with advanced glaucomatous loss and so probably needs to be interpreted with caution when relating to this group of subjects.

More recently, a sectoral comparison of 110 glaucoma, glaucoma suspect and normal eyes was performed using the HRT-II and the 24-2 SITA algorithm (Danesh-Meyer et al., 2006). Using linear regression, the strongest correlation for global measures was found using global RA and global MD ($r = 0.35$, $p = 0.0018$), in keeping with previous studies which used the earlier HRT model (Iester et al., 1997b; Lan et al., 2003). The IT RA sector was found to have the strongest correlation with both global MD ($r = 0.47$, $p < 0.0001$) and its respective sectoral MD value ($r = 0.46$, $p < 0.0001$), followed by the SN RA sector.

2.5.2.2 Cross sectional data - GDx-VCC

As the GDx-VCC is a relatively new instrument, structural and functional comparisons are fairly limited. Using an older scanning laser polarimeter with fixed corneal compensation, Weinreb and co-workers (Weinreb et al., 1995a) compared VF indices and retinal nerve fibre thickness in 53 POAG subjects. Nerve fibre thickness was correlated with MD both globally and locally. However, there was no significant correlation when hemifields were examined in isolation.

Reus and Lemij (2004b) have correlated HFA-II results (both full threshold and SITA) with GDx-VCC measurements in 47 healthy subjects and 101 glaucoma subjects. Statistically

significant correlations were found between DLS and peripapillary RNFL retardation in all sectors other than the temporal in the glaucomatous eyes (Spearman rank correlation coefficient = 0.77, 0.52, 0.46, 0.51, 0.38, $p < 0.001$, for the ST, SN, N, IN, IT sectors, respectively). No significant correlations were found in the healthy subjects, other than the SN sector. The relationship between retardation and DLS using the logarithmic decibel scale was curvilinear. By using unlogged DLS measurements (1/Decalambert) the relationship became linear. These observations are entirely in keeping with the work of Schlottmann et al., (2004) who additionally showed that the strength of correlations with SAP were greater for images acquired using variable, compared to fixed, corneal compensation. Reus and Lemij (2005) have subsequently compared the relationship between SAP and both GDx-VCC and HRT measurements in 46 healthy subjects and 76 glaucoma subjects. A curvilinear relationship was observed for both HRT RA and GDx-VCC retardation with DLS (in decibel scale) both globally and sectorally. There was a linear correlation between GDx-VCC and HRT measurements in all sectors other than the temporal.

2.5.2.3 Cross sectional data - OCT

A study has been conducted by the San Diego group comparing RNFL thickness measured by the OCT 2000 and SAP in 43 eyes from subjects deemed to have glaucomatous optic neuropathy on the basis of stereoscopic disc appearance (El Beltagi et al., 2003). The RNFL thickness measurements around the ONH were divided by clock hour and were considered outside normal limits if they were thinner than 97.5% of values derived from their clinic's normative database of 99 subjects. VF sectors were classified as depressed on the basis of the presence of test-points with a pattern deviation of < 5%, with the field divided into the 21 sectors described by Weber and Ulrich (1991). By comparing disc sectors with RNFL thicknesses outside normal limits and VF sectors depressed outside normal limits using linear regression, inferior and inferotemporal RNFL areas were best correlated to the superior arcuate and nasal step field regions ($R^2 = 0.34\text{-}0.57$, $p < 0.01$).

Most recently, the San Diego group have assessed structure-function relationships by comparing threshold sensitivities with $STRATUS_{OCT}$ RNFL thickness measurements, HRT-II RA and RNFL thickness measurements and GDx-VCC RNFL thickness measurements (Bowd et al., 2006). The results, from 127 glaucoma and glaucoma suspect subjects and 127

normal controls suggest that the strongest structure-function associations are found using the $STRATUS_{OCT}$, with GDx-VCC and HRT-II relationships being of similar magnitude but with weaker significance. HRT-II RA was more strongly associated with SAP than HRT-II RNFL measurements, which is unsurprising as RNFL measurements on the HRT-II are measured indirectly. The $STRATUS_{OCT}$ RNFL thickness measurements are clearly more strongly associated with SAP measurements globally and in the inferotemporal sector. The results of this study are out of keeping with previously mentioned reports (Schlottmann et al., 2004; Reus and Lemij, 2004b) in that the associations are no better if expressed by a logarithmic as opposed to a linear fit.

2.5.2.4 Longitudinal data

Given the relatively short length of time in which quantitative ONH and RNFL imaging devices have been available, the paucity of studies assessing structure and function longitudinally using these devices is understandable. Most reports available in the literature have been performed using the HRT as this has been available commercially for the longest period of time. The seminal work of Kamal et al., (1999; 2000) which demonstrated that objective imaging devices are capable of detecting change prior to conventional perimetry has already been discussed.

The Halifax group have reported a prospective longitudinal study in which HRT progression was assessed using TCA (Chauhan et al., 2001). 77 patients with early glaucomatous damage were followed up for a median of five years with bi-annual HRT imaging and 30-2, full threshold Humphrey VF testing. Field progression was assessed using the Statpac GCP program. 29% of subjects progressed by HRT and SAP, 40% progressed by HRT alone and 4% progressed by SAP only. Of the subjects progressing by both modalities, 45% progressed by HRT first, compared to 41% by SAP first and 14% at the same time. In this study, the specificities of HRT and SAP were not matched, which means that the comparison between the two techniques is not necessarily valid. The same group latterly performed a comparison of event- and trend-based progression techniques using the HRT, SAP and high pass resolution perimetry in 84 glaucoma subjects and 41 normal controls (Artes and Chauhan, 2005). A poor agreement between the three modalities as regards progression was identified regardless of the stringency of the progression criteria applied, with agreement varying from

4% to 19% in the glaucoma group. A later study performed using the OCT has identified a similarly poor level of agreement with conventional perimetry as regards progression (Wollstein et al., 2005b).

2.5.3 Results from histological studies

The work of Quigley, comparing retinal ganglion cell loss with kinetic perimetry (Quigley et al., 1982) and subsequently with SAP (Quigley et al., 1989), is frequently cited. It was reported that half the retinal ganglion cells could be lost before a repeatable central field defect could be detected (Quigley et al., 1982). Using SAP, 20% ganglion cell loss was associated with a 5 dB field defect and 40% ganglion cell loss was associated with a 10 dB field defect. These results are supported by the work of Harwerth et al., (1999) who assessed ganglion cell losses in a primate experimental glaucoma model, using primates trained to perform SAP. A 30-50% ganglion cell loss was required before a repeatable white-on-white defect could be detected. Both of these studies suggest a poor relationship between ganglion cell loss and VF sensitivity at the early to moderate stages of ganglion cell loss. At later stages of disease, these studies indicate a stronger, linear association between structure and function.

These studies are not, however, without caveats. A small number of eyes have been included in both human and primate groups. The number of human retinal ganglion cells is compared to a normative database, which is itself made up from a small number of eyes, in which there is a wide inter-individual variation; in the primate model the fellow eye is used as a non-glaucomatous control. The experimental primate model involves far higher IOP levels than would be encountered in POAG, resulting in significant glaucomatous damage over a short period of time with a pattern of damage different from that encountered in human POAG. Garway-Heath et al., (1998b) have pointed out that the conversion factor used to correspond ganglion cell areas to the visual field at 250°/mm is probably 12.5% too small, with the potential effect that sampled retinal areas may not have corresponded well with the field data. There was also no allowance made for the lateral displacement of ganglion cells from the fovea, potentially affecting the results from the central four test-points. The clinical interpretation of the results of these histological studies should therefore be approached with a degree of caution.

Quigley's group have latterly compared the number of retinal ganglion cells (RGCs) topographically mapped to VF data in 17 eyes of 13 subjects with glaucoma and 17 eyes of 17 age-matched controls (Kerrigan-Baumrind et al., 2000). This data has recently been reanalysed by Harwerth and Quigley (2006), by applying a model designed to predict ganglion cell density underlying a given VF sensitivity and location within the field, based on Harwerth's primate data (Harwerth et al., 2004). The model accounts for the effect of eccentricity and was shown to predict ganglion cell densities from VF threshold sensitivities in a primate model of glaucoma (Harwerth et al., 2004). The model was applied unchanged to the Kerrigan-Baumrind data and was shown to predict the general pattern of functional loss with RGC loss in humans (Harwerth and Quigley, 2006). However, the absolute topographical predictions were less precise and this is most likely due to variability caused by delay between last VF and histological examination (up to two years in five of the eyes), threshold variability, possible inclusion of amacrine cells in the RGC counts and the fact that the areas sampled histologically were greater than those tested in automated perimetry. Given these diverse sorces of error, the generalised agreement between the structural and functional parameters was encouraging.

2.5.4 The importance of scaling

A curvilinear or 'bilinear' relationship between structure and function has been reported by a number of groups, using both histological data (Quigley et al., 1982; Quigley et al., 1989; Harwerth et al., 1999) and structural data acquired through clinical examination (Airaksinen et al., 1985b; Jonas and Grundler, 1997). Garway-Heath et al., (1999; 2000b) illustrated that estimated ganglion cell numbers, adjusted for local spatial summation, had a curvilinear relationship with DLS when expressed in the decibel, logarithmic scale. When the DLS was expressed in a linear, unlogged scale (units = 1/decalamberts) the relationship with ganglion cell count was linear. On the assumption that spatial summation remains unchanged with progressive glaucoma, it is possible that a linear scaling of light sensitivity may be able to detect changes earlier than the standard decibel scale. Subsequent studies have similarly demonstrated that the structure-function relationship may be best characterised by a quadratic model using decibel DLS and by a linear model using 1/decalambert DLS, both with the GDx-VCC and with the HRT (Garway-Heath et al., 2002; Schlottmann et al., 2004; Reus

and Lemij, 2004b). The same relationship has also been found when comparing pattern electro-retinogram amplitude to differential light sensitivity (Garway-Heath et al., 2002). The group from San Diego have been unable to replicate the result (Bowd et al., 2006)(Racette et al. *IOVS* 2003; 44: ARVO E-Abstract 77), describing a linear relationship between structural parameters and decibel-scaled DLS.

3 SECTION III: Investigations

3.1 Aims and plan of research

The aims of the research are as follows:

1. In the first experiment (3.2) the test-retest variability of all stereometric parameters acquired using both the HRT and HRT-II is assessed, with the aim of identifying the most repeatable parameter and the factors which affect its variability. In the second experiment (3.3), methods of improving the repeatability of the stereometric parameter identified in the previous experiment are designed and tested with the aim of providing the basis for new HRT progression strategies.
2. A novel HRT trend analysis, based on parameter linear regression over time and weighted according to parameter variability, is applied to longitudinal HRT images acquired from a cohort of ocular hypertensive and control subjects (3.4). A novel HRT event analysis, with thresholds for change based on the parameter's coefficient of repeatability and weighted according to image quality, is tested using the same longitudinal data (3.5). Specificity, detection rates and agreement with established VF progression algorithms are assessed, with the aim of identifying optimal methods for monitoring glaucomatous progression in clinical practice.
3. A novel spatial filter, based on the physiological relationship between test-point sensitivities, is assessed: firstly by comparing the 'functional' relationship with an established anatomical, structural map (3.6) and secondly (3.7) by assessing its impact on the measurement of glaucomatous VF progression in the same cohorts utilised in 3.4-3.5. The aim of this final part of the research is to assess the potential clinical role of spatial filters in the monitoring of progression and to identify possible improvements in their application.

3.2-3.4 Test-retest variability of the HRT and HRT-II

3.2 Factors affecting test-retest variability

3.2.1 Background

Clinical examination of the ONH is of limited value to detect glaucomatous progression because of inter-observer variation (Lichter, 1976). An objective approach – longitudinal quantitative imaging of the ONH – may be more useful for the detection of glaucomatous progression.

One imaging method is scanning laser tomography, as implemented by the HRT and more recently by the HRT-II. The HRT-II is intended for use in the clinical milieu by more than one operator, any one of whom may not possess the same level of experience of operating the device as that required for the successful use of the HRT (Heidelberg Engineering, 2003). Both devices generate three-dimensional mean topography images from which a range of stereometric parameter values can be calculated. These parameters can be measured longitudinally to detect progression. It is useful to estimate the test-retest repeatability of stereometric parameters, so that changes due to disease progression, and not measurement error, can be identified correctly.

3.2.2 Purpose

The purpose of this study was to evaluate the test-retest variability of stereometric parameter measurements made with the HRT and HRT-II, and to establish which parameter was most repeatable and reliable. An investigation into the factors that may affect the repeatability of this parameter was carried out.

3.2.3 Methods

3.2.3.1 Subject selection

74 subjects – 43 OHT and 31 POAG – were recruited from the Ocular Hypertension Clinic at Moorfields Eye Hospital. OHT was defined as IOP greater than 21 mmHg on two or more occasions, and a baseline Humphrey 24-2 full threshold AGIS score of 0 (AGIS, 1994). POAG

was defined as a consistent AGIS VF score greater than 0 and a pre-treatment IOP greater than 21 mmHg on two or more occasions. All subjects had previous experience of scanning laser tomography. From each subject, a single eye was selected on the basis of having a refractive error less than 12 dioptres of spherical power and no history of previous intraocular surgery. In subjects with lens opacity, the eye with the greater degree of opacity was preferentially selected, although the presence of lens opacity itself was not a criterion for subject selection. This study adhered to the tenets of the Declaration of Helsinki and had local ethical committee approval, as well as subjects' informed consent.

3.2.3.2 Testing protocol

Image acquisition was carried out by two experienced observers (ETW and NGS) at each of two visits within six weeks of each other. The testing sequences were performed using both the HRT (Version 2.01b) and HRT-II (Heidelberg Engineering, Heidelberg, Germany; Eye Explorer Version 1.7.0). In each subject, the scan focus (HRT and HRT-II) and depth of focus (HRT) used in the first visit were also used in the second visit. A series of three scans was acquired by each observer at a 10° field of view for the HRT and at 15° for the HRT-II (the two different scanning angles have the same degree of resolution). The following imaging protocol was adhered to for all subjects:

VISIT 1 ETW then NGS then ETW

VISIT 2 ETW then NGS

Following IOP measurement at Visit 1, the eye was dilated using tropicamide 1% enabling a single observer (NGS) to carry out lens grading. Subjective grading was carried out using the Lens Opacity Classification System III (LOCS III) (Chylack et al., 1993). Nuclear opalescence (NO, range 0.1 to 6.9), nuclear colour (NC, range 0.1 to 6.9), posterior subcapsular (P, range 0.1 to 5.9) and cortical (C, range 0.1 to 5.9) scores were graded against a standardised transparency. Scheimpflug photography was performed using the Case 2000 series (Marcher Diagnostics, Hereford, UK). The central nuclear dip (CND) value, derived from digitised densitograms, was used as an objective lens score (Hammond et al., 2000).

3.2.3.3 Image analysis

Heidelberg Eye Explorer (Version 1.7.0), the operating system of the HRT-II, was used to generate mean topography images and to perform image analysis. The term 'HRT-II Explorer'

has been used to indicate when Explorer was used to analyse the HRT-II mean topographies. The HRT topographies were imported into the HRT-II operating platform as HRT-Port files. HRT mean topographies were generated and analysed using the same Explorer software as the HRT-II images (this system has been termed 'HRT Explorer'). HRT mean topographies were also generated and analysed using an option on the Explorer software called 'HRT-Classic' which is derived from the older MS-DOS HRT software. HRT and HRT-II images may be examined interchangeably (and therefore longitudinally) using Explorer; HRT-II images are not compatible with HRT-Classic. Contour lines were drawn by a single observer (NGS) for the baseline mean topographies, and these were exported to the subsequent images. Four different image sequences were analysed for both imaging devices: intra-observer/intra-visit (ETW then ETW, same visit), inter-observer/intra-visit (ETW then NGS, same visit), intra-observer/inter-visit (ETW then ETW, different visits) and inter-observer/inter-visit (ETW then NGS, different visits). The standard RP was used for all analyses in this study. MPHSD was recorded for each mean topography as a proxy measure of image quality.

3.2.3.4 Statistics

Within-subject coefficient of variation was used to examine the repeatability of each stereometric parameter. Within subject coefficient of variation was calculated with the following equations:

$$\mathbf{s_w} = \frac{1}{\sqrt{2n}}\sqrt{\Sigma\left(obs1-obs2\right)^2}$$

$$\mathbf{CV_w} = 100 \times \mathbf{s_w} \text{ /mean of all repeated measurements}$$

Where $\mathbf{s_w}$ is the common standard deviation of repeated measurements (within subject standard deviation) and $\mathbf{CV_w}$ is the within subject coefficient of variation.

Test-retest repeatability was also assessed by constructing Bland-Altman plots and by estimating the repeatability coefficient (RC) as:

$$\mathbf{RC} = \text{sqrt}(2) \times 1.96 s_w$$

This statistic was applied when no relationship was observed between observation magnitude and observation difference, and when the observation differences were normally distributed (Bland and Altman, 1986)(Bland, J.M. *Personal communication*, 2004).

Intraclass correlation coefficient (ICC) was used to estimate the reliability of the parameters generated.

Scatter plots and regression lines were constructed to identify which factors influenced test-retest variation with significant associations assumed at $p < 0.05$. The factors evaluated were age, refractive error (spherical and cylindrical power), IOP, lens score (NO, NC, PS, C and CND), MPHSD, inter-test reference height difference, disc area and baseline RA.

All statistical analyses were performed using Medcalc Version 7.4.2.0 (Medcalc Software, Mariakerke, Belgium) and SPSS Version 11.5 (SPSS Inc., Chicago, IL, USA).

3.2.4 Results

The male:female ratio of the subjects was 41:33 and the right:left eye ratio was 43:31. The baseline subject characteristics are summarised in Table 3-1.

	Mean	SD	Range
Age (Years)	68.2	10.2	20.4 - 84.8
Mean Deviation (dB)	-2.2	2.4	-11.3 - 1.3
Disc Area (mm^2)	1.9	0.4	1.0 - 3.4
Baseline Rim Area (mm^2)	1.2	0.4	0.4 - 2.2
Spherical Power (D)	-0.2	2.8	-7.7 - 5.0
Cylindrical Power (D)	1.0	0.8	0 - 4.2
Spherical Equivalent (D)	0.4	2.7	-7.4 - 5.7
LOCS III Nuclear Opalescence	2.2	0.9	0.4 - 5.3
LOCS III Nuclear Colour	2.0	0.8	0.3 - 5.1
LOCS III Posterior Subcapsular	0.4	0.5	0.1 - 3.8
LOCS III Cortical	0.8	1.0	0.1 - 3.8
Central Nuclear Dip	17	3	12 - 29
MPHSD (HRT)	31	22	11 - 121
MPHSD (HRT-II)	27	21	10 - 06

Table 3-1. Summary of baseline characteristics of test-retest subjects

Judged by coefficient of variation, RA and mean cup depth demonstrated the highest repeatability (Table 3-2).

Stereometric parameter	Coefficient of variation values (%)											
	HRT-Classic				HRT-Explorer				HRT II-Explorer			
	I	II	III	IV	I	II	III	IV	I	II	III	IV
Cup area	26	21	16	27	25	25	25	24	25	25	23	19
Rim area	7	11	7	10	9	10	9	10	9	12	7	8
Cup volume	26	27	23	30	27	30	31	30	32	37	29	26
Rim volume	16	19	15	17	18	19	19	19	18	22	17	18
Reference height	11	14	11	13	11	15	13	16	17	17	13	13
Height variation contour	14	12	15	15	13	16	14	16	20	15	20	16
Maximum cup depth	8	7	10	8	8	7	10	11	12	13	10	12
Mean cup depth	8	8	9	7	7	8	9	11	11	11	9	10
Mean retinal nerve fibre layer thickness	21	21	32	19	20	23	18	22	31	27	25	22
Retinal nerve fibre layer cross-sectional area	22	21	22	19	20	23	18	22	31	27	25	22
Cup shape measure	19	28	28	23	24	32	32	27	24	26	28	29

Table 3-2. Coefficient of variation values for the stereometric parameters generated in the test-retest study (I = intra-observer/intra-visit; II = inter-observer/intra-visit; III = intra-observer/inter-visit; IV = inter-observer/inter-visit). Low coefficient values equate to high repeatability

Judged by ICC, mean cup depth, cup volume, cup area and RA were the most reliable parameters (Table 3-3). There is no significant difference between the coefficients generated for these parameters in the situation most likely to be encountered in the longitudinal setting (inter-observer/inter-visit - IV).

Stereometric Parameter	Intraclass Correlation Coefficient											
	HRT-Classic				HRT-Explorer				HRT II-Explorer			
	I	II	III	IV	I	II	III	IV	I	II	III	IV
Cup area	0.97	0.94	0.97	0.96	0.94	0.93	0.93	0.95	0.95	0.92	0.96	0.96
Rim area	0.95	0.90	0.96	0.94	0.92	0.90	0.91	0.93	0.93	0.89	0.95	0.95
Cup volume	0.97	0.97	0.96	0.95	0.96	0.96	0.95	0.96	0.95	0.92	0.97	0.97
Rim volume	0.87	0.81	0.90	0.84	0.84	0.80	0.86	0.87	0.84	0.79	0.88	0.87
Reference height	0.86	0.85	0.88	0.84	0.81	0.80	0.83	0.81	0.84	0.74	0.88	0.88
Height variation contour	0.77	0.87	0.81	0.82	0.86	0.73	0.82	0.81	0.65	0.75	0.66	0.78
Maximum cup depth	0.92	0.96	0.89	0.95	0.91	0.97	0.91	0.93	0.76	0.85	0.90	0.88
Mean cup depth	0.97	0.97	0.96	0.98	0.98	0.97	0.97	0.97	0.93	0.95	0.97	0.95
Mean retinal nerve fibre layer thickness	0.82	0.75	0.83	0.79	0.79	0.76	0.81	0.76	0.77	0.78	0.80	0.85
Retinal nerve fibre layer cross-sectional area	0.87	0.82	0.89	0.83	0.79	0.77	0.82	0.79	0.85	0.66	0.85	0.85
Cup shape measure	0.93	0.92	0.89	0.92	0.93	0.90	0.88	0.88	0.87	0.87	0.86	0.88

Table 3-3. Intraclass correlation coefficient values for the stereometric parameters generated in the test-retest study (I = intra-observer/intra-visit; II = inter-observer/intra-visit; III = intra-observer/inter-visit; IV = inter-observer/inter-visit). High coefficient values equate to high reliability

RA and mean cup depth demonstrated the most consistent repeatability and reliability. As RA represents the more clinically meaningful measure, subsequent analyses were performed on this parameter.

RA inter-observer/inter-visit $\mathbf{CV_w}$ (%) values were 10.3% (HRT Classic), 10.2% (HRT Explorer) and 7.8% (HRT-II Explorer). RA RCs were similar for HRT Classic, HRT Explorer and HRT-II Explorer, irrespective of observer or visit (Table 3-4). There was a tendency

towards more repeatable measurements using the HRT Classic, compared with the HRT Explorer, software.

HRT type	Rim area repeatability coefficients (mm^2)			
	I	II	III	IV
HRT-Classic	0.21	0.29	0.19	0.24
HRT-Explorer	0.28	0.31	0.30	0.26
HRT II-Explorer	0.28	0.34	0.24	0.23

Table 3-4. Rim area repeatability coefficients obtained with different types of HRT at different image sequences (I = intra-observer/intra-visit; II = inter-observer/intra-visit; III = intra-observer/inter-visit; IV = inter-observer/inter-visit). Low coefficient values equate to high repeatability; the difference of two measurements will be within this value in 95% of cases

Bland-Altman plots (Figure 3-1) illustrate similar inter-observer/inter-visit repeatability for the three software platform analyses. The mean inter-test difference in all cases approximates zero.

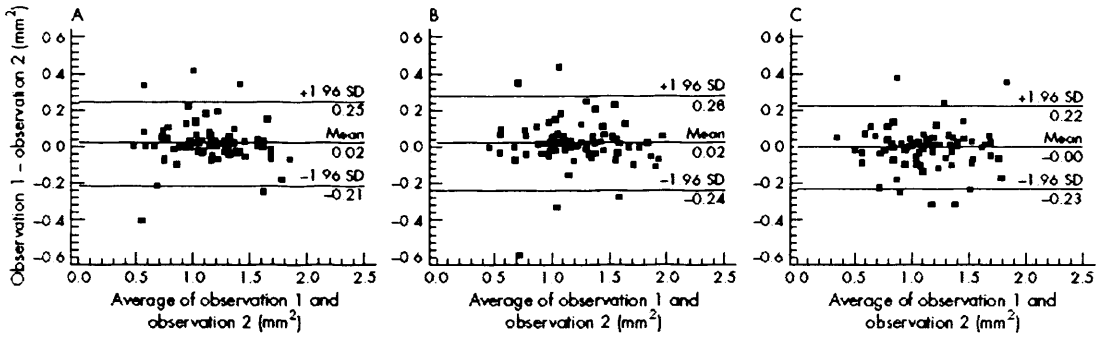

Figure 3-1. Bland-Altman plots of inter-observer/inter-visit rim area obtained with HRT-Classic (A), HRT-Explorer (B) and HRT-II Explorer (C)

3.2.4.1 Factors affecting repeatability

Inter-test reference height difference and mean image MPHSD were the two factors which consistently had a strong relationship ($R^2 > 0.5$) with inter-test RA difference for all testing permutations. Figures 3-2 and 3-3 show scatter plots, with a regression line, of intra-observer/intra-visit RA difference against mean MPHSD and inter-test reference height difference, respectively. Weaker relationships ($R^2 < 0.5$) of inter-test RA difference were observed with CND, NC and NO scores and cylindrical power. Table 3-5 summarises these relationships for intra-observer/intra-visit RA.

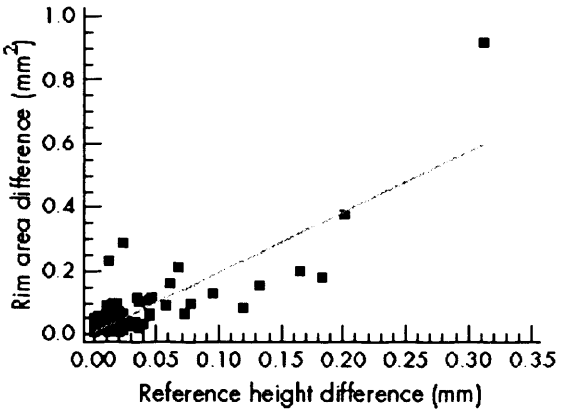

Figure 3-2. Scatter plot of intra-observer/intra-visit rim area difference (mm^2) against reference height difference (mm) using HRT-Explorer. The regression line is also shown ($R^2 = 0.7$, $p < 0.0001$)

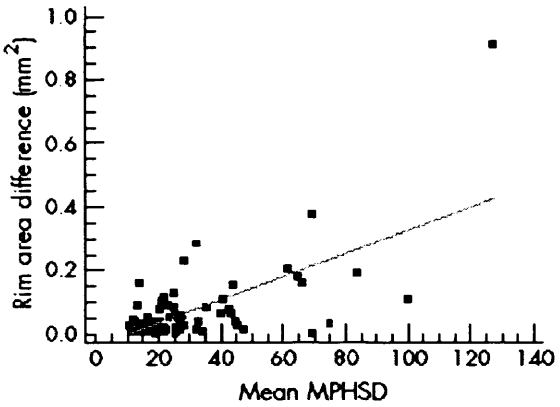

Figure 3-3. Scatter plot of intra-observer/intra-visit rim area difference (mm^2) against mean image quality (MPHSD) using HRT-Explorer. The regression line is also shown ($R^2 = 0.4$, $p < 0.0001$)

Source of Variability	HRT-Classic		HRT-Explorer		HRT II-Explorer	
	R^2	p	R^2	P	R^2	P
Reference height difference	0.7	<0.0001	0.7	<0.0001	0.5	<0.0001
Mean MPHSD	0.5	<0.0001	0.4	<0.0001	0.5	<0.0001
CND	0.1	0.005	0.3	<0.0001	0.2	<0.0001
NO	0.1	0.001	0.2	0.0006	0.2	<0.0001
NC	0.03	0.1	0.1	0.001	0.2	<0.0001
Cylindrical power	0.2	<0.0001	0.03	0.4	0.1	0.005
Spherical power	0.07	0.02	0.02	0.2	0.04	0.1
Spherical equivalent	0.04	0.08	0.01	0.3	0.02	0.2
Age	0.05	0.05	0.04	0.1	0.07	0.02
Baseline Rim Area	0.05	0.05	0.02	0.2	0.0003	0.9
Disc Area	0.001	0.8	0.01	0.5	0.001	0.8
IOP	0.05	0.05	0.05	0.07	0.01	0.4
P	0.01	0.4	0.001	0.8	0.005	0.6
C	0.0001	0.9	0.005	0.6	0.01	0.5

Table 3-5. Association (r^2) between sources of variability and intra-observer/intra-visit rim area differences (mm^2)

A multiple regression was performed, with RA difference as the dependent variable and the factors identified as influencing RA difference (i.e. reference height difference, MPHSD, CND, NO, NC, age and cylindrical power) defined as the independent variables. Reference height difference ($p < 0.0001$) and MPHSD ($p = 0.05$) were the only two significant variables ($R^2 = 0.7$).

To elucidate which factors influenced image quality (as determined by MPHSD), a multiple regression was carried out for intra-observer/intra-visit HRT Explorer, with MPHSD as the dependent variable and CND (used as a single, objective measure of lens opacity), age and cylindrical power as independent variables ($R^2 = 0.5$ for the multiple regression). CND and cylindrical power displayed a highly significant relationship ($p < 0.0001$ for both), and age showed a weaker but significant relationship ($p = 0.03$).

3.2.5 Discussion

Scanning laser tomography is an established technique which has been shown to be reproducible (Kruse et al., 1989; Dreher et al., 1991). The topographic measures produced by the HRT and its predecessor, the laser tomographic scanner (LTS, Heidelberg Engineering, Heidelberg, Germany) have been demonstrated to be repeatable (Rohrschneider et al., 1993; Rohrschneider et al., 1994), and to have less variation compared with other techniques such as computer-assisted planimetry (Garway-Heath et al., 1999). Little has been published about the reproducibility of the HRT-II (Sihota et al., 2002; Verdonck et al., 2002). As the HRT-II is intended as a 'clinical' instrument, its reproducibility under such conditions needs to be established. Our subject profile was heterogeneous – in terms of demographics, disease stage, refractive error, media opacity and image quality – thereby simulating the situation encountered in clinic. Image quality has previously been shown to be associated with pupil size and degree of lens opacity (both objective scoring and LOCS III graded NC, NO and P). Image quality was seen to improve with pupillary dilation but the improvements were often small (Zangwill et al., 1997b). Pupil size was therefore not taken into consideration in our study. None of the subjects were taking miotic medications at the time of the study, although this was not a recruitment criterion.

Since the publication of the original reproducibility studies of the HRT (Mikelberg et al., 1993; Rohrschneider et al., 1994), the Windows-based Explorer platform has been introduced. From this perspective, this study is the first to examine the repeatability of HRT-defined morphometric parameters using the newer software.

RA and mean cup depth were the most repeatable parameters for both devices. Some caution is required when interpreting coefficients of variability as some parameters, such as cup area and cup shape measure, have mean values of low magnitude (approaching zero). It is also difficult to interpret differences between ICC values of a similar magnitude. There is therefore unlikely to be any real difference in reliability between mean cup depth, cup area, cup volume and RA. One should also note that the ICC values depend on the variability of the sample population. As our sample was enriched with eyes with lenticular opacity the ICC values may not be applicable to other populations with less cataract.

Overall, RA and mean cup depth consistently demonstrated the best repeatability and reliability of the parameters measured. This concurs with previous findings of our group (Tan et al., 2003b). Another report, concerning the HRT-II, identified mean cup depth and cup area as the least variable parameters (Sihota et al., 2002). RA, as it contains the retinal ganglion cell axons, constitutes a meaningful parameter for physicians. RA has also been shown to discriminate between normal, glaucoma and OHT subjects (Zangwill et al., 1996; Wollstein et al., 1998; Kiriyama et al., 2003). There is no advantage to using cup area as this is merely the difference between disc area (kept constant in Explorer) and RA. RA is therefore an appropriate candidate for the examination of progression.

In this study, the repeatability of RA measurements was similar for both devices (RC = 0.2-0.3 mm^2) regardless of observer or visit. Similar repeatability between imaging performed at the same visit or at different visits is consistent with a previous study in which no difference was identified in the short-term and long-term variability of topographical measurements (Chauhan and Macdonald, 1995). The HRT-II performs at least as well as the HRT. The similar level of RA repeatability between HRT-II and HRT Explorer analyses indicates that the two methods could theoretically be used interchangeably in a longitudinal setting.

The sources of variability for the HRT, in terms of patient/scanner misalignment (Orgul et al., 1996) and different observers drawing the optic disc contour line have been documented

(Garway-Heath et al., 1999; Iester et al., 2001; Miglior et al., 2002). The present study identifies inter-test reference height difference to be the most consistent factor related to test-retest variability. Our group has previously reported a reduction in RA variability when using a 320μm RP compared with the standard RP (Tan et al., 2003a). Image quality, as recorded by MPHSD, was the other factor that was consistently found to influence variability. MPHSD is a gauge of the variability of pixel-height measurements across the three topographic images used to construct the mean image (Dreher et al., 1991). The present study shows that image quality was, in turn, influenced by lens opacity, age and degree of astigmatism. Sihota et al., (2002) also found a significant correlation between the test-retest variability of the HRT-II with both age and degree of astigmatism. The results of the present study suggest that MPHSD may be an appropriate summary measure for the effect of these factors. It is, therefore, possible to predict repeatability coefficients for various levels of image quality without having to measure the patient's age, degree of media opacity or of astigmatism.

In conclusion, this study indicates that RA consistently demonstrates excellent repeatability and reliability. It may therefore be an appropriate measure when monitoring glaucoma progression. RA repeatability is similar for both the HRT and HRT-II, irrespective of observer or visit. Reference height difference and image quality were found to be the factors which most influenced RA variability. The findings of this study will be used as the basis for suggesting strategies for improving the test-retest variability. Once variability is ameliorated, strategies for monitoring of stereometric parameter progression can be devised and tested.

3.3 Improving the repeatability of HRT and HRT-II rim area measurements

3.3.1 Background

In the previous study (3.2), RA and mean cup depth consistently demonstrated high repeatability and reliability (Strouthidis et al., 2005a). Of the two parameters, RA is the more clinically meaningful and constitutes an appropriate candidate for the monitoring of glaucomatous progression. RA variability was influenced by the inter-test reference height difference and by image quality. RA variability may be improved by the adoption of an alternative to the standard RP and by taking into account image quality. The RP (described in detail in section 2.3.2.4) is located parallel to the retinal surface and delineates structures superior to the plane as 'neuroretinal rim' and inferior as 'cup'. The standard RP is located 50μm posterior to the height of the contour line at the temporal disc margin. The 320μm RP is a fixed, off-set plane located 320μm posterior to a reference ring located in the image periphery. This reference ring is used to define the stable, zero-plane of the topographical image.

3.3.2 Purpose

To devise and test strategies to reduce RA measurement error using a series of longitudinal HRT data in order to assess whether they may be used to improve the detection of stereometric parameter progression.

3.3.3 Methods

3.3.3.1 Test-retest data acquisition

The test-retest subject selection and acquisition protocol have been described in sections 3.2.3.1 and 3.2.3.2, respectively.

3.3.3.2 Image analysis

Heidelberg Eye Explorer (Version 1.7.0; Heidelberg Engineering, Heidelberg, Germany) was used to generate and analyse the mean topographies for both HRT and HRT-II images (HRT Explorer and HRT-II Explorer). In addition the HRT images were analysed using the HRT

'Classic' option on the Explorer platform (which simulates the older DOS software). The default 'standard' RP was applied.

3.3.3.3 Improving repeatability

The test-retest RA values were re-calculated using the 320μm RP. The effect of this RP on RA repeatability, compared with the standard RP, was analysed using Bland-Altman plots (Bland and Altman, 1986). Eyes with poor quality images were then excluded, and repeatability was assessed using only good-quality images (MPHSD < 25).

3.3.3.4 Estimation of measurement error

RC is the method of defining measurement error that has been adopted by the British Standards Institution (1979), and is calculated as:

$$RC = 2 * \left(\sqrt{\frac{\sum (observation1 - observation2)^2}{n(observations)}} \right)$$

where 95% of inter-test differences will be within this error. Subject eyes were classified according to image quality: good-quality (MPHSD < 21), medium-quality (MPHSD 21-35) and poor-quality (MPHSD > 35). The follow-up scenario encountered in a clinical setting was simulated by generating a baseline reference RA value (the mean from two images taken on the same day by a single observer – ETW). A follow-up RA obtained from the image taken on a subsequent day by a different observer (NGS) was then compared to this baseline mean value. An RA RC, derived for images analysed with the 320μm RP, was calculated for each of the three image-quality categories.

3.3.3.5 Longitudinal HRT series - patient selection

The improvement strategies were also tested on a longitudinal data-set in which RA was expected to change over time (unlike the test-retest set where RA is expected to stay constant). The data-set was obtained from a cohort of OHT subjects recruited to take part in a betaxolol *versus* placebo study, the details of which have been described elsewhere (Kamal et al., 2003). The study adhered to the tenets of the Declaration of Helsinki and had local ethical committee approval, as well as subjects' informed consent. These subjects underwent regular HRT imaging, initially at yearly intervals for the first two years of their involvement, and four-monthly subsequently. HRT imaging at this latter frequency was continued until 2001, when imaging was continued using the HRT-II. 30 subjects, identified as converting to

glaucoma based on having developed a consistent AGIS VF score greater than 0 (AGIS, 1994), were selected. The mean age of these subjects was 61.8 years (range 43.4-71.7 years) and the mean number of HRT tests was 11 (range 9-16). Mean length of follow-up was 6.3 years (median 6.2 years, range 4.8 to 7.2 years).

3.3.3.6 Application of 'improved' strategy to longitudinal HRT series

The global RA was calculated for each image in a series using the standard RP. Images of all qualities were included. In a longitudinal image series of approximately 11 images, the exclusion of poorer quality images (e.g. MPHSD > 25) would have resulted in a substantial loss of valuable data. When using the Explorer software, the contour line is drawn around the disc margin of the baseline image and then automatically exported to all follow-up images. The automatic exportation sometimes gives rise to contour line misalignment. This occurs particularly when follow-up images with higher MPHSD values and image magnification differences are included. A novel manual alignment facility has been introduced for the Explorer platform, which adjusts for these anomalies (Figure 3-4). Manual alignment is achieved by selecting a minimum of four common landmarks, such as vessel bifurcations, between the baseline and follow-up images. A flicker chronoscopy, or 'toggle', facility enables the closeness of fit to be assessed prior to accepting the re-alignment.

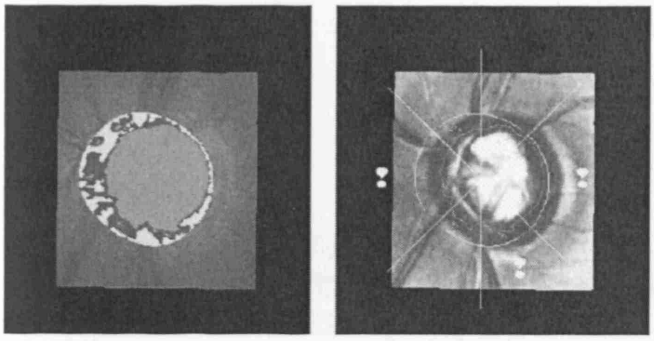

Figure 3-4. An example of a misplaced contour line on a follow-up HRT image in the Explorer software. Manual alignment is achieved by selecting a minimum of four common landmarks between the baseline and follow-up images to attain the best approximation of alignment

The global RA for each image in a series was then re-calculated using the 320µm RP and with manual adjustment when any magnification changes or contour line misplacements were encountered.

Linear regression of global RA over time (in years) was plotted using: (i) standard RP, non-aligned images; (ii) standard RP, aligned images; (iii) 320µm RP, non-aligned images and (iv) 320µm RP, aligned images. The residual standard deviation (RSD) of the linear regression was used to gauge the variability of each image series (Altman, 1980). All statistical analyses were performed using Medcalc Version 7.4.2.0 (Medcalc Software, Mariakerke, Belgium) and SPSS Version 11.5 (SPSS Inc., Chicago, IL, USA).

3.3.4 Results

3.3.4.1 Test-retest data

Bland-Altman plots illustrate the improved HRT Explorer inter-observer/inter-visit RA repeatability obtained when the 320µm RP was used (Figure 3-5B), compared with the standard RP (Figure 3-5A). The distribution was tighter, with narrower limits of agreement, when the 320µm RP was used. Repeatability was further improved when only good-quality images (MPHSD < 25) were used (Figure 3-5C), although this reduced the number of subjects from 74 to 35.

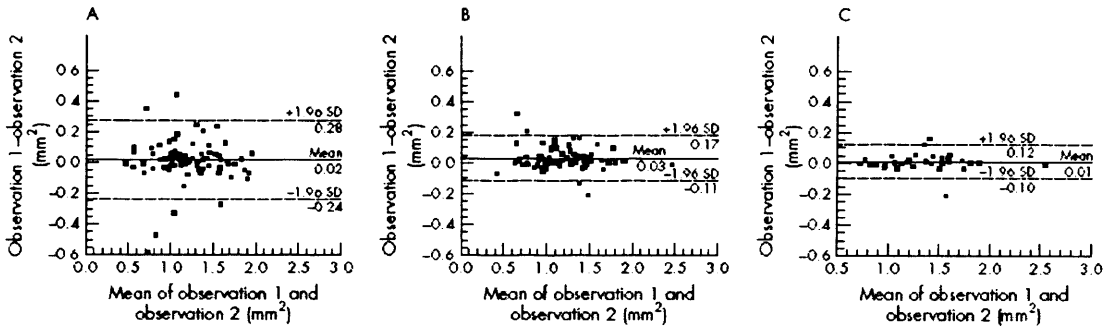

Figure 3-5. Bland-Altman plots of HRT-Explorer inter-observer/inter-visit rim area (mm^2) using the standard reference plane (A), the 320µm reference plane (B) and the 320µm reference plane with inclusion of only good-quality (MPHSD <25) images (C).

The inter-observer/inter-visit RA RC was reduced from 0.24 mm^2 (HRT Classic), 0.26 mm^2 (HRT Explorer) and 0.23 mm^2 (HRT-II Explorer), using the standard RP, to 0.16 mm^2 (HRT Classic), 0.16 mm^2 (HRT Explorer) and 0.20 mm^2 (HRT-II Explorer), using the 320μm RP. This coefficient was further reduced to 0.09 mm^2 (HRT Classic), 0.11 mm^2 (HRT Explorer) and 0.10 mm^2 (HRT-II Explorer) when only good-quality images (MPHSD < 25) were used (Table 3-6).

HRT Type	Strategy	Rim area repeatability coefficient values (mm^2)			
		I	II	III	IV
HRT-Classic	Standard reference plane	0.21	0.29	0.19	0.24
	320μm reference plane	0.10	0.14	0.16	0.16
	320μm reference plane; MPHSD <25	0.04	0.09	0.07	0.09
HRT-Explorer	Standard reference plane	0.28	0.31	0.30	0.26
	320μm reference plane	0.13	0.16	0.16	0.16
	320μm reference plane; MPHSD <25	0.07	0.09	0.09	0.11
HRT II-Explorer	Standard reference plane	0.28	0.34	0.24	0.23
	320μm reference plane	0.17	0.17	0.18	0.20
	320μm reference plane; MPHSD <25	0.08	0.07	0.09	0.10

Table 3-6. Application of different strategies to test-retest data - rim area repeatability for HRT Classic, HRT Explorer and HRT-II Explorer in various test-retest protocol permutations (I = intra-observer/intra-visit; II = inter-observer/intra-visit; III = intra-observer/inter-visit; IV = inter-observer/inter-visit)

3.3.4.1 Measurement error

The measurement error for good-quality images (MPHSD < 21) was similar for all three methods, with a mean RC value of 0.06 mm^2 (Table 3-7).

Image quality	HRT-Classic		HRT-Explorer		HRT-II Explorer	
	No subjects	RC	*No subjects*	RC	*No subjects*	RC
Good-image quality (MPHSD < 21)	28	0.05	28	0.08	38	0.07
Medium-image quality (MPHSD 21-35)	27	0.16	27	0.13	23	0.09
Poor-image quality (MPHSD > 35)	19	0.20	19	0.19	13	0.27

Table 3-7. Interobserver/intervisit rim area repeatability coefficients (mm^2) obtained with different image qualities and using different types of HRT

A step-wise increase in measurement error was first seen with medium-quality images (MPHSD 21–35) and then with poor-quality images (MPHSD > 35). The incremental change of measurement error from good to medium-quality image for the HRT-II was minimal (0.07 to 0.09 mm^2), compared with the HRT (0.05 to 0.16 mm^2, using HRT Classic). By contrast, the measurement error for poorer quality images was larger for the HRT-II compared with the HRT (0.27 and 0.20 mm^2, respectively).

3.3.4.1 Longitudinal analysis

The use of a 320μm RP significantly reduced the magnitude of the residuals compared with those using the standard RP (paired t-test, $p < 0.0001$). There was a further small, but significant, reduction in the residuals when the 320μm RP, manually aligned series was

compared with the automatically aligned 320μm RP series (paired t-test, $p < 0.0001$). The reduction in residuals was small when standard RP images were manually aligned (paired t-test, $p = 0.02$). A mean of four (median 4, range 0-11 images) longitudinal images required manual alignment in each image series. (Table 3-8).

Strategy used for longitudinal image series	**Residual Standard Deviation Values (mm^2)**		
	Mean	Median	Range
Standard reference plane; non-aligned	0.10	0.10	0.01-0.40
Standard reference plane; Aligned	0.09	0.08	0.01-0.40
320μm reference plane; non-aligned	0.05	0.04	0.01-0.10
320μm reference plane; aligned	0.04	0.03	0.01-0.10

Table 3-8. Standard deviations of residuals for longitudinal HRT image series analysed using HRT-Explorer

The scatter plots with regression lines and residuals plots of global RA over time for an example patient (Figure 3-6) illustrate the improvement gained with the 320μm RP and with manual alignment. These plots are from a 71-year-old female subject (left eye) examined over a 6.1 year period with 12 HRT tests. A closer relationship between RA and time was observed with the 320μm RP compared with the standard RP (Figures 3-6A and 3-6B). Further narrowing of the 95% confidence limits of the regression slope was noted when manual

alignment was carried out (Figure 3-6C). The residual differences also narrowed successively when the 320µm RP was used first, followed by manual alignment (Figures 3-6D-F).

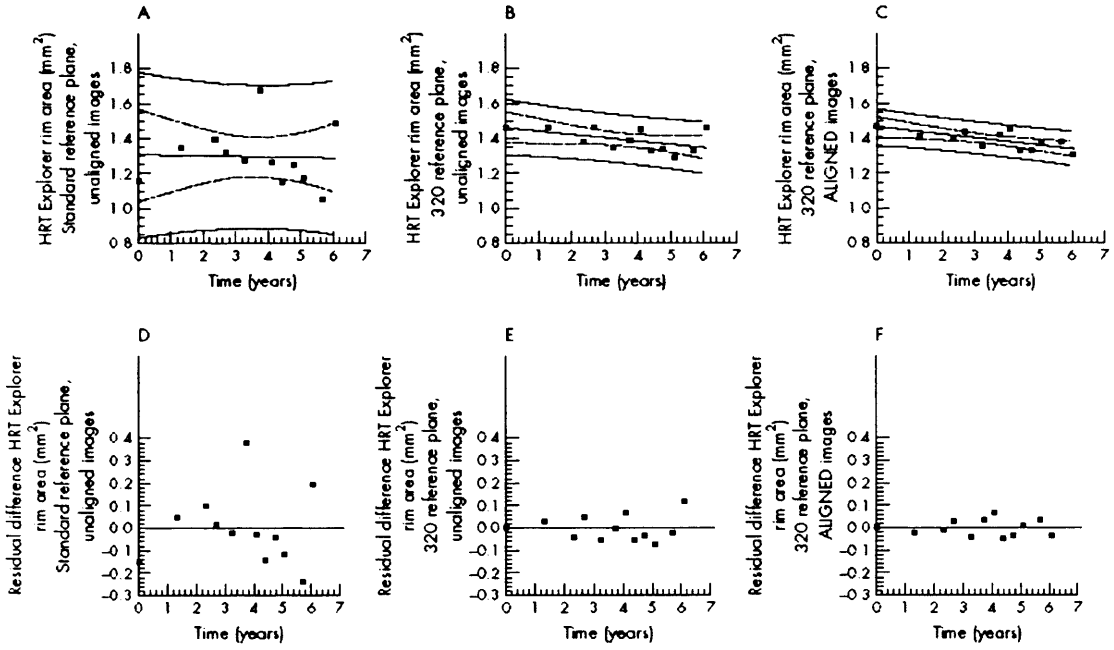

Figure 3-6. Linear regression of HRT-Explorer global rim area over time using the standard reference plane (A), 320µm reference plane (B) and 320µm reference plane with manual alignment (C).In these graphs the solid line represents the regression line, the dashed lines represent the 95% confidence limits and the dotted lines represent the 95% prediction limits. Plots of the residuals from the linear regression analysis are shown in D-F

3.3.5 Discussion

A disadvantage of stereometric parameters is their dependence on the position of the RP. The location of the standard RP was selected on the basis of the mean surface inclination angle of the ONH (Burk et al., 2000), and because it coincides with the papillomacular bundle – a site predicted to be minimally affected until the later stages of glaucoma. This has not been supported by retinal thickness measurements derived using the OCT in glaucoma subjects (Chen et al., 2001). Indeed, the mean retinal nerve fibre layer thickness as estimated by OCT has been used as the landmark for a novel RP which may be useful in the detection of early glaucoma, particularly in tilted optic discs (Park and Caprioli, 2002). The previous study (Section 3.2) (Strouthidis et al., 2005a) has indicated that there is variability in inter-test reference height and therefore in the height of the contour line at the temporal ONH margin. This indicates that the standard RP may change location between successive images, thereby causing variation in RA measurements. In the current study, the 320μm RP results in a reduction in test-retest RA variability. The advantage of the fixed-offset location of the 320μm RP is that it is stable in relation to changes in the disc margin contour line height. This feature helps to explain the improved repeatability in both the test-retest data and the improved repeatability of the longitudinal image series.

The 320μm RP does however have weaknesses, such as underestimation of RA in nerve heads with oblique insertion and overestimation of RA in discs with advanced peripapillary damage, where the height of the reference ring is affected (Burk et al., 2000). These factors are important when differentiating between different stages of the glaucomatous process in a single isolated topography (Tuulonen et al., 1994).

A newer, experimental RP has been described by Tan and Hitchings (2003c). It is intended to have an unchanging height relationship with the ONH in an imaging series. The position of the RP is calculated from a combination of the mean height of the contour line in relation to the reference ring, the contour line's lowest region and the point below the lowest region with the least RA variability. This RP has demonstrated better reproducibility of HRT images compared with the standard and 320μm RP, and has been used in a novel approach to measure glaucomatous change (Tan and Hitchings, 2003c; Tan and Hitchings, 2003d). However, because the RP height is linked to the height of the disc margin contour, it might be

expected to shift posteriorly as glaucoma progresses. The rates of RA change with the various RP options have yet to be compared.

In this study, estimates of inter-observer/inter-visit RA measurement error have been made for different degrees of image quality. These values may be used to establish probability limits for change when comparing RA between two isolated HRT or HRT-II images separated in time. An RA difference exceeding the RC at the appropriate mean image quality can be defined as surpassing a 'threshold' for change, at which glaucomatous change is distinct from measurement noise. These thresholds are used as the basis for the formulation of a novel event analysis technique described in this thesis (Section 3.5).

3.4-3.5 Measuring disc and field progression

3.4 Trend analysis

3.4.1 Background

HRT imaging has been shown to be reproducible and to identify structural changes prior to detection of repeatable VF loss in glaucoma (3.2) (Kamal et al., 1999; Kamal et al., 2000; Tan et al., 2003b; Strouthidis et al., 2005a). This latter observation is consistent with the popularly-held view that structural damage occurs prior to functional loss in glaucoma, although the exact nature of the structure-function relationship has yet to be clarified (Section 2.5.2).

A number of different strategies has been proposed for monitoring VF and HRT progression. These strategies may be broadly categorised as either 'event analyses', whereby progression is defined as the surpassing of a predetermined threshold for change, or 'trend analyses', whereby the behaviour of a measurement is assessed over time. The former approach has been particularly useful in defining VF end-points in large-scale clinical trials (AGIS, 1994; Musch et al., 1999; Heijl et al., 2003). Several event analyses have also been described for monitoring HRT RA change (Kamal et al., 2000; Tan and Hitchings, 2003d). Trend analyses have a useful advantage over event analyses in clinical practice in that, instead of a binary outcome, a rate of change may be estimated. This is particularly useful at the earliest stages of the disease process and in OHT. A measured rate of progression may assist in the assessment of a patient's risk of developing functionally significant visual loss and in the decision to commence or alter treatment.

3.4.2 Purpose

To compare ONH and VF progression in a group of OHT and control subjects followed prospectively as part of a clinical trial. A novel trend analysis of HRT RA progression is described and is compared with established PLR VF techniques. By assessing agreement of structural and functional methods in OHT subjects, it is hoped that insight might be gained into the nature of the structure-function relationship at the earliest stages of the glaucomatous process. Secondarily, by assessing method agreement, this study examines the feasibility of

using a single test (either structural or functional) to monitor progression. For a test to become redundant, an alternative test should provide the investigator with, at a minimum, the same information on progression.

3.4.3 Methods

3.4.3.1 Subject selection

Subjects were selected from a cohort of 255 OHT patients originally recruited to a betaxolol *versus* placebo study which took place at Moorfields Eye Hospital between 1992 and 1997. Eligibility criteria for this study are described in detail elsewhere (Kamal et al., 2003). Briefly, OHT was defined as an IOP > 22 mmHg and < 35mmHg on two or more occasions within a 2-week period, and a baseline mean AGIS (1994) VF score of zero (Humphrey Field Analyzer, full threshold 24-2 program). Subjects had a visual acuity at recruitment of 6/12 or better with no co-existent ocular or neurological disease.

Control subjects were selected from a cohort of 30 subjects who were recruited among senior citizens and retirees, or were the spouses or friends of subjects in the OHT cohort (Kamal et al., 1999). These subjects had a baseline IOP < 21 mmHg and a normal baseline VF test (same criteria as in the OHT group). Control subjects were excluded if there was a family history of glaucoma or any co-existent ocular or neurological pathology.

The same eye was analysed in the current study as had originally been randomised in the betaxolol *versus* placebo study. Briefly, randomisation was stratified according to risk of conversion to glaucoma, based on pattern electro-retinogram testing performed on each subject at recruitment, cup/disc ratio and IOP (Kamal et al., 2003). The choice of control eye was based on simple randomisation. A subject eye was included in the study if five or more of both VF tests and HRT mean topographies were available for the study period.

Subjects in both groups underwent four-monthly VF testing from the time of recruitment until September 2001. ONH imaging with the HRT was introduced into the protocol in 1994. Imaging initially took place at yearly intervals for the first two years of involvement, and subsequently at four monthly intervals until September 2001.

All images and VFs, regardless of quality, were included for analysis; this was done so that a minimum amount of potentially useful data was discarded. The study adhered to the tenets of

the Declaration of Helsinki and had local ethical committee approval, as well as subjects' informed consent.

3.4.3.2 Visual field analysis

PLR of each subject's VF series was performed using PROGRESSOR (Institute of Ophthalmology, London, UK). Two strategies were used to identify progression, one less stringent and the other stringent:

1. *Standard Criteria* – a point is flagged as progressing if it shows a significant negative slope of at least -1 dB/year, with a significance level of $p < 0.01$. This is the most commonly used PLR method in published studies (McNaught et al., 1996; Viswanathan et al., 1997; Nouri-Mahdavi et al., 2005).
2. *3-omitting Criteria* – a point is flagged as progressing if it satisfies the standard criteria in each of three slopes. The first slope is constructed using all time points up to time point *n*, the second slope is constructed omitting point *n* and including the next point in the series (*n + 1*), and the final slope is constructed omitting points *n* and *n + 1* with the inclusion of the next point in the series (*n + 2*). Increased specificity, compared with the standard criteria, has been demonstrated applying the three-omitting criteria to simulated VF data (Gardiner and Crabb, 2002a).

VF series were identified as demonstrating significant improvement using the same two strategies, except with a positive slope direction ($\geq +1$ dB/year).

3.4.3.3 HRT analysis

HRT mean topographies were generated and analysed using Heidelberg Eye Explorer (Version 1.7.0, Heidelberg Engineering GmbH, Dossenheim, Germany). Contour lines were drawn by a single observer (NGS) onto the baseline mean topographies, and these were exported automatically to the subsequent images. A manual alignment facility was used to correct contour line position if the automatically placed contour line was misplaced or if there was a magnification change (Figure 3-4). Where satisfactory contour line position could not be achieved, the mean topography was excluded from the analysis. Eight mean topographies were excluded from analysis, as a result either of a 'double image' being present or if the image was so grainy as to preclude visualisation of Elschnig's ring.

RA measurements were calculated for the six Explorer-defined disc sectors (N, T, SN, ST, IN, IT). RA was selected in favour of other stereometric parameters as it is consistently repeatable and reproducible and constitutes a clinically meaningful parameter (3.2)(Tan et al., 2003b; Strouthidis et al., 2005a). All analyses were performed using the 320μm RP as it results in less RA variability than the Standard RP (3.3)(Tan et al., 2003a; Strouthidis et al., 2005b). Linear regression of sectoral RA over time was performed for each subject's HRT series. The RSD was calculated for each linear regression analysis. 'Residuals' refer to the difference between the values observed and those predicted by the regression equation; RSD may be used to estimate the variability of the series (Altman, 1980). High RSD values equate to high variability and *vice versa* (Figure 3-7).

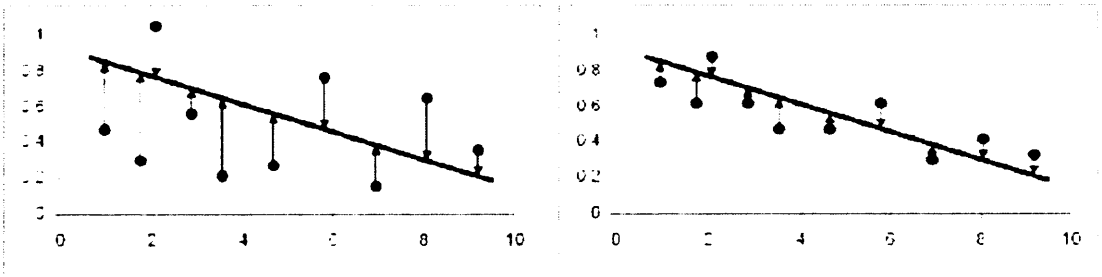

Figure 3-7. Two scatter plots with linear regression slopes constructed using simulated numerical data to demonstrate different levels of variability. *Left:* The graph on the left demonstrates large residuals (arrows), equating to a high residual standard deviation (RSD) and high variability for the series. *Right:* The graph on the right demonstrates much smaller residuals indicating a low RSD and low variability for the series

The RSD values generated were ranked in order of magnitude within each HRT sector. The 50th centile RSD value for each sector was used as a cut-off to define the variability of the subject's HRT series; RSD values less than the 50th centile were defined as having low variability and those greater than the 50th centile as having high variability. The P value at

which a linear regression was considered 'significant' was adjusted according to the RSD value, with tighter significance levels selected for the high RSD series. This approach was adopted to account for the inclusion of all image qualities in the analysis as poorer quality images tend to generate higher RA variability (3.2)(Strouthidis et al., 2005a).

Progression in any disc sector was determined if a slope exceeding -1 % of baseline RA/year was observed, with significant improvement occurring where the slope exceeds +1 %/year. The slope value was selected as it is approximately double the value of age-related RA loss estimated histologically and using cross-sectional HRT data (Johnson et al., 1987; Garway-Heath et al., 1997).

3.4.3.4 Comparing disc and field progression

In the absence of any established independent reference standard for measuring glaucoma progression, the estimated specificity of both tests should be closely matched (or 'anchored') for the comparison between them to be valid. Two proxy measures were used to estimate specificity:

1. Number of subjects progressing in the control cohort
2. Number of subjects (in both the OHT and control cohort) demonstrating significant improvement.

Specificity estimates were made for the PLR standard and 3-omitting criteria. Two HRT progression strategies (a less stringent and a stringent strategy) were devised by adjustment of the significance levels of the regression equation such that the estimated specificities closely matched those of the two PLR VF techniques.

Agreement between VF and RA progression at the end of the study period was assessed in the OHT group with specificity anchored at the two different levels. Where agreement existed, congruity between disc and field sectors was assessed using a map designed to compare the anatomical relationship between VF test points in the Humphrey 24-2 test pattern and regions of the ONH (Figure 2-8).

A further comparison between HRT RA progression and VF progression in the OHT group was made using matched numbers of VF and HRT tests, performed on the same day. This was executed using only the standard PLR criteria, as sufficient data points may not have

been available to perform the confirmatory tests required of the 3-omitting criteria. The 'thinned' standard VF progression was compared against the 'less stringent' HRT criteria. All statistical analyses were performed using Medcalc Version 7.4.2.0 (Medcalc Software, Mariakerke, Belgium).

3.4.4 Results

198 OHT subjects and 21 control subjects were included for analysis in the study. Male:female ratio was 105:93 in the OHT group, compared with 14:7 in the control group. There were 95 right eyes in the OHT group and 11 in the control group. The demographics of subjects in both groups are depicted in Table 3-9.

	OHT	CONTROL
No. of subjects	198	21
Age/years	60 (32-79)	65 (41-77)
Follow-up/years	6.0 (2.3-7.2)	5.3 (3.1-6.8)
No. of HRT exams	10 (5-16)	9 (8-11)
No. of visual field exams	17 (5-33)	9 (7-14)
Baseline mean defect (dB)	+ 0.1 (+ 3.0-2.7)	+ 0.1 (+ 2.6-2.4)
Baseline global rim area (mm^2)	1.24 (0.63-2.31)	1.35 (0.86–2.51)
Image quality (MPHSD)	20 (7-186)	23 (9–80)

Table 3-9. Demographic details of ocular hypertensive and control subjects included in the study. Figures given are median (range)

3.4.4.1 Estimation of specificity

A specificity range of 85.7-95.4% was estimated using standard PLR criteria and 95.2-98.2% using 3-omitting criteria (Table 3-10).

	Standard criteria	3-omitting criteria
No significant improvement	209 /219 = **95.4%**	215 /219 = **98.2%**
95 % confidence interval	91.8-97.5%	95.4-99.3%
No progression in control cohort	18 /21 = **85.7%**	20 /21 = **95.2%**
95 % confidence interval	65.4-95.0%	77.3-99.2%
Specificity estimate	**85.7-95.4%**	**95.2-98.2%**

Table 3-10 Estimation of specificity for visual field point-wise linear regression for both standard and 3-omitting criteria

The specificity estimate for the less stringent HRT progression strategy (significant slope > 1 % /year with significance levels $p < 0.05$ for low variability series and $p < 0.01$ for high variability series) was 88.1-90.5% (Table 3-11.).The specificity estimate for the stringent HRT progression strategy (significant slope > 1 % /year with significance levels $p < 0.001$ for low variability series and $p < 0.0001$ for high variability series) was 95.2-98.2% (Table 3-12).

	Less stringent *	Stringent †
No significant improvement	193 /219 = **88.1%**	215 /219 = **98.2%**
95 % confidence interval	83.2-91.8%	95.4-99.3%
No progression in control cohort	19 /21 = **90.5%**	20 /21 = **95.2%**
95 % confidence interval	71.1-97.4%	77.3-99.2%
Specificity estimates	**88.1-90.5%**	**95.2-98.2%**

Table 3-11. The estimation of specificity for two different HRT progression techniques

* **Slope > 1 % baseline sector RA/year; p < 0.05 for low variability series, p < 0.01 for high variability series**

† **Slope > 1 % baseline sector RA/year; p < 0.001 for low variability series, p < 0.0001 for high variability series**

3.4.4.2 Comparison of disc and field progression

Using the less stringent criteria (specificity for both tests anchored at approximately 90%), there was agreement between HRT and VF for progression 24 subjects within the OHT group. A further 42 subjects progressed by HRT alone compared with 40 by VF alone (Figure 3-8).

Using the stringent criteria (specificity anchored at approximately 97%), 7 subjects within the OHT cohort progressed by both HRT and by VF. A further 17 subjects progressed by HRT alone compared with 30 subjects by VF alone (Figure 3-9).

Of the 24 subjects progressing by disc and field with the less stringent criteria, there was congruity in at least one disc and field sector in 14 subjects (58.3%), compared with seven of seven subjects (100%) when the stringent criteria were applied. There was congruity in four sectors in one subject, in two sectors in four subjects and in one sector in eight subjects using the less stringent criteria. Using the less stringent criteria, congruity was detected in one sector in all seven subjects.

Using an equal number of HRT and VF examinations, performed on the same day (ie 'thinned' VF data), 22 subjects (11.1%) within the OHT cohort progressed by both HRT and

by VF. A further 44 subjects (22.2%) progressed by HRT alone compared with 25 subjects (12.6%) by VF alone.

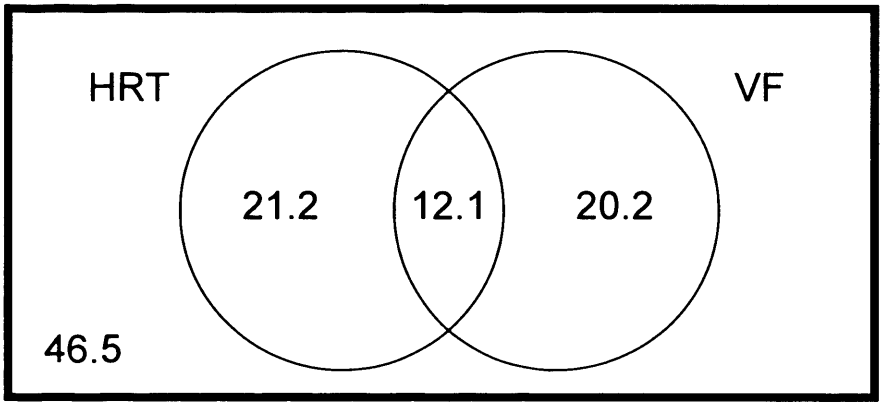

Figure 3-8. Venn diagram comparing HRT and field progression within the OHT cohort, expressed as a percentage of subjects. Specificity of both the HRT progression strategy ('less stringent') and the VF progression strategy ('standard PLR') is anchored at approximately 90%. 46.5% of subjects were not progressing

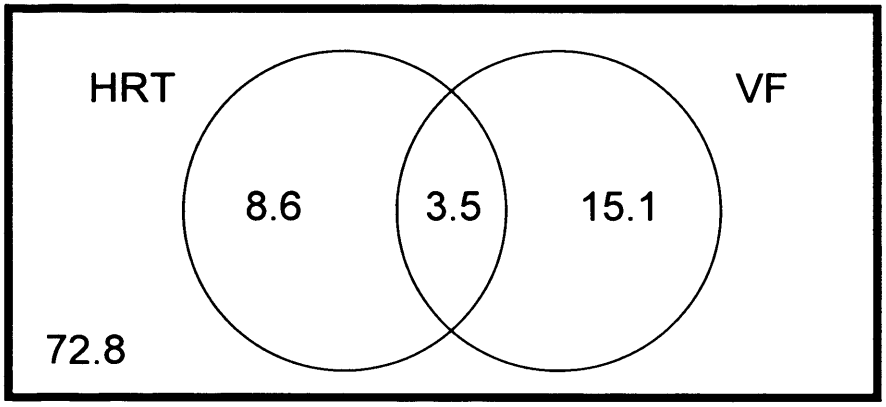

Figure 3-9. Venn diagram comparing HRT and field progression within the OHT cohort, expressed as a percentage of subjects. Specificity of both the HRT progression strategy ('stringent') and the visual field progression strategy ('3-omitting') is anchored at approximately 97%. 72.8% of subjects were not progressing

3.4.4.3 Example patient

Subject 9 was male, aged 58 years and was followed up for 6.5 years; the left eye was analysed. He underwent 15 VF examinations (baseline MD, -1.17 dB) and 11 HRT examinations (baseline global RA, 1.27 mm^2). The range of MPHSD values was 13-26, median 20. Figure 3-10 depicts the HRT mean topographies at baseline and at the conclusion of the study. Scatter plots show significant decay of sectoral RA over time (less stringent criteria). The following slopes of RA/time were generated: ST sector - 3.8 %/year ($p = 0.005$, $R^2 = 0.6$), IT sector - 3.8 %/year ($p < 0.0001$, $R^2 = 0.9$), SN sector - 3.9 %/year ($p < 0.0001$, $R^2 = 0.9$) and IN sector - 5.0 %/year ($p = 0.003$, $R^2 = 0.6$). Within the final VF grey-scale, points progressing by standard PLR criteria are highlighted. There was complete congruity between the four disc and field sectors identified as progressing.

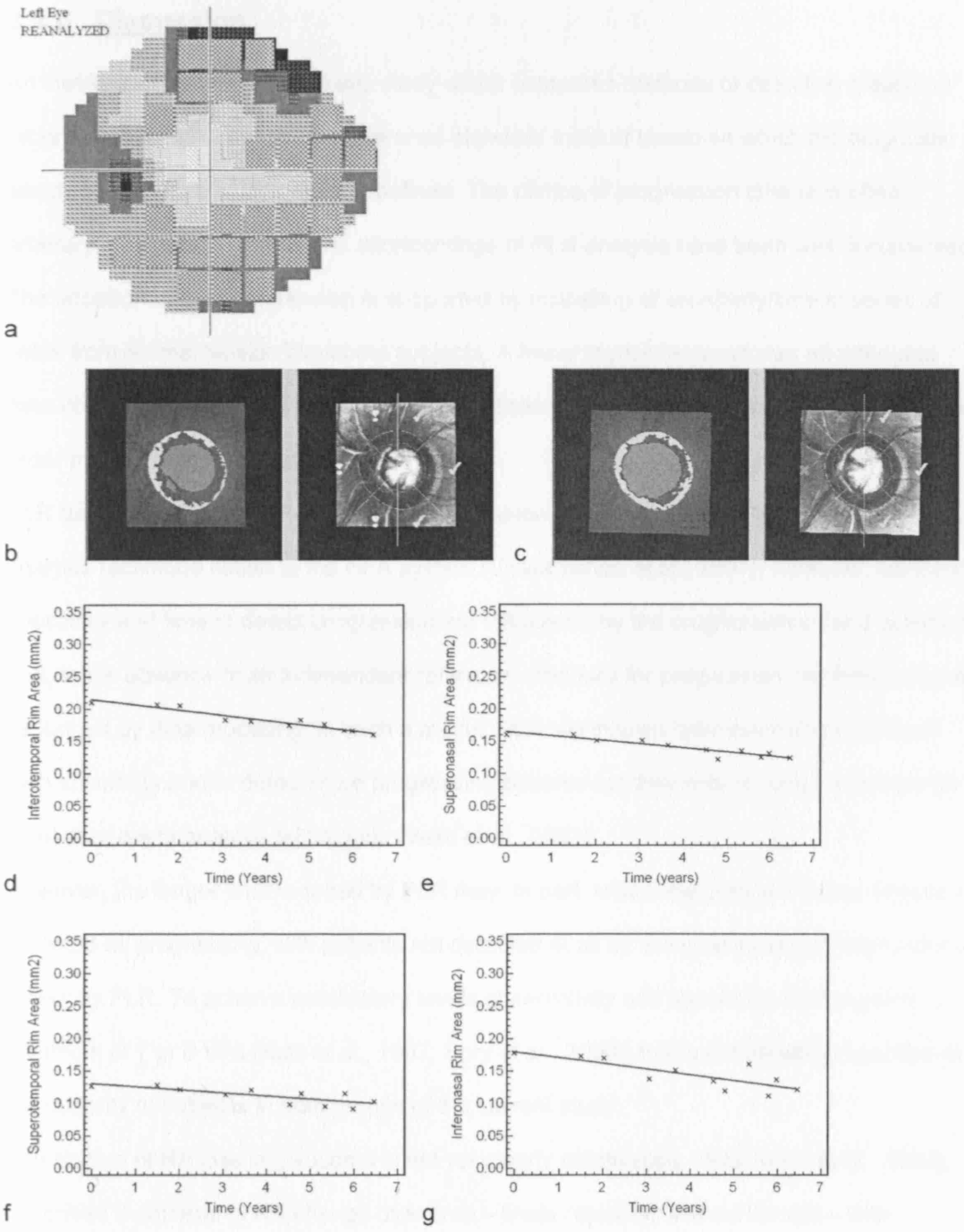

Figure 3-10. Disc and field progression in subject 9 (a) Visual field grey-scale at the conclusion of the study; the hatched squares indicate the test-points flagged as progressing using the standard point-wise linear regression criteria; (b) baseline mean topography; (c) mean topography at the conclusion of the study period. The graphs labelled (d) to (g) are scatter plots with regression line for sectoral rim area against time

3.4.5 Discussion

An inevitable shortcoming with any study which compares methods of detecting glaucoma progression is the absence of a reference standard method based on which the diagnostic accuracy of the tests used may be defined. The choice of progression criteria is often arbitrary. The relative merits and shortcomings of PLR analysis have been well documented. The adoption of linear regression is supported by modelling of sensitivity/time in series of fields from normal tension glaucoma subjects. A linear model demonstrates an adequate data-fit and also generates more accurate prediction of future perimetric change than higher-order models (McNaught et al., 1995).

PLR using PROGRESSOR may detect progression earlier than STATPAC 2, an event analysis technique native to the HFA system (Viswanathan et al., 1997). However, sensitivity, specificity and time to detect progression are influenced by the progression criteria selected and, in the absence of an independent reference standard for progression, performance may be judged by data modelling. In such a model, PLR techniques have been shown to have high specificity and to detect more progressing patients but they may require more tests (or time) than event analysis techniques (Vesti et al., 2003).

However, the longer time required by PLR may, in part, reflect the greater number of patients detected as progressing, with patients not detected at all by 'event analyses' taking longer to detect by PLR. To achieve satisfactory levels of sensitivity and specificity, PLR requires a minimum of 7 or 8 VFs (Katz et al., 1997; Spry et al., 2000); this is comfortably exceeded in the majority of subjects in both groups of the current study.

The pattern of RA loss in glaucoma is not yet clearly established. (Airaksinen et al., 1992), described 3 patterns of RA change over time – linear, episodic and curvilinear – with approximately half of both OHT and glaucoma subjects demonstrating a linear decay. This observation supports the adoption of a linear model to detect HRT RA progression, although linear regression may miss some episodic change, particularly if it occurs in a highly variable series. In addition, it should be appreciated that measurement noise may mimic stepwise and non-linear change. As with PLR, detection of progression is improved with a greater amount of data included in the analysis. In this study, there were fewer HRT examinations, compared with VF examinations, in the OHT group, due to less frequent HRT imaging. Some subjects

have a particularly high number of VF examinations as VF 'conversion' was the study end-point. These subjects were tested intensively over 3-month periods when VF 'conversion' was suspected. This may introduce some bias favouring the detection of VF progression, as subjects deemed to have converted to glaucoma within the original study have a greater number of VF examinations relative to HRT examinations. This has been confirmed by repeating the comparison using a matched number of HRT and VF examinations. This resulted in a much lower detection rate by VF (12.6% compared to 20.2%), although it had very little effect on the level of agreement as regards progression status (11.1% compared to 12.1%). A much higher detection rate of progression by VF was observed in this study compared to previously published reports with similar length of follow-up (Gordon et al., 2002; Miglior et al., 2005); this is most likely a reflection of the use of linear regression-based techniques which have been shown to have higher detection rates than event-analysis techniques when sufficient data and length of follow-up are available (Vesti et al., 2003). In addition, as optic disc appearance was not an entry criterion for the study, there may have been more OHT subjects in the present study with early glaucomatous damage than there were in the similar studies. High rates of structural progression may be explained by the detection method. Analysis of structural progression in the present study was a quantitative analysis of CSLO images, which has been shown in a primate model of glaucoma to be more sensitive than the subjective evaluation of stereo ONH photographs (Ervin et al., 2002).

The estimation of specificity in this study was derived from proxy measures based on two assumptions. Firstly, significant RA and DLS improvement over time should not occur. Secondly, RA and DLS loss at a much greater rate than the age-related estimate should not be observed in control subjects. One may argue that these assumptions are not wholly valid. VF sensitivity may improve because of a learning effect. However, significant learning effects are unlikely in this study because it was required that subjects had reproducibly normal and reliable VFs at baseline (Kamal et al., 2003). When using TCA to monitor HRT progression, positive topographical changes may be seen when there are also areas of topographic depression (Chauhan et al., 2000). However, isolated 'improvement' is rare. It is uncertain whether such changes exert any sustained influence over the longitudinal RA trend in a given sector. Both RA and VF sensitivity probably decline with ageing. Our rate criteria were set to

be higher than average (estimated) rates, but individuals are likely to age at different rates, so it is possible that some true, age-related, change was detected. Thus, our estimates of specificity may, in fact, constitute an underestimation of true specificity.

The specificity estimates relate to the analysis performed in this study, with progression rates calculated only at the end of the observation period. Were the same criteria applied in the clinical setting, lower specificity would result because the clinician analyses data for progression at each patient visit, rather than at the end of a specified period. The result is reduced specificity from 'multiple testing'.

In this study there was poor agreement between ONH progression and VF progression in OHT subjects, regardless of the specificity of the progression criteria applied. A similar result was reported in a group of subjects with established glaucomatous VF loss followed longitudinally (Artes and Chauhan, 2005). In that study, event- and trend-based progression analysis methods were assessed using SAP, high-pass resolution perimetry and HRT. For the trend-based analysis, agreement between all three tests was observed in 2.4 to 7.1% of subjects, depending on the stringency of the criteria. This closely matches the results of the current study, with agreement for progression of 3.5 to 10.6%. The results of these 2 studies suggest that poor agreement is seen regardless of the stage of disease and criteria for monitoring progression. One may therefore conclude that, as both VF and HRT testing are providing additive information on progression, the 2 cannot be used interchangeably. Therefore a single test, either of structure or of function, is not yet sufficient for monitoring glaucoma progression in isolation.

Structural damage and loss of visual function are both features of glaucoma. There is a popularly held view that structural changes are detectable prior to functional changes in progressive glaucoma using currently available techniques. Some structural changes may occur without concomitant changes in function. This theory was expounded by (Fuchs, 1916), and has been supported more recently by descriptions of lamina bowing and astrocytic remodelling in experimental glaucoma work (Hayreh et al., 1999a; Hernandez et al., 2000). Another possibility is that functional loss may occur without concomitant structural alteration; electrophysiological evidence of IOP-mediated ganglion cell dysfunction in primate retina has recently been described (Weber and Harman, 2005). An explanation for the high frequency of

detected VF progression in the present study, in the absence of concomitant identifiable structural progression in many eyes, is that a 'functional reserve' may have been expended prior to the time of entering into the study. This may be pertinent, as the appearance of the ONH was not taken into account at the time of recruitment. However, this theory is not supported by the results of (Artes and Chauhan, 2005), where a similarly poor level of agreement was observed in subjects with established glaucoma. A recent study, also at odds with the view that structural damage precedes functional damage, has demonstrated evidence of electrophysiological changes detectable prior to structural changes in OHT subjects (Parisi et al., 2006).

A likely explanation for the apparent structure-function dissociation lies in measurement variability. Even if disc and VF progression rates were identical, differences in measurement noise between the two testing modalities may result in progression being detected by one modality, but not the other.

By taking steps to 'tailor' the HRT progression criteria according to RA variability, the effect of differing image qualities and measurement 'noise' on false-positive progression detection has been reduced. This has not been possible for the VF analysis, primarily because there is no satisfactory metric with which to measure visual field reliability (Bengtsson, 2000; Henson et al., 2000). The issue of VF variability over time is a complex one, particularly as variability increases in areas of established depressed sensitivity (Heijl et al., 1989a; Chauhan et al., 1993), and is beyond the scope of the current study.

It is possible that improved agreement may be observed with further refinement of imaging and visual function tests and data analysis techniques. Machine-learning classifiers, both supervised and unsupervised, may prove useful in detecting true progression from measurement noise (Sample et al., 2005; Tucker et al., 2005). Monitoring topographic changes with a recently-described technique, SIM, may be more useful than monitoring stereometric parameters (Patterson et al., 2005). The adoption of VF spatial filtering techniques may also ameliorate our ability to discriminate perimetric progression (3.7). However, until these developments are fully tested and validated, the results of this study indicate that both structural and functional tests should be monitored to identify progression in OHT subjects.

3.5 Event analysis

3.5.1 Background

The ability to discriminate true change, over and beyond measurement variability, is recognised as a central requirement of any progression technique. Event analyses identify progression when a measurement exceeds a predetermined threshold for change (or an 'event'); it is assumed that any change below threshold represents measurement variability and changes above threshold represent true disease change.

A robust estimate of RA measurement precision is necessary to define a threshold for glaucomatous change. The British Standards Institution (1979) defines measurement precision according to RC, whereby 95% of inter-test differences are expected to lie within this range. RC values for global RA at different levels of HRT image quality, as measured by MPHSD, have been calculated (3.3)(Strouthidis et al., 2005b). As a strategy for monitoring glaucomatous progression, it is likely that global RA will not identify focal RA changes. A more suitable approach would therefore be to estimate RC values for RA sectors.

3.5.2 Purpose

To describe a novel HRT event analysis developed using RC values derived from inter-observer/inter-visit sectoral RA measurements (3.3)(Strouthidis et al., 2005b). The new technique is applied to longitudinal HRT data collected from OHT and control subjects – specificity and progression rates are estimated. The HRT event analysis is also compared to an established VF event analysis, an RA trend analysis and a VF trend analysis, applied to the same longitudinal data-set.

3.5.3 Methods

3.5.3.1 Defining thresholds for change

The subject selection and test-retest acquisition protocol have been described fully in sections 3.2.3.1 and 3.2.3.2. Single topographies acquired using the HRT were imported into Heidelberg Eye Explorer (Version 1.7.0; Heidelberg Engineering GmbH, Heidelberg, Germany); the 320μm reference plane was adopted throughout the study. Explorer defines 6

RA sectors – ST, IT, T, SN, IN and N. In order to simulate the situation likely to be encountered in a clinical setting, the RC values for inter-observer/inter-visit sectoral RA were calculated, as per section 3.3.3.4. A baseline reference sectoral RA value (observation 1) was generated from the mean of two images taken on the same day by a single observer (ETW). The follow-up sectoral RA (observation 2) was acquired from an image taken on a subsequent day by a different observer (NGS). RC was calculated as:

$$RC = 2 * \left(\sqrt{\frac{\sum (observation1 - observation2)^2}{n(observations)}} \right)$$

As per section 3.3.3.4, subject eyes were classified according to image quality: good-quality (mean MPHSD < 21), medium-quality (mean MPHSD 21-35) and poor-quality (mean MPHSD > 35). RC values were calculated for each of the six HRT sectors at each level of image quality.

3.5.3.2 Defining the novel event analysis

The RC values generated equate to estimates of inter-observer/inter-visit sectoral RA repeatability, whereby 95% of differences between repeated sectoral RA measurements will be within the RC value. An inter-test difference that exceeds the RC threshold is suggestive of change due to causes other than measurement error, such as genuine disease progression. Calling progression when the RC is exceeded on just one occasion is liable to result in a high false positive rate over a long series of images, primarily because the change analysis is applied repeatedly over time (there is a 5% chance of erroneously identifying change at each visit). Schulzer (Schulzer et al., 1991; Schulzer, 1994) has indicated that the false positive rate, and therefore specificity, may be increased by including additional confirmatory tests or by raising the threshold for change.

As the RC values are pre-defined according to image quality, the threshold for change identification may be raised by increasing the number of disc sectors required to satisfy the progression criteria and by requiring change confirmation. The requirement for both spatial and temporal criteria to confirm progression has parallels with GPA. GPA confirms progression when deterioration beyond the 5th percentile of test-retest variability is observed at three test locations on three consecutive tests (Artes et al., 2005).

The following event analysis strategies were tested in this study:

1) Two of three criteria in one or more disc sector (EA1)

Progression is suggested if:

Follow-up - Baseline sector RA (sector RA difference) > sector RC for the level of image quality, with image quality defined as the mean MPHSD ((baseline + follow-up MPHSD)/2).

Progression is confirmed if:

Sector RA difference > RC in at least one of the next two consecutive follow-up images, in one or more sectors.

2) Two of three criteria in two or more disc sectors (EA2)

As for the previous strategy, except change is required in two or more disc sectors.

3) Three of three criteria in one or more disc sector (EA3)

Progression is suggested if:

Follow-up - Baseline sector RA > sector RC for the level of image quality.

Progression is confirmed if:

Sector RA difference > RC in the next two consecutive follow-up images, in one or more sectors.

4) Three of three criteria in two or more disc sectors (EA4)

As for the previous strategy, except change is required in two or more disc sectors.

Significant improvement for all four strategies is identified if an increase in sectoral RA occurs from baseline to follow-up image, and the difference exceeds the RC value of that sector for the level of image quality.

3.5.2.3 Testing the novel event analysis

Strategies EA1-4 were applied to longitudinal HRT images acquired from a cohort of 198 OHT subjects and 21 control subjects, described in section 3.4.3.1 and in Table 3-9.

HRT mean topographies were generated and analysed using Heidelberg Eye Explorer (Version 1.7.0, Heidelberg Engineering GmbH, Heidelberg, Germany). The 320μm RP was used for all analyses. Contour lines were drawn by a single observer (NGS) onto the baseline mean topographies and were exported automatically to the subsequent images. A manual alignment facility was used to correct contour line position if the automatically placed contour

line was misplaced, or if there was a magnification change (Figure 3-4). A minimum of five HRT mean topographies was available for each subject, with images of all qualities selected for analysis except where satisfactory contour line alignment could not be achieved. In total, eight mean topographies were excluded from the study, either as a result of 'double imaging' or if the image was so grainy as to prevent adequate visualization of Elschnig's ring. For each longitudinal series, the baseline image was taken as the first mean topography available for each subject; the baseline VF was taken as the test which coincided with the baseline HRT mean topography. When HRT testing was introduced to the betaxolol *versus* placebo study, imaging took place at yearly intervals. It was, therefore, not possible to construct a mean baseline image from two mean topography images. This is in contrast with the calculation of the EA thresholds for change where two images acquired on the same day are utilised to generate a mean baseline image.

Specificity (1 - false positives) was estimated for EA1-4 using two proxy measures; the number of control subjects (of 21) progressing and the number of subjects (of 219) demonstrating significant improvement. The number of OHT subjects identified as progressing ('positive hit rate') was also compared for the four strategies.

3.5.3.4 Comparison with other progression strategies

As part of the ongoing examination of subjects recruited to the betaxolol *versus* placebo study, subjects underwent full-threshold 24-2 Humphrey VF testing at approximately 4 monthly intervals. AGIS VF scoring was performed for each subject's VF series (AGIS, 1994). VF progression was identified if the AGIS VF score increased from 0 to 1 or more and which was reproducible in three consecutive VF tests in the same region of the VF. A glaucoma expert independently confirmed VF series that were identified as progressing. Previous studies have estimated the specificity of the AGIS VF strategy, an event analysis, at between 91-100 % (Vesti et al., 2003; Mayama et al., 2004; Zahari et al., 2006).

Agreement with regard to progression status was assessed for the two event analyses (HRT and VF), using the HRT technique with an estimated specificity closely approximating that of the AGIS VF criteria. Time to identified progression was also compared; this was taken as the date of the final confirmatory test.

The 'high stringency' HRT trend analysis and 3-omitting PLR VF criterion both achieved specificity estimates of 95.2-98.2 %, using the same longitudinal data (Section 3.4.4.1)(Strouthidis et al., 2006a). Agreement with regard to progression status was assessed for these two trend analyses, the AGIS VF strategy and the novel HRT event analysis. In order to validate the comparison between the four progression criteria, the estimated specificity for each needed to be matched; an HRT event analysis strategy with specificity approaching 95% was therefore selected.

The study adhered to the tenets of the Declaration of Helsinki and had local ethical committee approval, in addition to subjects' informed consent. All statistical analyses were performed using Medcalc Version 7.4.2.0 (Medcalc Software, Mariakerke, Belgium).

3.5.4 Results

The thresholds for change, identified by calculating inter-observer / inter-visit RA RCs, are summarised in Table 3-12.

Rim Area Repeatability Coefficients	T	N	ST	IT	SN	IN
Good Image Quality (MPHSD < 21)	0.054 (0.050)	0.016 (0.014)	0.013 (0.012)	0.028 (0.026)	0.007 (0.008)	0.006 (0.007)
Medium Image Quality (MPHSD 21 – 35)	0.042 (0.058)	0.030 (0.031)	0.022 (0.026)	0.023 (0.026)	0.021 (0.022)	0.014 (0.015)
Poor Image Quality (MPHSD > 35)	0.096 (0.109)	0.079 (0.068)	0.047 (0.057)	0.042 (0.046)	0.042 (0.049)	0.029 (0.029)

Table 3-12. Repeatability coefficients for interobserver / intervisit sectoral rim area measurements (mm^2). Baseline rim area has been calculated using two images acquired on the same day by the same observer. Figures in parentheses are for repeatability coefficients calculated using only a single image to derive the baseline rim area. Repeatability coefficients are stratified according to HRT image quality, measured by mean pixel height standard deviation

The RC values for 'good quality' images were higher than those of 'medium quality' images in the T and the IT disc sectors. For the purposes of the event analyses, the RC value for the good quality images (0.054 in T sector, 0.028 in IT sector), were adopted as the threshold for change for both good and medium quality images in that sector. The baseline RA values used to define the thresholds for change are generated from the mean of two HRT images acquired by the same observer at the same visit; the figures in parentheses in Table 3-12 represent the RCs generated when RA values from a single baseline HRT image were used. In general 'single image' baseline RA values generated slightly higher RCs for medium and poor quality images and slightly lower RCs for good quality images compared with the 'two image' baseline. The estimated specificities for EA1-4 are summarised in Table 3-13.

Event Analysis	**EAI**	**EA2**	**EA3**	**EA4**
Subjects without significant improvement	191 /219 = **87.2%**	206 /219 = **94.1%**	199 /219 = **91.0%**	217 /219 = **99.1%**
95% Confidence Limits	82.1-91.0%	90.1-96.5%	86.3-94.0%	96.7-99.7%
Controls without progression	18 /21 = **85.7%**	20 /21 = **95.2%**	19 /21 = **90.5%**	21 /21 = **100%**
95% Confidence Limits	65.4-95.0 %	77.3-99.1%	71.1-97.3%	84.5-100%
Specificity Estimate	**85.7-87.2-%**	**94.1-95.2 %**	**90.5-91.0%**	**99.1-100%**

Table 3-13. Estimation of specificity for four novel HRT event analysis strategies

EA1, 2, 3 and 4 identified 89 (45%), 56 (28%), 59 (30%) and 34 (17%) OHT subjects, respectively, as progressing at the end of the study period. EA2 achieved a specificity estimate of approximately 95%; this strategy was therefore selected for the comparison with AGIS VF criteria and with the HRT and VF trend analyses.

Comparing EA2 with AGIS VF criteria, 24 OHT subjects were identified as progressing by both disc and by VF. A further 32 OHT subjects progressed by HRT alone and 19 by VF alone (Figure 3-11.). The age, MD, global RA at baseline and MPHSD throughout the series

for subjects progressing by HRT alone or by VF alone are summarised in table 3-14. There was a significant difference in baseline MD (p = 0.02, unpaired t-test) and MPHSD throughout the series (p = 0.0001, unpaired t-test) between the two groups, with those progressing by HRT alone having better image quality and more positive MD. The median time to detection of progression in the OHT group was 3.2 years (range 1.2-5.5 years) using EA2 and 3.6 years (range 1.0-7.2 years) using AGIS VF criteria. The time to identification of progression in the OHT cohort, using the 2 strategies, is compared in the Kaplan-Meier survival curve shown in Figure 3-12.

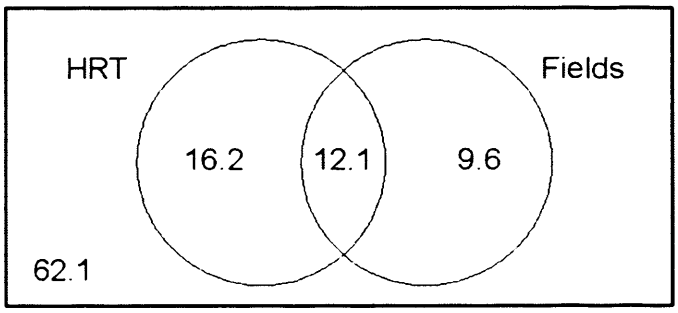

Figure 3-11. Venn diagram comparing HRT progression (2 of 3, in 2 or more sectors, strategy) and AGIS visual field progression in the OHT cohort, expressed as a percentage of subjects (estimated specificity is 95%)

Ocular Hypertensive Subjects' Characteristics	HRT - EA2	VF – AGIS	p VALUES†
Baseline age (years)	63.0 (45.4-78.9)	69.9 (41.0-74.1)	0.23
Image quality throughout study (MPHSD*)	18 (8-186)	30 (9-114)	< 0.0001
Baseline global Rim Area (mm^2)	1.1 (0.8-1.6)	1.2 (0.6-2.1)	0.17
Baseline Mean Deviation (dB)	0.4 (-1.9-+ 2.9)	-0.2 (-1.5-+ 2.4)	0.02

†Unpaired t-test

Table 3-14. Characteristics of subjects progressing by optic disc alone (HRT - EA2) and by visual field alone (VF - AGIS). Values given are median (range)

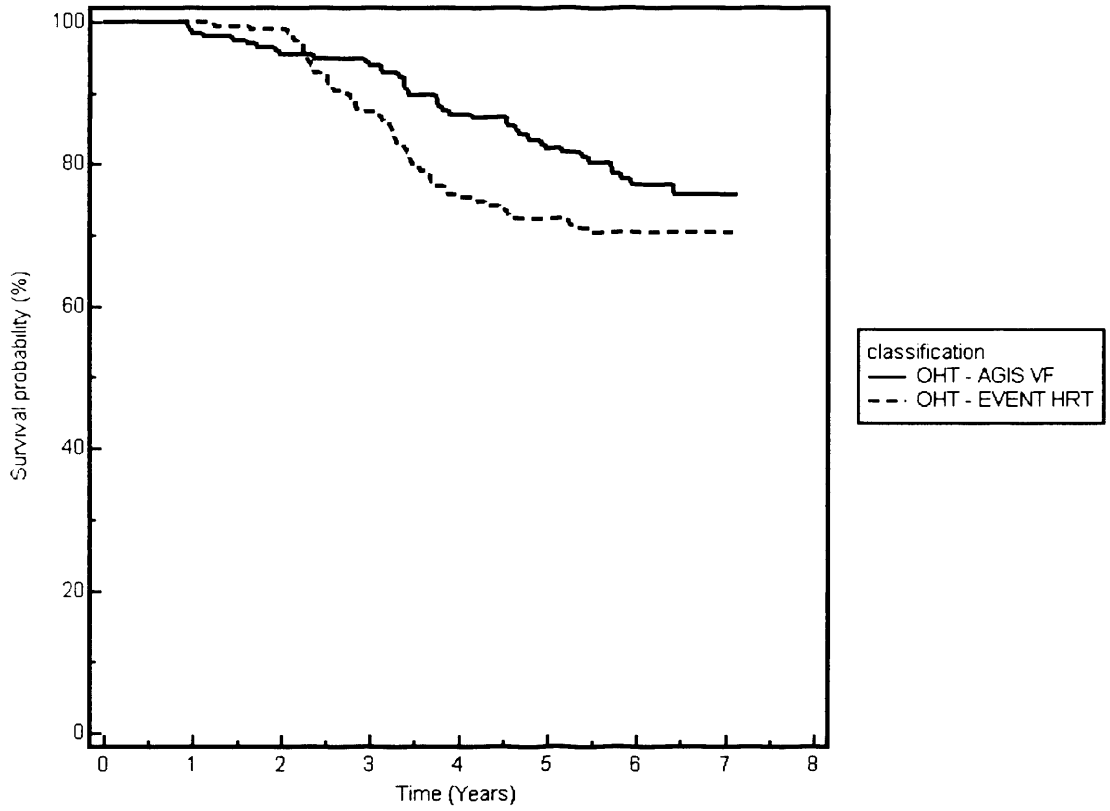

Figure 3-12. Kaplan-Meier survival curve comparing time to detection of progression in the OHT cohort using the HRT event analysis, EA2 (2 of 3 in 2 or more sectors), and AGIS visual field criteria

Comparing EA2 with the 'high stringency' RA trend analysis (slope > 1 % baseline sector RA/year; $p < 0.001$ for low variability series, $p < 0.0001$ for high variability series) within the OHT cohort, 19 subjects (9.6%) had progressed by both strategies at the end of the study period. A further 37 subjects (18.7%) progressed by EA2 alone and a further 5 subjects (2.5%) progressed by HRT trend analysis alone. Comparing AGIS VF criteria and 3-omitting PLR in the OHT cohort, 26 subjects progressed by both strategies, 17 subjects progressed by AGIS criteria alone and 11 subjects progressed by 3-omitting alone. Five subjects progressed by all four techniques. The number of OHT subjects identified as progressing by each technique at the end of the study is compared in Figure 3-13.

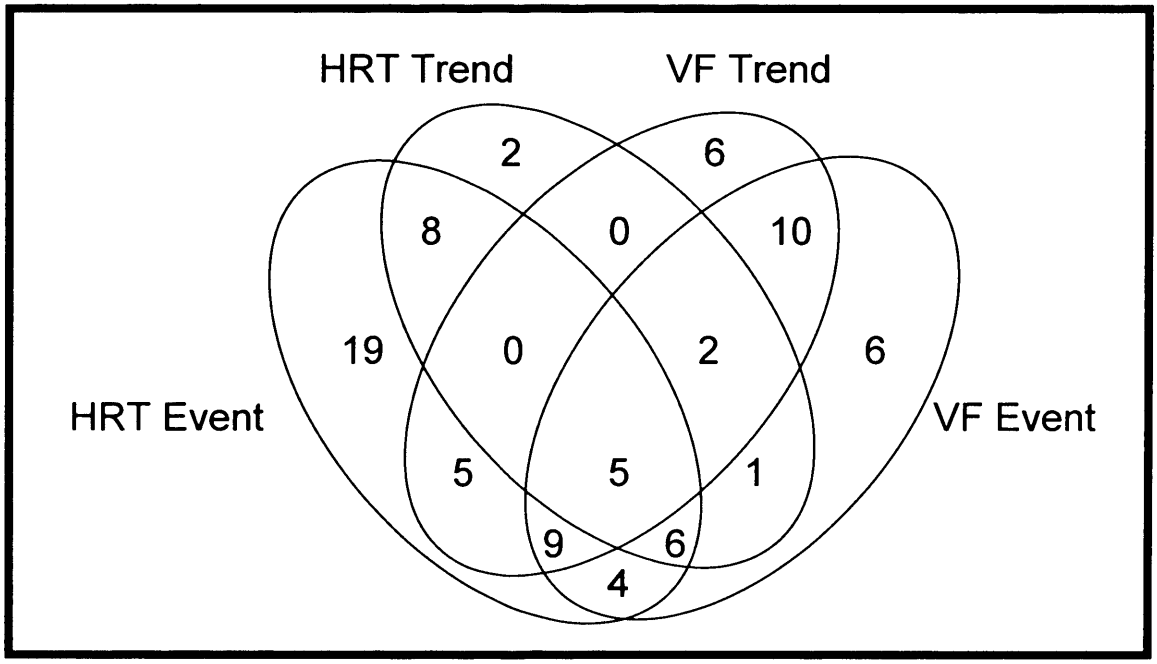

Figure 3-13. Venn diagram comparing the number of ocular hypertensive subjects identified as progressing at the end of the study period by four progression strategies; HRT Event Analysis – 2 of 3 in 2 or more sectors (EA2), VF Event Analysis – AGIS visual field criteria, HRT Trend Analysis – Slope > 1% baseline sector RA/year; $p < 0.001$ for low variability series, $p < 0.0001$ for high variability series, VF Trend Analysis – 3-omitting pointwise linear regression of sensitivity / time.

The specificity for the four techniques is matched at approximately 95%

3.5.5 Discussion

The ideal attributes for any strategy implemented for the detection of glaucomatous progression are high sensitivity, high specificity, the ability to detect progression early and resistance to high levels of measurement variability. Kamal et al., (1999; 2000) estimated normal RA variability by deriving 95% confidence limits for change from RA differences measured in sequential HRT images acquired from control subjects. In terms of defining a threshold for change, this method does not take into account the variation in inter-individual measurement error (images from some eyes are more variable than others). Tan and Hitchings (2004a; 2003d) avoided this problem by deriving limits for RA change for each eye from the single topography images acquired at each visit in a longitudinal series. Using the same 'two of three' confirmatory strategy used in EA2, Tan reported a 'sensitivity' (identified HRT progression in those meeting the AGIS VF criteria for progression) of 85% and a specificity of 95%. A comparable figure in this study is 56%. It should be noted that an experimental RP was adopted in the application of Tan's progression strategy and not the 320μm RP which was used in the HRT progression strategies used in the current study (Tan and Hitchings, 2003d). A major drawback of the 'limits of variability' strategy is that single topography measures are not readily available on current Explorer software (both for the HRT-II and, more recently, for the HRT-III); it is therefore not yet possible to estimate the variability limits for RA change in this context. The current study estimates RA measurement error from repeated acquisitions from a cohort of OHT subjects and a cohort of glaucoma subjects. The recruitment of subjects for the test-retest study was artificially 'enriched' by including the eye with greater lenticular opacity compared to its fellow (3.2)(Strouthidis et al., 2005a). This was done to ensure a wide degree of measurement variability. The subjects recruited were also highly variable in terms of their stage of disease and included those with pre-perimetric/early glaucoma, advanced glaucoma, and OHT subjects with no glaucomatous features. An advantage of the test-retest data-set is that it was repeated using the HRT-II. Thresholds for change are therefore accessible for images acquired using the newer device. Similarly, thresholds can be calculated for HRT-II acquisitions analysed using the HRT-III software in which a new image alignment algorithm operates. A potential weakness is that the

test-retest data may not be equally applicable to other populations with different racial and physiological characteristics.

A unique element in the novel event analysis is the stratification according to image quality. Although it is not clear whether MPHSD truly equates to a subjective appreciation of image quality, it is a measure of variability (of pixel height) and has been shown to influence RA variability (3.2)(Dreher et al., 1991; Strouthidis et al., 2005a). Applying differing thresholds for change according to image quality (MPHSD) should result in minimisation of false positive progression. Estimated specificity in this study was increased by two techniques: firstly by increasing the number of confirmatory images and secondly by requiring change in more than one disc sector. A potential weakness of the latter strategy is that it may result in a diminution of spatial resolution. The T and N HRT sectors have the highest RC values, regardless of image quality. Fluctuation in reference height has more impact upon RA variability in the temporal portion of the rim, resulting in the greater degree of 'noise' in this sector, because the temporal neuroretinal rim has a gentler contour than other disc sectors. In less steep portions of the disc small changes in reference height results in greater changes in RA magnitude. This effect was observed despite the use of the more stable 320μm RP. This may be particularly prevalent in discs with oblique insertion into the globe. Greater RA variability at the N sector is likely to be a manifestation of the distribution of larger blood vessels in that sector. The position and size of blood vessels will vary according to the patient's pulse, blood pressure and fixation – factors unlikely to be constant between image acquisitions. As a greater proportion of larger blood vessels are located in the N sector, RA measurements are likely to be more variable than in sectors with fewer blood vessels.

In comparing structural and functional progression, the choice of VF event analysis was pragmatic. In the absence of a method for external verification, there is no optimal single VF progression strategy. AGIS VF scoring was part of the protocol of the betaxolol *versus* placebo study and this was continued after the completion of the study in 1998, until the conclusion of the current study. Shortcomings of the AGIS VF criteria compared to other VF event analyses are emphasised in the literature. These include high rates of 'reversal' – a lack of maintained progression status (Katz, 1999a; Nouri-Mahdavi et al., 2005), and being excessively conservative, with similar specificity but lower detection rates than CIGTS VF

criteria (Vesti et al., 2003). The VF event analysis used in EMGT examines changes in the pattern deviation (Heijl et al., 2003). This technique is utilised in GPA – the native progression algorithm for the HFA-2. This technique may screen out field loss due to cataract; pattern deviation strategies have relatively poor agreement with total deviation-based strategies (Katz et al., 1997). A recent report has suggested, however, that pattern deviation systems may underestimate VF progression in the absence of increasing media opacity (Artes et al., 2005). At present, it is not possible to apply the commercially available EMGT strategy to retrospective full threshold VF series as used in this study.

A considerable proportion of subjects (79%) identified as progressing by the HRT trend analysis were also identified by the novel HRT event analysis. Given similar levels of specificity, the event analysis has a much higher detection rate, with an additional 19 subjects progressing by HRT event analysis alone. 51% of subjects identified as progressing by VF trend analysis also progressed by HRT event analysis, compared to 56% of subjects identified by the AGIS VF criteria. Although there is a widely held view that structural changes are detected before functional changes using current testing techniques, there was no significant difference in the time to detection of progression by the different event analyses. This may reflect subjects commencing the study at different stages of the disease process – this is particularly pertinent as optic disc appearance was not taken into consideration at the time of recruitment. The results of the study show that eyes progressing by VF criteria alone had a lower MD, on average, at baseline.

The new HRT event analysis represents a simple technique that performs at least as well, if not better in terms of detection rate, as other established techniques. A potential weakness of the use of RCs to define threshold for change is that the HRT test-retest RA 'noise' is not normally distributed but is best characterised by a hyperbolic distribution (Owen et al., 2006). However, for the purposes of this study, the use of empirical estimates of test specificity as well as temporal and spatial confirmatory steps, should counteract any imprecision likely to have resulted from the distribution of RA variability. In the present study, only a single mean topography was available at baseline and the thresholds for change in the event analyses were based on two mean topographies acquired on the same day. As the RCs tend to be slightly greater when derived from a single baseline image, the specificity estimates are lower

than expected. Thus, the present analysis reflects a 'worst case scenario' and an analysis with longitudinal data with a baseline of two mean images is likely to have higher specificity. The RCs generated in this study suggest that the acquisition of two images to generate a baseline may be of particular benefit with medium and poor quality images; a single baseline image should suffice for good quality images.

Further modifications to progression strategies are unlikely to yield an improvement in agreement. The discrepancy may be due to functional changes occurring without structural changes (such as IOP-dependent ganglion cell dysfunction) or vice versa (such as lamina bowing or astrocyte loss). It is also possible that a degree of the disagreement may be due to differences in measurement variability between the two modalities in individual patients. Our results support this hypothesis, with eyes progressing by HRT criteria alone having better image quality than those progressing by VF alone. Future developments in the identification of glaucomatous progression will need to limit the influence of measurement variability by improving the acquisition and the processing of both images and visual fields.

3.6-3.7 Spatial filtering

3.6 Comparing structure and function

3.6.1 Background

The detection of VF progression by SAP is confounded by the inter-test and intra-test variability inherent within the testing process. Threshold sensitivity may be influenced by factors including patient-response fluctuation, patient experience and patient fatigue (Bebie et al., 1976b; Wild et al., 1989; Hudson et al., 1994; Henson et al., 2000). Variability has also been shown to increase in areas of glaucomatous deficit where there is established reduced sensitivity (Heijl et al., 1989a; Chauhan et al., 1993; Henson et al., 2000) .For progression to be detected reliably, the VF change due to glaucoma needs to be distinguished from this measurement 'noise'.

One approach to reducing measurement variability is the post-hoc application of a spatial filter. The concept of spatial filtering has been discussed in section 2.4.6. A novel spatial filter has been designed with the intention that it closely mimics the physiological relationship between VF test-points (Gardiner et al., 2004). This filter predicts the sensitivity of each test-point based on the sensitivities at other locations in the field, weighted according to the predictive power of each of those locations. Predictive power was determined by examining the correlations and covariances between sensitivities among all pairs of test locations, within a large database of 98,821 predominantly glaucomatous visual fields. The derivation of this filter has generated an array of inter-point absolute correlation values for the entire field. These values effectively constitute a mathematically derived 'functional map' based on physiological data. The relationship between points demonstrated by the filter should therefore closely mirror the structural pattern of the nerve fibre layer, although it may be influenced by idiosyncrasies of the HFA testing algorithm used.

3.6.2 Purpose

To identify whether the magnitude of functional correlation between points, as described by the novel spatial filter, is related to the relative proximity of the points at the ONH and in the

retinal periphery. This information may give insight to the anatomical organisation of the ONH, the glaucomatous disease process, and enable the refinement of filters applied to the VF series to reduce measurement noise.

3.6.3 Methods

3.6.3.1 Description and application of the anatomical map

A map based on the anatomical structure of the ONH and RNFL (Garway-Heath et al., 2000a) has been described earlier in this thesis (section 2.5.1.2 and Figure 2-8.). The map was derived from 69 RNFL photographs from 69 NTG patients in which the course of discrete RNFL defects or prominent nerve fibre bundles could easily be traced. Using this method, the ONH location, in degrees, corresponding to each test point was calculated, with the temporal meridian designated 0° and measured in a clock-wise fashion for the left eye and counter clock-wise for the right eye. In the current study, the angular distances between all possible pairings of test-points were calculated using the map. Where the angular distances exceeded 180°, a correction was incorporated so that the shortest angular distance between points was calculated, by subtracting the distance from 360°. Angular distance between test-points at the ONH was designated ONHd (Figure 3-14).

The distance between test-points within the peripheral retina was calculated using the Humphrey Visual Field Analyzer 24-2 template (Humphrey Instruments Inc., Dublin, California, USA). Within the template there is a 6° separation between horizontally or vertically adjacent points and 8.5° between diagonally adjacent points (using Pythagoras' theorem, $h^2 = a^2 + b^2$). In this study the 'retinal' distance between all possible pairs of test-points was calculated and designated RETd (Figure 3-14). This was calculated for the global VF and for pairings within the upper and lower hemispheres.

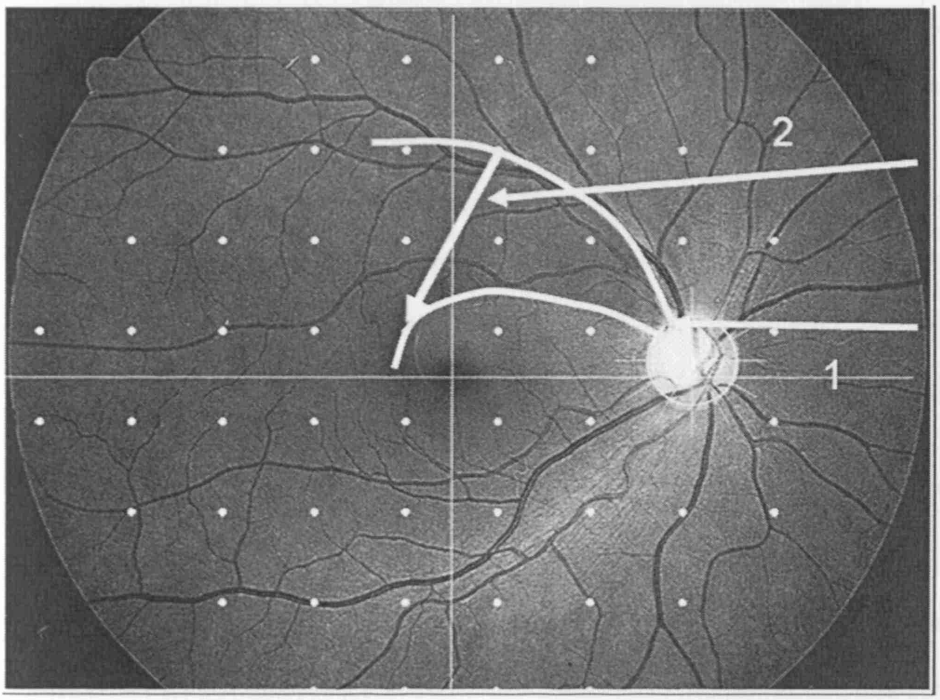

Figure 3-14. Diagram illustrating how 1) optic nerve head distance (ONHd) and 2) inter-point retinal distance (RETd) are calculated. The Humphrey 24-2 template has been superimposed onto a retinal nerve fibre layer (RNFL)photograph. The boundaries of a prominent RNFL defect have been demarcated; the distance between the limits of the defect both at the optic nerve head and in the retina have also been marked

3.6.3.2 Description and application of the functional map

The derivation of the novel spatial filter has been described in detail elsewhere (Gardiner et al., 2004). Briefly, the filter was derived from VFs from the Moorfields Eye Hospital database. This contains 98,821 VFs, taken from 14,675 individual suspected glaucoma patients. The tests performed were all standard white-on-white, full threshold tests; only complete 24-2 tests were used in the generation of the filter, although all levels of test reliability were included. The relationship between individual test-points was elucidated by examining the covariances and correlations between the sensitivities of all test-point pairings throughout the database. These inter-point correlation values (52*51 = 2652 in total) were used in this study

as a gauge of 'functional relationship' between points, and the basis of the comparison with the physical distances obtained from the anatomical map.

3.6.3.3 Comparison of the anatomical map and the functional map

Inter-point correlation values were compared to RETd and ONHd using Pearson correlation coefficient analysis and multiple regression analysis. Comparisons were performed for the entire template, for the upper and lower hemispheres and between hemispheres. Linear models for predicting VF correlation values (FC) from ONHd and RETd were assessed. The application of the prediction model to derive a 'physiological' filter was illustrated for one VF test-point. Firstly, FC values predicted for that test-point were generated; R^2 values were generated by squaring the predicted FC values. An R^2 cut-off value of 0.7 was selected to identify which test-point pairings should be included in the filter for that test-point. All statistical analyses were performed using S (AT & T Bell Laboratories, USA). This study adhered to the tenets of the Declaration of Helsinki.

3.6.4 Results

A strong negative association was observed between FC values and the angular distance at the ONH (R^2 = 0.60). That is, points corresponding to locations closer together at the ONH tended to be better correlated than those further apart (Figure 3-15). A weaker negative association was observed between FC and the retinal distance (R^2 = 0.33) (Figure 3-16). These results, for the entire VF template, are summarised in Table 3-15.

	ONHd	RETd
ONHd	1	0.34
RETd	0.34	1
FC	0.60	0.33

Table 3-15. Matrix demonstrating R^2 values for the interactions between the anatomical and functional relationships.

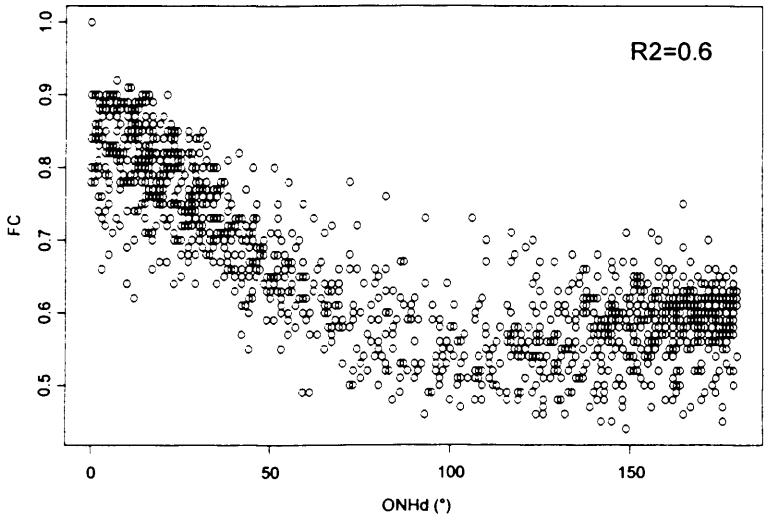

Figure 3-15. Scatter-plot demonstrating the relationship between inter-point functional correlation (FC) and optic nerve head distance (ONHd). A linear trend is observed from 0 to 90 degrees angular distance from the test point of interest. The R^2 value of 0.6 assumes a linear relationship between FC and ONHd

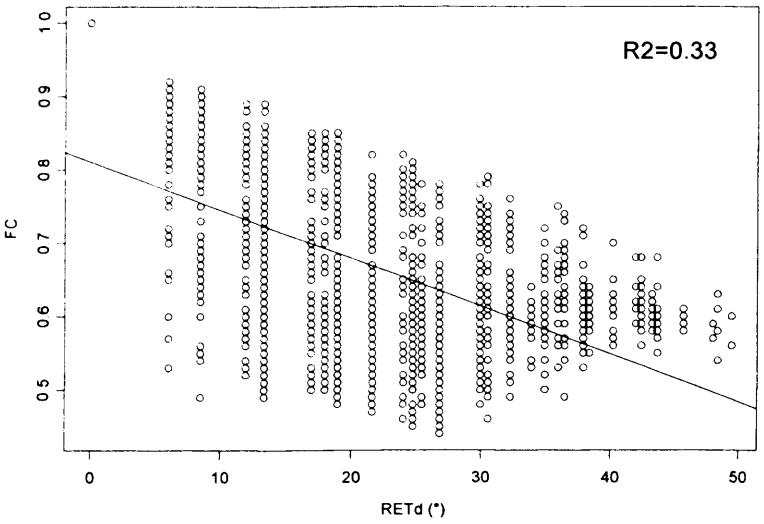

Figure 3-16. Scatter-plot demonstrating the relationship between inter-point functional correlation (FC) and retinal distance (RETd). A weak linear relationship is observed, with an R^2 value of 0.33

In order to elucidate whether the two distances are independent predictors of functional inter-point correlation, 'best-fit' models incorporating both distances were investigated. A multiple regression model incorporating ONHd, RETd and the product of the two (ONHd * RETd) was identified as having the highest R^2 value when plotted against functional inter-point correlation (R^2 = 0.75, Figure 3-17.). The interaction coefficient of the regression model is very low (0.0001), though still significant ($p < 0.00001$) due to the large number of points involved. However, when the interaction between the 2 variables is removed from the model, the linear relationship between the raw VF values and the combination of ONHd and RETd is still present. The results of the regression models are summarised in Table 3-16.

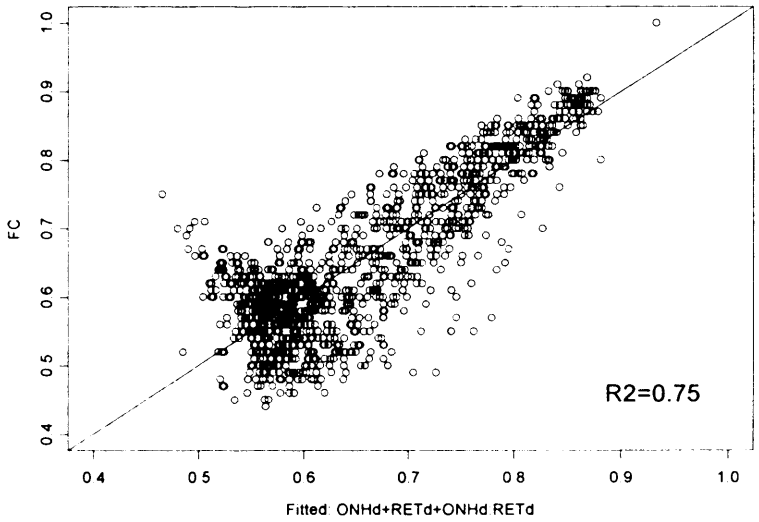

Figure 3-17. Scatter-plot demonstrating a linear relationship between inter-point functional correlation values (FC) and a multiple regression model incorporating distance at the optic nerve head (ONHd), distance at the retina (RETd) and the product of the two (ONHd * RETd)

	Intercept	ONHd	RETd	ONHd*RETd
Coefficient	0.9325	-0.0029	-0.0077	0.0001
P-value	< 0.00001	< 0.00001	< 0.00001	< 0.00001

Table 3-16. Table illustrating the multiple regression coefficients and p-values for the interactions between FC and ONHd, RETd and the combined product of the two, ONHd*RETd

Figure 3-18 illustrates a plot of inter-point correlation against angular distance for both the upper and lower hemispheres. The association between functional correlations and anatomical distance was much better when restricted to one hemisphere at a time (Figure 3-19).

The best-fit model for predicting FC was therefore:

FC = 0.9325 – (0.0029*ONHd) – (0.0077*RETd) + (0.0001*ONHd*RETd)

A new filter was derived for test-point number 49 using this predictive model; its derivation is illustrated in Figure 3-20. The ONHd values (Figure 3-20a.) and RETd values (Figure 3-20b.) for point 49 were calculated. Using the regression equation, FC values were predicted for each test-point in relation to point 49; the FC results were squared to generate R^2 values (Figure 3-20c). The test-points included in the filter were those with R^2 values of ≥ 0.7 (highlighted in bold in Figure 3-20c). Finally, the weightings by which each test-point's sensitivity influences the sensitivity of point 49 were calculated by dividing each R^2 value by the sum of all R^2 values included in the filter (Figure 3-20d).

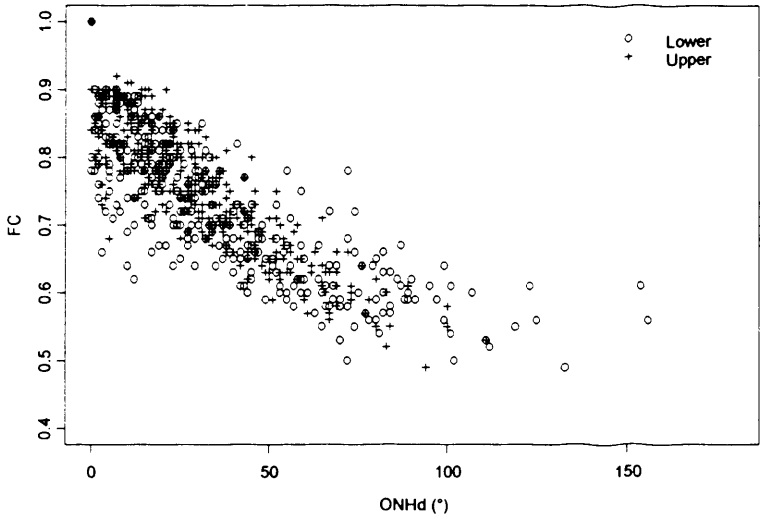

Figure 3-18. Scatter plot demonstrating the relationship between inter-point functional correlation (FC) and distance at the optic nerve head (ONHd) for each hemisphere in isolation. A linear relationship between FC and ONHd is observed for test points in the upper hemisphere (crosses) and in the lower hemisphere (circles)

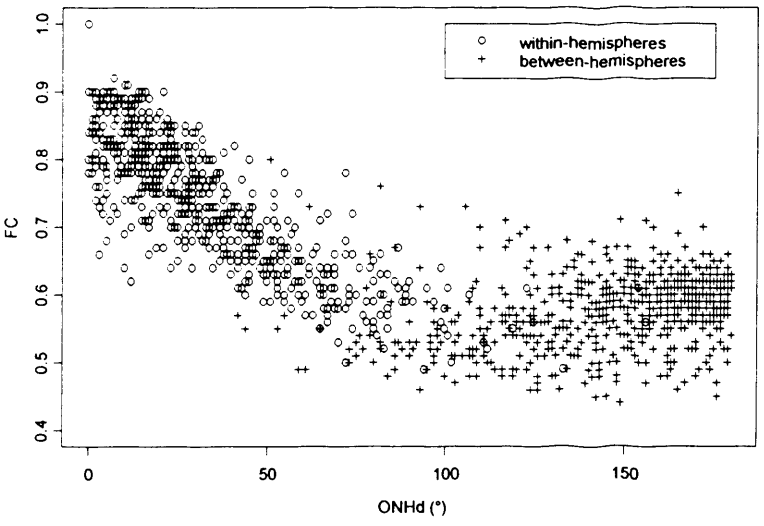

Figure 3-19. Scatter plot comparing the relationship between inter-point functional correlation (FC) and distance at the optic nerve head (ONHd) within the same hemispheres (circles) and between different hemispheres (crosses). A linear association is observed from 0 to 90 degrees

a)

		164	174	179	173			
	166	179	166	160	167	177		
148	172	158	143	145	150	156	170	
137		123	112	129	143	150	156	170
86		68	70	47	26	13	5	2
55	14	21	33	25	15	3	4	
	31	12	1	4	X	7		
		27	19	14	12			

b)

		40.2	37.9	36.5	36.0			
	36.4	34.9	32.3	30.6	30.0	30.6		
38.4	33.9	30.0	26.8	24.7	24.0	24.7	26.8	
34.9		25.5	21.6	18.9	18.0	18.9	21.6	25.5
32.3		21.6	18.9	13.4	12.0	13.4	16.9	21.6
30.6	24.7	18.9	13.4	8.5	6.0	8.5	13.4	
	24.0	18.0	12.0	6.0	X	6.0		
		18.9	13.4	8.5	6.0			

c)

		0.65	0.63	0.62	0.60			
	0.63	0.59	0.55	0.52	0.52	0.53		
0.60	0.57	0.51	0.48	0.46	0.45	0.46	0.47	
0.55		0.48	0.47	0.43	0.40	0.40	0.43	0.46
0.51		0.51	0.51	0.57	0.63	0.66	0.63	0.58
0.49	0.54	0.59	0.60	0.67	**0.73**	**0.74**	0.68	
	0.54	0.61	**0.70**	**0.77**	**0.87**	**0.76**		
		0.58	0.64	**0.70**	**0.74**			

d)

				0.12	0.12	
			0.11	0.13	**0.16**	0.13
				0.12	0.12	

e)

					0.02	
				0.03		0.16
			0.04	0.22	**0.22**	0.18
				0.05	0.08	

Figure 3-20. The derivation of a new filter for test-point 49 based on the regression equation

FC = 0.9325 – (0.0029*ONHd) – (0.0077*RETd) + (0.0001*ONHd*RETd)

a) **The angular distances (°) between each test-point and point 49 at the optic nerve head (ONHd) are illustrated. Point 49 is marked with an X; ONHd is 0 at this point.**

b) **The angular distances (°) between each test-point and point 49 in the retinal periphery (RETd) are illustrated. Point 49 is marked with an X; RETd is 0 at this point.**

c) **R^2 values generated by squaring the FC values predicted by the regression equation are illustrated. Values achieving an R^2 cut-off value of 0.7 are highlighted in bold. These test points are included in the filter for point 49.**

d) **The 'weightings' for each test-point in the filter based on the predictive model for point 49 are shown (Point 49 is highlighted in bold). The weightings are**

estimated by dividing each point's R^2 value by the sum of R^2 values included in the filter. When applying the filter, the sensitivity value for each test point is multiplied by its relative weighting; the 'weighted' sensitivities are summed for each point included in the filter to generate the 'filtered' sensitivity for point 49.

e) **The weightings for each test point associated with point 49, based on the physiologically derived filter described by Gardiner, et al (Gardiner et al., 2004).**

3.6.5 Discussion

A more useful approach to constructing a spatial filter, rather than using the arbitrary three-by-three grid organisation of the Gaussian filter (Figure 2-7) would be to exploit the functional or anatomical relationship between test-points. Initially, the point by point spatial dependence was determined by multiple regression analysis of sensitivity values for each test-point in a data-set of 440 Humphrey VFs (Crabb et al., 1997a). A similar investigation (Gonzalez de la Rosa et al., 2002) reports the relationship between sensitivities of test-points using the 32 program of Octopus 1-2-3 (Interzeag, Schlieren-Zurich, Switzerland). In this study, linear regression analysis among each of the locations and the rest of the points in the field was performed. The methodology used in the construction of the novel filter was similar, although the mathematical relationship between sensitivities was assessed using covariances and correlations and the number of fields assessed was much larger. In particular, all available VF data were used in the construction of the filter, so as to be truly representative of a glaucoma clinic population. It may therefore not be suitable for use in normal subjects or subjects with non-glaucomatous, such as neurological, field defects. Using simulated progressing VF data, the novel filter was found to improve both specificity and sensitivity (Gardiner et al., 2004). When used on a 50 patient sample of longitudinal field data, the filter has been shown to reduce variability and to not reduce detection of loss using Total Deviation maps (Artes et al. *IOVS* 2005; 46: ARVO E-Abstract 3732). This represents a clear improvement on the performance of the Gaussian filter; the effect of the novel filter is assessed using prospective clinical data in section 3.7. An additional observation from Artes' study is that the filter improved the 'pattern' of progression compared to unfiltered VFs such that it more resembled

the defect appearance expected in glaucoma. This should be expected if the physiological relationships exploited in the construction of the filter are valid.

An encouraging level of agreement between the magnitude of functional correlation between points and the relative location of the points at the ONH and the retinal periphery was observed in this study. There was a negative association between FC and both ONHd and with RETd. A multiple regression model using the product of ONHd and RETd was able to predict inter-point correlation values. It should be noted that the model continues to predict FC well with the interaction term removed, which may indicate that the dependent association of ONHd and RETd with inter-point sensitivity correlation may not be large. However, although the coefficient for the interaction term is small (0.0001) it cannot be dismissed completely, as an increase in R^2 value from 0.6 to 0.75 was observed when the interaction is included. The interaction term is intended to account for the non-linearity observed in the models shown in Figures 3-15 and 3-16. The minimal impact of the interaction term on the predictive model may suggest that the non-linearity observed has a negligible influence. The regression equation used to construct the example filter was therefore derived from a predictive model which included the interaction between ONHd and RETd. In the construction of the filter, only predicted FC values with ONHd correlations > 0.84 ($R^2 \geq 0.7$) were included, and the ONHd/FC relation is clearly linear over this range (Figure 3-18). However, as should be expected, the relationship between ONHd and the VF correlation values appears to be wholly valid (and linear) within the same hemisphere but not between hemispheres (Figure 3-19).

As glaucomatous damage is believed to manifest itself at the ONH, it seems logical that VF locations which correspond to similar regions of the ONH should be well correlated; damage to that area of the ONH will affect all such points. In this study, retinal proximity was also found to be a predictor of the strength of correlation between two points. This observation has implications for both disease process and anatomical organisation, although with the caveat that it is unknown whether the finding is real or spurious. If the observation is 'real', it may support the hypothesis that RNFL bundles from similar peripheral eccentricities are closely located at the optic nerve head. Experimental studies in different species of the macaque monkey have generally suggested that a degree of retinotopic organisation exists with respect to the eccentricity of axonal origin, although they tend to differ in terms of exact detail (Ogden,

1974; Radius and Anderson, 1979b; Minckler, 1980; Ogden, 1983a). To date, there has been little by way of clinical observation to support this hypothesis (Read and Spaeth, 1974), although the results of this study may support such a finding in the context of a disease model where glaucomatous damage occurs at the ONH. An alternative explanation applies to a model where damage occurs primarily in the retina. In this situation, damage may propagate from dysfunctional or dying retinal ganglion cells locally within the retina. ONHd has a much higher coefficient of determination than RETd, suggesting that the glaucomatous process more likely occurs at the ONH, although the ONH and retinal models are not mutually exclusive. The FC/RETd relationship, however, may in part be spurious, resulting from measurement error. The error may be systematic, perhaps related to inaccuracies in the anatomical map. Random error may relate to inter-individual variation of ONH position in relation to the fovea (Garway-Heath et al., 2000a), or to fixation losses occurring during VF testing.

The comparison between inter-point functional correlation and the anatomical map is dependent on the assumption that the relationships described by the anatomical map are valid. Alternative maps have been described which were developed using similar techniques (2.5.1.2). The map used in the current study has previously been used in structure-function studies in glaucoma (Strouthidis and Garway-Heath, 2003; Schlottmann et al., 2004; Reus and Lemij, 2004b). The adoption of an alternative map, such as that developed by Junemann (Junemann et al., 2000), has been based upon the simplicity of use, as opposed to any perceived greater integrity compared to the map used in our study (Artes and Chauhan, 2005). Recently, a map has been described which was developed using both SAP and HRT data (Gardiner et al., 2005). This newer map therefore differs from the map used in our study in that it incorporated both structural and functional information in its development, although the result is similar to the map used in the current study.

Structural data have been incorporated into the construction of a spatial filter, based on the multiple regression predictive model which incorporates the angular distance between test-points at the ONH, the angular distance between test-points in the retinal periphery and the interaction between the two distances. In the example used in this study, which is for a single test-point, the filter has a similar distribution of test-point associations compared to those

generated using the 'physiological' filter of (Gardiner et al., 2004). Both filters follow an 'arcuate' pattern, in keeping with what might be expected given the distribution of the RNFL. The newly developed 'structural' filter does, however, include fewer points, which have more similar weightings relative to each other, as compared to the physiological filter. This may be explained by the fact that all the points, bar one, included in the structural filter are directly adjacent to the point of interest and as such may be expected to have a similar relation, according to a linear model. The method for constructing the physiological filter downplayed points which strongly co-varied with, but had lower predictive value than, other predicting points. This has not been done in the new structural filter. By not downplaying strongly associated points, measurement noise reduction may be improved through increased signal averaging; however, whether this confers an advantage in the detection of signal needs to be tested and is the subject of further work. The use of the predictive equation developed in this study enables the construction of filters which may be customised on a point-wise basis. A 'bespoke' spatial filter is particularly useful if one wishes to exclude test-points from a longitudinal series if they are consistently depressed by a mechanism other than glaucoma – for example, due to lid artefact or due to chorioretinal scarring. Likewise, the physiological filter is limited as it is designed for use with the 24-2 program of the HFA. A point-wise customisable filter may be adopted in the context of different Humphrey programs (such as 10-2) and may also be used in alternative proprietary perimeters.

The associations identified in our study help to validate the structure and function relationship in glaucoma and give insight into the anatomic organisation of the ONH and glaucomatous disease process. The incorporation of structural data may be of benefit in the future development of more refined spatial filters to reduce measurement noise in VF testing.

3-7 Measuring progression

3.7.1 Background

A fundamental challenge in the management of POAG and OHT is the discrimination between stable and progressing disease. In cases of established POAG, the accurate detection of disease progression enables the assessment of the effect of a particular treatment regimen; in subjects with OHT, it will influence the decision on whether to commence IOP-lowering treatment. Despite the availability of devices such as HRT, the determination of disease progression in routine clinical practice remains largely based on the scrutinization of longitudinal series of standard automated VF examinations. In order to detect progression reliably, a true glaucomatous change needs to be distinguished from measurement variability. One proposed method of for reducing visual field measurement variability, spatial filtering, has been discussed previously in this thesis (sections 2.4.6 and 3.6). A novel spatial filter has been introduced which is derived by the inter-point functional correlations of threshold sensitivities (Gardiner et al., 2004). The 'functional map' described by the novel spatial has been shown to correlate well with the expected structural patterns, both at the ONH and in the retinal periphery (Section 3.6)(Strouthidis et al., 2006b).

3.7.2 Purpose

To apply the novel spatial filter to real longitudinal VF data and to compare estimated specificity, progression rates and time to progression using the filter and without using the filter. The application of the filter is also compared to a VF progression technique which required multiple confirmatory testing (3-omitting PLR analysis). The level of concordance in identified progression by VF and imaging techniques has been reported to be poor (Artes and Chauhan, 2005; Strouthidis et al., 2006a) and one explanation is that measurement noise results in failure to identify some progressing eyes and in the false detection of stable eyes. Noise reduction, therefore, potentially may improve concordance. The effect of the filter on the concordance of VF progression with HRT structural progression, was therefore also assessed.

3.7.3 Methods

3.7.3.1 Subject selection

198 OHT and 21 control subjects as described in section 3.4.3.1 and in Table 3-9.

3.7.3.2 Visual field analysis

Each subject had a minimum of five Humphrey VF tests obtained over the study period, with the baseline test date taken as the date when the first HRT image was acquired. Five Humphrey VF tests were selected as this is the minimum number of tests with which one may perform 3-omitting PLR (three tests to generate a linear regression, and two further confirmatory tests). In order to evaluate the performance of the spatial filter in a dataset containing a range of VF variability, all available VF tests were included in the analysis irrespective of reliability criteria.

VF examinations from the subjects selected for analysis in this study were not used in the construction of the novel spatial filter.

VF progression was assessed by PLR using a version of PROGRESSOR (Institute of Ophthalmology, London, UK) which had been adapted to include the novel spatial filter. Each subject's VF series was analysed using the 'standard' PLR criteria (as in section 3.4.3.2) with the post-hoc application of the spatial filter (referred to as 'filtered' VF data). Results for standard PLR applied without application of the spatial filter (i.e. with 'raw' VF sensitivity data, referred to as 'unfiltered' VF data) and for the more stringent 3-omitting PLR without application of the spatial filter (referred to as 'unfiltered' 3-omitting PLR) have been reported in section 3.4.4 and by Strouthidis et al., (2006a). The number of subjects identified as demonstrating significant progression or improvement at the end of the study period was compared using each technique (filtered standard PLR, unfiltered standard PLR and unfiltered three-omitting PLR), as was the time to identification of significant change in these subjects. Ranges of specificity were estimated for both unfiltered and filtered VF data using two proxy measures – the number of control subjects demonstrating progression and the total number of subjects (both OHT and control) demonstrating improvement (VFs with one or more points changing with a slope of +1 dB/Year at $p < 0.01$). All statistical analyses were performed using Medcalc Version 7.4.2.0 (Medcalc Software, Mariakerke, Belgium).

3.7.3.3 HRT analysis

Progression by HRT was assessed using the RA trend analysis strategy as described in section 3.4.3.3 (Strouthidis et al., 2006a). The 'low stringency' and 'high stringency' criteria achieved specificity estimates of 88.1-90.5% and 95.2-98.2%, respectively, when applied to HRT images acquired in the same longitudinal data-set as the current study. The number of subjects progressing by HRT was compared with the number of subjects progressing by VF, using both unfiltered and filtered data.

3.7.4 Results

Specificity estimates have been made using 'false improvement' in all subjects and 'false progression' in control subjects; these estimates are summarised in table 3-16. The number of control subjects available (21) was low, and as such the power to estimate specificity using control subjects was relatively poor. These estimates may therefore be considered as supplementary, supportive, evidence to the estimates derived from 'false improvement', which have greater power being obtained from 219 subjects. A specificity range of 85.7-95.4% was therefore estimated using 'unfiltered' standard PLR criteria compared with 84.5-100% using 'filtered' standard PLR criteria (Table 3-17); the difference between estimates approached statistical significance ($p = 0.07$, McNemar test). There was a statistically significant difference between specificity estimates using unfiltered standard PLR criteria and unfiltered 3-omitting PLR criteria ($p = 0.04$, McNemar test), although there was no difference between filtered standard PLR criteria and unfiltered 3-omitting PLR criteria ($p=0.9$, McNemar test). As specificity was closely matched, at approximately 90%, the unfiltered VF PLR progression in the OHT cohort was compared with HRT progression using the lower stringency strategy. The filtered VF PLR progression in the OHT cohort was compared with HRT progression using the higher stringency strategy, with specificity matched at approximately 97%. Using the unfiltered VFs, 64 OHT subjects (positive detection rate 32%, 95% confidence limits 26-39%) were identified as progressing, of whom 24 also progressed by the HRT low stringency strategy. A further 42 subjects (21%) progressed by HRT alone (Figure 3-8). 57 OHT subjects (positive detection rate 29%, 95% confidence limits 23-36%) progressed by filtered VFs, of

whom seven also progressed by the HRT high stringency strategy. A further 17 subjects (9%) progressed by HRT alone (Figure 3-21).

	Unfiltered Standard PLR	**Unfiltered 3-omitting PLR**	**Filtered Standard PLR**
Subjects without significant improvement	209/219 = **95.4%**	215/219 = **98.2%**	212/219 = **96.8%**
95 % Confidence limits	91.8-97.5%	95.4-99.3%	93.5-98.4%
Controls without progression	18/21 = **85.7%**	20/21 = **95.2%**	21/21 = **100%**
95 % Confidence limits	65.4-95.0%	77.3-99.1%	84.5-100%

Table 3-17. Estimation of specificity for visual field point-wise linear regression using standard criteria (PLR) with and without the application of a novel spatial filter and using unfiltered 3-omitting criterion PLR

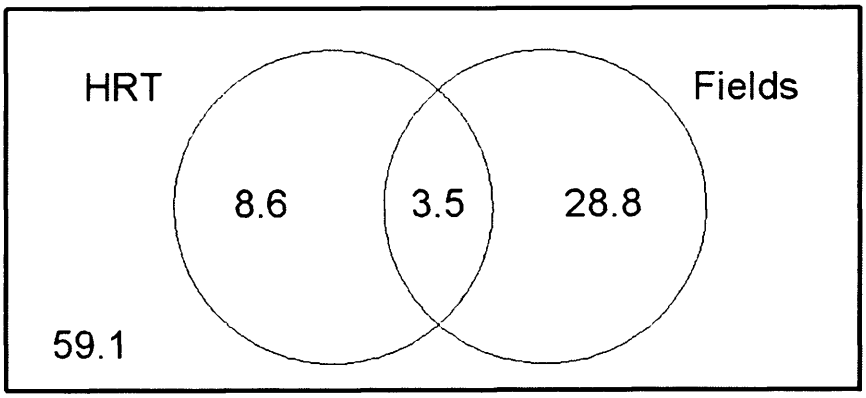

Figure 3-21. Venn diagram comparing HRT and filtered field progression within the OHT cohort, expressed as a percentage of subjects. Specificity of both the HRT progression strategy ('high stringency') and the filtered visual field progression is anchored at approximately 97%

Filtered standard PLR generated similar specificity estimates as unfiltered 3-omitting PLR. Figure 3-22 illustrates the agreement between 3-omitting PLR and the high stringency HRT progression strategy (specificity for both techniques was approximately 97%). Using unfiltered 3-omitting PLR, 37 subjects (positive detection rate 19%, 95% confidence limits 14-25%) were identified as progressing. The same percentage of OHT subjects (3.5%) demonstrated agreement with structural progression as with the filter; however the use of confirmatory criteria was associated with a 10% reduction in VF positive 'hit rate'. There was a significant difference in positive detection rate between filtered standard PLR and unfiltered 3-omitting PLR ($p=0.0001$, McNemar test). By comparing low stringency HRT progression with filtered VF results, where specificity is not closely matched, a similar level of agreement (11.1%) was noted as for unfiltered VF data (Figure 3-23).

36 OHT subjects progressed by all 3 PLR techniques (unfiltered standard PLR, unfiltered 3-omitting PLR and filtered standard PLR). A single subject progressed only by filtered standard PLR; no subjects progressed by 3-omitting PLR alone (Figure 3-24). 3 subjects (both OHT and control) improved by all 3 PLR techniques. A single subject improved only by filtered standard PLR (Figure 3-25).

The application of the filter did not significantly alter time to detection of VF change (Figures 3-26 and 3-27). Median time to identification of significant change was 2.5 years (range 0.4-6.8 years) for unfiltered VF data compared with 2.6 years (range 0.3-6.4 years) for filtered VF data. The adoption of the 3-omitting criterion was associated with an increased time to detection of progression, compared with both the filtered and unfiltered standard PLR (Figures 3-26 and 3-27).

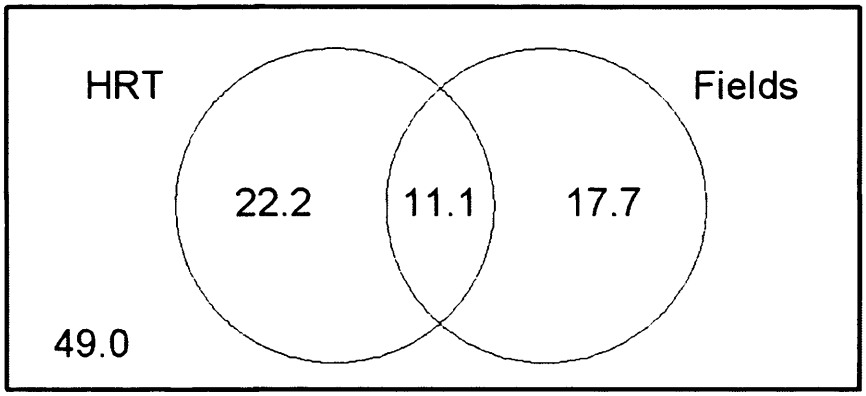

Figure 3-22. Venn diagram comparing HRT (low stringency) and field progression (filtered standard PLR) within the OHT cohort, expressed as a percentage of subjects. Specificity of the HRT progression was estimated at approximately 90 %, and of visual field progression at approximately 97%

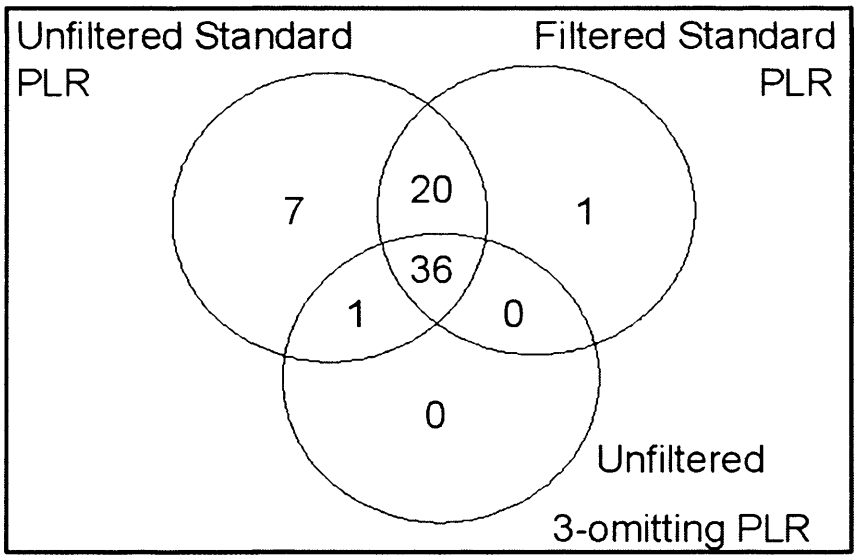

Figure 3-23. Venn diagram comparing the number of ocular hypertensive subjects progressing at the end of the study period using three different PLR techniques – unfiltered standard PLR, filtered standard PLR and unfiltered 3-omitting PLR

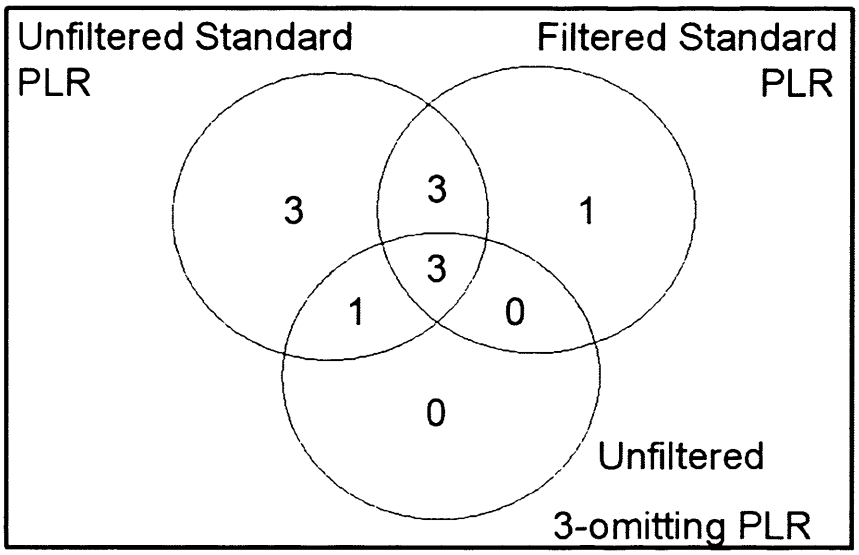

Figure 3-24. Venn diagram comparing number of subjects (both ocular hypertensive and control) demonstrating significant improvement at the end of the study period using three different PLR techniques – unfiltered standard PLR, filtered standard PLR and unfiltered 3-omitting PLR

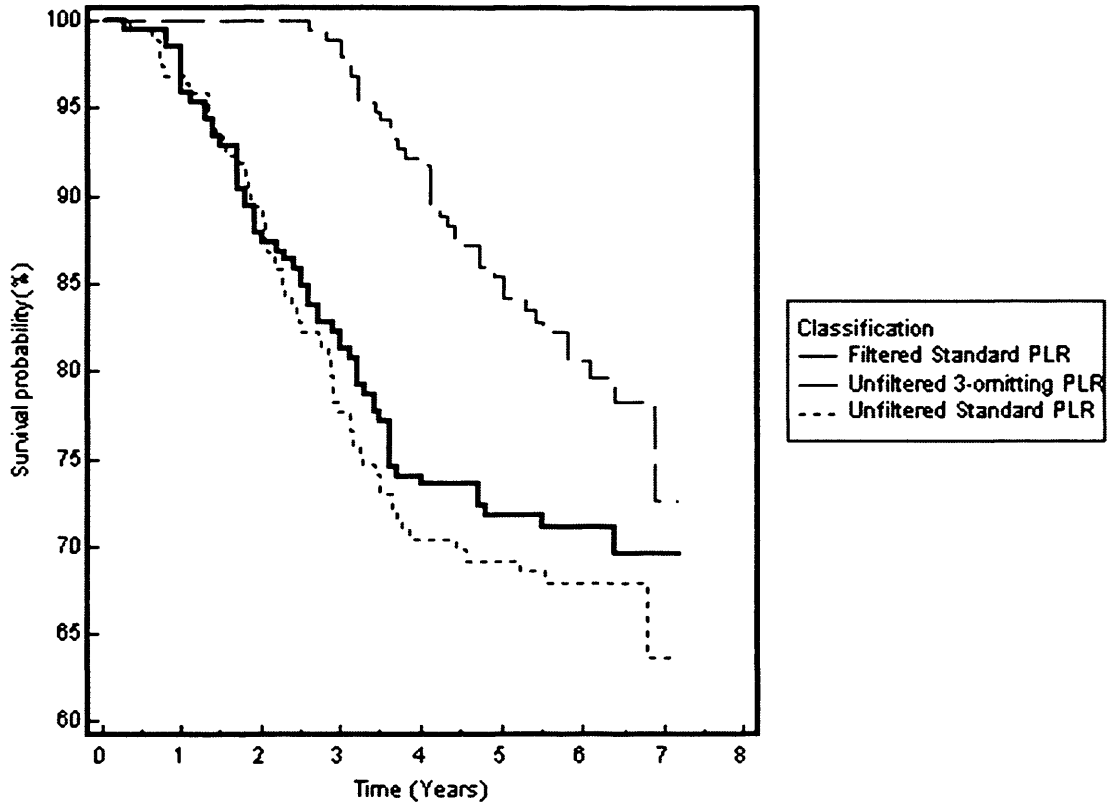

Figure 3-25. Kaplan-Meier survival curves comparing time to identification of progression using both raw visual field data ('unfiltered' – both standard PLR and 3-omitting PLR) and visual field data following application of a novel spatial filter ('filtered' – standard PLR) in the ocular hypertensive cohort

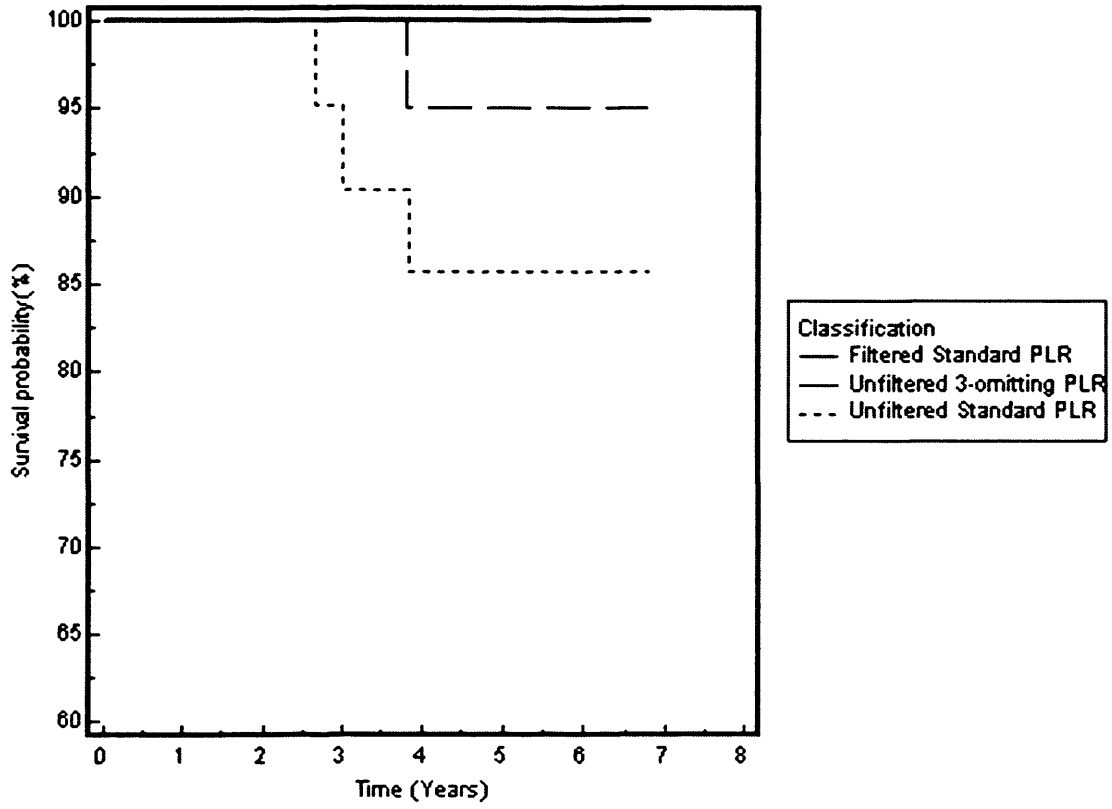

Figure 3-26. Kaplan-Meier survival curves comparing time to identification of progression using both raw visual field data ('unfiltered' – both standard PLR and 3-omitting PLR) and visual field data following application of a novel spatial filter ('filtered' – standard PLR) in the control cohort

3.7.5 Discussion

In this study, the effect of a novel spatial filter on the monitoring of glaucomatous VF progression has been assessed. There is insufficient power to prove that the new filter confers an improvement in specificity compared to standard PLR criteria (without use of the filter), although the difference approached statistical significance. However, there was a statistically significant difference in specificity between the standard PLR (without use of the filter) and 3-omitting PLR (without use of the filter). This suggests that the use of confirmatory tests (in this case two) is associated with an appreciable improvement in specificity. There was no significant difference in specificity between the use of the spatial filter with standard PLR technique and the 3-omitting PLR technique without filtering. The use of the spatial filter therefore results in similar specificity compared to confirmatory testing but with the advantage of an increase in positive hit rate and with a shorter time to identification of progression. The difference in the detection rates comparing filtered and unfiltered standard PLR may be explained by the slightly higher specificity of the filtered PLR. However, the difference in detection rates between filtered PLR and unfiltered 3-omitting PLR cannot be explained by lower specificity of filtered PLR compared with 3-omitting. The maximum false positive rate (in the confidence intervals) for filtered PLR is 6.5% and the minimum false positive rate for 3-omitting PLR is 0.7% – a maximum difference of 5.8%. This represents a 'worst-case scenario' in which filtered standard PLR is much less specific than the unfiltered 3-omitting PLR. It is highly likely, therefore, that the 10% difference in detection rate is a consequence of the new filter identifying more instances of progression that are genuine and not false positives, compared to 3-omitting PLR.

Confirmatory tests are an approach to counteract the inter-test measurement variability, or long-term fluctuation, which represent the primary barrier to the identification of true change within a longitudinal series of VFs (Heijl et al., 1989a; Boeglin et al., 1992). Additional tests to confirm progression have the benefit of lessening the effect of poor overall performance in a VF test in a series (which may affect many points in the VF), but with the caveat that increased costs are incurred due to additional visits (Hutchings et al., 2000). It is likely that confirmation tests and spatial filtering will prove complementary. The concept of spatial processing represents an attractive proposition as it does not require the collection of further

test data or any modification to the testing process itself, as it is applied 'post-hoc' to previously acquired VF data. The first spatial filter applied to VF data – the Gaussian, or simple averaging, filter – has been shown to be capable of dampening the effect of long-term variability. Its performance is, however, unsatisfactory where localised but significant VF loss exists. In this circumstance, the field loss may be obscured by the spatial processing technique. (Spry et al., 2002) observed that Gaussian filtering, when applied to simulated VF data, resulted in a modest specificity gain but considerable sensitivity depreciation for small, progressive VF losses; a small specificity loss was also observed for large, progressive defects. In Spry's study, temporal processing, effectively a running average of threshold sensitivity over time, was propounded as a more predictable method for increasing sensitivity gain. This technique exerts a 'smoothing' effect of variability over time; its benefit is decreased with an increasing number of available tests. Unlike the spatial filter used in the current study, neither the temporal nor the Gaussian filter was designed along physiological principles.

There was likely a small improvement in specificity when the novel spatial filter was applied, and this was associated with a similar decline in the proportion of eyes identified as progressing. (Gardiner et al., 2004) originally tested the novel spatial filter using VF computer simulations; these were based on robust and realistic estimates of the VF noise (Henson et al., 2000; Gardiner and Crabb, 2002b). Localised defects for each point in the VF were tested, including some consisting of just 2 progressing points. Results indicated that, as expected, the Gaussian filter blurred many of the progressive defects whereas the new filter improved detection rate in more than 90% of the defects tested.

Specificity estimates approaching 100% have been achieved previously for PLR techniques, without spatial filtering, using glaucomatous VF data with simulated measurement variability (Vesti et al., 2003). The progression criteria applied were far more rigid than those used in the current study, requiring a significant regression slope of -1.0 dB/year, $p < 0.01$ in the same three test-points in three of four consecutive tests. By excluding the necessity for 'cluster' test-point progression, the PLR technique used in the current study may be predisposed to lower specificity because of the wide range of variability at individual test locations. Lower specificity may also be expected as no confirmatory tests were included to counter long-term fluctuation.

In the absence of an independent 'gold standard' based on which to classify a subject as having progressed, estimates of specificity were derived from surrogate measures based on two assumptions. Firstly, that threshold sensitivity should not improve over time and secondly, that threshold sensitivity decay over time should not exceed age-related decay in control subjects. With respect to the former assumption, all subjects included in the analysis had reproducibly normal and reliable VFs at baseline and were therefore unlikely to exhibit prolonged learning effects over time, which may have resulted in some positive threshold sensitivity change (Kamal et al., 2003). With respect to the latter assumption, it is possible that, as individuals may age at different rates, some threshold sensitivity loss due to normal aging may have been flagged as progression in the control cohort. However, no progression was seen in the normal subjects following the application of the novel spatial filter.

Likewise, in the absence of an independent 'gold standard' for disease progression, it is not possible to obtain a direct measure of test sensitivity. Given the high estimates of specificity, both for unfiltered and filtered PLR, it is very likely that the great majority of 'progressors' identified by either technique are likely to represent true disease progression. Spatial processing resulted in a small decrease in detected progression or 'positive hit-rate' of 3.6%, which may equate to a relatively small diminution of sensitivity. In the current study, progressing defects are expected to be smaller as the subjects are ocular hypertensive with normal VF tests at baseline. In a previous study using the Gaussian filter, a sensitivity loss of up to 50% has been estimated for small progressive defects (2 progressing points) at a true progression rate of -1dB/Year using 10 visual field tests, compared with up to 20% for larger defects (18 progressing points) (Spry et al., 2002).

A particular problem identified in the VF progression techniques adopted in large-scale clinical trials is the number of false-positive results. 'Reversal' of progression was examined in subjects from OHTS; only 12% of VF tests returned to normal after 3 consistent abnormal VF tests, compared with 66% when only two abnormal VFs were used (Keltner et al., 2005). These results suggested that, for the VF progression criteria used in OHTS, the adoption of two additional confirmatory VF tests would improve stability and specificity. A high false-positive detection of field progression is also suggested when a single test-point is used to flag progression by PLR, as in the current study (Heijl et al., 1998; Nouri-Mahdavi et al.,

2005). The high specificity achieved by application of the novel spatial processing technique suggests that the number of false-positive progressors would be limited. Whether this removes the necessity for confirmatory testing is not clear. Within the original betaxolol *versus* placebo study period (1994–1998), a change in AGIS VF score from 0 to greater than 1 at the same test-point location on 3 occasions was required to confirm progression (Kamal et al., 2003). Individuals who were suspected of disease progression were therefore subjected to episodes of increased frequency of VF testing whilst the investigators were seeking to confirm progression. In general, subjects were tested at a frequency of three times per year, which has previously been identified as an appropriate frequency by which to detect progression (Gardiner and Crabb, 2002b). A recent study has suggested, however, that an 'adaptive' test interval, shortened at periods when progression is suspected, may detect progression earlier than at a fixed interval rate (Jansonius, 2006). An indicator that application of the spatial filter may limit the requirement for confirmatory testing is the observation that it achieves similar estimates of specificity as the 3-omitting technique. However, the use of confirmatory criteria is at the cost of a significant decrease in positive detection rate as compared with filtered standard PLR.

Explanations for poor structural and functional correlation may include structural changes occurring without concomitant functional change (such as lamina cribrosa bowing) and functional changes occurring without structural alteration (such as ganglion cell dysfunction). Another possible theory is that the poor correlation arises from differences in the amount of measurement variability between the two testing modalities. It is, however, difficult to identify improvement in agreement using the spatial filter because of the large reduction in hit rate using the HRT with the more stringent progression criteria. By comparing the filtered VF results with the low stringency HRT strategy, albeit with the caveat that the specificities are not matched, one can observe that there is very little reduction (and no improvement) in the agreement between disc and field progression with the application of the filter.

The novel spatial filtering technique used in this study, which was designed to mimic the physiological relationship between test-point pairings within the VF, has been shown to achieve similar specificity as using PLR with confirmatory criteria, with an increased rate of detected progression. The filter, therefore, may be useful in the detection of glaucomatous

progression and might be suitable in examining data from clinical trials. As it is applied post-hoc to data which have already been collected, it does not require additional costs in terms of clinic time and repeat VF testing. The filter was, however, constructed and tested using full-threshold VF tests (albeit from a different group of subjects). It has yet to be applied to VF series acquired using SITA. It may be necessary for the spatial filter to be reconstructed using a database of SITA fields to obtain optimal performance in that context.

4 SECTION IV: Discussion and summary

4.1 Test-retest variability of the HRT and HRT-II

4.1.1 Summary

In the first test-retest study (section 3.2), RA and mean cup depth were found to be the most repeatable and reliable stereometric parameters generated by the HRT and HRT-II. The factors which affected RA variability were reference height and image quality. Image quality, in itself, was affected by the patient's age, refractive error and by degree of lenticular opacity. In the second test-retest study (section 3.3), the repeatability of RA measurements was shown to improve by using an alternative to the standard RP, the 320μm RP, and by exclusion of poor quality images. The use of a manual alignment facility to correct the position of automatically misplaced contour lines was shown to offer a marginal improvement in RA variability, where exclusion by image quality may not be practical.

4.1.2 Implications

The test-retest studies have confirmed, in keeping with numerous other studies, that the HRT can image the ONH reliably and reproducibly. Very little has been published regarding the test-retest variability of the HRT's successor, the HRT-II. The test-retest studies described in this thesis have confirmed that imaging with the HRT-II is as reliable and reproducible as with the HRT. In theory it should therefore be possible to use HRT and HRT-II images interchangeably in a longitudinal series, as long as the software platform permits such an analysis.

RA is a clinically meaningful parameter with low test-retest variability. As such it may be useful for monitoring glaucomatous structural progression, and RCs may be used to define 'limits for change'. The results of the test-retest studies suggest that the HRT progression algorithms should use RA and a fixed off-set 320μm RP to minimise measurement error. The importance of good quality image acquisition is stressed; this may not be possible in subjects with increasing lenticular opacity. RCs for inter-test RA have been generated for differing levels of image quality which may be useful to compensate for the inclusion of poorer quality images.

4.1.3 Further work

Since the test-retest studies were carried out, a newer iteration of the HRT software, HRT-III has been introduced. Although there has been no alteration in the mechanism of image acquisition, the newer platform aligns images differently. Principally, the HRT-III no longer truncates the peripheral parts of the image ('letter-boxing') when trying to approximate rotational alignment. This means that the position of the reference ring in the image periphery will be more stable in successive images; resulting in a more stable 320μm RP. The test-retest images acquired using the HRT-II should therefore be re-analysed using the HRT-III software to assess whether the newer alignment algorithm results in more stable RA measurements. Likewise it would be of interest to replicate the second test-retest study (3.3) using alternative RPs, in particular the RP described by (Tan and Hitchings, 2003c). A logical method of applying the RP may be to apply the standard RP at baseline and then fix it at that level with respect to the reference height for follow-up images. Heidelberg Engineering has recently developed such an RP and it would therefore be important to assess its effect on RA variability.

Since the test-retest studies were performed, and published (Strouthidis et al., 2005a; Strouthidis et al., 2005b), our group have subsequently used the data to characterise the distribution of HRT RA measurements (Owen et al., 2006). The distribution of 'noise' was applied in computer simulations of disease progression. The modelling showed that patients with poor quality images need to be imaged more frequently in order to detect progression and that sensitivity of detection improves with more frequent testing.

The test-retest acquisition protocol represents a clear and robust method for examining reliability and reproducibility. It would serve as a useful template for the assessment of newer imaging devices as they are introduced into the clinical setting.

4.2 Measuring disc and field progression

4.2.1 Summary

2 HRT progression algorithms, based on the observation that RA is the most repeatable, clinically meaningful, stereometric parameter, have been designed and tested. The trend analysis assesses progression by the linear regression of sectoral RA over time (section 3.4). The stringency of the significance criteria are tailored according to the variability of the image series (according to the RSD for each linear regression), such that 'tighter' criteria are applied to highly variable series and 'looser' criteria are applied to less variable series. The event analysis assesses progression by defining the thresholds for change according to inter-observer, inter-visit RA RCs (section 3.5). The inclusion of confirmatory criteria and spatial inclusion criteria result in increased estimated specificity.

Agreement with functional progression was poor, regardless of estimated specificity and regardless of whether a trend analysis or event analysis was used. The HRT event analysis has a marginally higher 'positive detection rate' at the same specificity than the HRT trend analysis.

4.2.2 Implications

The most important observation of these 2 studies relates to the poor agreement as regards progression. Despite the widely accepted dogma that structure precedes function using currently available methods of detection, the discrepancy observed in these studies seems counter-intuitive. Structure and function seem to be progressing at equal frequency, but in different patients. Given the length of follow-up in these studies, it should be expected that a greater degree of overlap should occur between subjects. Indeed, the level of agreement as regards progression between event or trend analyses monitoring the same parameter (either RA or threshold sensitivity) is also depressingly low. Given the manipulations performed in order to generate the high levels of specificity observed in these studies, one can assume that the progression observed by either modality is likely to be genuine. One must therefore conclude that monitoring of progression using both structure and function is essential, even at the earliest stages of the disease.

4.2.3 Further work

The trend analysis method needs to be verified using an alternative longitudinal data-set, as the criteria applied are specific to the OHT and control cohort described in this thesis. This is with particular reference to the 'variability' of RA over time; the test-retest studies indicate that RA variability is not influenced by the magnitude of RA, thereby suggesting that variability is not influenced by stage of GON. It is not known, however, whether this observation is true in practice. It would therefore be essential to apply the trend analysis to subjects with advanced glaucomatous damage, as well as another OHT cohort.

The issue of whether discrepancies in measurement variability affect agreement between structure and function should be explored further. In theory, subjects with highly variable disc and field series should agree less frequently than subjects with less variable series. A major confounding factor is that the variability of threshold sensitivities increases with progressing glaucomatous field loss. It is therefore difficult to separate true measurement noise from variability which is a consequence of glaucoma. Henson (Henson et al., 2000) have provided an equation:

Log_e(Standard deviation) = -0.081*Sensitivity(dB) + 3.27

which might be capable of 'normalising' visual field threshold sensitivities by attenuating the effect of glaucoma on measurement variability. An alternative, statistical approach, might be to use 'de-trended fluctuation analysis', a method which can identify the extent of long range correlations within a time series. The methodology has been applied to such diverse phenomena as financial markets and to the study of the El Nino meteorological system; its applications in medical research are, to date, limited.

4.3 Spatial filtering

4.3.1 Summary

The novel spatial filter, designed by Stuart Gardiner, is based on the inter-point correlation of threshold sensitivities. The functional 'map' described by the filter was effectively verified by comparing the FC values with the distance between test-points at the ONH and at the retinal periphery (using the anatomical map described by Garway-Heath). A good level of agreement was found between the structural and the functional maps (section 3.6). A multiple regression model which included ONHd, RETd and the product of the two was found to best predict the structure-function relationship. This model was used to construct an example of a 'bespoke' point-wise spatial filter.

The application of the spatial filter to real patient longitudinal data offered a small, non-significant, improvement in estimated specificity (section 3.7). The estimated specificity using the filter was equivalent to that achieved using the highly stringent 3-omitting criteria, except with a higher positive detection rate and a shorter time to detected progression. The application of the novel spatial filter does not appear to improve agreement as regards structural and functional progression.

4.3.2 Implications

The novel spatial filter appears to be more clinically useful than its predecessor, the Gaussian filter. The particular benefit of the filter is that it can achieve similar levels of specificity as 3-omitting PLR, without recourse to 2 additional VF tests and the additional costs associated with this. Application of the newer filter, unlike the Gaussian filter, results in a minimal diminution of positive detection rate and little effect on time to detected progression. Given the good level of correlation with the structural map, it is safe to assume that the rationale behind the construction of the filter is valid. The concept of 'bespoke' point-wise filtering may be useful in the monitoring of glaucoma subjects with persistent non-glaucomatous defects, such as those due to chorioretinal scars or dermatochalasis.

4.3.3 Further work

Perhaps the most exciting prospect for spatial filters would be the development of a 'three-dimensional' filter. It may be possible to combine functional interpoint correlation data with structural data acquired using the newer objective imaging devices. Such a filter may be capable of 'smoothing' both ONH images and VF tests on the basis of expected patterns of agreement. There may also be some benefit in combining a filter and a confirmation (two-omitting) criterion, as this may be able to deal with the 'bad field' in a series scenario.

5 SECTION V: Supporting publications

5.1 Papers, articles and book chapters

Strouthidis, N.G. and Garway-Heath, D.F. (2004) The correlation between change in optic disc neuroretinal rim area and differential light sensitivity. *Perimetry Update 2002/2003* (Eds, Henson, D. B. and Wall, M.) Kugler Publications, The Hague, pp. 317-327.

Strouthidis, N.G., White, E.T., Ho, T.A., Hammond, C.J. and Garway-Heath, D.F. (2005) Factors affecting the test-Retest variability of the Heidelberg retina tomograph and the Heidelberg retina tomography-II. *Br J Ophthalmol*, 89,1427-1432.

Strouthidis, N.G., White, E.T., Ho, T.A. and Garway-Heath, D.F. (2005) Improving the repeatability of Heidelberg retina tomograph and Heidelberg retina tomograph II rim area measurements. *Br J Ophthalmol*, 89,1433-1437.

Strouthidis, N.G., Scott, A., Peter, N.M. and Garway-Heath, D.F. (2006) A comparison of optic disc and visual field progression in ocular hypertensive subjects; detection rates, specificity and agreement. *Invest Ophthalmol Vis Sci*, 47, 2904-2910.

Owen, V.M.F., Strouthidis, N.G., Garway-Heath, D.F. and Crabb, D.P. (2006) Measurement variability in Heidelberg Retina Tomograph imaging of neuroretinal rim area. *Invest Ophthalmol Vis Sci*, 47, 5322-30.

Strouthidis, N.G., Vinciotti, V., Tucker, A.J., Gardiner, S.K., Crabb, D.P. and Garway-Heath, D.F. (2006) Structure and function in glaucoma; the relationship between a functional visual field map and an anatomical retinal map. *Invest Ophthalmol Vis Sci*, 47, 5356-62.

Strouthidis, N.G., Scott, A., Viswanathan, A.C., Crabb, D.P. and Garway-Heath, D.F. (2006) Monitoring glaucomatous visual field progression; the effect of a novel spatial filter. *Invest Ophthalmol Vis Sci* (in press)

Fayers, T., Strouthidis, N.G. and Garway-Heath, D.F. Monitoring glaucomatous progression using a novel HRT event analysis. (Sept 2006 – under review, *Ophthalmology*)

6 SECTION VI: References

AGIS (1994) Advanced Glaucoma Intervention Study. 2. Visual field test scoring and reliability, *Ophthalmology,* 101, 1445-55.

AGIS (2000) The Advanced Glaucoma Intervention Study (AGIS): 7. The relationship between control of intraocular pressure and visual field deterioration.The AGIS Investigators, *Am J Ophthalmol,* 130, 429-40.

Ahn, J. K. and Park, K. H. (2002) Morphometric change analysis of the optic nerve head in unilateral disk hemorrhage cases, *Am J Ophthalmol,* 134, 920-2.

Airaksinen, P. J., Drance, S. M., Douglas, G. R. and Schulzer, M. (1985a) Neuroretinal rim areas and visual field indices in glaucoma, *Am J Ophthalmol,* 99, 107-10.

Airaksinen, P. J., Drance, S. M., Douglas, G. R., Schulzer, M. and Wijsman, K. (1985b) Visual field and retinal nerve fiber layer comparisons in glaucoma, *Arch Ophthalmol,* 103, 205-7.

Airaksinen, P. J., Mustonen, E. and Alanko, H. I. (1981) Optic disc haemorrhages precede retinal nerve fibre layer defects in ocular hypertension, *Acta Ophthalmol (Copenh),* 59, 627-41.

Airaksinen, P. J. and Tuulonen, A. (1984) Early glaucoma changes in patients with and without an optic disc haemorrhage, *Acta Ophthalmol (Copenh),* 62, 197-202.

Airaksinen, P. J., Tuulonen, A. and Alanko, H. I. (1992) Rate and pattern of neuroretinal rim area decrease in ocular hypertension and glaucoma, *Arch Ophthalmol,* 110, 206-10.

Albon, J., Karwatowski, W. S., Easty, D. L., Sims, T. J. and Duance, V. C. (2000a) Age related changes in the non-collagenous components of the extracellular matrix of the human lamina cribrosa, *Br J Ophthalmol,* 84, 311-7.

Albon, J., Purslow, P. P., Karwatowski, W. S. and Easty, D. L. (2000b) Age related compliance of the lamina cribrosa in human eyes, *Br J Ophthalmol,* 84, 318-23.

Altman, D. G. (1980) Statistics and ethics in medical research. VI--Presentation of results, *Br Med J,* 281, 1542-4.

Anderson, D. R. (1969) Ultrastructure of human and monkey lamina cribrosa and optic nerve head, *Arch Ophthalmol,* 82, 800-14.

Anderson, D. R. and Braverman, S. (1976) Reevaluation of the optic disk vasculature, *Am J Ophthalmol,* 82, 165-74.

Anton, A., Andrada, M. T., Mujica, V., Calle, M. A., Portela, J. and Mayo, A. (2004) Prevalence of primary open-angle glaucoma in a Spanish population: the Segovia study, *J Glaucoma,* 13, 371-6.

Anton, A., Yamagishi, N., Zangwill, L., Sample, P. A. and Weinreb, R. N. (1998) Mapping structural to functional damage in glaucoma with standard automated perimetry and confocal scanning laser ophthalmoscopy, *Am J Ophthalmol,* 125, 436-46.

Armaly, M. F. (1965) On the Distribution of Applanation Pressure. I. Statistical Features and the Effect of Age, Sex, and Family History of Glaucoma, *Arch Ophthalmol,* 73, 11-8.

Armaly, M. F., Krueger, D. E., Maunder, L., Becker, B., Hetherington, J., Jr., Kolker, A. E., Levene, R. Z., Maumenee, A. E., Pollack, I. P. and Shaffer, R. N. (1980) Biostatistical analysis of the collaborative glaucoma study. I. Summary report of the risk factors for glaucomatous visual-field defects, *Arch Ophthalmol,* 98, 2163-71.

Arndt, S., Cizadlo, T., Andreasen, N. C., Heckel, D., Gold, S. and O'Leary, D. S. (1996) Tests for comparing images based on randomization and permutation methods, *J Cereb Blood Flow Metab,* 16, 1271-9.

Artes, P. H. and Chauhan, B. C. (2005) Longitudinal changes in the visual field and optic disc in glaucoma, *Prog Retin Eye Res,* 24, 333-54.

Artes, P. H., Iwase, A., Ohno, Y., Kitazawa, Y. and Chauhan, B. C. (2002) Properties of perimetric threshold estimates from Full Threshold, SITA Standard, and SITA Fast strategies, *Invest Ophthalmol Vis Sci,* 43, 2654-9.

Artes, P. H., Nicolela, M. T., LeBlanc, R. P. and Chauhan, B. C. (2005) Visual field progression in glaucoma: total versus pattern deviation analyses, *Invest Ophthalmol Vis Sci,* 46, 4600-6.

Aung, T., Ocaka, L., Ebenezer, N. D., Morris, A. G., Brice, G., Child, A. H., Hitchings, R. A., Lehmann, O. J. and Bhattacharya, S. S. (2002) Investigating the association between OPA1 polymorphisms and glaucoma: comparison between normal tension and high tension primary open angle glaucoma, *Hum Genet,* 110, 513-4.

Autzen, T., Pugesgaard, T. and Work, K. (1990) Automated static perimetry and nerve fibre layer defects in glaucoma and controls, *Acta Ophthalmol (Copenh),* 68, 677-80.

Azuara-Blanco, A., Katz, L. J., Spaeth, G. L., Vernon, S. A., Spencer, F. and Lanzl, I. M. (2003) Clinical agreement among glaucoma experts in the detection of glaucomatous changes of the optic disk using simultaneous stereoscopic photographs, *Am J Ophthalmol,* 136, 949-50.

Bagga, H., Greenfield, D. S. and Knighton, R. W. (2003) Scanning laser polarimetry with variable corneal compensation: identification and correction for corneal birefringence in eyes with macular disease, *Invest Ophthalmol Vis Sci,* 44, 1969-76.

Balazsi, A. G., Drance, S. M., Schulzer, M. and Douglas, G. R. (1984) Neuroretinal rim area in suspected glaucoma and early chronic open-angle glaucoma. Correlation with parameters of visual function, *Arch Ophthalmol,* 102, 1011-4.

Bankes, J. L., Perkins, E. S., Tsolakis, S. and Wright, J. E. (1968) Bedford glaucoma survey, *Br Med J,* 1, 791-6.

Bathija, R., Zangwill, L., Berry, C. C., Sample, P. A. and Weinreb, R. N. (1998) Detection of early glaucomatous structural damage with confocal scanning laser tomography, *J Glaucoma,* 7, 121-7.

Bebie, H., Fankhauser, F. and Spahr, J. (1976a) Static perimetry: strategies, *Acta Ophthalmol (Copenh),* 54, 325-38.

Bebie, H., Fankhauser, F. and Spahr, J. (1976b) Static perimetry: accuracy and fluctuations, *Acta Ophthalmol (Copenh),* 54, 339-48.

Bechetoille, A. and Bresson-Dumont, H. (1994) Diurnal and nocturnal blood pressure drops in patients with focal ischemic glaucoma, *Graefes Arch Clin Exp Ophthalmol,* 232, 675-9.

Bengtsson, B. (1976) The variation and covariation of cup and disc diameters, *Acta Ophthalmol (Copenh),* 54, 804-18.

Bengtsson, B. (1980) The alteration and asymmetry of cup and disc diameters, *Acta Ophthalmol (Copenh),* 58, 726-32.

Bengtsson, B. (2000) Reliability of computerized perimetric threshold tests as assessed by reliability indices and threshold reproducibility in patients with suspect and manifest glaucoma, *Acta Ophthalmol Scand,* 78, 519-22.

Bengtsson, B., Heijl, A. and Olsson, J. (1998) Evaluation of a new threshold visual field strategy, SITA, in normal subjects. Swedish Interactive Thresholding Algorithm, *Acta Ophthalmol Scand,* 76, 165-9.

Bengtsson, B., Leske, M. C., Hyman, L. and Heijl, A. (2006) Fluctuation of Intraocular Pressure and Glaucoma Progression in the Early Manifest Glaucoma Trial, *Ophthalmology* (e-pub ahead of print).

Bengtsson, B., Lindgren, A., Heijl, A., Lindgren, G., Asman, P. and Patella, M. (1997a) Perimetric probability maps to separate change caused by glaucoma from that caused by cataract, *Acta Ophthalmol Scand,* 75, 184-8.

Bengtsson, B., Olsson, J., Heijl, A. and Rootzen, H. (1997b) A new generation of algorithms for computerized threshold perimetry, SITA, *Acta Ophthalmol Scand,* 75, 368-75.

Bengtsson, B. O. (1989) Incidence of manifest glaucoma, *Br J Ophthalmol,* 73, 483-7.

Betz, P., Camps, F., Collignon-Brach, J., Lavergne, G. and Weekers, R. (1982) Biometric study of the disc cup in open-angle glaucoma, *Graefes Arch Clin Exp Ophthalmol,* 218, 70-4.

Bhandari, A., Crabb, D. P., Poinoosawmy, D., Fitzke, F. W., Hitchings, R. A. and Noureddin, B. N. (1997) Effect of surgery on visual field progression in normal-tension glaucoma, *Ophthalmology,* 104, 1131-7.

Birch, M. K., Wishart, P. K. and O'Donnell, N. (1995) Determining progressive visual field loss. Perimetry Update 1994/1995. R. P. Mills and M. Wall. Amsterdam, Kugler & Ghedini: 31-36.

Bjerrum, J. (1889) Om en tilföjelse til den saedvanlige synfeltsundersökelse samt om synsfeltet ved glaukom, *Nord Ophthalmol. Tskr (Copenhagen),* 2, 141-185.

Bland, J. M. and Altman, D. G. (1986) Statistical methods for assessing agreement between two methods of clinical measurement, *Lancet,* 1, 307-10.

Blumenthal, E. Z. and Frenkel, S. (2005) Inter-device reproducibility of the scanning laser polarimeter with variable cornea compensation, *Eye,* 19, 308-11.

Blumenthal, E. Z., Williams, J. M., Weinreb, R. N., Girkin, C. A., Berry, C. C. and Zangwill, L. M. (2000) Reproducibility of nerve fiber layer thickness measurements by use of optical coherence tomography, *Ophthalmology,* 107, 2278-82.

Boden, C., Blumenthal, E. Z., Pascual, J., McEwan, G., Weinreb, R. N., Medeiros, F. and Sample, P. A. (2004) Patterns of glaucomatous visual field progression identified by three progression criteria, *Am J Ophthalmol,* 138, 1029-36.

Boeglin, R. J., Caprioli, J. and Zulauf, M. (1992) Long-term fluctuation of the visual field in glaucoma, *Am J Ophthalmol,* 113, 396-400.

Boehm, M. D., Nedrud, C., Greenfield, D. S. and Chen, P. P. (2003) Scanning laser polarimetry and detection of progression after optic disc hemorrhage in patients with glaucoma, *Arch Ophthalmol,* 121, 189-94.

Bonomi, L., Marchini, G., Marraffa, M., Bernardi, P., De Franco, I., Perfetti, S., Varotto, A. and Tenna, V. (1998) Prevalence of glaucoma and intraocular pressure distribution in a defined population. The Egna-Neumarkt Study, *Ophthalmology,* 105, 209-15.

Bonomi, L., Marchini, G., Marraffa, M., Bernardi, P., Morbio, R. and Varotto, A. (2000) Vascular risk factors for primary open angle glaucoma: the Egna-Neumarkt Study, *Ophthalmology,* 107, 1287-93.

Bourne, R. R., Medeiros, F. A., Bowd, C., Jahanbakhsh, K., Zangwill, L. M. and Weinreb, R. N. (2005) Comparability of retinal nerve fiber layer thickness measurements of optical coherence tomography instruments, *Invest Ophthalmol Vis Sci,* 46, 1280-5.

Bourne, R. R., Sukudom, P., Foster, P. J., Tantisevi, V., Jitapunkul, S., Lee, P. S., Johnson, G. J. and Rojanapongpun, P. (2003) Prevalence of glaucoma in Thailand: a population based survey in Rom Klao District, Bangkok, *Br J Ophthalmol,* 87, 1069-74.

Bowd, C., Chan, K., Zangwill, L. M., Goldbaum, M. H., Lee, T. W., Sejnowski, T. J. and Weinreb, R. N. (2002) Comparing neural networks and linear discriminant functions for glaucoma detection using confocal scanning laser ophthalmoscopy of the optic disc, *Invest Ophthalmol Vis Sci,* 43, 3444-54.

Bowd, C., Medeiros, F. A., Zhang, Z., Zangwill, L. M., Hao, J., Lee, T. W., Sejnowski, T. J., Weinreb, R. N. and Goldbaum, M. H. (2005) Relevance vector machine and support

vector machine classifier analysis of scanning laser polarimetry retinal nerve fiber layer measurements, *Invest Ophthalmol Vis Sci,* 46, 1322-9.

Bowd, C., Zangwill, L. M., Medeiros, F. A., Tavares, I. M., Hoffmann, E. M., Bourne, R. R., Sample, P. A. and Weinreb, R. N. (2006) Structure-function relationships using confocal scanning laser ophthalmoscopy, optical coherence tomography, and scanning laser polarimetry, *Invest Ophthalmol Vis Sci,* 47, 2889-95.

Brigatti, L. and Caprioli, J. (1995) Correlation of visual field with scanning confocal laser optic disc measurements in glaucoma, *Arch Ophthalmol,* 113, 1191-4.

Brigatti, L., Weitzman, M. and Caprioli, J. (1995) Regional test-retest variability of confocal scanning laser tomography, *Am J Ophthalmol,* 120, 433-40.

British, S. I. (1979) Precision of test methods I: Guide for the determination and reproducibility for a standard test method. London, BSI. BS 5497, part 1.

Britton, R. J., Drance, S. M., Schulzer, M., Douglas, G. R. and Mawson, D. K. (1987) The area of the neuroretinal rim of the optic nerve in normal eyes, *Am J Ophthalmol,* 103, 497-504.

Bron, A. J., Tripathi, R. C. and Tripathi, B. J. (1997) Wolff's anatomy of the eye and orbit. London, Chapman and Hall Medical.

Budde, W. M. and Jonas, J. B. (2004) Enlargement of parapapillary atrophy in follow-up of chronic open-angle glaucoma, *Am J Ophthalmol,* 137, 646-54.

Budenz, D. L., Chang, R. T., Huang, X., Knighton, R. W. and Tielsch, J. M. (2005) Reproducibility of retinal nerve fiber thickness measurements using the stratus OCT in normal and glaucomatous eyes, *Invest Ophthalmol Vis Sci,* 46, 2440-3.

Buhrmann, R. R., Quigley, H. A., Barron, Y., West, S. K., Oliva, M. S. and Mmbaga, B. B. (2000) Prevalence of glaucoma in a rural East African population, *Invest Ophthalmol Vis Sci,* 41, 40-8.

Bullmore, E. T., Suckling, J., Overmeyer, S., Rabe-Hesketh, S., Taylor, E. and Brammer, M. J. (1999) Global, voxel, and cluster tests, by theory and permutation, for a difference between two groups of structural MR images of the brain, *IEEE Trans Med Imaging,* 18, 32-42.

Bunce, C. and Wormald, R. (2006) Leading causes of certification for blindness and partial sight in England & Wales, *BMC Public Health,* 6, 58.

Burgoyne, C. F., Downs, J. C., Bellezza, A. J., Suh, J. K. and Hart, R. T. (2005) The optic nerve head as a biomechanical structure: a new paradigm for understanding the role of IOP-related stress and strain in the pathophysiology of glaucomatous optic nerve head damage, *Prog Retin Eye Res,* 24, 39-73.

Burgoyne, C. F., Quigley, H. A., Thompson, H. W., Vitale, S. and Varma, R. (1995a) Early changes in optic disc compliance and surface position in experimental glaucoma, *Ophthalmology,* 102, 1800-9.

Burgoyne, C. F., Quigley, H. A., Thompson, H. W., Vitale, S. and Varma, R. (1995b) Measurement of optic disc compliance by digitized image analysis in the normal monkey eye, *Ophthalmology,* 102, 1790-9.

Burgoyne, C. F., Varma, R., Quigley, H. A., Vitale, S., Pease, M. E. and Lenane, P. L. (1994) Global and regional detection of induced optic disc change by digitized image analysis, *Arch Ophthalmol,* 112, 261-8.

Burk, R. O., Vihanninjoki, K., Bartke, T., Tuulonen, A., Airaksinen, P. J., Volcker, H. E. and Konig, J. M. (2000) Development of the standard reference plane for the Heidelberg retina tomograph, *Graefes Arch Clin Exp Ophthalmol,* 238, 375-84.

Burk, R. O. W., Noack, H., Rohrschneider, K. and Volcker, H. E. (1998) Prediction of glaucomatous visual field defects by reference plane independent three-dimensional optic nerve head parameters. Perimetry Update1998/1999. M. Wall and J. M. Wild. The Hague, Walter Kugler: 463-474.

Caprioli, J. (1994) Clinical evaluation of the optic nerve in glaucoma, *Trans Am Ophthalmol Soc,* 92, 589-641.

Caprioli, J. and Miller, J. M. (1987) Optic disc rim area is related to disc size in normal subjects, *Arch Ophthalmol,* 105, 1683-5.

Caprioli, J., Prum, B. and Zeyen, T. (1996) Comparison of methods to evaluate the optic nerve head and nerve fiber layer for glaucomatous change, *Am J Ophthalmol,* 121, 659-67.

Caprioli, J. and Spaeth, G. L. (1985) Comparison of the optic nerve head in high- and low-tension glaucoma, *Arch Ophthalmol,* 103, 1145-9.

Carel, R. S., Korczyn, A. D., Rock, M. and Goya, I. (1984) Association between ocular pressure and certain health parameters, *Ophthalmology,* 91, 311-4.

Carpel, E. F. and Engstrom, P. F. (1981) The normal cup-disk ratio, *Am J Ophthalmol,* 91, 588-97.

Cartwright, M. J. and Anderson, D. R. (1988) Correlation of asymmetric damage with asymmetric intraocular pressure in normal-tension glaucoma (low-tension glaucoma), *Arch Ophthalmol,* 106, 898-900.

Casson, E. J., Shapiro, L. R. and Johnson, C. A. (1990) Short-term fluctuation as an estimate of variability in visual field data, *Invest Ophthalmol Vis Sci,* 31, 2459-63.

Cedrone, C., Culasso, F., Cesareo, M., Zapelloni, A., Cedrone, P. and Cerulli, L. (1997) Prevalence of glaucoma in Ponza, Italy: a comparison with other studies, *Ophthalmic Epidemiol,* 4, 59-72.

Centofanti, M., Oddone, F., Parravano, M., Gualdi, L., Bucci, M. G. and Manni, G. (2005) Corneal birefringence changes after laser assisted in situ keratomileusis and their influence on retinal nerve fibre layer thickness measurement by means of scanning laser polarimetry, *Br J Ophthalmol,* 89, 689-93.

Chandler, P. A. and Grant, W. M. (1965). Lectures on Glaucoma. Philadelphia, Lea and Febiger: 14-16, 112-113.

Chauhan, B. C. (2005) Detection of glaucomatous changes in the optic disc. The essential HRT primer. M. Fingeret, J. G. Flanagan and J. M. Liebmann. San Ramon, California, Jocoto Advertising, Inc.: 53-65.

Chauhan, B. C., Blanchard, J. W., Hamilton, D. C. and LeBlanc, R. P. (2000) Technique for detecting serial topographic changes in the optic disc and peripapillary retina using scanning laser tomography, *Invest Ophthalmol Vis Sci,* 41, 775-82.

Chauhan, B. C., Drance, S. M. and Douglas, G. R. (1990) The use of visual field indices in detecting changes in the visual field in glaucoma, *Invest Ophthalmol Vis Sci,* 31, 512-20.

Chauhan, B. C. and Johnson, C. A. (1999) Test-retest variability of frequency-doubling perimetry and conventional perimetry in glaucoma patients and normal subjects, *Invest Ophthalmol Vis Sci,* 40, 648-56.

Chauhan, B. C., LeBlanc, R. P., McCormick, T. A. and Rogers, J. B. (1994) Test-retest variability of topographic measurements with confocal scanning laser tomography in patients with glaucoma and control subjects, *Am J Ophthalmol,* 118, 9-15.

Chauhan, B. C., LeBlanc, R. P., Shaw, A. M., Chan, A. B. and McCormick, T. A. (1997) Repeatable diffuse visual field loss in open-angle glaucoma, *Ophthalmology,* 104, 532-8.

Chauhan, B. C. and Macdonald, C. A. (1995) Influence of time separation on variability estimates of topographical measurements with confocal scanning laser tomography, *Journal of Glaucoma,* 4, 189-193.

Chauhan, B. C. and McCormick, T. A. (1995) Effect of the cardiac cycle on topographic measurements using confocal scanning laser tomography, *Graefes Arch Clin Exp Ophthalmol,* 233, 568-72.

Chauhan, B. C., McCormick, T. A., Nicolela, M. T. and LeBlanc, R. P. (2001) Optic disc and visual field changes in a prospective longitudinal study of patients with glaucoma: comparison of scanning laser tomography with conventional perimetry and optic disc photography, *Arch Ophthalmol,* 119, 1492-9.

Chauhan, B. C., Tompkins, J. D., LeBlanc, R. P. and McCormick, T. A. (1993) Characteristics of frequency-of-seeing curves in normal subjects, patients with suspected glaucoma, and patients with glaucoma, *Invest Ophthalmol Vis Sci,* 34, 3534-40.

Chen, E., Gedda, U. and Landau, I. (2001) Thinning of the papillomacular bundle in the glaucomatous eye and its influence on the reference plane of the Heidelberg retinal tomography, *J Glaucoma,* 10, 386-9.

Cheng, C. Y., Liu, C. J., Chiou, H. J., Chou, J. C., Hsu, W. M. and Liu, J. H. (2001) Color Doppler imaging study of retrobulbar hemodynamics in chronic angle-closure glaucoma, *Ophthalmology,* 108, 1445-51.

Choplin, N., Reus, N. and Lemij, H. (2005) Interpretation of GDx VCC printouts. Optic nerve head and retinal nerve fibre analysis. M. Iester, D. F. Garway-Heath and H. Lemij. Savona, Editrice Dogma: 103-106.

Choplin, N. T., Zhou, Q. and Knighton, R. W. (2003) Effect of individualized compensation for anterior segment birefringence on retinal nerve fiber layer assessments as determined by scanning laser polarimetry, *Ophthalmology,* 110, 719-25.

Chylack, L. T., Jr., Wolfe, J. K., Singer, D. M., Leske, M. C., Bullimore, M. A., Bailey, I. L., Friend, J., McCarthy, D. and Wu, S. Y. (1993) The Lens Opacities Classification System III. The Longitudinal Study of Cataract Study Group, *Arch Ophthalmol,* 111, 831-6.

Cockerham, K. P., Pal, C., Jani, B., Wolter, A. and Kennerdell, J. S. (1997) The prevalence and implications of ocular hypertension and glaucoma in thyroid-associated orbitopathy, *Ophthalmology,* 104, 914-7.

Coffey, M., Reidy, A., Wormald, R., Xian, W. X., Wright, L. and Courtney, P. (1993) Prevalence of glaucoma in the west of Ireland, *Br J Ophthalmol,* 77, 17-21.

Coleman, A. L., Sommer, A., Enger, C., Knopf, H. L., Stamper, R. L. and Minckler, D. S. (1996) Interobserver and intraobserver variability in the detection of glaucomatous progression of the optic disc, *J Glaucoma,* 5, 384-9.

Colton, T. and Ederer, F. (1980) The distribution of intraocular pressures in the general population, *Surv Ophthalmol,* 25, 123-9.

Congdon, N., O'Colmain, B., Klaver, C. C., Klein, R., Munoz, B., Friedman, D. S., Kempen, J., Taylor, H. R. and Mitchell, P. (2004) Causes and prevalence of visual impairment among adults in the United States, *Arch Ophthalmol,* 122, 477-85.

Congdon, N. G., Broman, A. T., Bandeen-Roche, K., Grover, D. and Quigley, H. A. (2006) Central corneal thickness and corneal hysteresis associated with glaucoma damage, *Am J Ophthalmol,* 141, 868-75.

Coops, A., Henson, D. B., Kwartz, A. J. and Artes, P. H. (2006) Automated analysis of heidelberg retina tomograph optic disc images by glaucoma probability score, *Invest Ophthalmol Vis Sci,* 47, 5348-55.

Crabb, D. P., Fitzke, F. W. and McNaught, A. I. (1997a) A profile of the spatial dependence of pointwise sensitivity across the glaucomatous visual field. Perimetry Update 1996/1997. A. Heijl and M. Wall. Amsterdam, Kugler Publications: 301-311.

Crabb, D. P., Fitzke, F. W., McNaught, A. I., Edgar, D. F. and Hitchings, R. A. (1997b) Improving the prediction of visual field progression in glaucoma using spatial processing, *Ophthalmology,* 104, 517-24.

Crichton, A., Drance, S. M., Douglas, G. R. and Schulzer, M. (1989) Unequal intraocular pressure and its relation to asymmetric visual field defects in low-tension glaucoma, *Ophthalmology,* 96, 1312-4.

Cursiefen, C., Wisse, M., Cursiefen, S., Junemann, A., Martus, P. and Korth, M. (2000) Migraine and tension headache in high-pressure and normal-pressure glaucoma, *Am J Ophthalmol,* 129, 102-4.

Da Pozzo, S., Fuser, M., Vattovani, O., Di Stefano, G. and Ravalico, G. (2006) GDx-VCC performance in discriminating normal from glaucomatous eyes with early visual field loss, *Graefes Arch Clin Exp Ophthalmol,* 244, 689-695.

Dandona, L., Dandona, R., Srinivas, M., Mandal, P., John, R. K., McCarty, C. A. and Rao, G. N. (2000) Open-angle glaucoma in an urban population in southern India: the Andhra Pradesh eye disease study, *Ophthalmology,* 107, 1702-9.

Danesh-Meyer, H. V., Ku, J. Y., Papchenko, T. L., Jayasundera, T., Hsiang, J. C. and Gamble, G. D. (2006) Regional correlation of structure and function in glaucoma, using the Disc Damage Likelihood Scale, Heidelberg Retina Tomograph, and visual fields, *Ophthalmology,* 113, 603-11.

David, R., Zangwill, L. M., Tessler, Z. and Yassur, Y. (1985) The correlation between intraocular pressure and refractive status, *Arch Ophthalmol,* 103, 1812-5.

de Voogd, S., Ikram, M. K., Wolfs, R. C., Jansonius, N. M., Hofman, A. and de Jong, P. T. (2005) Incidence of open-angle glaucoma in a general elderly population: the Rotterdam Study, *Ophthalmology,* 112, 1487-93.

Demailly, P., Cambien, F., Plouin, P. F., Baron, P. and Chevallier, B. (1984) Do patients with low tension glaucoma have particular cardiovascular characteristics?, *Ophthalmologica,* 188, 65-75.

Dielemans, I., de Jong, P. T., Stolk, R., Vingerling, J. R., Grobbee, D. E. and Hofman, A. (1996) Primary open-angle glaucoma, intraocular pressure, and diabetes mellitus in the general elderly population. The Rotterdam Study, *Ophthalmology,* 103, 1271-5.

Dielemans, I., Vingerling, J. R., Wolfs, R. C., Hofman, A., Grobbee, D. E. and de Jong, P. T. (1994) The prevalence of primary open-angle glaucoma in a population-based study in The Netherlands. The Rotterdam Study, *Ophthalmology,* 101, 1851-5.

Dolman, C. L., McCormick, A. Q. and Drance, S. M. (1980) Aging of the optic nerve, *Arch Ophthalmol,* 98, 2053-8.

Drance, S., Anderson, D. R. and Schulzer, M. (2001) Risk factors for progression of visual field abnormalities in normal-tension glaucoma, *Am J Ophthalmol,* 131, 699-708.

Drance, S. M. (1991) Diffuse visual field loss in open-angle glaucoma, *Ophthalmology,* 98, 1533-8.

Drance, S. M., Douglas, G. R., Wijsman, K., Schulzer, M. and Britton, R. J. (1988) Response of blood flow to warm and cold in normal and low-tension glaucoma patients, *Am J Ophthalmol,* 105, 35-9.

Drance, S. M., Fairclough, M., Butler, D. M. and Kottler, M. S. (1977) The importance of disc hemorrhage in the prognosis of chronic open angle glaucoma, *Arch Ophthalmol,* 95, 226-8.

Drance, S. M., Schulzer, M., Thomas, B. and Douglas, G. R. (1981) Multivariate analysis in glaucoma. Use of discriminant analysis in predicting glaucomatous visual field damage, *Arch Ophthalmol,* 99, 1019-22.

Drance, S. M., Sweeney, V. P., Morgan, R. W. and Feldman, F. (1973) Studies of factors involved in the production of low tension glaucoma, *Arch Ophthalmol,* 89, 457-65.

Dreher, A. W., Tso, P. C. and Weinreb, R. N. (1991) Reproducibility of topographic measurements of the normal and glaucomatous optic nerve head with the laser tomographic scanner, *Am J Ophthalmol,* 111, 221-9.

Drexler, W., Morgner, U., Ghanta, R. K., Kartner, F. X., Schuman, J. S. and Fujimoto, J. G. (2001) Ultrahigh-resolution ophthalmic optical coherence tomography, *Nat Med,* 7, 502-7.

Duijm, H. F., van den Berg, T. J. and Greve, E. L. (1997) Choroidal haemodynamics in glaucoma, *Br J Ophthalmol,* 81, 735-42.

Edmunds, B., Thompson, J. R., Salmon, J. F. and Wormald, R. P. (1999) The National Survey of Trabeculectomy. I. Sample and methods, *Eye,* 13 (Pt 4), 524-30.

Ehlers, N. (1970) On corneal thickness and intraocular pressure. II. A clinical study on the thickness of the corneal stroma in glaucomatous eyes, *Acta Ophthalmol (Copenh),* 48, 1107-12.

El Beltagi, T. A., Bowd, C., Boden, C., Amini, P., Sample, P. A., Zangwill, L. M. and Weinreb, R. N. (2003) Retinal nerve fiber layer thickness measured with optical coherence tomography is related to visual function in glaucomatous eyes, *Ophthalmology,* 110, 2185-91.

Elkington, A. R., Inman, C. B., Steart, P. V. and Weller, R. O. (1990) The structure of the lamina cribrosa of the human eye: an immunocytochemical and electron microscopical study, *Eye,* 4 (Pt 1), 42-57.

Ellis, J. D., Morris, A. D. and MacEwen, C. J. (1999) Should diabetic patients be screened for glaucoma? DARTS/MEMO Collaboration, *Br J Ophthalmol,* 83, 369-72.

Emdadi, A., Zangwill, L., Sample, P. A., Kono, Y., Anton, A. and Weinreb, R. N. (1998) Patterns of optic disk damage in patients with early focal visual field loss, *Am J Ophthalmol,* 126, 763-71.

Emery, J. M., Landis, D., Paton, D., Boniuk, M. and Craig, J. M. (1974) The lamina cribrosa in normal and glaucomatous human eyes, *Trans Am Acad Ophthalmol Otolaryngol,* 78, OP290-7.

Emre, M., Orgul, S., Haufschild, T., Shaw, S. G. and Flammer, J. (2005) Increased plasma endothelin-1 levels in patients with progressive open angle glaucoma, *Br J Ophthalmol,* 89, 60-3.

Ernest, J. T. and Potts, A. M. (1968) Pathophysiology of the distal portion of the optic nerve. I. Tissue pressure relationships, *Am J Ophthalmol,* 66, 373-80.

Ervin, J. C., Lemij, H. G., Mills, R. P., Quigley, H. A., Thompson, H. W. and Burgoyne, C. F. (2002) Clinician change detection viewing longitudinal stereophotographs compared

to confocal scanning laser tomography in the LSU Experimental Glaucoma (LEG) Study, *Ophthalmology,* 109, 467-81.

Essock, E. A., Zheng, Y. and Gunvant, P. (2005) Analysis of GDx-VCC polarimetry data by Wavelet-Fourier analysis across glaucoma stages, *Invest Ophthalmol Vis Sci,* 46, 2838-47.

Findl, O., Rainer, G., Dallinger, S., Dorner, G., Polak, K., Kiss, B., Georgopoulos, M., Vass, C. and Schmetterer, L. (2000) Assessment of optic disk blood flow in patients with open-angle glaucoma, *Am J Ophthalmol,* 130, 589-96.

Fingert, J. H., Heon, E., Liebmann, J. M., Yamamoto, T., Craig, J. E., Rait, J., Kawase, K., Hoh, S. T., Buys, Y. M., Dickinson, J., Hockey, R. R., Williams-Lyn, D., Trope, G., Kitazawa, Y., Ritch, R., Mackey, D. A., Alward, W. L., Sheffield, V. C. and Stone, E. M. (1999) Analysis of myocilin mutations in 1703 glaucoma patients from five different populations, *Hum Mol Genet,* 8, 899-905.

Fitzgibbon, T. and Taylor, S. F. (1996) Retinotopy of the human retinal nerve fibre layer and optic nerve head, *J Comp Neurol,* 375, 238-51.

Fitzke, F. W., Crabb, D. P., McNaught, A. I., Edgar, D. F. and Hitchings, R. A. (1995) Image processing of computerised visual field data, *Br J Ophthalmol,* 79, 207-12.

Fitzke, F. W., Hitchings, R. A., Poinoosawmy, D., McNaught, A. I. and Crabb, D. P. (1996) Analysis of visual field progression in glaucoma, *Br J Ophthalmol,* 80, 40-8.

Flammer, J., Drance, S. M., Augustiny, L. and Funkhouser, A. (1985) Quantification of glaucomatous visual field defects with automated perimetry, *Invest Ophthalmol Vis Sci,* 26, 176-81.

Flammer, J., Drance, S. M., Fankhauser, F. and Augustiny, L. (1984a) Differential light threshold in automated static perimetry. Factors influencing short-term fluctuation, *Arch Ophthalmol,* 102, 876-9.

Flammer, J., Drance, S. M. and Schulzer, M. (1984b) Covariates of the long-term fluctuation of the differential light threshold, *Arch Ophthalmol,* 102, 880-2.

Flammer, J., Drance, S. M. and Zulauf, M. (1984c) Differential light threshold. Short- and long-term fluctuation in patients with glaucoma, normal controls, and patients with suspected glaucoma, *Arch Ophthalmol,* 102, 704-6.

Flammer, J., Haefliger, I. O., Orgul, S. and Resink, T. (1999) Vascular dysregulation: a principal risk factor for glaucomatous damage?, *J Glaucoma,* 8, 212-9.

Flammer, J., Pache, M. and Resink, T. (2001) Vasospasm, its role in the pathogenesis of diseases with particular reference to the eye, *Prog Retin Eye Res,* 20, 319-49.

Fontana, L., Bhandari, A., Fitzke, F. W. and Hitchings, R. A. (1998a) In vivo morphometry of the lamina cribrosa and its relation to visual field loss in glaucoma, *Curr Eye Res,* 17, 363-9.

Fontana, L., Poinoosawmy, D., Bunce, C. V., O'Brien, C. and Hitchings, R. A. (1998b) Pulsatile ocular blood flow investigation in asymmetric normal tension glaucoma and normal subjects, *Br J Ophthalmol,* 82, 731-6.

Ford, B. A., Artes, P. H., McCormick, T. A., Nicolela, M. T., LeBlanc, R. P. and Chauhan, B. C. (2003) Comparison of data analysis tools for detection of glaucoma with the Heidelberg Retina Tomograph, *Ophthalmology,* 110, 1145-50.

Foster, P. J., Baasanhu, J., Alsbirk, P. H., Munkhbayar, D., Uranchimeg, D. and Johnson, G. J. (1996) Glaucoma in Mongolia. A population-based survey in Hovsgol province, northern Mongolia, *Arch Ophthalmol,* 114, 1235-41.

Foster, P. J., Oen, F. T., Machin, D., Ng, T. P., Devereux, J. G., Johnson, G. J., Khaw, P. T. and Seah, S. K. (2000) The prevalence of glaucoma in Chinese residents of Singapore: a cross-sectional population survey of the Tanjong Pagar district, *Arch Ophthalmol,* 118, 1105-11.

Franceschetti, A. and Bock, R. H. (1950) Megalopapilla; a new congenital anomaly, *Am J Ophthalmol,* 33, 227-35.

Frenkel, S., Slonim, E., Horani, A., Molcho, M., Barzel, I. and Blumenthal, E. Z. (2005) Operator learning effect and interoperator reproducibility of the scanning laser polarimeter with variable corneal compensation, *Ophthalmology,* 112, 257-61.

Fuchs, E. (1916) Uer die lamina cribrosa, *Albrecht von Graefes Arch Ophthalmol,* 91, 435-485.

Funk, J., Bornscheuer, C. and Grehn, F. (1988) Neuroretinal rim area and visual field in glaucoma, *Graefes Arch Clin Exp Ophthalmol,* 226, 431-4.

Funk, J., Dieringer, T. and Grehn, F. (1989) Correlation between neuroretinal rim area and age in normal subjects, *Graefes Arch Clin Exp Ophthalmol,* 227, 544-8.

Gardiner, S. K. and Crabb, D. P. (2002a) Examination of different pointwise linear regression methods for determining visual field progression, *Invest Ophthalmol Vis Sci,* 43, 1400-7.

Gardiner, S. K. and Crabb, D. P. (2002b) Frequency of testing for detecting visual field progression, *Br J Ophthalmol,* 86, 560-4.

Gardiner, S. K., Crabb, D. P., Fitzke, F. W. and Hitchings, R. A. (2004) Reducing noise in suspected glaucomatous visual fields by using a new spatial filter, *Vision Res,* 44, 839-48.

Gardiner, S. K., Johnson, C. A. and Cioffi, G. A. (2005) Evaluation of the structure-function relationship in glaucoma, *Invest Ophthalmol Vis Sci,* 46, 3712-7.

Gardiner, S. K., Johnson, C. A. and Spry, P. G. (2006) Normal age-related sensitivity loss for a variety of visual functions throughout the visual field, *Optom Vis Sci,* 83, 438-43.

Garway-Heath, D. F., Caprioli, J., Fitzke, F. W. and Hitchings, R. A. (2000b) Scaling the hill of vision: the physiological relationship between light sensitivity and ganglion cell numbers, *Invest Ophthalmol Vis Sci,* 41, 1774-82.

Garway-Heath, D. F. and Hitchings, R. A. (1998) Sources of bias in studies of optic disc and retinal nerve fibre layer morphology, *Br J Ophthalmol,* 82, 986.

Garway-Heath, D. F., Holder, G. E., Fitzke, F. W. and Hitchings, R. A. (2002) Relationship between electrophysiological, psychophysical, and anatomical measurements in glaucoma, *Invest Ophthalmol Vis Sci,* 43, 2213-20.

Garway-Heath, D. F., Poinoosawmy, D., Fitzke, F. W. and Hitchings, R. A. (2000a) Mapping the visual field to the optic disc in normal tension glaucoma eyes, *Ophthalmology,* 107, 1809-15.

Garway-Heath, D. F., Poinoosawmy, D., Wollstein, G., Viswanathan, A., Kamal, D., Fontana, L. and Hitchings, R. A. (1999) Inter- and intraobserver variation in the analysis of optic disc images: comparison of the Heidelberg retina tomograph and computer assisted planimetry, *Br J Ophthalmol,* 83, 664-9.

Garway-Heath, D. F., Ruben, S. T., Viswanathan, A. and Hitchings, R. A. (1998a) Vertical cup/disc ratio in relation to optic disc size: its value in the assessment of the glaucoma suspect, *Br J Ophthalmol,* 82, 1118-24.

Garway-Heath, D. F., Rudnicka, A. R., Lowe, T., Foster, P. J., Fitzke, F. W. and Hitchings, R. A. (1998b) Measurement of optic disc size: equivalence of methods to correct for ocular magnification, *Br J Ophthalmol,* 82, 643-9.

Garway-Heath, D. F., Wollstein, G. and Hitchings, R. A. (1997) Aging changes of the optic nerve head in relation to open angle glaucoma, *Br J Ophthalmol,* 81, 840-5.

Gasser, P. and Flammer, J. (1991) Blood-cell velocity in the nailfold capillaries of patients with normal-tension and high-tension glaucoma, *Am J Ophthalmol,* 111, 585-8.

Geijssen, H. C. and Greve, E. L. (1987) The spectrum of primary open angle glaucoma. I: Senile sclerotic glaucoma versus high tension glaucoma, *Ophthalmic Surg,* 18, 207-13.

Girkin, C. A. (2005) Principles of confocal scanning laser ophthalmoscopy for the clinician. The essential HRT primer. M. Fingeret, J. G. Flanagan and J. Liebmann. San Ramon, California, Jocoto Advertising, Inc.: 2-7.

Girkin, C. A., McGwin, G., Jr., McNeal, S. F. and Owsley, C. (2006) Is there an association between pre-existing sleep apnoea and the development of glaucoma?, *Br J Ophthalmol,* 90, 679-81.

Girkin, C. A., McGwin, G., Jr., Xie, A. and Deleon-Ortega, J. (2005) Differences in optic disc topography between black and white normal subjects, *Ophthalmology,* 112, 33-9.

Giuffre, G., Giammanco, R., Dardanoni, G. and Ponte, F. (1995) Prevalence of glaucoma and distribution of intraocular pressure in a population. The Casteldaccia Eye Study, *Acta Ophthalmol Scand,* 73, 222-5.

Goldberg, I., Hollows, F. C., Kass, M. A. and Becker, B. (1981) Systemic factors in patients with low-tension glaucoma, *Br J Ophthalmol,* 65, 56-62.

Goldmann, H. and Schmidt, T. (1957) [Applanation tonometry.], *Ophthalmologica,* 134, 221-42.

Goldschmidt, E. (1973) The heredity of glaucoma, *Acta Ophthalmol Suppl,* 120, 27-31.

Gonzalez de la Rosa, M., Gonzalez-Hernandez, M., Abraldes, M. and Azuara-Blanco, A. (2002) Quantification of interpoint topographic correlations of threshold values in glaucomatous visual fields, *J Glaucoma,* 11, 30-4.

Gordon, M. O., Beiser, J. A., Brandt, J. D., Heuer, D. K., Higginbotham, E. J., Johnson, C. A., Keltner, J. L., Miller, J. P., Parrish, R. K., 2nd, Wilson, M. R. and Kass, M. A. (2002) The Ocular Hypertension Treatment Study: baseline factors that predict the onset of primary open-angle glaucoma, *Arch Ophthalmol,* 120, 714-20; discussion 829-30.

Graham, S. L. and Drance, S. M. (1999) Nocturnal hypotension: role in glaucoma progression, *Surv Ophthalmol,* 43 Suppl 1, S10-6.

Graham, S. L., Drance, S. M., Wijsman, K., Douglas, G. R. and Mikelberg, F. S. (1995) Ambulatory blood pressure monitoring in glaucoma. The nocturnal dip, *Ophthalmology,* 102, 61-9.

Greenfield, D. S., Knighton, R. W. and Huang, X. R. (2000) Effect of corneal polarization axis on assessment of retinal nerve fiber layer thickness by scanning laser polarimetry, *Am J Ophthalmol,* 129, 715-22.

Guo, L., Tsatourian, V., Luong, V., Podoleanu, A. G., Jackson, D. A., Fitzke, F. W. and Cordeiro, M. F. (2005) En face optical coherence tomography: a new method to analyse structural changes of the optic nerve head in rat glaucoma, *Br J Ophthalmol,* 89, 1210-6.

Gupta, N. and Weinreb, R. N. (1997) New definitions of glaucoma, *Curr Opin Ophthalmol,* 8, 38-41.

Guthauser, U., Flammer, J. and Niesel, P. (1987) The relationship between the visual field and the optic nerve head in glaucomas, *Graefes Arch Clin Exp Ophthalmol,* 225, 129-32.

Haas, J. S. and Nootens, R. H. (1974) Glaucoma secondary to benign adrenal adenoma, *Am J Ophthalmol,* 78, 497-500.

Halkiadakis, I., Anglionto, L., Ferensowicz, M., Triebwasser, R. W., van Westenbrugge, J. A. and Gimbel, H. V. (2005) Assessment of nerve fiber layer thickness before and after laser in situ keratomileusis using scanning laser polarimetry with variable corneal compensation, *J Cataract Refract Surg,* 31, 1035-41.

Hammond, C. J., Snieder, H., Spector, T. D. and Gilbert, C. E. (2000) Genetic and environmental factors in age-related nuclear cataracts in monozygotic and dizygotic twins, *N Engl J Med,* 342, 1786-90.

Hart, W. M., Jr. and Becker, B. (1982) The onset and evolution of glaucomatous visual field defects, *Ophthalmology,* 89, 268-79.

Hart, W. M., Jr., Yablonski, M., Kass, M. A. and Becker, B. (1979) Multivariate analysis of the risk of glaucomatous visual field loss, *Arch Ophthalmol,* 97, 1455-8.

Harwerth, R. S., Carter-Dawson, L., Shen, F., Smith, E. L., 3rd and Crawford, M. L. (1999) Ganglion cell losses underlying visual field defects from experimental glaucoma, *Invest Ophthalmol Vis Sci,* 40, 2242-50.

Harwerth, R. S., Carter-Dawson, L., Smith, E. L., 3rd, Barnes, G., Holt, W. F. and Crawford, M. L. (2004) Neural losses correlated with visual losses in clinical perimetry, *Invest Ophthalmol Vis Sci,* 45, 3152-60.

Harwerth, R. S. and Quigley, H. A. (2006) Visual field defects and retinal ganglion cell losses in patients with glaucoma, *Arch Ophthalmol,* 124, 853-9.

Hatch, W. V., Flanagan, J. G., Etchells, E. E., Williams-Lyn, D. E. and Trope, G. E. (1997) Laser scanning tomography of the optic nerve head in ocular hypertension and glaucoma, *Br J Ophthalmol,* 81, 871-6.

Hayreh, S. S. (1975) Segmental nature of the choroidal vasculature, *Br J Ophthalmol,* 59, 631-48.

Hayreh, S. S. (1978) Structure and blood supply of the optic nerve. Glaucoma: conceptions of a disease. K. Heilmann and K. T. Richardson. Stuttgart, Thieme: 104-137.

Hayreh, S. S. (1990) In vivo choroidal circulation and its watershed zones, *Eye,* 4 (Pt 2), 273-89.

Hayreh, S. S. (2001) The blood supply of the optic nerve head and the evaluation of it - myth and reality, *Prog Retin Eye Res,* 20, 563-93.

Hayreh, S. S., Pe'er, J. and Zimmerman, M. B. (1999a) Morphologic changes in chronic high-pressure experimental glaucoma in rhesus monkeys, *J Glaucoma,* 8, 56-71.

Hayreh, S. S., Podhajsky, P. and Zimmerman, M. B. (1999b) Role of nocturnal arterial hypotension in optic nerve head ischemic disorders, *Ophthalmologica,* 213, 76-96.

Hayreh, S. S., Zimmerman, M. B., Podhajsky, P. and Alward, W. L. (1994) Nocturnal arterial hypotension and its role in optic nerve head and ocular ischemic disorders, *Am J Ophthalmol,* 117, 603-24.

Healey, P. R., Mitchell, P., Smith, W. and Wang, J. J. (1998) Optic disc hemorrhages in a population with and without signs of glaucoma, *Ophthalmology,* 105, 216-23.

Heidelberg Engineering. (2006) Operating manual for the Heidelberg Retina Tomograph III. Heidelberg, Heidelberg Engineering.

Heidelberg Engineering. (2003) Operation manual for the Heidelberg Retina Tomograph II. Heidelberg, Heidelberg Engineering.

Heijl, A., Bengtsson, B. and Lindgren, G. (1998) Visual field progression in glaucoma, *Br J Ophthalmol,* 82, 1097-8.

Heijl, A., Bengtsson, B. and Patella, V. M. (2000) Glaucoma follow-up when converting from long to short perimetric threshold tests, *Arch Ophthalmol,* 118, 489-93.

Heijl, A., Leske, M. C., Bengtsson, B. and Hussein, M. (2003) Measuring visual field progression in the Early Manifest Glaucoma Trial, *Acta Ophthalmol Scand,* 81, 286-93.

Heijl, A., Leske, M. C., Bengtsson, B., Hyman, L. and Hussein, M. (2002) Reduction of intraocular pressure and glaucoma progression: results from the Early Manifest Glaucoma Trial, *Arch Ophthalmol,* 120, 1268-79.

Heijl, A., Lindgren, A. and Lindgren, G. (1989a) Test-retest variability in glaucomatous visual fields, *Am J Ophthalmol,* 108, 130-5.

Heijl, A., Lindgren, G., Lindgren, A., Olsson, J., Åsman, P., Myers, S. and Patella, M. (1990) Extended empirical statistical package for evaluation of single and multiple fileds in glaucoma: Statpac 2. Perimetry Update 1990/1. R. Mills and A. Heijl. Amsterdam/New York, Kluger Publications: 303-15.

Heijl, A., Lindgren, G. and Olsson, J. (1987) Normal variability of static perimetric threshold values across the central visual field, *Arch Ophthalmol,* 105, 1544-9.

Heijl, A., Lindgren, G., Olsson, J. and Asman, P. (1989b) Visual field interpretation with empiric probability maps, *Arch Ophthalmol,* 107, 204-8.

Henderer, J. D., Liu, C., Kesen, M., Altangerel, U., Bayer, A., Steinmann, W. C. and Spaeth, G. L. (2003) Reliability of the disk damage likelihood scale, *Am J Ophthalmol,* 135, 44-8.

Henson, D. B. (1998) Visual Fields. Oxford, Butterworth Heinemann.

Henson, D. B., Artes, P. H. and Chauhan, B. C. (1999) Diffuse loss of sensitivity in early glaucoma, *Invest Ophthalmol Vis Sci,* 40, 3147-51.

Henson, D. B., Chaudry, S., Artes, P. H., Faragher, E. B. and Ansons, A. (2000) Response variability in the visual field: comparison of optic neuritis, glaucoma, ocular hypertension, and normal eyes, *Invest Ophthalmol Vis Sci,* 41, 417-21.

Hernandez, M. R. (1992) Ultrastructural immunocytochemical analysis of elastin in the human lamina cribrosa. Changes in elastic fibers in primary open-angle glaucoma, *Invest Ophthalmol Vis Sci,* 33, 2891-903.

Hernandez, M. R. (2000) The optic nerve head in glaucoma: role of astrocytes in tissue remodeling, *Prog Retin Eye Res,* 19, 297-321.

Hernandez, M. R., Andrzejewska, W. M. and Neufeld, A. H. (1990) Changes in the extracellular matrix of the human optic nerve head in primary open-angle glaucoma, *Am J Ophthalmol,* 109, 180-8.

Hernandez, M. R., Luo, X. X., Andrzejewska, W. and Neufeld, A. H. (1989) Age-related changes in the extracellular matrix of the human optic nerve head, *Am J Ophthalmol,* 107, 476-84.

Hernandez, M. R., Luo, X. X., Igoe, F. and Neufeld, A. H. (1987) Extracellular matrix of the human lamina cribrosa, *Am J Ophthalmol,* 104, 567-76.

Hernandez, M. R., Pena, J. D., Selvidge, J. A., Salvador-Silva, M. and Yang, P. (2000) Hydrostatic pressure stimulates synthesis of elastin in cultured optic nerve head astrocytes, *Glia,* 32, 122-36.

Hernandez, M. R., Ye, H. and Roy, S. (1994) Collagen type IV gene expression in human optic nerve heads with primary open angle glaucoma, *Exp Eye Res,* 59, 41-51.

Herndon, L. W., Weizer, J. S. and Stinnett, S. S. (2004) Central corneal thickness as a risk factor for advanced glaucoma damage, *Arch Ophthalmol,* 122, 17-21.

Herschler, J. and Osher, R. H. (1980) Baring of the circumlinear vessel. An early sign of optic nerve damage, *Arch Ophthalmol,* 98, 865-9.

Hitchings, R. A. and Spaeth, G. L. (1976) The optic disc in glaucoma. I: Classification, *Br J Ophthalmol,* 60, 778-85.

Hitchings, R. A. and Spaeth, G. L. (1977) Fluorescein angiography in chronic simple and low-tension glaucoma, *Br J Ophthalmol,* 61, 126-32.

Hogan, M. J., Alvarado, J. A. and Esperson Weddell, J. (1971) Histology of the human eye: an atlas and textbook. Philadelphia, W.B. Saunders Company.

Hoh, S. T., Ishikawa, H., Greenfield, D. S., Liebmann, J. M., Chew, S. J. and Ritch, R. (1998) Peripapillary nerve fiber layer thickness measurement reproducibility using scanning laser polarimetry, *J Glaucoma,* 7, 12-5.

Hollo, G. (1997) Scanning laser Doppler flowmeter study of retinal and optic disk blood flow in glaucomatous patients, *Am J Ophthalmol,* 123, 859-60.

Hollo, G., Katsanos, A., Kothy, P., Kerek, A. and Suveges, I. (2003) Influence of LASIK on scanning laser polarimetric measurement of the retinal nerve fibre layer with fixed angle and customised corneal polarisation compensation, *Br J Ophthalmol,* 87, 1241-6.

Hollo, G., Nagy, Z. Z., Vargha, P. and Suveges, I. (2002) Influence of post-LASIK corneal healing on scanning laser polarimetric measurement of the retinal nerve fibre layer thickness, *Br J Ophthalmol,* 86, 627-31.

Hollo, G., Suveges, I., Nagymihaly, A. and Vargha, P. (1997) Scanning laser polarimetry of the retinal nerve fibre layer in primary open angle and capsular glaucoma, *Br J Ophthalmol,* 81, 857-61.

Holmes, A. P., Blair, R. C., Watson, J. D. and Ford, I. (1996) Nonparametric analysis of statistic images from functional mapping experiments, *J Cereb Blood Flow Metab,* 16, 7-22.

Horani, A., Frenkel, S. and Blumenthal, E. Z. (2006) The effect of pupil dilation on scanning laser polarimetry with variable corneal compensation, *Ophthalmic Surg Lasers Imaging,* 37, 212-6.

Horton, J. C., Greenwood, M. M. and Hubel, D. H. (1979) Non-retinotopic arrangement of fibres in cat optic nerve, *Nature,* 282, 720-2.

Hoyng, P. F., de Jong, N., Oosting, H. and Stilma, J. (1992) Platelet aggregation, disc haemorrhage and progressive loss of visual fields in glaucoma. A seven year follow-up study on glaucoma, *Int Ophthalmol,* 16, 65-73.

Hoyt, W. F. (1976) Fundoscopic changes in the retinal nerve-fibre layer in chronic and acute optic neuropathies, *Trans Ophthalmol Soc U K,* 96, 368-71.

Hoyt, W. F., Frisen, L. and Newman, N. M. (1973) Fundoscopy of nerve fiber layer defects in glaucoma, *Invest Ophthalmol,* 12, 814-29.

Hoyt, W. F. and Luis, O. (1962) Visual fiber anatomy in the infrageniculate pathway of the primate, *Arch Ophthalmol,* 68, 94-106.

Hoyt, W. F. and Newman, N. M. (1972) The earliest observable defect in glaucoma?, *Lancet,* 1, 692-3.

Huang, D., Swanson, E. A., Lin, C. P., Schuman, J. S., Stinson, W. G., Chang, W., Hee, M. R., Flotte, T., Gregory, K., Puliafito, C. A. and et al. (1991) Optical coherence tomography, *Science,* 254, 1178-81.

Huang, X. R. and Knighton, R. W. (2002) Linear birefringence of the retinal nerve fiber layer measured in vitro with a multispectral imaging micropolarimeter, *J Biomed Opt,* 7, 199-204.

Huang, X. R. and Knighton, R. W. (2005) Microtubules contribute to the birefringence of the retinal nerve fiber layer, *Invest Ophthalmol Vis Sci,* 46, 4588-93.

Hudson, C., Wild, J. M. and O'Neill, E. C. (1994) Fatigue effects during a single session of automated static threshold perimetry, *Invest Ophthalmol Vis Sci,* 35, 268-80.

Hutchings, N., Wild, J. M., Hussey, M. K., Flanagan, J. G. and Trope, G. E. (2000) The long-term fluctuation of the visual field in stable glaucoma, *Invest Ophthalmol Vis Sci,* 41, 3429-36.

Iacono, P., Da Pozzo, S., Fuser, M., Marchesan, R. and Ravalico, G. (2006) Intersession reproducibility of retinal nerve fiber layer thickness measurements by GDx-VCC in healthy and glaucomatous eyes, *Ophthalmologica,* 220, 266-71.

Iester, M., Broadway, D. C., Mikelberg, F. S. and Drance, S. M. (1997a) A comparison of healthy, ocular hypertensive, and glaucomatous optic disc topographic parameters, *J Glaucoma,* 6, 363-70.

Iester, M., Mikelberg, F. S., Courtright, P., Burk, R. O., Caprioli, J., Jonas, J. B., Weinreb, R. N. and Zangwill, L. (2001) Interobserver variability of optic disk variables measured by confocal scanning laser tomography, *Am J Ophthalmol,* 132, 57-62.

Iester, M., Mikelberg, F. S., Courtright, P. and Drance, S. M. (1997b) Correlation between the visual field indices and Heidelberg retina tomograph parameters, *J Glaucoma,* 6, 78-82.

Iester, M., Mikelberg, F. S. and Drance, S. M. (1997c) The effect of optic disc size on diagnostic precision with the Heidelberg retina tomograph, *Ophthalmology,* 104, 545-8.

Iester, M., Swindale, N. V. and Mikelberg, F. S. (1997d) Sector-based analysis of optic nerve head shape parameters and visual field indices in healthy and glaucomatous eyes, *J Glaucoma,* 6, 370-6.

Ishida, K., Yamamoto, T., Sugiyama, K. and Kitazawa, Y. (2000) Disk hemorrhage is a significantly negative prognostic factor in normal-tension glaucoma, *Am J Ophthalmol,* 129, 707-14.

Iwase, A., Suzuki, Y., Araie, M., Yamamoto, T., Abe, H., Shirato, S., Kuwayama, Y., Mishima, H. K., Shimizu, H., Tomita, G., Inoue, Y. and Kitazawa, Y. (2004) The prevalence of primary open-angle glaucoma in Japanese: the Tajimi Study, *Ophthalmology,* 111, 1641-8.

Iwata, K., Kurosawa, A. and Sawaguchi, S. (1985) Wedge-shaped retinal nerve fiber layer defects in experimental glaucoma preliminary report, *Graefes Arch Clin Exp Ophthalmol,* 223, 184-9.

Jacob, A., Thomas, R., Koshi, S. P., Braganza, A. and Muliyil, J. (1998) Prevalence of primary glaucoma in an urban south Indian population, *Indian J Ophthalmol,* 46, 81-6.

Jansonius, N. M. (2006) Towards an optimal perimetric strategy for progression detection in glaucoma: from fixed-space to adaptive inter-test intervals, *Graefes Arch Clin Exp Ophthalmol,* 244, 390-3.

Javitt, J. C., McBean, A. M., Nicholson, G. A., Babish, J. D., Warren, J. L. and Krakauer, H. (1991) Undertreatment of glaucoma among black Americans, *N Engl J Med,* 325, 1418-22.

Javitt, J. C., Spaeth, G. L., Katz, L. J., Poryzees, E. and Addiego, R. (1990) Acquired pits of the optic nerve. Increased prevalence in patients with low-tension glaucoma, *Ophthalmology,* 97, 1038-43; discussion 1043-4.

Jay, J. L. and Murdoch, J. R. (1993) The rate of visual field loss in untreated primary open angle glaucoma, *Br J Ophthalmol,* 77, 176-8.

Jay, J. L. and Murray, S. B. (1988) Early trabeculectomy versus conventional management in primary open angle glaucoma, *Br J Ophthalmol,* 72, 881-9.

Johnson, B. M., Miao, M. and Sadun, A. A. (1987) Age-related decline of human optic nerve axon populations, *Age,* 10, 5-9.

Johnson, C. A., Sample, P. A., Zangwill, L. M., Vasile, C. G., Cioffi, G. A., Liebmann, J. R. and Weinreb, R. N. (2003) Structure and function evaluation (SAFE): II. Comparison of optic disk and visual field characteristics, *Am J Ophthalmol,* 135, 148-54.

Jonas, J. B. and Budde, W. M. (2000) Diagnosis and pathogenesis of glaucomatous optic neuropathy: morphological aspects, *Prog Retin Eye Res,* 19, 1-40.

Jonas, J. B., Budde, W. M. and Panda-Jonas, S. (1999) Ophthalmoscopic evaluation of the optic nerve head, *Surv Ophthalmol,* 43, 293-320.

Jonas, J. B., Fernandez, M. C. and Naumann, G. O. (1992a) Glaucomatous parapapillary atrophy. Occurrence and correlations, *Arch Ophthalmol,* 110, 214-22.

Jonas, J. B. and Grundler, A. E. (1997) Correlation between mean visual field loss and morphometric optic disk variables in the open-angle glaucomas, *Am J Ophthalmol,* 124, 488-97.

Jonas, J. B., Gusek, G. C. and Naumann, G. O. (1988a) Optic disc, cup and neuroretinal rim size, configuration and correlations in normal eyes, *Invest Ophthalmol Vis Sci,* 29, 1151-8.

Jonas, J. B., Gusek, G. C. and Naumann, G. O. (1988b) Optic disk morphometry in high myopia, *Graefes Arch Clin Exp Ophthalmol,* 226, 587-90.

Jonas, J. B., Martus, P., Horn, F. K., Junemann, A., Korth, M. and Budde, W. M. (2004) Predictive factors of the optic nerve head for development or progression of glaucomatous visual field loss, *Invest Ophthalmol Vis Sci,* 45, 2613-8.

Jonas, J. B., Nguyen, X. N., Gusek, G. C. and Naumann, G. O. (1989) Parapapillary chorioretinal atrophy in normal and glaucoma eyes. I. Morphometric data, *Invest Ophthalmol Vis Sci,* 30, 908-18.

Jonas, J. B., Schmidt, A. M., Muller-Bergh, J. A., Schlotzer-Schrehardt, U. M. and Naumann, G. O. (1992b) Human optic nerve fiber count and optic disc size, *Invest Ophthalmol Vis Sci,* 33, 2012-8.

Jonas, J. B. and Xu, L. (1994) Optic disk hemorrhages in glaucoma, *Am J Ophthalmol,* 118, 1-8.

Junemann, A. G., Martus, P., Wisse, M. and Jonas, J. (2000) Quantitative analysis of visual field and optic disk in glaucoma: retinal nerve fiber bundle-associated analysis, *Graefes Arch Clin Exp Ophthalmol,* 238, 306-14.

Kahn, H. A., Leibowitz, H. M., Ganley, J. P., Kini, M. M., Colton, T., Nickerson, R. S. and Dawber, T. R. (1977a) The Framingham Eye Study. I. Outline and major prevalence findings, *Am J Epidemiol,* 106, 17-32.

Kahn, H. A., Leibowitz, H. M., Ganley, J. P., Kini, M. M., Colton, T., Nickerson, R. S. and Dawber, T. R. (1977b) The Framingham Eye Study. II. Association of ophthalmic pathology with single variables previously measured in the Framingham Heart Study, *Am J Epidemiol,* 106, 33-41.

Kaiser, H. J., Flammer, J., Graf, T. and Stumpfig, D. (1993) Systemic blood pressure in glaucoma patients, *Graefes Arch Clin Exp Ophthalmol,* 231, 677-80.

Kamal, D., Garway-Heath, D., Ruben, S., O'Sullivan, F., Bunce, C., Viswanathan, A., Franks, W. and Hitchings, R. (2003) Results of the betaxolol versus placebo treatment trial in ocular hypertension, *Graefes Arch Clin Exp Ophthalmol,* 241, 196-203.

Kamal, D. S., Garway-Heath, D. F., Hitchings, R. A. and Fitzke, F. W. (2000) Use of sequential Heidelberg retina tomograph images to identify changes at the optic disc in ocular hypertensive patients at risk of developing glaucoma, *Br J Ophthalmol,* 84, 993-8.

Kamal, D. S., Viswanathan, A. C., Garway-Heath, D. F., Hitchings, R. A., Poinoosawmy, D. and Bunce, C. (1999) Detection of optic disc change with the Heidelberg retina tomograph before confirmed visual field change in ocular hypertensives converting to early glaucoma, *Br J Ophthalmol,* 83, 290-4.

Kashiwagi, K., Hosaka, O., Kashiwagi, F., Taguchi, K., Mochizuki, J., Ishii, H., Ijiri, H., Tamura, K. and Tsukahara, S. (2001) Systemic circulatory parameters. comparison between patients with normal tension glaucoma and normal subjects using ambulatory monitoring, *Jpn J Ophthalmol,* 45, 388-96.

Kass, M. A., Heuer, D. K., Higginbotham, E. J., Johnson, C. A., Keltner, J. L., Miller, J. P., Parrish, R. K., 2nd, Wilson, M. R. and Gordon, M. O. (2002) The Ocular Hypertension Treatment Study: a randomized trial determines that topical ocular hypotensive medication delays or prevents the onset of primary open-angle glaucoma, *Arch Ophthalmol,* 120, 701-13.

Katsanos, A., Kothy, P., Nagy, Z. Z. and Hollo, G. (2004) Scanning laser polarimetry of retinal nerve fibre layer thickness after laser assisted in situ keratomileusis (LASIK): stability of the values after the third post-LASIK month, *Acta Physiol Hung,* 91, 119-30.

Katsanos, A., Kothy, P., Papp, A. and Hollo, G. (2005) Influence of subfoveal choroidal neovascularisation on macular imaging with scanning laser polarimetry of the retinal nerve fibre layer, *Eye,* 19, 117-22.

Katz, J. (1999a) Scoring systems for measuring progression of visual field loss in clinical trials of glaucoma treatment, *Ophthalmology,* 106, 391-5.

Katz, J. (2000) A comparison of the pattern- and total deviation-based Glaucoma Change Probability programs, *Invest Ophthalmol Vis Sci,* 41, 1012-6.

Katz, J., Congdon, N. and Friedman, D. S. (1999b) Methodological variations in estimating apparent progressive visual field loss in clinical trials of glaucoma treatment, *Arch Ophthalmol,* 117, 1137-42.

Katz, J., Gilbert, D., Quigley, H. A. and Sommer, A. (1997) Estimating progression of visual field loss in glaucoma, *Ophthalmology,* 104, 1017-25.

Katz, J. and Sommer, A. (1986) Asymmetry and variation in the normal hill of vision, *Arch Ophthalmol,* 104, 65-8.

Keltner, J. L., Johnson, C. A., Levine, R. A., Fan, J., Cello, K. E., Kass, M. A. and Gordon, M. O. (2005) Normal visual field test results following glaucomatous visual field end points in the Ocular Hypertension Treatment Study, *Arch Ophthalmol,* 123, 1201-6.

Keltner, J. L., Johnson, C. A., Quigg, J. M., Cello, K. E., Kass, M. A. and Gordon, M. O. (2000) Confirmation of visual field abnormalities in the Ocular Hypertension Treatment Study. Ocular Hypertension Treatment Study Group, *Arch Ophthalmol,* 118, 1187-94.

Kerr, J., Nelson, P. and O'Brien, C. (1998) A comparison of ocular blood flow in untreated primary open-angle glaucoma and ocular hypertension, *Am J Ophthalmol,* 126, 42-51.

Kerr, J., Nelson, P. and O'Brien, C. (2003) Pulsatile ocular blood flow in primary open-angle glaucoma and ocular hypertension, *Am J Ophthalmol,* 136, 1106-13.

Kerrigan-Baumrind, L. A., Quigley, H. A., Pease, M. E., Kerrigan, D. F. and Mitchell, R. S. (2000) Number of ganglion cells in glaucoma eyes compared with threshold visual field tests in the same persons, *Invest Ophthalmol Vis Sci,* 41, 741-8.

Kiriyama, N., Ando, A., Fukui, C., Nambu, H., Nishikawa, M., Terauchi, H., Kuwahara, A. and Matsumura, M. (2003) A comparison of optic disc topographic parameters in patients with primary open angle glaucoma, normal tension glaucoma, and ocular hypertension, *Graefes Arch Clin Exp Ophthalmol,* 241, 541-5.

Kirsch, R. E. and Anderson, D. R. (1973) Clinical recognition of glaucomatous cupping, *Am J Ophthalmol,* 75, 442-54.

Kitazawa, Y., Shirato, S. and Yamamoto, T. (1986) Optic disc hemorrhage in low-tension glaucoma, *Ophthalmology,* 93, 853-7.

Klaver, J. H., Greve, E. L., Goslinga, H., Geijssen, H. C. and Heuvelmans, J. H. (1985) Blood and plasma viscosity measurements in patients with glaucoma, *Br J Ophthalmol,* 69, 765-70.

Klein, B. E., Klein, R. and Linton, K. L. (1992a) Intraocular pressure in an American community. The Beaver Dam Eye Study, *Invest Ophthalmol Vis Sci,* 33, 2224-8.

Klein, B. E., Klein, R., Meuer, S. M. and Goetz, L. A. (1993) Migraine headache and its association with open-angle glaucoma: the Beaver Dam Eye Study, *Invest Ophthalmol Vis Sci,* 34, 3024-7.

Klein, B. E., Klein, R. and Moss, S. E. (1984) Intraocular pressure in diabetic persons, *Ophthalmology,* 91, 1356-60.

Klein, B. E., Klein, R. and Moss, S. E. (1997) Incidence of self reported glaucoma in people with diabetes mellitus, *Br J Ophthalmol,* 81, 743-7.

Klein, B. E., Klein, R., Sponsel, W. E., Franke, T., Cantor, L. B., Martone, J. and Menage, M. J. (1992b) Prevalence of glaucoma. The Beaver Dam Eye Study, *Ophthalmology,* 99, 1499-504.

Knighton, R. W. and Huang, X. R. (2002) Linear birefringence of the central human cornea, *Invest Ophthalmol Vis Sci,* 43, 82-6.

Kono, Y., Chi, Q. M., Tomita, G., Yamamoto, T., Kitazawa, Y. and Chi, Q. (1997) High-pass resolution perimetry and a Humphrey Field Analyzer as indicators of glaucomatous optic disc abnormalities. A comparative study, *Ophthalmology,* 104, 1496-502.

Kruse, F. E., Burk, R. O., Volcker, H. E., Zinser, G. and Harbarth, U. (1989) Reproducibility of topographic measurements of the optic nerve head with laser tomographic scanning, *Ophthalmology,* 96, 1320-4.

Lagrange, F. (1922) Du glaucome et de l'hypotonie; leur traitement chirurgical., *Paris: Librarie Octave Doin.*

Lan, Y. W., Henson, D. B. and Kwartz, A. J. (2003) The correlation between optic nerve head topographic measurements, peripapillary nerve fibre layer thickness, and visual field indices in glaucoma, *Br J Ophthalmol,* 87, 1135-41.

Lee, B. L. and Wilson, M. R. (2003) Ocular Hypertension Treatment Study (OHTS) commentary, *Curr Opin Ophthalmol,* 14, 74-7.

Leibowitz, H. M., Krueger, D. E., Maunder, L. R., Milton, R. C., Kini, M. M., Kahn, H. A., Nickerson, R. J., Pool, J., Colton, T. L., Ganley, J. P., Loewenstein, J. I. and Dawber, T. R. (1980) The Framingham Eye Study monograph: An ophthalmological and epidemiological study of cataract, glaucoma, diabetic retinopathy, macular

degeneration, and visual acuity in a general population of 2631 adults, 1973-1975, *Surv Ophthalmol,* 24, 335-610.

Leighton, D. A. and Phillips, C. I. (1972) Systemic blood pressure in open-angle glaucoma, low tension glaucoma, and the normal eye, *Br J Ophthalmol,* 56, 447-53.

Leighton, D. A. and Tomlinson, A. (1973) Ocular tension and axial length of the eyeball in open-angle glaucoma and low tension glaucoma, *Br J Ophthalmol,* 57, 499-502.

Leske, M. C., Connell, A. M., Schachat, A. P. and Hyman, L. (1994) The Barbados Eye Study. Prevalence of open angle glaucoma, *Arch Ophthalmol,* 112, 821-9.

Leske, M. C., Connell, A. M., Wu, S. Y., Hyman, L. and Schachat, A. P. (1997) Distribution of intraocular pressure. The Barbados Eye Study, *Arch Ophthalmol,* 115, 1051-7.

Leske, M. C., Connell, A. M., Wu, S. Y., Hyman, L. G. and Schachat, A. P. (1995) Risk factors for open-angle glaucoma. The Barbados Eye Study, *Arch Ophthalmol,* 113, 918-24.

Leske, M. C., Connell, A. M., Wu, S. Y., Nemesure, B., Li, X., Schachat, A. and Hennis, A. (2001) Incidence of open-angle glaucoma: the Barbados Eye Studies. The Barbados Eye Studies Group, *Arch Ophthalmol,* 119, 89-95.

Leske, M. C., Heijl, A., Hussein, M., Bengtsson, B., Hyman, L. and Komaroff, E. (2003) Factors for glaucoma progression and the effect of treatment: the early manifest glaucoma trial, *Arch Ophthalmol,* 121, 48-56.

Leske, M. C., Wu, S. Y., Nemesure, B. and Hennis, A. (2002) Incident open-angle glaucoma and blood pressure, *Arch Ophthalmol,* 120, 954-9.

Leung, C. K., Chan, W. M., Yung, W. H., Ng, A. C., Woo, J., Tsang, M. K. and Tse, R. K. (2005) Comparison of macular and peripapillary measurements for the detection of glaucoma: an optical coherence tomography study, *Ophthalmology,* 112, 391-400.

Levy, N. S. and Crapps, E. E. (1984) Displacement of optic nerve head in response to short-term intraocular pressure elevation in human eyes, *Arch Ophthalmol,* 102, 782-6.

Li, J., Herndon, L. W., Asrani, S. G., Stinnett, S. and Allingham, R. R. (2004) Clinical comparison of the Proview eye pressure monitor with the Goldmann applanation tonometer and the Tonopen, *Arch Ophthalmol,* 122, 1117-21.

Lichter, P. R. (1976) Variability of expert observers in evaluating the optic disc, *Trans Am Ophthalmol Soc,* 74, 532-72.

Lieberman, M. F., Maumenee, A. E. and Green, W. R. (1976) Histologic studies of the vasculature of the anterior optic nerve, *Am J Ophthalmol,* 82, 405-23.

Liu, J. and Roberts, C. J. (2005) Influence of corneal biomechanical properties on intraocular pressure measurement: quantitative analysis, *J Cataract Refract Surg,* 31, 146-55.

Lleo-Perez, A., Ortuno-Soto, A., Rahhal, M. S., Martinez-Soriano, F. and Sanchis-Gimeno, J. A. (2004) Intraobserver reproducibility of retinal nerve fiber layer measurements using scanning laser polarimetry and optical coherence tomography in normal and ocular hypertensive subjects, *Eur J Ophthalmol,* 14, 523-30.

Mainster, M. A., Timberlake, G. T., Webb, R. H. and Hughes, G. W. (1982) Scanning laser ophthalmoscopy. Clinical applications, *Ophthalmology,* 89, 852-7.

Manassakorn, A., Nouri-Mahdavi, K., Koucheki, B., Law, S. K. and Caprioli, J. (2006) Pointwise linear regression analysis for detection of visual field progression with absolute versus corrected threshold sensitivities, *Invest Ophthalmol Vis Sci,* 47, 2896-903.

Marcus, D. M., Costarides, A. P., Gokhale, P., Papastergiou, G., Miller, J. J., Johnson, M. H. and Chaudhary, B. A. (2001) Sleep disorders: a risk factor for normal-tension glaucoma?, *J Glaucoma,* 10, 177-83.

Mardin, C. Y., Horn, F. K., Jonas, J. B. and Budde, W. M. (1999) Preperimetric glaucoma diagnosis by confocal scanning laser tomography of the optic disc, *Br J Ophthalmol,* 83, 299-304.

Mardin, C. Y., Hothorn, T., Peters, A., Junemann, A. G., Nguyen, N. X. and Lausen, B. (2003) New glaucoma classification method based on standard Heidelberg Retina Tomograph parameters by bagging classification trees, *J Glaucoma,* 12, 340-6.

Martus, P., Stroux, A., Budde, W. M., Mardin, C. Y., Korth, M. and Jonas, J. B. (2005) Predictive factors for progressive optic nerve damage in various types of chronic open-angle glaucoma, *Am J Ophthalmol,* 139, 999-1009.

Mason, R. P., Kosoko, O., Wilson, M. R., Martone, J. F., Cowan, C. L., Jr., Gear, J. C. and Ross-Degnan, D. (1989) National survey of the prevalence and risk factors of glaucoma in St. Lucia, West Indies. Part I. Prevalence findings, *Ophthalmology,* 96, 1363-8.

Mastropasqua, L., Lobefalo, L., Mancini, A., Ciancaglini, M. and Palma, S. (1992) Prevalence of myopia in open angle glaucoma, *Eur J Ophthalmol,* 2, 33-5.

Mayama, C., Araie, M., Suzuki, Y., Ishida, K., Yamamoto, T., Kitazawa, Y., Shirakashi, M., Abe, H., Tsukamoto, H., Mishima, H. K., Yoshimura, K. and Ohashi, Y. (2004) Statistical evaluation of the diagnostic accuracy of methods used to determine the progression of visual field defects in glaucoma, *Ophthalmology,* 111, 2117-25.

McNaught, A. I., Crabb, D. P., Fitzke, F. W. and Hitchings, R. A. (1995) Modelling series of visual fields to detect progression in normal-tension glaucoma, *Graefes Arch Clin Exp Ophthalmol,* 233, 750-5.

McNaught, A. I., Crabb, D. P., Fitzke, F. W. and Hitchings, R. A. (1996) Visual field progression: comparison of Humphrey Statpac2 and pointwise linear regression analysis, *Graefes Arch Clin Exp Ophthalmol,* 234, 411-8.

Medeiros, F. A., Sample, P. A. and Weinreb, R. N. (2003a) Corneal thickness measurements and visual function abnormalities in ocular hypertensive patients, *Am J Ophthalmol,* 135, 131-7.

Medeiros, F. A., Sample, P. A., Zangwill, L. M., Bowd, C., Aihara, M. and Weinreb, R. N. (2003b) Corneal thickness as a risk factor for visual field loss in patients with preperimetric glaucomatous optic neuropathy, *Am J Ophthalmol,* 136, 805-13.

Medeiros, F. A., Zangwill, L. M., Bowd, C., Vessani, R. M., Susanna, R., Jr. and Weinreb, R. N. (2005b) Evaluation of retinal nerve fiber layer, optic nerve head, and macular thickness measurements for glaucoma detection using optical coherence tomography, *Am J Ophthalmol,* 139, 44-55.

Medeiros, F. A., Zangwill, L. M., Bowd, C. and Weinreb, R. N. (2004) Comparison of the GDx VCC scanning laser polarimeter, HRT II confocal scanning laser ophthalmoscope, and stratus OCT optical coherence tomograph for the detection of glaucoma, *Arch Ophthalmol,* 122, 827-37.

Michelson, G., Langhans, M. J. and Groh, M. J. (1996) Perfusion of the juxtapapillary retina and the neuroretinal rim area in primary open angle glaucoma, *J Glaucoma,* 5, 91-8.

Michelson, G., Langhans, M. J., Harazny, J. and Dichtl, A. (1998a) Visual field defect and perfusion of the juxtapapillary retina and the neuroretinal rim area in primary open-angle glaucoma, *Graefes Arch Clin Exp Ophthalmol,* 236, 80-5.

Michelson, G., Welzenbach, J., Pal, I. and Harazny, J. (1998b) Automatic full field analysis of perfusion images gained by scanning laser Doppler flowmetry, *Br J Ophthalmol,* 82, 1294-300.

Migdal, C., Gregory, W. and Hitchings, R. (1994) Long-term functional outcome after early surgery compared with laser and medicine in open-angle glaucoma, *Ophthalmology,* 101, 1651-6.

Miglior, S., Albe, E., Guareschi, M., Rossetti, L. and Orzalesi, N. (2002) Intraobserver and interobserver reproducibility in the evaluation of optic disc stereometric parameters by Heidelberg Retina Tomograph, *Ophthalmology,* 109, 1072-7.

Miglior, S., Brigatti, L., Lonati, C., Rossetti, L., Pierrottet, C. and Orzalesi, N. (1996) Correlation between the progression of optic disc and visual field changes in glaucoma, *Curr Eye Res,* 15, 145-9.

Miglior, S., Guareschi, M., Albe, E., Gomarasca, S., Vavassori, M. and Orzalesi, N. (2003) Detection of glaucomatous visual field changes using the Moorfields regression analysis of the Heidelberg retina tomograph, *Am J Ophthalmol,* 136, 26-33.

Miglior, S., Zeyen, T., Pfeiffer, N., Cunha-Vaz, J., Torri, V. and Adamsons, I. (2005) Results of the European Glaucoma Prevention Study, *Ophthalmology,* 112, 366-75.

Mikelberg, F. S., Douglas, G. R., Schulzer, M., Cornsweet, T. N. and Wijsman, K. (1984a) Reliability of optic disk topographic measurements recorded with a video-ophthalmograph, *Am J Ophthalmol,* 98, 98-102.

Mikelberg, F. S. and Drance, S. M. (1984b) The mode of progression of visual field defects in glaucoma, *Am J Ophthalmol,* 98, 443-5.

Mikelberg, F. S., Parfitt, C. M., Swindale, N. V., Graham, S. L., Drance, S. M. and Gosine, R. (1995) Ability of the Heidelberg Retinal Tomograph to detect early glaucomatous visual field loss, *J Glaucoma,* 4, 242-247.

Mikelberg, F. S., Schulzer, M., Drance, S. M. and Lau, W. (1986) The rate of progression of scotomas in glaucoma, *Am J Ophthalmol,* 101, 1-6.

Mikelberg, F. S., Wijsman, K. and Schulzer, M. (1993) Reproducibility of topographic parameters obtained with the Heidelberg retina tomograph, *J Glaucoma,* 2, 101-103.

Miller, K. M. and Quigley, H. A. (1988) The clinical appearance of the lamina cribrosa as a function of the extent of glaucomatous optic nerve damage, *Ophthalmology,* 95, 135-8.

Minckler, D. S. (1980) The organization of nerve fiber bundles in the primate optic nerve head, *Arch Ophthalmol,* 98, 1630-6.

Minckler, D. S. (1986) Correlations between anatomic features and axonal transport in primate optic nerve head, *Trans Am Ophthalmol Soc,* 84, 429-52.

Minckler, D. S. (1989) Histology of optic nerve damage in ocular hypertension and early glaucoma, *Surv Ophthalmol,* 33 Suppl, 401-2; discussion 409-11.

Minckler, D. S., Bunt, A. H. and Johanson, G. W. (1977) Orthograde and retrograde axoplasmic transport during acute ocular hypertension in the monkey, *Invest Ophthalmol Vis Sci,* 16, 426-41.

Minckler, D. S., McLean, I. W. and Tso, M. O. (1976) Distribution of axonal and glial elements in the rhesus optic nerve head studied by electron microscopy, *Am J Ophthalmol,* 82, 179-87.

Minckler, D. S. and Spaeth, G. L. (1981) Optic nerve damage in glaucoma, *Surv Ophthalmol,* 26, 128-48.

Mitchell, P., Hourihan, F., Sandbach, J. and Wang, J. J. (1999) The relationship between glaucoma and myopia: the Blue Mountains Eye Study, *Ophthalmology,* 106, 2010-5.

Mitchell, P., Smith, W., Attebo, K. and Healey, P. R. (1996) Prevalence of open-angle glaucoma in Australia. The Blue Mountains Eye Study, *Ophthalmology,* 103, 1661-9.

Mitchell, P., Smith, W., Chey, T. and Healey, P. R. (1997) Open-angle glaucoma and diabetes: the Blue Mountains eye study, Australia, *Ophthalmology,* 104, 712-8.

Mojon, D. S., Hess, C. W., Goldblum, D., Fleischhauer, J., Koerner, F., Bassetti, C. and Mathis, J. (1999) High prevalence of glaucoma in patients with sleep apnea syndrome, *Ophthalmology,* 106, 1009-12.

Monemi, S., Spaeth, G., DaSilva, A., Popinchalk, S., Ilitchev, E., Liebmann, J., Ritch, R., Heon, E., Crick, R. P., Child, A. and Sarfarazi, M. (2005) Identification of a novel

adult-onset primary open-angle glaucoma (POAG) gene on 5q22.1, *Hum Mol Genet,* 14, 725-33.

Morgan, J. E., Jeffery, G. and Foss, A. J. (1998) Axon deviation in the human lamina cribrosa, *Br J Ophthalmol,* 82, 680-3.

Morgan, J. E., Uchida, H. and Caprioli, J. (2000) Retinal ganglion cell death in experimental glaucoma, *Br J Ophthalmol,* 84, 303-10.

Morrison, J. C., Dorman-Pease, M. E., Dunkelberger, G. R. and Quigley, H. A. (1990) Optic nerve head extracellular matrix in primary optic atrophy and experimental glaucoma, *Arch Ophthalmol,* 108, 1020-4.

Morrison, J. C., Jerdan, J. A., Dorman, M. E. and Quigley, H. A. (1989) Structural proteins of the neonatal and adult lamina cribrosa, *Arch Ophthalmol,* 107, 1220-4.

Moya, F. J., Brigatti, L. and Caprioli, J. (1999) Effect of aging on optic nerve appearance: a longitudinal study, *Br J Ophthalmol,* 83, 567-72.

Mukesh, B. N., McCarty, C. A., Rait, J. L. and Taylor, H. R. (2002) Five-year incidence of open-angle glaucoma: the visual impairment project, *Ophthalmology,* 109, 1047-51.

Munoz, B., West, S. K., Rubin, G. S., Schein, O. D., Quigley, H. A., Bressler, S. B. and Bandeen-Roche, K. (2000) Causes of blindness and visual impairment in a population of older Americans: The Salisbury Eye Evaluation Study, *Arch Ophthalmol,* 118, 819-25.

Musch, D. C., Lichter, P. R., Guire, K. E. and Standardi, C. L. (1999) The Collaborative Initial Glaucoma Treatment Study: study design, methods, and baseline characteristics of enrolled patients, *Ophthalmology,* 106, 653-62.

Nassif, N., Cense, B., Park, B. H., Yun, S. H., Chen, T. C., Bouma, B. E., Tearney, G. J. and de Boer, J. F. (2004) In vivo human retinal imaging by ultrahigh-speed spectral domain optical coherence tomography, *Opt Lett,* 29, 480-2.

Nemesure, B., Wu, S. Y., Hennis, A. and Leske, M. C. (2003) Corneal thickness and intraocular pressure in the Barbados eye studies, *Arch Ophthalmol,* 121, 240-4.

Nichols, T. E. and Holmes, A. P. (2002) Nonparametric permutation tests for functional neuroimaging: a primer with examples, *Hum Brain Mapp,* 15, 1-25.

Nicolela, M. T. and Drance, S. M. (1996a) Various glaucomatous optic nerve appearances: clinical correlations, *Ophthalmology,* 103, 640-9.

Nicolela, M. T., Drance, S. M., Rankin, S. J., Buckley, A. R. and Walman, B. E. (1996b) Color Doppler imaging in patients with asymmetric glaucoma and unilateral visual field loss, *Am J Ophthalmol,* 121, 502-10.

Nicolela, M. T., McCormick, T. A., Drance, S. M., Ferrier, S. N., LeBlanc, R. P. and Chauhan, B. C. (2003) Visual field and optic disc progression in patients with different types of optic disc damage: a longitudinal prospective study, *Ophthalmology,* 110, 2178-84.

Nicolela, M. T., Walman, B. E., Buckley, A. R. and Drance, S. M. (1996c) Ocular hypertension and primary open-angle glaucoma: a comparative study of their retrobulbar blood flow velocity, *J Glaucoma,* 5, 308-10.

Nicolela, M. T., Walman, B. E., Buckley, A. R. and Drance, S. M. (1996d) Various glaucomatous optic nerve appearances. A color Doppler imaging study of retrobulbar circulation, *Ophthalmology,* 103, 1670-9.

Noureddin, B. N., Poinoosawmy, D., Fietzke, F. W. and Hitchings, R. A. (1991) Regression analysis of visual field progression in low tension glaucoma, *Br J Ophthalmol,* 75, 493-5.

Nouri-Mahdavi, K., Brigatti, L., Weitzman, M. and Caprioli, J. (1995) Outcomes of trabeculectomy for primary open-angle glaucoma, *Ophthalmology,* 102, 1760-9.

Nouri-Mahdavi, K., Brigatti, L., Weitzman, M. and Caprioli, J. (1997) Comparison of methods to detect visual field progression in glaucoma, *Ophthalmology,* 104, 1228-36.

Nouri-Mahdavi, K., Caprioli, J., Coleman, A. L., Hoffman, D. and Gaasterland, D. (2005) Pointwise linear regression for evaluation of visual field outcomes and comparison with the advanced glaucoma intervention study methods, *Arch Ophthalmol,* 123, 193-9.

Nouri-Mahdavi, K., Hoffman, D., Coleman, A. L., Liu, G., Li, G., Gaasterland, D. and Caprioli, J. (2004) Predictive factors for glaucomatous visual field progression in the Advanced Glaucoma Intervention Study, *Ophthalmology,* 111, 1627-35.

Nyman, K., Tomita, G., Raitta, C. and Kawamura, M. (1994) Correlation of asymmetry of visual field loss with optic disc topography in normal-tension glaucoma, *Arch Ophthalmol,* 112, 349-53.

O'Brart, D. P., de Souza Lima, M., Bartsch, D. U., Freeman, W. and Weinreb, R. N. (1997) Indocyanine green angiography of the peripapillary region in glaucomatous eyes by confocal scanning laser ophthalmoscopy, *Am J Ophthalmol,* 123, 657-66.

O'Brien, C. and Schwartz, B. (1992) Point by point linear regression analysis of automated visual fields in primary open angle glaucoma. Perimetry Update 1992/3. R. P. Mills. Amsterdam/New York, Kluger Publications: 149-52.

Ogden, T. E. (1974) The nerve-fiber layer of the primate retina: an autoradiographic study, *Invest Ophthalmol,* 13, 95-100.

Ogden, T. E. (1978) Nerve fiber layer astrocytes of the primate retina: morphology, distribution, and density, *Invest Ophthalmol Vis Sci,* 17, 499-510.

Ogden, T. E. (1983a) Nerve fiber layer of the macaque retina: retinotopic organization, *Invest Ophthalmol Vis Sci,* 24, 85-98.

Ogden, T. E. (1983b) Nerve fiber layer of the owl monkey retina: retinotopic organization, *Invest Ophthalmol Vis Sci,* 24, 265-9.

Ogden, T. E. (1983c) Nerve fiber layer of the primate retina: thickness and glial content, *Vision Res,* 23, 581-7.

Ogden, T. E., Duggan, J., Danley, K., Wilcox, M. and Minckler, D. S. (1988) Morphometry of nerve fiber bundle pores in the optic nerve head of the human, *Exp Eye Res,* 46, 559-68.

Ohtsuka, K. and Nakamura, Y. (2000) Open-angle glaucoma associated with Graves disease, *Am J Ophthalmol,* 129, 613-7.

Olver, J. M., Spalton, D. J. and McCartney, A. C. (1990) Microvascular study of the retrolaminar optic nerve in man: the possible significance in anterior ischaemic optic neuropathy, *Eye,* 4 (Pt 1), 7-24.

Olver, J. M., Spalton, D. J. and McCartney, A. C. (1994) Quantitative morphology of human retrolaminar optic nerve vasculature, *Invest Ophthalmol Vis Sci,* 35, 3858-66.

Onda, E., Cioffi, G. A., Bacon, D. R. and Van Buskirk, E. M. (1995) Microvasculature of the human optic nerve, *Am J Ophthalmol,* 120, 92-102.

Orgul, S., Cioffi, G. A., Bacon, D. R. and Van Buskirk, E. M. (1996) Sources of variability of topometric data with a scanning laser ophthalmoscope, *Arch Ophthalmol,* 114, 161-4.

Orgul, S. and Flammer, J. (1994) Interocular visual-field and intraocular-pressure asymmetries in normal-tension-glaucoma, *Eur J Ophthalmol,* 4, 199-201.

Osher, R. H. and Herschler, J. (1981) The significance of baring of the circumlinear vessel. A prospective study, *Arch Ophthalmol,* 99, 817-8.

Owen, M. F., Strouthidis, N. G., Garway-Heath, D. F. and Crabb, D. P. (2006) Measurement variability in Heidelberg Retina Tomograph imaging of neuroretinal rim area, *Invest Ophthalmol Vis Sci,* 47, 5322-30.

Parisi, V., Miglior, S., Manni, G., Centofani, M. and Bucci, M. G. (2006) Clinical Ability of Pattern Electroretinograms and Visual Evoked Potentials in Detecting Visual Dysfunction in Ocular Hypertension and Glaucoma, *Ophthalmology,* 113, 216-228.

Park, K. H. and Caprioli, J. (2002) Development of a novel reference plane for the Heidelberg retina tomograph with optical coherence tomography measurements, *J Glaucoma,* 11, 385-91.

Parrish, R. K., 2nd (2006) The European Glaucoma Prevention Study and the Ocular Hypertension Treatment Study: why do two studies have different results?, *Curr Opin Ophthalmol,* 17, 138-41.

Parrish, R. K., 2nd, Schiffman, J. C., Feuer, W. J., Anderson, D. R., Budenz, D. L., Wells-Albornoz, M. C., Vandenbroucke, R., Kass, M. A. and Gordon, M. O. (2005) Test-retest reproducibility of optic disk deterioration detected from stereophotographs by masked graders, *Am J Ophthalmol,* 140, 762-4.

Patterson, A. J., Garway-Heath, D. F., Strouthidis, N. G. and Crabb, D. P. (2005) A new statistical approach for quantifying change in series of retinal and optic nerve head topography images, *Invest Ophthalmol Vis Sci,* 46, 1659-67.

Paunescu, L. A., Schuman, J. S., Price, L. L., Stark, P. C., Beaton, S., Ishikawa, H., Wollstein, G. and Fujimoto, J. G. (2004) Reproducibility of nerve fiber thickness, macular

thickness, and optic nerve head measurements using StratusOCT, *Invest Ophthalmol Vis Sci,* 45, 1716-24.

Pederson, J. E. and Anderson, D. R. (1980) The mode of progressive disc cupping in ocular hypertension and glaucoma, *Arch Ophthalmol,* 98, 490-5.

Perkins, E. S. and Phelps, C. D. (1982) Open angle glaucoma, ocular hypertension, low-tension glaucoma, and refraction, *Arch Ophthalmol,* 100, 1464-7.

Phelps, C. D. and Corbett, J. J. (1985) Migraine and low-tension glaucoma. A case-control study, *Invest Ophthalmol Vis Sci,* 26, 1105-8.

Polansky, J. R., Fauss, D. J., Chen, P., Chen, H., Lutjen-Drecoll, E., Johnson, D., Kurtz, R. M., Ma, Z. D., Bloom, E. and Nguyen, T. D. (1997) Cellular pharmacology and molecular biology of the trabecular meshwork inducible glucocorticoid response gene product, *Ophthalmologica,* 211, 126-39.

Portney, G. L. (1976) Photogrammetric analysis of the three-dimensional geometry of normal and glaucomatous optic cups, *Tr Am Acad Ophth & Otol,* 81, 239-246.

Quigley, H. and Anderson, D. R. (1976) The dynamics and location of axonal transport blockade by acute intraocular pressure elevation in primate optic nerve, *Invest Ophthalmol,* 15, 606-16.

Quigley, H. A. (1977) The pathogenesis of reversible cupping in congenital glaucoma, *Am J Ophthalmol,* 84, 358-70.

Quigley, H. A. (1986) Examination of the retinal nerve fiber layer in the recognition of early glaucoma damage, *Trans Am Ophthalmol Soc,* 84, 920-66.

Quigley, H. A. (1996) Number of people with glaucoma worldwide, *Br J Ophthalmol,* 80, 389-93.

Quigley, H. A. and Addicks, E. M. (1981) Regional differences in the structure of the lamina cribrosa and their relation to glaucomatous optic nerve damage, *Arch Ophthalmol,* 99, 137-43.

Quigley, H. A. and Addicks, E. M. (1982) Quantitative studies of retinal nerve fiber layer defects, *Arch Ophthalmol,* 100, 807-14.

Quigley, H. A., Addicks, E. M. and Green, W. R. (1982) Optic nerve damage in human glaucoma. III. Quantitative correlation of nerve fiber loss and visual field defect in

glaucoma, ischemic neuropathy, papilledema, and toxic neuropathy, *Arch Ophthalmol,* 100, 135-46.

Quigley, H. A., Addicks, E. M., Green, W. R. and Maumenee, A. E. (1981) Optic nerve damage in human glaucoma. II. The site of injury and susceptibility to damage, *Arch Ophthalmol,* 99, 635-49.

Quigley, H. A. and Anderson, D. R. (1977) Distribution of axonal transport blockade by acute intraocular pressure elevation in the primate optic nerve head, *Invest Ophthalmol Vis Sci,* 16, 640-4.

Quigley, H. A. and Broman, A. T. (2006) The number of people with glaucoma worldwide in 2010 and 2020, *Br J Ophthalmol,* 90, 262-7.

Quigley, H. A., Brown, A. E., Morrison, J. D. and Drance, S. M. (1990) The size and shape of the optic disc in normal human eyes, *Arch Ophthalmol,* 108, 51-7.

Quigley, H. A., Dorman-Pease, M. E. and Brown, A. E. (1991) Quantitative study of collagen and elastin of the optic nerve head and sclera in human and experimental monkey glaucoma, *Curr Eye Res,* 10, 877-88.

Quigley, H. A., Dunkelberger, G. R. and Green, W. R. (1988) Chronic human glaucoma causing selectively greater loss of large optic nerve fibers, *Ophthalmology,* 95, 357-63.

Quigley, H. A., Dunkelberger, G. R. and Green, W. R. (1989) Retinal ganglion cell atrophy correlated with automated perimetry in human eyes with glaucoma, *Am J Ophthalmol,* 107, 453-64.

Quigley, H. A. and Green, W. R. (1979) The histology of human glaucoma cupping and optic nerve damage: clinicopathologic correlation in 21 eyes, *Ophthalmology,* 86, 1803-30.

Quigley, H. A., Hohman, R. M., Addicks, E. M., Massof, R. W. and Green, W. R. (1983) Morphologic changes in the lamina cribrosa correlated with neural loss in open-angle glaucoma, *Am J Ophthalmol,* 95, 673-91.

Quigley, H. A., Katz, J., Derick, R. J., Gilbert, D. and Sommer, A. (1992) An evaluation of optic disc and nerve fiber layer examinations in monitoring progression of early glaucoma damage, *Ophthalmology,* 99, 19-28.

Quigley, H. A., Sanchez, R. M., Dunkelberger, G. R., L'Hernault, N. L. and Baginski, T. A. (1987) Chronic glaucoma selectively damages large optic nerve fibers, *Invest Ophthalmol Vis Sci,* 28, 913-20.

Quigley, H. A. and Sommer, A. (1987) How to use nerve fiber layer examination in the management of glaucoma, *Trans Am Ophthalmol Soc,* 85, 254-72.

Quigley, H. A., Tielsch, J. M., Katz, J. and Sommer, A. (1996) Rate of progression in open-angle glaucoma estimated from cross-sectional prevalence of visual field damage, *Am J Ophthalmol,* 122, 355-63.

Quigley, H. A. and Vitale, S. (1997) Models of open-angle glaucoma prevalence and incidence in the United States, *Invest Ophthalmol Vis Sci,* 38, 83-91.

Quigley, H. A., West, S. K., Rodriguez, J., Munoz, B., Klein, R. and Snyder, R. (2001) The prevalence of glaucoma in a population-based study of Hispanic subjects: Proyecto VER, *Arch Ophthalmol,* 119, 1819-26.

Racette, L., Wilson, M. R., Zangwill, L. M., Weinreb, R. N. and Sample, P. A. (2003) Primary open-angle glaucoma in blacks: a review, *Surv Ophthalmol,* 48, 295-313.

Radius, R. L. (1987) Anatomy of the optic nerve head and glaucomatous optic neuropathy, *Surv Ophthalmol,* 32, 35-44.

Radius, R. L. and Anderson, D. R. (1979a) The histology of retinal nerve fiber layer bundles and bundle defects, *Arch Ophthalmol,* 97, 948-50.

Radius, R. L. and Anderson, D. R. (1979b) The course of axons through the retina and optic nerve head, *Arch Ophthalmol,* 97, 1154-8.

Radius, R. L. and de Bruin, J. (1981) Anatomy of the retinal nerve fiber layer, *Invest Ophthalmol Vis Sci,* 21, 745-9.

Radius, R. L. and Gonzales, M. (1981) Anatomy of the lamina cribrosa in human eyes, *Arch Ophthalmol,* 99, 2159-62.

Rahman, M. M., Rahman, N., Foster, P. J., Haque, Z., Zaman, A. U., Dineen, B. and Johnson, G. J. (2004) The prevalence of glaucoma in Bangladesh: a population based survey in Dhaka division, *Br J Ophthalmol,* 88, 1493-7.

Ramakrishnan, R., Nirmalan, P. K., Krishnadas, R., Thulasiraj, R. D., Tielsch, J. M., Katz, J., Friedman, D. S. and Robin, A. L. (2003) Glaucoma in a rural population of southern India: the Aravind comprehensive eye survey, *Ophthalmology,* 110, 1484-90.

Rankin, S. J., Walman, B. E., Buckley, A. R. and Drance, S. M. (1995) Color Doppler imaging and spectral analysis of the optic nerve vasculature in glaucoma, *Am J Ophthalmol,* 119, 685-93.

Rasker, M. T., van den Enden, A., Bakker, D. and Hoyng, P. F. (1997) Deterioration of visual fields in patients with glaucoma with and without optic disc hemorrhages, *Arch Ophthalmol,* 115, 1257-62.

Rasker, M. T., van den Enden, A., Bakker, D. and Hoyng, P. F. (2000) Rate of visual field loss in progressive glaucoma, *Arch Ophthalmol,* 118, 481-8.

Read, R. M. and Spaeth, G. L. (1974) The practical clinical appraisal of the optic disc in glaucoma: the natural history of cup progression and some specific disc-field correlations, *Trans Am Acad Ophthalmol Otolaryngol,* 78, OP255-74.

Repka, M. X. and Quigley, H. A. (1989) The effect of age on normal human optic nerve fiber number and diameter, *Ophthalmology,* 96, 26-32.

Resnikoff, S., Pascolini, D., Etya'ale, D., Kocur, I., Pararajasegaram, R., Pokharel, G. P. and Mariotti, S. P. (2004) Global data on visual impairment in the year 2002, *Bull World Health Organ,* 82, 844-51.

Reus, N. J. and Lemij, H. G. (2004a) Diagnostic accuracy of the GDx VCC for glaucoma, *Ophthalmology,* 111, 1860-5.

Reus, N. J. and Lemij, H. G. (2004b) The relationship between standard automated perimetry and GDx VCC measurements, *Invest Ophthalmol Vis Sci,* 45, 840-5.

Reus, N. J. and Lemij, H. G. (2005) Relationships between standard automated perimetry, HRT confocal scanning laser ophthalmoscopy, and GDx VCC scanning laser polarimetry, *Invest Ophthalmol Vis Sci,* 46, 4182-8.

Reyes, R. D., Tomita, G. and Kitazawa, Y. (1998) Retinal nerve fiber layer thickness within the area of apparently normal visual field in normal-tension glaucoma with hemifield defect, *J Glaucoma,* 7, 329-35.

Rezaie, T., Child, A., Hitchings, R., Brice, G., Miller, L., Coca-Prados, M., Heon, E., Krupin, T., Ritch, R., Kreutzer, D., Crick, R. P. and Sarfarazi, M. (2002) Adult-onset primary open-angle glaucoma caused by mutations in optineurin, *Science,* 295, 1077-9.

Ricard, C. S., Pena, J. D. and Hernandez, M. R. (1999) Differential expression of neural cell adhesion molecule isoforms in normal and glaucomatous human optic nerve heads, *Brain Res Mol Brain Res,* 74, 69-82.

Ridley (1951) Television in ophthalmology. Acta XVI Concilium Ophthalmologicum. London, British Medical Association. 2: 1397-1404.

Ritch, R., Shields, M. B. and Krupin, T. (1989) The glaucomas. St. Louis, Missouri, Mosby-Year Book.

Robinson, R., Deutsch, J., Jones, H. S., Youngson-Reilly, S., Hamlin, D. M., Dhurjon, L. and Fielder, A. R. (1994) Unrecognised and unregistered visual impairment, *Br J Ophthalmol,* 78, 736-40.

Rockwood, E. J. and Anderson, D. R. (1988) Acquired peripapillary changes and progression in glaucoma, *Graefes Arch Clin Exp Ophthalmol,* 226, 510-5.

Rohrschneider, K., Burk, R. O., Kruse, F. E. and Volcker, H. E. (1994) Reproducibility of the optic nerve head topography with a new laser tomographic scanning device, *Ophthalmology,* 101, 1044-9.

Rohrschneider, K., Burk, R. O. and Volcker, H. E. (1993) Reproducibility of topometric data acquisition in normal and glaucomatous optic nerve heads with the laser tomographic scanner, *Graefes Arch Clin Exp Ophthalmol,* 231, 457-464.

Rotchford, A. P. and Johnson, G. J. (2002) Glaucoma in Zulus: a population-based cross-sectional survey in a rural district in South Africa, *Arch Ophthalmol,* 120, 471-8.

Rotchford, A. P., Kirwan, J. F., Muller, M. A., Johnson, G. J. and Roux, P. (2003) Temba glaucoma study: a population-based cross-sectional survey in urban South Africa, *Ophthalmology,* 110, 376-82.

Rozsival, P., Hampl, R., Obenberger, J., Starka, L. and Rehak, S. (1981) Aqueous humour and plasma cortisol levels in glaucoma and cataract patients, *Curr Eye Res,* 1, 391-6.

Sample, P. A., Boden, C., Zhang, Z., Pascual, J., Lee, T. W., Zangwill, L. M., Weinreb, R. N., Crowston, J. G., Hoffmann, E. M., Medeiros, F. A., Sejnowski, T. and Goldbaum, M.

(2005) Unsupervised machine learning with independent component analysis to identify areas of progression in glaucomatous visual fields, *Invest Ophthalmol Vis Sci,* 46, 3684-92.

Sato, Y., Tomita, G., Onda, E., Goto, Y., Oguri, A. and Kitazawa, Y. (2000) Association between watershed zone and visual field defect in normal tension glaucoma, *Jpn J Ophthalmol,* 44, 39-45.

Saw, S. M., Foster, P. J., Gazzard, G. and Seah, S. (2004) Causes of blindness, low vision, and questionnaire-assessed poor visual function in Singaporean Chinese adults: The Tanjong Pagar Survey, *Ophthalmology,* 111, 1161-8.

Schiefer, U., Flad, M., Stumpp, F., Malsam, A., Paetzold, J., Vonthein, R., Denk, P. O. and Sample, P. A. (2003) Increased detection rate of glaucomatous visual field damage with locally condensed grids: a comparison between fundus-oriented perimetry and conventional visual field examination, *Arch Ophthalmol,* 121, 458-65.

Schlottmann, P. G., De Cilla, S., Greenfield, D. S., Caprioli, J. and Garway-Heath, D. F. (2004) Relationship between visual field sensitivity and retinal nerve fiber layer thickness as measured by scanning laser polarimetry, *Invest Ophthalmol Vis Sci,* 45, 1823-9.

Schmidt, K. G., von Ruckmann, A. and Pillunat, L. E. (1998) Topical carbonic anhydrase inhibition increases ocular pulse amplitude in high tension primary open angle glaucoma, *Br J Ophthalmol,* 82, 758-62.

Schulzer, M. (1994) Errors in the diagnosis of visual field progression in normal-tension glaucoma, *Ophthalmology,* 101, 1589-94; discussion 1595.

Schulzer, M., Anderson, D. R. and Drance, S. M. (1991) Sensitivity and specificity of a diagnostic test determined by repeated observations in the absence of an external standard, *J Clin Epidemiol,* 44, 1167-79.

Schuman, J. S., Pedut-Kloizman, T., Hertzmark, E., Hee, M. R., Wilkins, J. R., Coker, J. G., Puliafito, C. A., Fujimoto, J. G. and Swanson, E. A. (1996) Reproducibility of nerve fiber layer thickness measurements using optical coherence tomography, *Ophthalmology,* 103, 1889-98.

Schwartz, B. (1973) Cupping and pallor of the optic disc, *Arch Ophthalmol,* 89, 272-7.

Schwartz, B., Rieser, J. C. and Fishbein, S. L. (1977) Fluorescein angiographic defects of the optic disc in glaucoma, *Arch Ophthalmol,* 95, 1961-74.

Seddon, J. M., Schwartz, B. and Flowerdew, G. (1983) Case-control study of ocular hypertension, *Arch Ophthalmol,* 101, 891-4.

Shimmyo, M., Ross, A. J., Moy, A. and Mostafavi, R. (2003) Intraocular pressure, Goldmann applanation tension, corneal thickness, and corneal curvature in Caucasians, Asians, Hispanics, and African Americans, *Am J Ophthalmol,* 136, 603-13.

Shuman, J. S., Puliafito, C. A. and Fujimoto, J. G. (2004) Optical Coherence Tomography of Ocular Diseases. New Jersey, Slack Incorporated.

Siegner, S. W. and Netland, P. A. (1996) Optic disc hemorrhages and progression of glaucoma, *Ophthalmology,* 103, 1014-24.

Sihota, R., Gulati, V., Agarwal, H. C., Saxena, R., Sharma, A. and Pandey, R. M. (2002) Variables affecting test-retest variability of Heidelberg Retina Tomograph II stereometric parameters, *J Glaucoma,* 11, 321-8.

Silver, D. M., Farrell, R. A., Langham, M. E., O'Brien, V. and Schilder, P. (1989) Estimation of pulsatile ocular blood flow from intraocular pressure, *Acta Ophthalmol Suppl,* 191, 25-9.

Smith, S. D., Katz, J. and Quigley, H. A. (1996) Analysis of progressive change in automated visual fields in glaucoma, *Invest Ophthalmol Vis Sci,* 37, 1419-28.

Sommer, A., Katz, J., Quigley, H. A., Miller, N. R., Robin, A. L., Richter, R. C. and Witt, K. A. (1991a) Clinically detectable nerve fiber atrophy precedes the onset of glaucomatous field loss, *Arch Ophthalmol,* 109, 77-83.

Sommer, A., Miller, N. R., Pollack, I., Maumenee, A. E. and George, T. (1977) The nerve fiber layer in the diagnosis of glaucoma, *Arch Ophthalmol,* 95, 2149-56.

Sommer, A., Pollack, I. and Maumenee, A. E. (1979a) Optic disc parameters and onset of glaucomatous field loss. I. Methods and progressive changes in disc morphology, *Arch Ophthalmol,* 97, 1444-8.

Sommer, A., Pollack, I. and Maumenee, A. E. (1979b) Optic disc parameters and onset of glaucomatous field loss. II. Static screening criteria, *Arch Ophthalmol,* 97, 1449-54.

Sommer, A., Tielsch, J. M., Katz, J., Quigley, H. A., Gottsch, J. D., Javitt, J. and Singh, K. (1991b) Relationship between intraocular pressure and primary open angle glaucoma among white and black Americans. The Baltimore Eye Survey, *Arch Ophthalmol,* 109, 1090-5.

Sonnsjo, B., Dokmo, Y. and Krakau, T. (2002) Disc haemorrhages, precursors of open angle glaucoma, *Prog Retin Eye Res,* 21, 35-56.

Spaeth, G. L. (1994) A new classification of glaucoma including focal glaucoma, *Surv Ophthalmol,* 38 Suppl, S9-17.

Spaeth, G. L., Henderer, J., Liu, C., Kesen, M., Altangerel, U., Bayer, A., Katz, L. J., Myers, J., Rhee, D. and Steinmann, W. (2002) The disc damage likelihood scale: reproducibility of a new method of estimating the amount of optic nerve damage caused by glaucoma, *Trans Am Ophthalmol Soc,* 100, 181-5; discussion 185-6.

Spaeth, G. L., Hitchings, R. A. and Sivalingam, E. (1976) The optic disc in glaucoma: pathogenetic correlation of five patterns of cupping in chronic open-angle glaucoma, *Trans Sect Ophthalmol Am Acad Ophthalmol Otolaryngol,* 81, 217-23.

Spahr, J. (1975) Optimization of the presentation pattern in automated static perimetry, *Vision Res,* 15, 1275-81.

Sponsel, W. E. (1989) Tonometry in question: can visual screening tests play a more decisive role in glaucoma diagnosis and management?, *Surv Ophthalmol,* 33 Suppl, 291-300.

Spry, P. G., Bates, A. B., Johnson, C. A. and Chauhan, B. C. (2000) Simulation of longitudinal threshold visual field data, *Invest Ophthalmol Vis Sci,* 41, 2192-200.

Spry, P. G. and Johnson, C. A. (2002) Identification of progressive glaucomatous visual field loss, *Surv Ophthalmol,* 47, 158-73.

Spry, P. G., Johnson, C. A., Bates, A. B., Turpin, A. and Chauhan, B. C. (2002) Spatial and temporal processing of threshold data for detection of progressive glaucomatous visual field loss, *Arch Ophthalmol,* 120, 173-80.

Stone, E. M., Fingert, J. H., Alward, W. L., Nguyen, T. D., Polansky, J. R., Sunden, S. L., Nishimura, D., Clark, A. F., Nystuen, A., Nichols, B. E., Mackey, D. A., Ritch, R., Kalenak, J. W., Craven, E. R. and Sheffield, V. C. (1997) Identification of a gene that causes primary open angle glaucoma, *Science,* 275, 668-70.

Strouthidis, N. G. (2005) The reference plane. Optic nerve head and retinal fibre analysis. M. Iester, D. F. Garway-Heath and J. Lemij. Savona, Editrice Dogma: 63-65.

Strouthidis, N. G. and Garway-Heath, D. F. (2003) The correlation between change in optic disc neuroretinal rim area and differential light sensitivity. Perimetry Update 2002/2003. D. B. Henson and M. Wall. The Hague, Kugler Publications: 317-327.

Strouthidis, N. G., Scott, A., Peter, N. M. and Garway-Heath, D. F. (2006a) Optic disc and visual field progression in ocular hypertensive subjects: detection rates, specificity, and agreement, *Invest Ophthalmol Vis Sci,* 47, 2904-10.

Strouthidis, N. G., Vinciotti, V., Tucker, A., Gardiner, S. K., Crabb, D. P. and Garway-Heath, D. F. (2006b) Structure and function in glaucoma; the relationship between a functional visual field map and an anatomical retinal map, *Invest Ophthalmol Vis Sci,* 47, 2904-2910.

Strouthidis, N. G., White, E. T., Owen, V. M., Ho, T. A. and Garway-Heath, D. F. (2005b) Improving the repeatability of Heidelberg retina tomograph and Heidelberg retina tomograph II rim area measurements, *Br J Ophthalmol,* 89, 1433-7.

Strouthidis, N. G., White, E. T., Owen, V. M., Ho, T. A., Hammond, C. J. and Garway-Heath, D. F. (2005a) Factors affecting the test-retest variability of Heidelberg retina tomograph and Heidelberg retina tomograph II measurements, *Br J Ophthalmol,* 89, 1427-32.

Sugiyama, K., Tomita, G., Kitazawa, Y., Onda, E., Shinohara, H. and Park, K. H. (1997) The associations of optic disc hemorrhage with retinal nerve fiber layer defect and peripapillary atrophy in normal-tension glaucoma, *Ophthalmology,* 104, 1926-33.

Sugiyama, K., Uchida, H., Tomita, G., Sato, Y., Iwase, A. and Kitazawa, Y. (1999) Localized wedge-shaped defects of retinal nerve fiber layer and disc hemorrhage in glaucoma, *Ophthalmology,* 106, 1762-7.

Sugiyama, T., Moriya, S., Oku, H. and Azuma, I. (1995) Association of endothelin-1 with normal tension glaucoma: clinical and fundamental studies, *Surv Ophthalmol,* 39 Suppl 1, S49-56.

Sutton, G. E., Motolko, M. A. and Phelps, C. D. (1983) Baring of a circumlinear vessel in glaucoma, *Arch Ophthalmol,* 101, 739-44.

Swindale, N. V., Stjepanovic, G., Chin, A. and Mikelberg, F. S. (2000) Automated analysis of normal and glaucomatous optic nerve head topography images, *Invest Ophthalmol Vis Sci,* 41, 1730-42.

Tan, J. C., Garway-Heath, D. F., Fitzke, F. W. and Hitchings, R. A. (2003a) Reasons for rim area variability in scanning laser tomography, *Invest Ophthalmol Vis Sci,* 44, 1126-31.

Tan, J. C., Garway-Heath, D. F. and Hitchings, R. A. (2003b) Variability across the optic nerve head in scanning laser tomography, *Br J Ophthalmol,* 87, 557-9.

Tan, J. C. and Hitchings, R. A. (2003c) Reference plane definition and reproducibility in optic nerve head images, *Invest Ophthalmol Vis Sci,* 44, 1132-7.

Tan, J. C. and Hitchings, R. A. (2003d) Approach for identifying glaucomatous optic nerve progression by scanning laser tomography, *Invest Ophthalmol Vis Sci,* 44, 2621-6.

Tan, J. C. and Hitchings, R. A. (2004a) Optimizing and validating an approach for identifying glaucomatous change in optic nerve topography, *Invest Ophthalmol Vis Sci,* 45, 1396-403.

Tan, J. C., Poinoosawmy, D. and Hitchings, R. A. (2004b) Tomographic identification of neuroretinal rim loss in high-pressure, normal-pressure, and suspected glaucoma, *Invest Ophthalmol Vis Sci,* 45, 2279-85.

Tanaka, C., Yamazaki, Y. and Yokoyama, H. (2001) Study on the Progression of Visual Field Defect and Clinical Factors in Normal-Tension Glaucoma, *Jpn J Ophthalmol,* 45, 117.

Tate, J. W. and Lynn, J. R. (1977) Principles of quantitative perimetry. New York, Grunne and Stratton.

Teikari, J. M. (1987) Genetic factors in open-angle (simple and capsular) glaucoma. A population-based twin study, *Acta Ophthalmol (Copenh),* 65, 715-20.

Tezel, G., Hernandez, M. R. and Wax, M. B. (2001) In vitro evaluation of reactive astrocyte migration, a component of tissue remodeling in glaucomatous optic nerve head, *Glia,* 34, 178-89.

Tezel, G., Kolker, A. E., Kass, M. A., Wax, M. B., Gordon, M. and Siegmund, K. D. (1997a) Parapapillary chorioretinal atrophy in patients with ocular hypertension. I. An evaluation as a predictive factor for the development of glaucomatous damage, *Arch Ophthalmol,* 115, 1503-8.

Tezel, G., Kolker, A. E., Wax, M. B., Kass, M. A., Gordon, M. and Siegmund, K. D. (1997b) Parapapillary chorioretinal atrophy in patients with ocular hypertension. II. An evaluation of progressive changes, *Arch Ophthalmol,* 115, 1509-14.

Tielsch, J. M., Katz, J., Quigley, H. A., Javitt, J. C. and Sommer, A. (1995) Diabetes, intraocular pressure, and primary open-angle glaucoma in the Baltimore Eye Survey, *Ophthalmology,* 102, 48-53.

Tielsch, J. M., Katz, J., Sommer, A., Quigley, H. A. and Javitt, J. C. (1994) Family history and risk of primary open angle glaucoma. The Baltimore Eye Survey, *Arch Ophthalmol,* 112, 69-73.

Tielsch, J. M., Sommer, A., Katz, J., Quigley, H. and Ezrine, S. (1991a) Socioeconomic status and visual impairment among urban Americans. Baltimore Eye Survey Research Group, *Arch Ophthalmol,* 109, 637-41.

Tielsch, J. M., Sommer, A., Katz, J., Royall, R. M., Quigley, H. A. and Javitt, J. (1991b) Racial variations in the prevalence of primary open-angle glaucoma. The Baltimore Eye Survey, *Jama,* 266, 369-74.

Toh, T., Liew, S. H., MacKinnon, J. R., Hewitt, A. W., Poulsen, J. L., Spector, T. D., Gilbert, C. E., Craig, J. E., Hammond, C. J. and Mackey, D. A. (2005) Central corneal thickness is highly heritable: the twin eye studies, *Invest Ophthalmol Vis Sci,* 46, 3718-22.

Trew, D. R. and Smith, S. E. (1991) Postural studies in pulsatile ocular blood flow: II. Chronic open angle glaucoma, *Br J Ophthalmol,* 75, 71-5.

Trope, G. E., Salinas, R. G. and Glynn, M. (1987) Blood viscosity in primary open-angle glaucoma, *Can J Ophthalmol,* 22, 202-4.

Tsai, C. S., Ritch, R., Shin, D. H., Wan, J. Y. and Chi, T. (1992) Age-related decline of disc rim area in visually normal subjects, *Ophthalmology,* 99, 29-35.

Tucker, A., Vinciotti, V., Liu, X. and Garway-Heath, D. (2005) A spatio-temporal Bayesian network classifier for understanding visual field deterioration, *Artif Intell Med,* 34, 163-77.

Tuulonen, A. and Airaksinen, P. J. (1991) Initial glaucomatous optic disk and retinal nerve fiber layer abnormalities and their progression, *Am J Ophthalmol,* 111, 485-90.

Tuulonen, A., Lehtola, J. and Airaksinen, P. J. (1993) Nerve fiber layer defects with normal visual fields. Do normal optic disc and normal visual field indicate absence of glaucomatous abnormality?, *Ophthalmology,* 100, 587-97; discussion 597-8.

Tuulonen, A., Vihanninjoki, K., Airaksinen, P. J., Alanko, H. and Nieminen, H. (1994) The effect of reference levels on neuroretinal rim area and rim volume measurements in the Heidelberg Retina Tomograph, *IOVS : Supplement,* 35, 1729.

Uchida, H., Brigatti, L. and Caprioli, J. (1996) Detection of structural damage from glaucoma with confocal laser image analysis, *Invest Ophthalmol Vis Sci,* 37, 2393-401.

Uchida, H., Ugurlu, S. and Caprioli, J. (1998) Increasing peripapillary atrophy is associated with progressive glaucoma, *Ophthalmology,* 105, 1541-5.

Usui, T., Iwata, K., Shirakashi, M. and Abe, H. (1991) Prevalence of migraine in low-tension glaucoma and primary open-angle glaucoma in Japanese, *Br J Ophthalmol,* 75, 224-6.

Varela, H. J. and Hernandez, M. R. (1997) Astrocyte responses in human optic nerve head with primary open-angle glaucoma, *J Glaucoma,* 6, 303-13.

Varma, R., Quigley, H. A. and Pease, M. E. (1992a) Changes in optic disk characteristics and number of nerve fibers in experimental glaucoma, *Am J Ophthalmol,* 114, 554-9.

Varma, R., Spaeth, G. L., Steinmann, W. C. and Katz, L. J. (1989) Agreement between clinicians and an image analyzer in estimating cup-to-disc ratios, *Arch Ophthalmol,* 107, 526-9.

Varma, R., Steinmann, W. C. and Scott, I. U. (1992b) Expert agreement in evaluating the optic disc for glaucoma, *Ophthalmology,* 99, 215-21.

Varma, R., Tielsch, J. M., Quigley, H. A., Hilton, S. C., Katz, J., Spaeth, G. L. and Sommer, A. (1994) Race-, age-, gender-, and refractive error-related differences in the normal optic disc, *Arch Ophthalmol,* 112, 1068-76.

Varma, R., Ying-Lai, M., Francis, B. A., Nguyen, B. B., Deneen, J., Wilson, M. R. and Azen, S. P. (2004) Prevalence of open-angle glaucoma and ocular hypertension in Latinos: the Los Angeles Latino Eye Study, *Ophthalmology,* 111, 1439-48.

Verdonck, N., Zeyen, T., Van Malderen, L. and Spileers, W. (2002) Short-term intra-individual variability in heidelberg retina tomograph II, *Bull Soc Belge Ophtalmol,* 11, 51-7.

Vesti, E., Johnson, C. A. and Chauhan, B. C. (2003) Comparison of different methods for detecting glaucomatous visual field progression, *Invest Ophthalmol Vis Sci,* 44, 3873-9.

Vesti, E. and Kivela, T. (2000) Exfoliation syndrome and exfoliation glaucoma, *Prog Retin Eye Res,* 19, 345-68.

Vijaya, L., George, R., Arvind, H., Baskaran, M., Raju, P., Ramesh, S. V., Paul, P. G., Kumaramanickavel, G. and McCarty, C. (2006) Prevalence and causes of blindness in the rural population of the Chennai Glaucoma Study, *Br J Ophthalmol,* 90, 407-10.

Viswanathan, A. C., Crabb, D. P., McNaught, A. I., Westcott, M. C., Kamal, D., Garway-Heath, D. F., Fitzke, F. W. and Hitchings, R. A. (2003) Interobserver agreement on visual field progression in glaucoma: a comparison of methods, *Br J Ophthalmol,* 87, 726-30.

Viswanathan, A. C., Fitzke, F. W. and Hitchings, R. A. (1997) Early detection of visual field progression in glaucoma: a comparison of PROGRESSOR and STATPAC 2, *Br J Ophthalmol,* 81, 1037-42.

von Graefe, A. (1857) Uber die iridktomie bei glaukom and uber den glaukomatosen prozess., *Albrecht Von Graefes Arch Ophthalmol,* 3, 456-650.

Vrabec, F. (1966) The temporal raphe of the human retina, *Am J Ophthalmol,* 62, 926-38.

Wang, J. J., Mitchell, P. and Smith, W. (1997) Is there an association between migraine headache and open-angle glaucoma? Findings from the Blue Mountains Eye Study, *Ophthalmology,* 104, 1714-9.

Watkins, R. J. and Broadway, D. C. (2005) Intraobserver and interobserver reliability indices for drawing scanning laser ophthalmoscope optic disc contour lines with and without the aid of optic disc photographs, *J Glaucoma,* 14, 351-7.

Webb, R. H. and Hughes, G. W. (1981) Scanning laser ophthalmoscope, *IEEE Trans Biomed Eng,* 28, 488-92.

Webb, R. H., Hughes, G. W. and Pomerantzeff, O. (1980) Flying spot TV ophthalmoscope, *Appl Opt,* 19, 2991-7.

Weber, A. J. and Harman, C. D. (2005) Structure-function relations of parasol cells in the normal and glaucomatous primate retina, *Invest Ophthalmol Vis Sci,* 46, 3197-207.

Weber, J., Dannheim, F. and Dannheim, D. (1990) The topographical relationship between optic disc and visual field in glaucoma, *Acta Ophthalmol (Copenh),* 68, 568-74.

Weber, J. and Ulrich, H. (1991) A perimetric nerve fiber bundle map, *Int Ophthalmol,* 15, 193-200.

Weinreb, R. N., Dreher, A. W., Coleman, A., Quigley, H., Shaw, B. and Reiter, K. (1990) Histopathologic validation of Fourier-ellipsometry measurements of retinal nerve fiber layer thickness, *Arch Ophthalmol,* 108, 557-60.

Weinreb, R. N., Lusky, M., Bartsch, D. U. and Morsman, D. (1993) Effect of repetitive imaging on topographic measurements of the optic nerve head, *Arch Ophthalmol,* 111, 636-8.

Weinreb, R. N., Shakiba, S., Sample, P. A., Shahrokni, S., van Horn, S., Garden, V. S., Asawaphureekorn, S. and Zangwill, L. (1995a) Association between quantitative nerve fiber layer measurement and visual field loss in glaucoma, *Am J Ophthalmol,* 120, 732-8.

Weinreb, R. N., Shakiba, S. and Zangwill, L. (1995b) Scanning laser polarimetry to measure the nerve fiber layer of normal and glaucomatous eyes, *Am J Ophthalmol,* 119, 627-36.

Wensor, M. D., McCarty, C. A., Stanislavsky, Y. L., Livingston, P. M. and Taylor, H. R. (1998) The prevalence of glaucoma in the Melbourne Visual Impairment Project, *Ophthalmology,* 105, 733-9.

Werner, E. B., Bishop, K. I., Koelle, J., Douglas, G. R., LeBlanc, R. P., Mills, R. P., Schwartz, B., Whalen, W. R. and Wilensky, J. T. (1988) A comparison of experienced clinical observers and statistical tests in detection of progressive visual field loss in glaucoma using automated perimetry, *Arch Ophthalmol,* 106, 619-23.

Wiggs, J. L., Allingham, R. R., Vollrath, D., Jones, K. H., De La Paz, M., Kern, J., Patterson, K., Babb, V. L., Del Bono, E. A., Broomer, B. W., Pericak-Vance, M. A. and Haines, J. L. (1998) Prevalence of mutations in TIGR/Myocilin in patients with adult and juvenile primary open-angle glaucoma, *Am J Hum Genet,* 63, 1549-52.

Wild, J. M., Dengler-Harles, M., Searle, A. E., O'Neill, E. C. and Crews, S. J. (1989) The influence of the learning effect on automated perimetry in patients with suspected glaucoma, *Acta Ophthalmol (Copenh),* 67, 537-45.

Wild, J. M., Hutchings, N., Hussey, M. K., Flanagan, J. G. and Trope, G. E. (1997) Pointwise univariate linear regression of perimetric sensitivity against follow-up time in glaucoma, *Ophthalmology,* 104, 808-15.

Wilson, M. R. (2002) Progression of visual field loss in untreated glaucoma patients and suspects in St Lucia, West Indies, *Trans Am Ophthalmol Soc,* 100, 365-410.

Wilson, M. R., Hertzmark, E., Walker, A. M., Childs-Shaw, K. and Epstein, D. L. (1987) A case-control study of risk factors in open angle glaucoma, *Arch Ophthalmol,* 105, 1066-71.

Wilson, R., Richardson, T. M., Hertzmark, E. and Grant, W. M. (1985) Race as a risk factor for progressive glaucomatous damage, *Ann Ophthalmol,* 17, 653-9.

Winder, A. F. (1977) Circulating lipoprotein and blood glucose levels in association with low-tension and chronic simple glaucoma, *Br J Ophthalmol,* 61, 641-5.

Wirtschafter, J. D., Becker, W. L., Howe, J. B. and Younge, B. R. (1982) Glaucoma visual field analysis by computed profile of nerve fiber function in optic disc sectors, *Ophthalmology,* 89, 255-67.

Wollstein, G., Garway-Heath, D. F. and Hitchings, R. A. (1998) Identification of early glaucoma cases with the scanning laser ophthalmoscope, *Ophthalmology,* 105, 1557-63.

Wollstein, G., Ishikawa, H., Wang, J., Beaton, S. A. and Schuman, J. S. (2005a) Comparison of three optical coherence tomography scanning areas for detection of glaucomatous damage, *Am J Ophthalmol,* 139, 39-43.

Wollstein, G., Schuman, J. S., Price, L. L., Aydin, A., Stark, P. C., Hertzmark, E., Lai, E., Ishikawa, H., Mattox, C., Fujimoto, J. G. and Paunescu, L. A. (2005b) Optical coherence tomography longitudinal evaluation of retinal nerve fiber layer thickness in glaucoma, *Arch Ophthalmol,* 123, 464-70.

Wong, T. Y., Klein, B. E., Klein, R., Knudtson, M. and Lee, K. E. (2003) Refractive errors, intraocular pressure, and glaucoma in a white population, *Ophthalmology,* 110, 211-7.

Woo, S. J., Park, K. H. and Kim, D. M. (2003) Comparison of localised nerve fibre layer defects in normal tension glaucoma and primary open angle glaucoma, *Br J Ophthalmol,* 87, 695-8.

Wu, S. Y. and Leske, M. C. (1997) Associations with intraocular pressure in the Barbados Eye Study, *Arch Ophthalmol,* 115, 1572-6.

Wu, S. Y., Nemesure, B. and Leske, M. C. (1999) Refractive errors in a black adult population: the Barbados Eye Study, *Invest Ophthalmol Vis Sci,* 40, 2179-84.

Wu, S. Y., Nemesure, B. and Leske, M. C. (2000) Glaucoma and myopia, *Ophthalmology,* 107, 1026-7.

Xu, L., Wang, Y., Li, Y., Cui, T., Li, J. and Jonas, J. B. (2006) Causes of Blindness and Visual Impairment in Urban and Rural Areas in Beijing The Beijing Eye Study, *Ophthalmology.*

Yamagishi, N., Anton, A., Sample, P. A., Zangwill, L., Lopez, A. and Weinreb, R. N. (1997) Mapping structural damage of the optic disk to visual field defect in glaucoma, *Am J Ophthalmol,* 123, 667-76.

Yamazaki, S., Inoue, Y. and Yoshikawa, K. (1996) Peripapillary fluorescein angiographic findings in primary open angle glaucoma, *Br J Ophthalmol,* 80, 812-7.

Yan, D. B., Coloma, F. M., Metheetrairut, A., Trope, G. E., Heathcote, J. G. and Ethier, C. R. (1994) Deformation of the lamina cribrosa by elevated intraocular pressure, *Br J Ophthalmol,* 78, 643-8.

Zafar, S., Gurses-Ozden, R., Vessani, R., Makornwattana, M., Liebmann, J. M., Tello, C. and Ritch, R. (2004) Effect of pupillary dilation on retinal nerve fiber layer thickness measurements using optical coherence tomography, *J Glaucoma,* 13, 34-7.

Zahari, M., Mukesh, B. N., Rait, J. L., Taylor, H. R. and McCarty, C. A. (2006) Progression of visual field loss in open angle glaucoma in the Melbourne Visual Impairment Project, *Clin Experiment Ophthalmol,* 34, 20-6.

Zangwill, L., Berry, C. A., Garden, V. S. and Weinreb, R. N. (1997a) Reproducibility of retardation measurements with the nerve fiber analyzer II, *J Glaucoma,* 6, 384-9.

Zangwill, L., Irak, I., Berry, C. C., Garden, V., de Souza Lima, M. and Weinreb, R. N. (1997b) Effect of cataract and pupil size on image quality with confocal scanning laser ophthalmoscopy, *Arch Ophthalmol,* 115, 983-90.

Zangwill, L. M., Abunto, T., Bowd, C., Angeles, R., Schanzlin, D. J. and Weinreb, R. N. (2005a) Scanning laser polarimetry retinal nerve fiber layer thickness measurements after LASIK, *Ophthalmology,* 112, 200-7.

Zangwill, L. M., van Horn, S., de Souza Lima, M., Sample, P. A. and Weinreb, R. N. (1996) Optic nerve head topography in ocular hypertensive eyes using confocal scanning laser ophthalmoscopy, *Am J Ophthalmol,* 122, 520-5.

Zangwill, L. M., Weinreb, R. N., Beiser, J. A., Berry, C. C., Cioffi, G. A., Coleman, A. L., Trick, G., Liebmann, J. M., Brandt, J. D., Piltz-Seymour, J. R., Dirkes, K. A., Vega, S., Kass, M. A. and Gordon, M. O. (2005b) Baseline topographic optic disc measurements are associated with the development of primary open-angle glaucoma: the Confocal Scanning Laser Ophthalmoscopy Ancillary Study to the Ocular Hypertension Treatment Study, *Arch Ophthalmol,* 123, 1188-97.

Zeyen, T., Miglior, S., Pfeiffer, N., Cunha-Vaz, J. and Adamsons, I. (2003) Reproducibility of evaluation of optic disc change for glaucoma with stereo optic disc photographs, *Ophthalmology,* 110, 340-4.

Zeyen, T. G. and Caprioli, J. (1993) Progression of disc and field damage in early glaucoma, *Arch Ophthalmol,* 111, 62-5.

Zinser, G. (2005) Heidelberg retina tomograph; the system. Optic nerve head and retinal nerve fibre analysis. Savona, Editrice Dogma: 59-61.